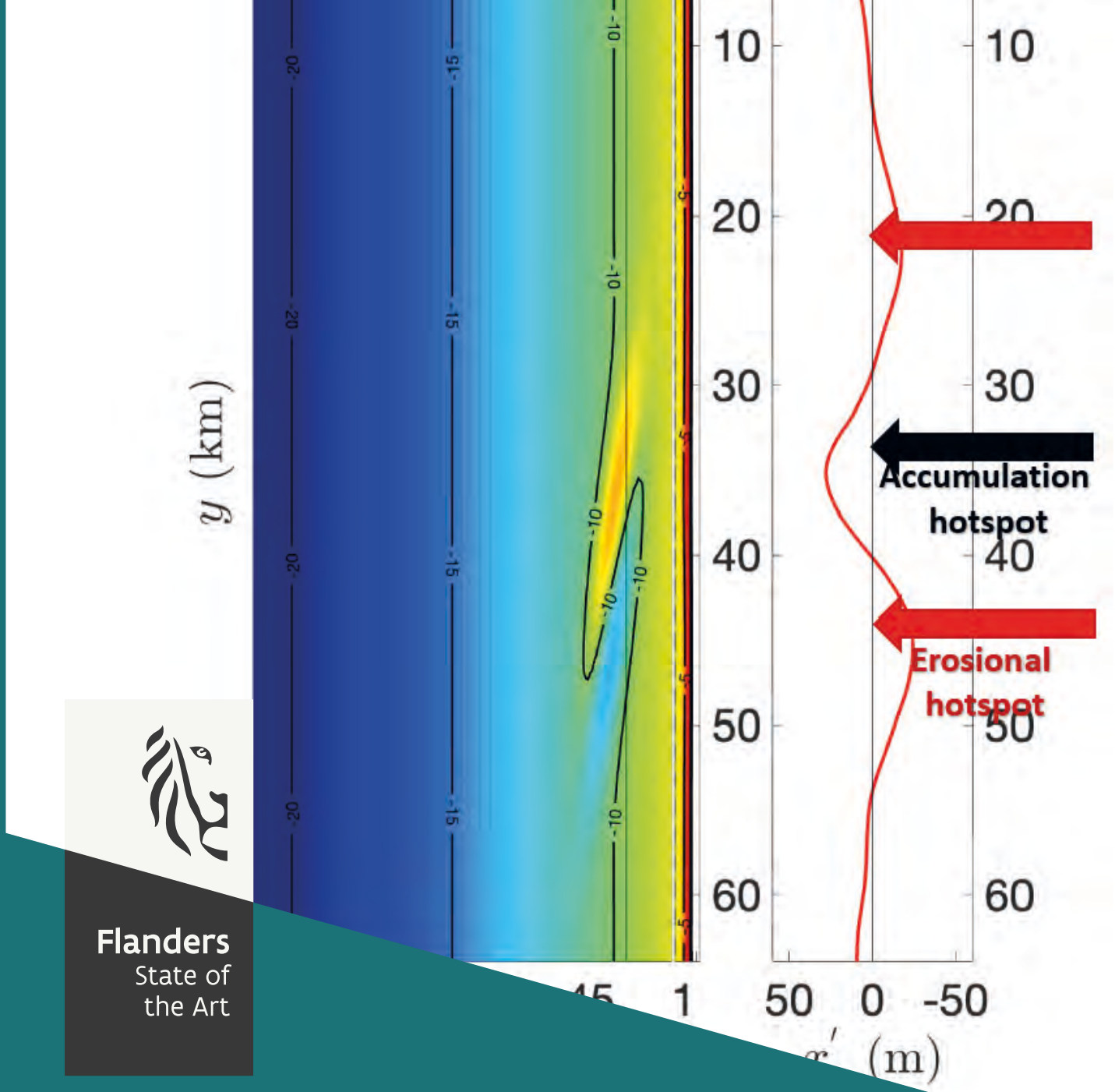

Flanders
State of the Art

20_079_3
FH reports

MOZES – Research on the Morphological Interaction between the Sea bottom and the Belgian Coastline

Working year 3

DEPARTMENT
MOBILITY &
PUBLIC
WORKS

www.flandershydraulics.be

MOZES – Research on the Morphological Interaction between the Sea bottom and the Belgian Coastline

Working year 3

Dujardin, A.; Houthuys, R.; Nnafie, A.; Röbke, B.; Nguyen, D.; de Bakker, A.; de Swart, H.E.; van der Werf, J.; Huisman, B.; De Maerschalck, B.; Dan, S.; Verwaest, T.

Flanders Hydraulics
Flanders State of the Art

Cover figure © The Government of Flanders, Department of Mobility and Public Works, Flanders Hydraulics

Legal notice

Copyright and citation

This publication should be cited as follows:

Dujardin, A.; Houthuys, R.; Nnafie, A.; Röbke, B.; Nguyen, D.; de Bakker, A.; de Swart, H.E.; van der Werf, J.; Huisman, B.; De Maerschalck, B.; Dan, S.; Verwaest, T. (2025). MOZES – Research on the Morphological Interaction between the Sea bottom and the Belgian Coastline: Working year 3. Version 4.0. FH Reports, 20_079_3. Flanders Hydraulics: Antwerp

Document identification

Customer:	Flanders Hydraulics / Coastal Division	Ref.:	WL2025R20_079_3
Keywords (3-5):	Coastal Morphology, Sediment Transport		
Knowledge domains:	Hydraulics and Sediment > Morphology > Erosion / Sedimentation > Literature and desktop study Hydraulics and Sediment > Morphology > Erosion / Sedimentation > Numerical modelling		
Text (p.):	131	Appendices (p.):	23
Confidential:	☒ No	☒ Available online	

Author(s):	Dujardin, A.; Houthuys, R.; Nnafie, A.; Röbke, B.; Nguyen, D.; de Bakker, A.

Control

	Name	Signature
Reviser(s):	De Maerschalck, B. Dan, S.	Signed by:De Maerschalck Bart Signed at:2025-09-16 11:44:04 +02:00 Reason:Ik keur dit document goed Signed by:Sebastian Dan (Signature) Signed at:2025-09-16 11:29:05 +02:00 Reason:I approve this document
Project leader:	Verwaest, T.	Signed by:Verwaest Toon Signed at:2025-09-16 10:41:19 +02:00 Reason:Ik keur dit document goed

Approval

Head of Division:	Bellafkih, K.	Signed by:Bellafkih Abdelkarim Signed at:2025-09-16 13:38:47 +02:00 Reason:Ik keur dit document goed

Abstract

The MOZES-project (**MO**rfolgische interactie kustnabije **ZE**ebodem en **S**trand) investigates the morphodynamic interaction between the Belgian offshore seabed (shelf and nearshore) and adjacent shoreline across varying time scales (days to centuries), aiming to improve regional morphodynamic understanding needed for effective coastal management.

This report outlines progress during the third year across four Work Packages (WP1, WP2, WP3 and WP4). WP1 analysed field data, WP2 further developed the idealized models (coupled shelf-shoreline model and morphodynamic model) established in the first two years, WP3 validated the Scaldis-Coast and FlemCo models by simulating nearshore wave directions, while WP4 began hindcasting shoreline and seabed changes near Knokke-Heist from 1999-2003. Key findings and highlights from each Work Package are listed below.

WP1:

- Vectorisation of historical topo-bathymetric maps continued in the third year, focusing on selected areas surveyed in the 1970s and around 1990.
- Over the past two centuries, shoreface-connected sand ridges (sfcr) migrated by up to 5 km eastwards, and several hundred metres landwards. The underlying driving forces are believed to be mainly the residual sediment transport and sea-level rise. While the area of tidal sand ridges (tsr) lost sediment, the area of sfcr accreted, although vertical change remained within depth uncertainty. The relative height of all sand ridges did not change.
- Dredging of navigation channels deprives the downdrift sandbanks and the point where they attach to the shore of sediment. A morphological analysis for Stroombank yields a longshore sediment transport estimate of about 300 m^3/m/year.

WP2:

- The coupled shelf-shoreline model, featuring synthetic sfcr and tsr resembling the Belgian shelf, successfully reproduces observed shoreline progradation near sfcr crests, retreat near channels, with tsr having smaller but non-negligible impact. These results are published in the *Journal of Geophysical Research.*
- The morphodynamic shelf model, for the first time, simulates the simultaneous development of sfcr and tsr under waves, wind, and tides. While the simulated ridges resemble those on the Belgian shelf, key differences exist: sfcr are less oblique and migrate faster in the model, while tsr are located more shoreward than in observations.
- The morphodynamic shelf model, for the first time, successfully simulates sfcr using sediment formulations other than those traditionally used, showing sfcr formation is not constrained by a specific sediment transport formulation.

WP3:

- Overall, the wave heights and directions as simulated with the Scaldis-Coast and FlemCo models agree with the observed wave heights and directions at the Flemish coast but the interaction between tides and waves in the Appelzak gully near the coast is not fully reproduced by both models.
- FlemCo slightly overestimates the wave directional spreading offshore, while Scaldis underestimates the spreading nearshore, leading to an exaggerated peak for waves from the northwest.

WP4:

- Overall, FlemCo produces the observed morphodynamics at the beach and shoreface of Knokke-Heist, though discrepancies increase seaward of the shoreface.
- The Scaldis-Coast model generally captures the main morphological changes during the period 1999-2002/2003: erosion in the nourishment area. However, deviations remain in the magnitude and spatial distribution of bed level changes in the broader area.
- Both models require further calibration and validation before being use to study erosion of nourishments of the coastline of Knokke-Heist coast in more detail.

Contents

List of tables

List of figures

1 Introduction

1.1 WP1: Data acquisition and analysis

WP1 consists of acquiring historical bathymetric and topographic data crucial for addressing the research questions within the MOZES project. These data are utilized to create Digital Elevation Models (DEMs) covering the entire area of interest at specific time points, spanning the last two centuries. The bathymetric datasets were examined for large-scale morphological change. These datasets are also available as input for numerical models, thereby contributing to research on the morphological evolution of nearshore channels and shoreface-connected sand ridges on decadal time scales.

In year 3 of MOZES, the following subtasks within WP1 were performed:

- Subtask 1: vectorise maps of the beach, shoreface, and inner shelf, with emphasis on the second half of the 20th-century maps. Continuation of the work achieved in the 1st and 2nd year of the project. In the 3rd year, the cover of beach and outer dunes in Spring 1992 is completed, an additional inner shelf cover for 1974-1978 has been realised and the Autumn 1989 and March 1990 nearshore bathymetry of the eastern part of the Belgian nearshore was vectorised, as well as the corresponding part of the Autumn 1989 beach topography.
- Subtask 2: analyse the large-scale morphological evolution of the Belgian inner shelf and the surrounding areas, using vectorised small-scale (in the order of 1/100,000) navigation charts of 1804, 1866, 1908 and 1938 and comparing these historic bathymetries with more recent bathymetries of the inner shelf and the 2022 bathymetric cover of the area.
- Subtask 3: obtain an additional estimate of the longshore sediment transport using the morphological evolution after the abandonment of the old access channel to Oostende, Rechtstreekse Kil, at its intersection with Stroombank.

1.2 Numerical modelling

1.2.1 WP2

To quantify potential impacts of the observed onshore and alongshore migrating sfcr on the decadal evolution of the Belgian shoreline, a coupled shelf-shoreline model is being developed within the MOZES project. This coupled model integrates a shelf model (Delft3D+SWAN) with a shoreline evolution model. In the first two years of the MOZES project, this coupled model was applied to the Belgian coast, where a synthetic field of morphostatic sfcr (i.e., the ridges and the shelf bathymetry did not evolve during the simulation) was placed on the shelf. Simulations with this model suggested that the observed onshore movement of ridges on the Belgian shelf is likely to enhance shoreline retreat near the channels and progradation near the ridge crests. A key limitation in that model, however, was the exclusion of tidal sand ridges on the shelf, which might also impact shoreline evolution on decadal scales. Another limitation was the assumption of a morphostatic shelf model, where the sfcr remained "frozen" during the simulation. This assumption implies a one-way coupling between the shelf and nearshore models, meaning that the shelf morphology influences the bed level of the nearshore zone and the shoreline, but not the other way around. Finally, another limitation was the use of a single sfcr on the shelf, whereas on the Belgian shelf, three sfcr are located. The use of more sfcr might induce non-linear interactions between the shoreline undulations induced by the individual ridges.

The considerations outlined above motivated the specific objectives of year 3 within Workpackage 2 (WP2) of the MOZES project, which are divided among activities 1 and 2. The overall objective in Activity 1 is to further refine the coupled shelf-shoreline model by implementing a ridge configuration resembling that of the Belgian shelf, whereby multiple sfcr and tsr are present on the shelf.

In Activity 2, the overall objective is to further develop the morphodynamic shelf model by 1) incorporating a wind climate more representative for the Belgian shelf and 2) including tides in the shelf model.

It is important to emphasise that the goal of this study is not to reconstruct the morphodynamic evolution of the sfcr and tsr on Belgian shelf and the adjacent shoreline over recent decades, but rather to gain fundamental insights into the effects of onshore migrating sfcr on the shoreline and the influence of tides on the shelf ridges. To achieve this, an idealised modelling approach is employed, in which the tides, waves, bathymetry and ridge configuration are schematised and serve as first-order approximations of reality.

1.2.2 WP3

Research conducted in working year 2 of the MOZES-project revealed that both the Scaldis-Coast (openTELEMAC-suite) and FlemCo (Delft3D Flexible Mesh) models predict comparable longshore sediment transport along the Belgian coast for an idealised setup, where

- the same wave model settings (as far as possible, given the different applied wave modelling software),
- constant wave and wind boundary conditions and
- no groynes in the FlemCo model are applied (Dujardin *et al*., 2024).

However, when the models are used with their calibrated settings (see Grasmeijer *et al*., 2020 and Röbke *et al.,* 2000 for FlemCo and Kolokythas *et al*., 2023 for Scaldis-Coast) and realistic boundary time series, the FlemCo model systematically predicts lower longshore sediment transport for the Belgian coast than the Scaldis-Coast model (Dujardin *et al*., 2024).

Sensitivity simulation runs performed with the two models based on different forcing combinations (tide, waves and wind) revealed that it is mainly the wave related longshore sediment transport that differs between the two models, while the tide related transports show a closer match. The observed discrepancies of the predicted waves between models is – apart from the different wave models used by Scaldis-Coast and FlemCo (TOMAWAC/SWAN) – related to

- different settings used in the two wave models, especially the applied bed friction coefficient (lower in Scaldis-Coast) and breaker index (higher in Scaldis-Coast),
- the fact that groynes in the Scaldis-Coast model are clearly smaller in dimension (interpolated as bathymetry on the computational grid) in the FlemCo model (fixed weirs with specified elevations), and therefore block the wave-induced longshore current to a smaller degree than in the FlemCo model,
- less directional spreading of waves in the nearshore zone in the Scaldis-Coast model resulting in more dominant wave directions and stronger wave-induced longshore currents than in the FlemCo model.

This altogether favours higher wave energy and/or more pronounced wave-induced longshore currents in the nearshore zone and by this higher longshore transport in the Scaldis-Coast than in the FlemCo model. In the absence of sufficient wave validation data nearshore for the applied simulation periods, the wave models could not yet been sufficiently calibrated and validated for the zone of Knokke-Heist, where tides in the Appelzak gully appear to have an important effect on the wave direction.

In the current study, both the Scaldis-Coast and FlemCo models are therefore applied for a different, more recent simulation period that allows for a more detailed calibration and validation of the wave models in the nearshore zone between Zeebrugge harbour and the Belgian-Dutch border, especially with regard to the predicted wave directions and wave heights.

Furthermore for the coastal zone between Zeebrugge harbour and the Belgian-Dutch border, the exact crest height and length of the groynes was examined. For the position above the low water mark a long-term dataset LiDar flights was used. To define the underwater part two multibeam soundings – executed by DEME within the framework of the 2023 – 2024 shoreface nourishment – and scans of the design plans were used. The derived crest heights and (underwater) length of the groynes were then implemented into the Scaldis-Coast model.

1.2.3 WP4

In the MOZES-project, task 4 is investigated based on the example of the Appelzak channel located off the coast of Knokke-Heist between Zeebrugge harbour and the Dutch border. After the extension of Zeebrugge harbour in the year 1986, a significant deepening of the Appelzak channel has been observed, while the Paardenmarkt ridge (located seaward of the Appelzak) experienced pronounced sedimentation. The morphological development of the Appelzak channel is most probably related to the extension of Zeebrugge harbour and the observed erosion along the harbour breakwaters as well as the sedimentation on the Paardenmarkt ridge (Dujardin *et al.*, 2023; Dujardin *et al.*, 2024). Moreover, intensive beach nourishments and the presence of groynes at Knokke-Heist slow down or even prevent landward migration of the Appelzak channel.

The sedimentary processes and morphodynamics of the Appelzak area will be studied in more detail in the fourth project year using the openTelemac Scaldis-Coast and the Delft3D Flexible Mesh FlemCo model. In order to calibrate the models for this application, we made a first attempt of a morphological hindcast in this study for the period summer 1999 to spring 2003.

2 Data Acquisition and Analysis

2.1 Vectorising pre-2000 maps of beach, shoreface and inner shelf

2.1.1 Outsourcing of vectorization of 2nd half 20th century beach, shoreface and inner shelf maps

This task continues the work started in the previous working years. Table 1 provides an overview of the work progress. It was updated for the parts in working year 2 that were finished after the report and the new work in year 3. The work was outsourced to Sparks bvba, 1601 Sint-Pieters-Leeuw.

Table 1 – Progress of the outsourced vectorisation work.

Work package	Sheets	Date commissioned	Date of delivery	Date of acceptance
Selection stage	A typical beach map: SIT_1985_1_OOST10.jpg (1 sheet) A typical nearshore map: VO_1986_1_8616.jpg (1 sheet) A typical inner shelf map: wie-sch1986.jpg (1 sheet)	16/06/2022	8/07/2022	12/07/2022
Deelopdracht 1	SIT_1985_1_OOST05 – 09, OOST11; SIT_1983_1_OOST05 – 08 (10 sheets) and ZUYWE_1987 en west-dh1984 (2 sheets)	20/07/2022	22/08/2022	29/08/2022
Deelopdracht 2	SIT_1983_1_OOST09 – 11; OOST03 – 04; MIWE28 – 32 (10 sheets)	5/09/2022	10/10/2022	11/10/2022
Deelopdracht 3	SIT_1983_1_MIWE01 – 09; VO_1987_2_87130	14/10/2022	14/11/2022	16/11/2022
Deelopdracht 4	SIT_1983_1_MIWE10 – 20	21/11/2022	4/01/2023	5/01/2023
Deelopdracht 5	SIT_1983_1_MIWE21 – 27	9/01/2023	3/02/2023	7/02/2023
Deelopdracht 6	ZuyWe1967.jpg (locally the first survey) wie-sch1962.jpg (the 1968 sheet was originally selected, but it covers only a small part of the inner shelf. Priority was given to a complete coverage of the inner shelf, for which 1962 was the closest in time)	27/03/2023	25/04/2023	27/04/2023

	WestDH1969.jpg (locally the first survey) ZuyWe1991.jpg WestDH1993.jpg WieSch1992.jpg			
Deelopdracht 7	8 nearshore plans of the Spring 1992 survey which was the first to cover the complete Belgian coast	5/05/2023	12/06/2023	15/06/2023
Deelopdracht 8	SIT_1992_1_MIWE21-30	23/06/2023	31/07/2023	2/08/2023
Deelopdracht 9	SIT_1992_1_OOST05-11	2/08/2023	26/09/2023	29/09/2023
Deelopdracht 10	SIT_1992_1_OOST01-04	2/10/2023	24/10/2023	26/10/2023
Deelopdracht 11	SIT_1992_1_MIWE01-09	27/10/2023	22/12/2023	26/12/2023
Deelopdracht 12	SIT_1992_1_MIWE10-20	15/03/2024	29/04/2024	3/05/2024
Deelopdracht 13	3 nearshore plans of the Autumn 1989 survey and the corresponding 3 nearshore plans of the March of Spring 1990 survey	8/05/2024	29/05/2021	3/06/2024
Deelopdracht 14	ZUYWE_1978.jpg ost-dh74-75.jpg (in two parts) wie-sch1976.jpg	4/06/2024	25/06/2024	27/06/2024
Deelopdracht 15a	SIT_1989_2_MIWE01-07	16/07/2024	21/08/2024	28/08/2024
Deelopdracht 15b	SIT_1989_2_MIWE24-30, SIT_1989_2_OOST01-04	16/09/2024	24/10/2024	2/11/2024
Deelopdracht 15c	SIT_1989_2_OOST05-11	To be assigned		

Preparation of each part involved georeferencing of the map images in Lambert 72 using all coordinate marks in the map area and using a spline transformation.

Each delivery was controlled using the acceptance criteria of the terms of reference.

Georeferenced plan packages, vectorisation work deliveries and the control reports can be found here: P:\20_079_MorfoInteract\3_Uitvoering\Deeltaak1_DataAcquisition\OudeKaarten\VectorisatieKustplannen in subfolders "plannen" (georeferenced plan packages sent out) and "lev" (delivery and report). The control and acceptance of each delivery of the vectorisation work was done according to section 5 of the work specifications (see Appendix 1 in Dujardin *et al.*, 2023).

Processing the deliveries into DEM rasters involves conversion from MOW Z or MLLWS to TAW, and completing the vectorised data with justified extrapolations around the data area, so that sections are completely covered in the sense needed to compute volumes per elevation slice (Houthuys *et al.*, 2022).

For older inner shelf maps, added depth contour lines may be needed to provide sufficiently dense data coverage for the DEM. Especially the beach plan deliveries require some intensive completion at the seawall and groins. Where needed to achieve a realistic DEM, points are added from the Lidar 2000_2 survey so as not to truncate groins and hard structures. The complete methodology was described in section 1.1.9 in Dujardin et al., 2023).

The following DEMs (Table 2) were made and are available on P:\20_079_MorfoInteract\3_Uitvoering\Deeltaak1_DataAcquisition\DEMs. The rasters are in ESRI raster format. They are referenced in Lambert72 and, while the source maps are either in Z MOW or MLLWS, they have been converted to TAW before making the DEMs. For the datum conversion MLLWS to TAW, use was made of *gllws_to_taw_vlaamsebanken_l72.tif*, a conversion raster borrowed from aMT available at FH on G:\Masterarchief\cnv. Some results are displayed in Figure 2 to Figure 4.

Table 2 – DEMs made of vectorised data.

Topic	Source of data	DEM	Area
Beach and dune foot maps (cell size 2 m)	SIT_1983_1_MIWE01-09.jpg	G_1983_1A	De Panne to Nieuwpoort
	SIT_1983_1_MIWE10-20.jpg	G_1983_1B	Nieuwprt to Oostende
	SIT_1983_1_MIWE21-31.jpg	G_1983_1C	Oostende to Wenduine
	SIT_1983_1_MIWE31-OOST04.jpg	G_1983_1D	Blankenberge to Zeebr.
	SIT_1983_1_OOST05-11.jpg	G_1983_1E	From Heist to Zwin
	SIT_1985_1_OOST05-11.jpg	G_1985_1E	From Heist to Zwin
Nearshore maps (cell size 10 m)	VO_1986_1_8616.jpg	G_vo1986_1_Knok	From Heist to Zwin
	VO_1987_2_87130	G_vo1987_2_Kks	De Panne to Oostduinkerke
	VO_1992_1 (8 sheets)	G_vo1992_1	Complete coast
Inner shelf maps (cell size 10 m)	ZuyWe1967.pdf	G_ZW1967_taw	Inner shelf western part
	WestDH1969.pdf	G_WD1969_taw	Inner shelf central part
	wie-sch1962.pdf	G_WS1962_taw	Inner shelf eastern part
	Mosaic 1962-1969	G_BS62_69_taw	Complete inner shelf
	Wie-sch1986.pdf	G_WS1986_TAW	Inner shelf eastern part
	West-dh1984.pdf	G_WD1984_TAW	Inner shelf central part

	ZUYWE_1987.pdf	G_ZW1987_TAW	Inner shelf western part
	Mosaic 1984-1987	G_BS84_87_TAW	Complete inner shelf
	ZuyWe1991.pdf	G_ZW1991_taw	Inner shelf western part
	WestDH1993.pdf	G_WD1993_taw	Inner shelf central part
	WieSch1992.pdf	G_WS1992_taw	Inner shelf eastern part
	Mosaic 1991-1993	G_BS91_93_taw	Complete inner shelf
Beach and dune foot maps (cell size 2 m)	SIT_1992_1_MIWE01-09.jpg	G_1992_1A	De Panne to Nieuwpoort
	SIT_1992_1_MIWE10-20.jpg	G_1992_1B	Nieuwprt to Oostende
	SIT_1992_1_MIWE21-31.jpg	G_1992_1C	Oostende to Wenduine
	SIT_1992_1_MIWE31-OOST04.jpg	G_1992_1D	Blankenberge to Zeebr.
	SIT_1992_1_OOST05-11.jpg	G_1992_1E	From Heist to Zwin
Nearshore maps (cell size 10 m)	VO_1989_2_89158.jpg VO_1989_2_89147.jpg VO_1989_2_89146.jpg	G_vo1989_2BrZ	From Bredene to Zwin
	VO_1990_0_maart1990.jpg VO_1990_1_90106.jpg VO_1990_1_90108.jpg	G_vo1990_1BrZ	From Bredene to Zwin
Inner shelf maps (cell size 10 m)	ZuyWe1978.pdf	G_ZW1978_taw	Inner shelf western part
	Ost-dh74-75.pdf	G_OD1974_taw	Inner shelf central part
	wie-sch1976.pdf	G_WS1976_taw	Inner shelf eastern part
	Mosaic 1974-1978	G_BS74_78_taw	Complete inner shelf
Beach and dune foot maps (cell size 2 m)	SIT_1989_2_MIWE01-07.jpg	G_1989_2A	De Panne to Oostdkerke
	SIT_1989_2_MIWE24-30.jpg	G_1989_2C	Bredene to Wenduine
	SIT_1989_2_OOST01-04.jpg	G_1989_2D	Blankenberge to Zeebr.

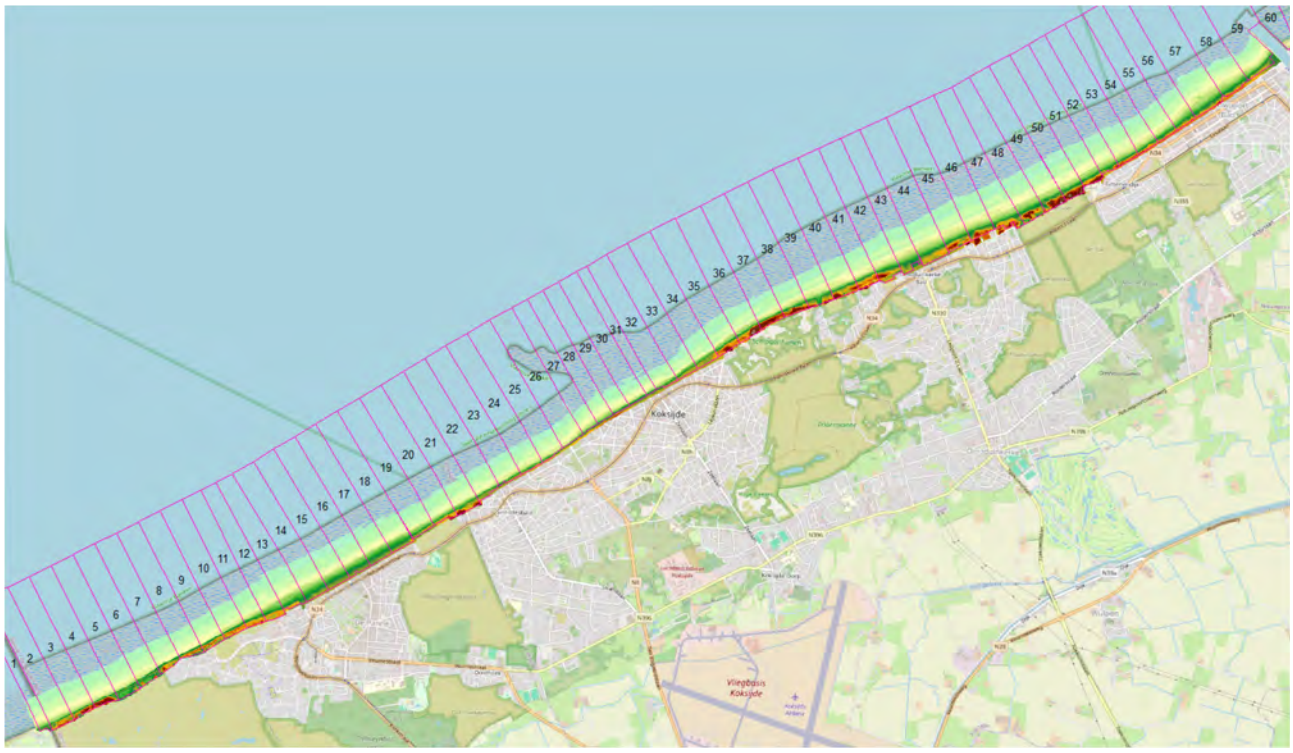

Figure 1 – 2 m-DEM of vectorised survey Spring 1992 between French border and Nieuwpoort. Land area is latest Openstreetmap.

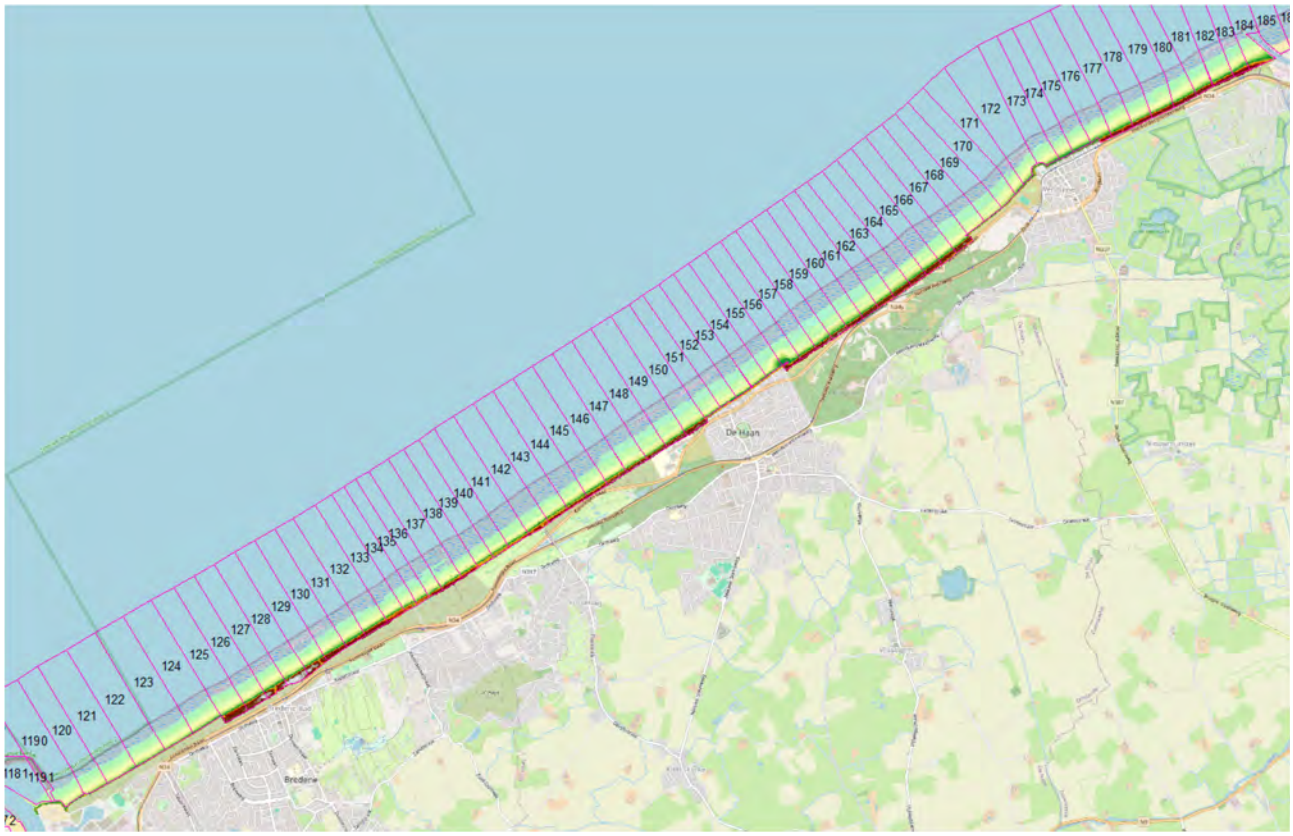

Figure 2 – 2 m-DEM of vectorised survey Spring 1992 between Oostende and Blankenberge.

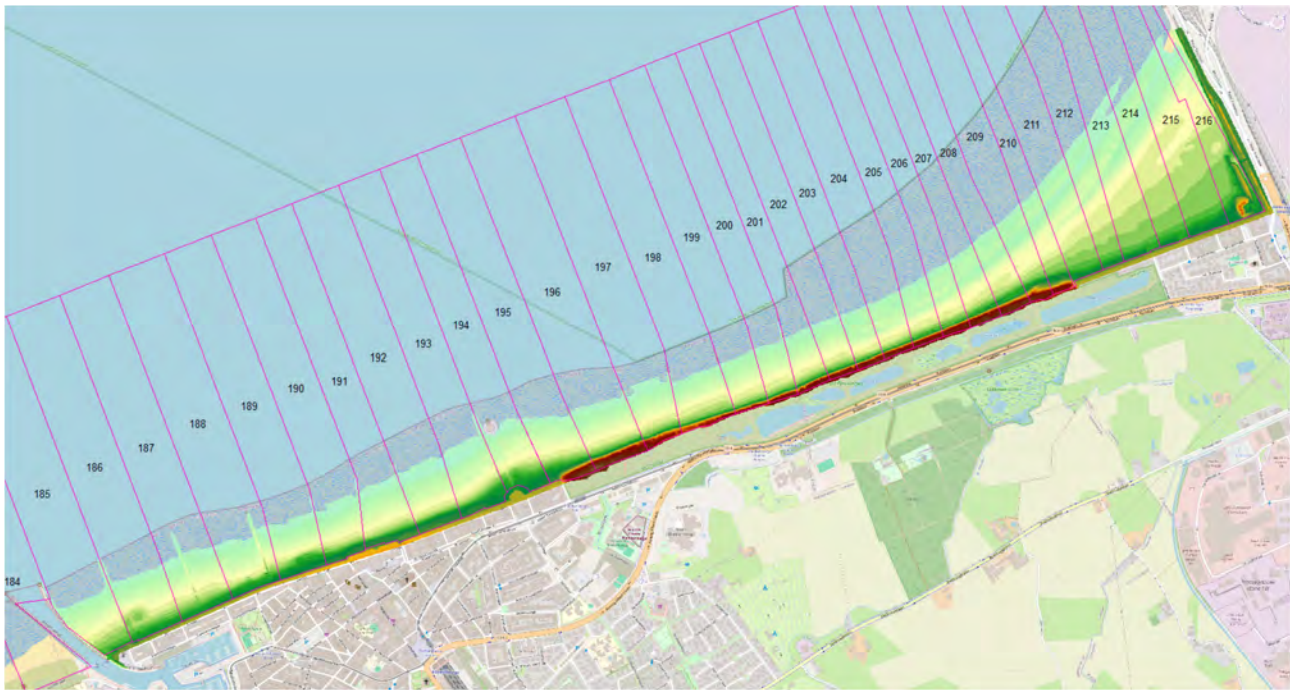

Figure 3 – 2 m-DEM of vectorised survey Spring 1992 between Blankenberge and Zeebrugge.

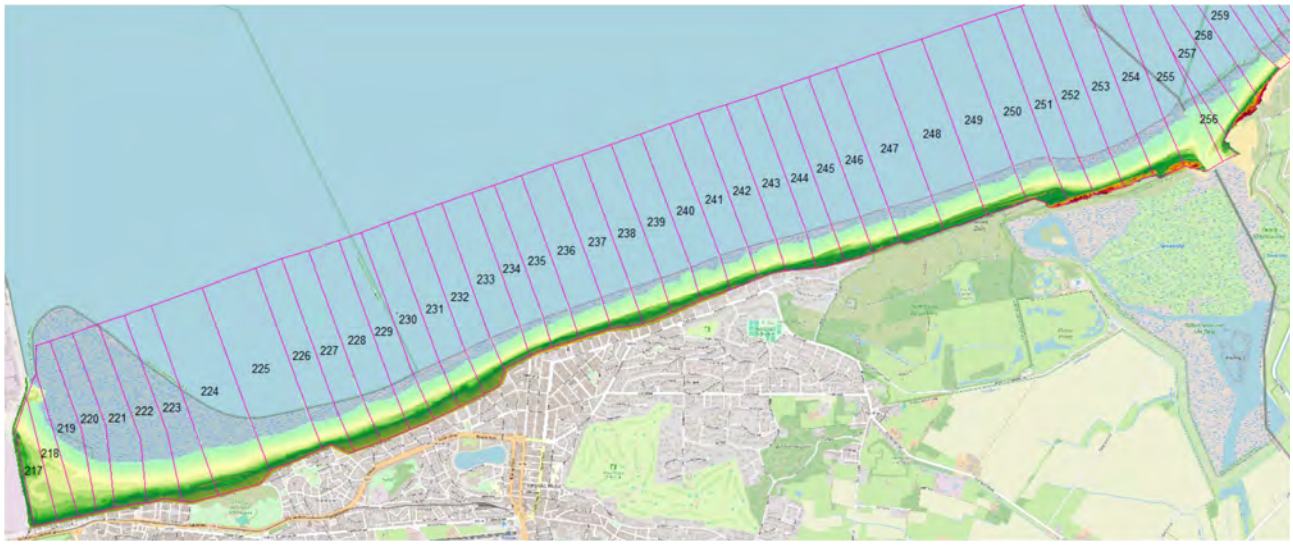

Figure 4 – 2 m-DEM of vectorised survey Spring 1992 between Zeebrugge and Zwin.

2.1.2 Flemish shelf maps 1804-1866-1908-1938

The hydrographic maps of the Belgian continental shelf allow studying large-scale morphological change on the time scale of two centuries. They were digitized in this project, and a 10 m-DEM was made of each available map.

Description

The 1866-1908-1938 maps were selected, scanned and used in the project Quest4D (Janssen *et al*., 2012). The 1804 maps are an additional source allowing pushing back the start of the observation period, at least for the inner shelf and the mouth of the Westerschelde. The maps were made under French rule to build an important harbour in Antwerp. They were measured using geometer principles and can therefore be considered as the first reliable map of the area (Baudez, 1989). Here are some metadata:

1804 (2 maps)

Name on the map: (1) Reconnoissance hydrographique de la côte Nord de France. Covers the inner shelf including the Flemish Banks from Gravelines to Oostende. (2) Carte réduite des côtes des Pays-Bas (depuis Ostende jusqu'à Hellevoetsluis).

Author: C.F. Beautemps-Beaupré

Coordinate system on the map: (1) for longitude: nautical miles east of Calais. Latitude not specified, probably orthonormal. Distances are in nautical miles (60 miles per degree: 1 mile = 1.852 km). (2) Lat-long. Longitude east with respect to the meridian of the Paris Royal Observatory (2°20'14,025" east of Greenwich)

Datum: local lower low water at spring tide. Depths are in feet (pied de France or pied du roi, set equal to 4500/13853 m = 0.3248 m in 1799) (fr.Wikipédia.org, Anciennes unités de mesure françaises) (conversion table to m available on map (2))

Survey period: (1) 1802 – 1803 (Baudez, 1989). Map mentions publishing date Vendemiaire An XI (September-October 1802); however, Baudez (1989) states it was published in 1804 (2) 1801 – 1811; the Westerschelde part in 1804 (Baudez, 1989). Map was published in 1817.

Map scale: 1/100,000

Figure 5 – Extract of the 1804 chart near Oostende.

1866

Name on the map: Carte Générale des Bancs de Flandres compris entre Gravelines et l'embouchure de l'Escaut

Author: A. Stessels

Coordinate system on the map: geographical coordinates, zero meridian of Paris (2°20'14,025" east of Greenwich)

Datum: local low water at spring tide (metres)

Survey period: not mentioned. Map was published in 1866.

Map scale: (1) 43 nautical miles in 0.9 m ≅ 1/88,500 (marks on map), probably same scale as next; (2) 1/88,888 (Baudez, 1989)

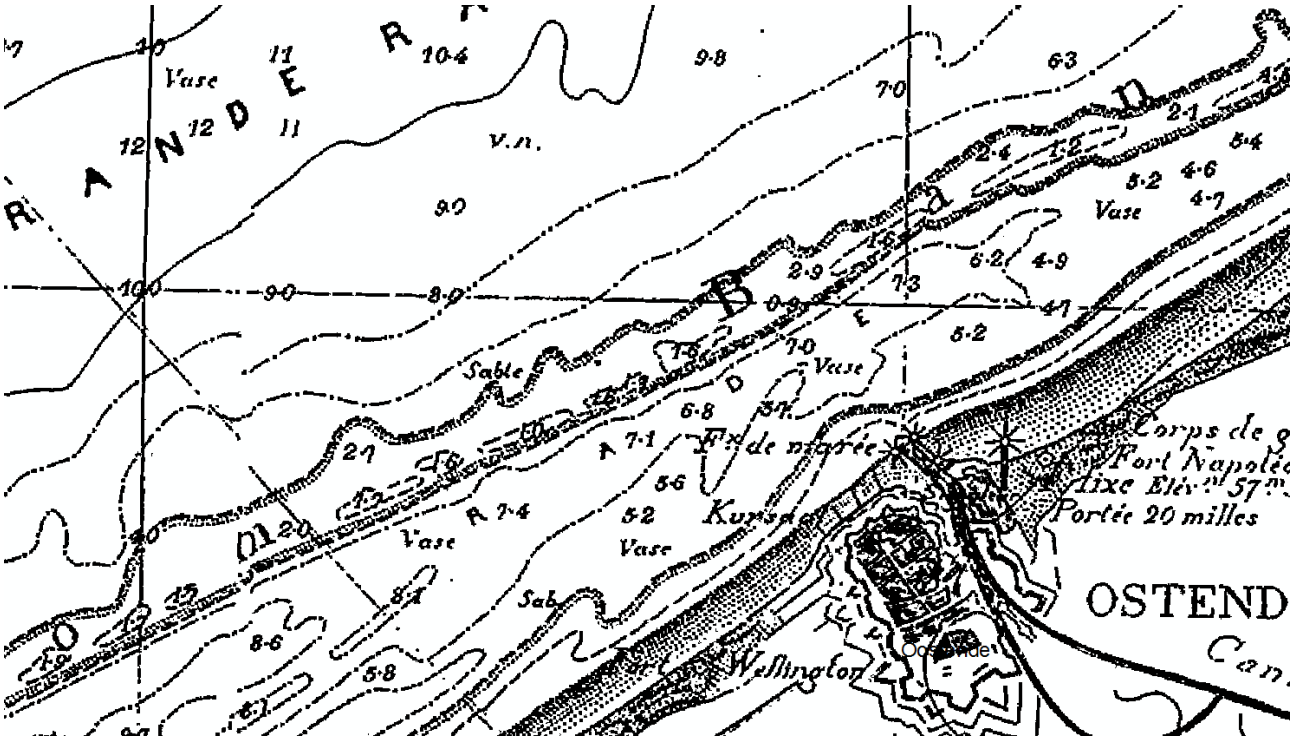

Figure 6 – Extract of the 1866 chart near Oostende.

1908

Name on the map: Mer du Nord – Dunkerque-Flessingue

Author: Ponts et Chaussées, Service special de la côte, Hydrographie

Coordinate system on the map: geographical coordinates, zero meridian of Greenwich

Datum: local low water at spring tide (decimetres)

Survey period: 1901-1908 + updated until 1st May 1911.

Map scale: 1/80,000

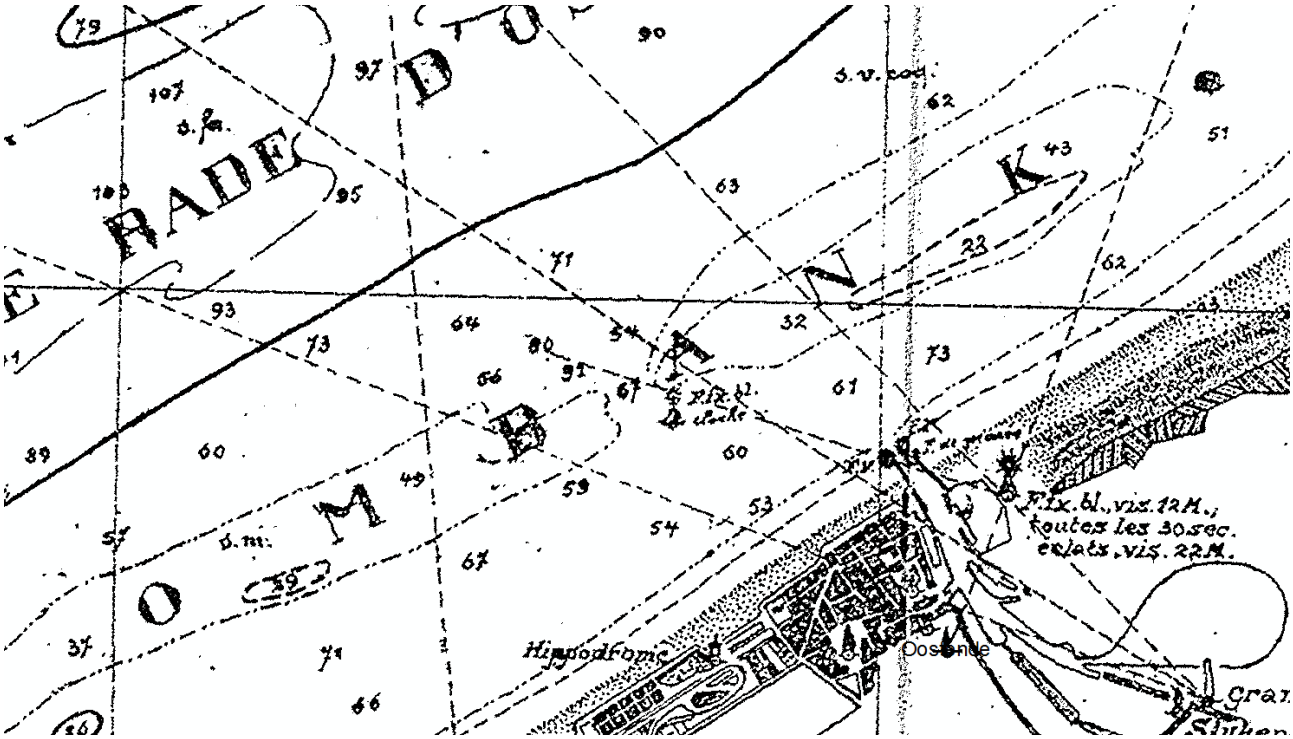

Figure 7 – Extract of the 1908 chart near Oostende.

1938

Name on the map: Noordzee, Vlaamsche Banken 1938

Author: M.J. Lauwers, assisted by P. Wessels and L. Vercruysse, Ministerie van Verkeerswezen, Beheer van het Zeewezen, Hydrographie

Coordinate system on the map: geographical coordinates, zero meridian of Greenwich

Datum: local low water at spring tide (decimetres)

Survey period: 1938 (probably also the preceding years).

Map scale: 1/100,000

The map was complemented by Dutch and French data in the periphery. The map contains insets of the ports of Dunkerque, Oostende, Zeebrugge, showing more detail for the local bathymetry.

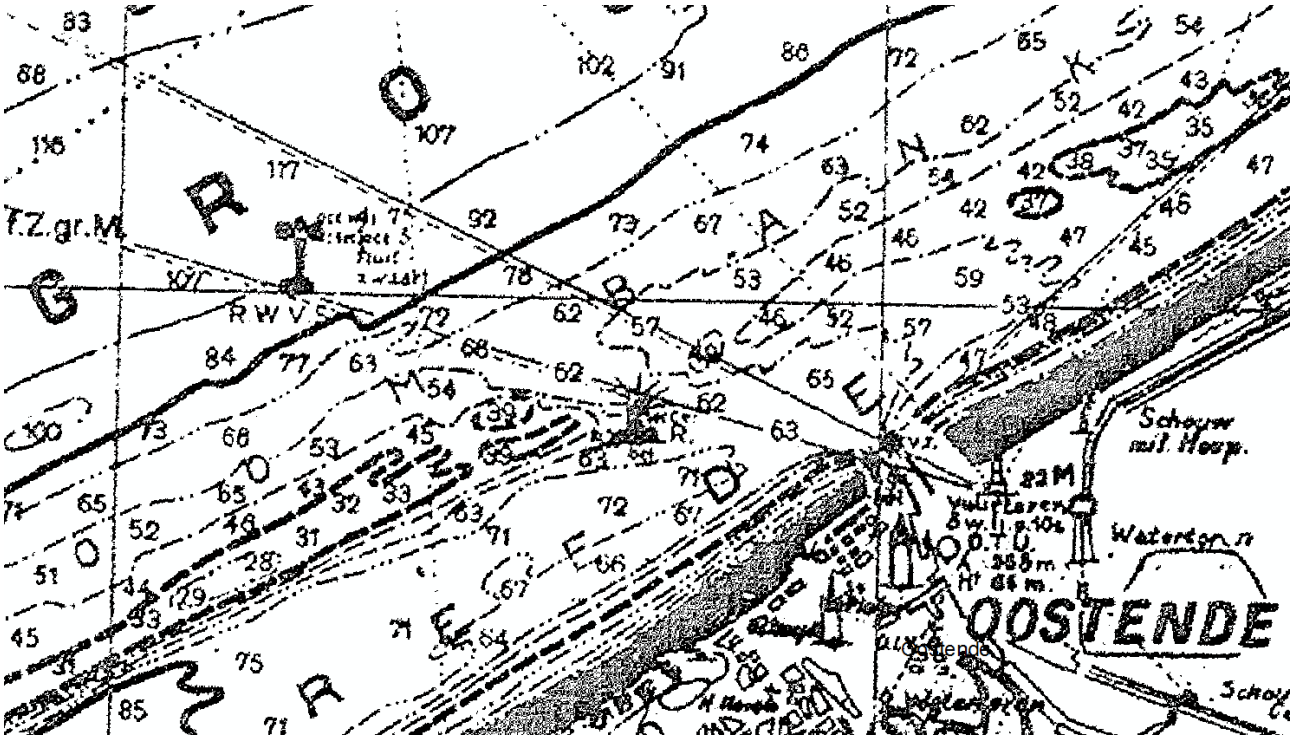

Figure 8 – Extract of the 1938 chart near Oostende.

Vectorisation

High-resolution scans of the 1804 charts were specially acquired for this project at KBR (Koninklijke Bibliotheek, Brussel). The scanned images are clearly readable.

The 1804 map "côte nord de France" (map 1) does not contain coordinate marks. It was georeferenced using all available church towers as reference points to the modern map, taking into account the present churches and towers that already existed around 1800. They include church towers from Calais in the west to Oostende in the East. Sixteen control points could be identified. Applying an affine transformation and then removing the four control points with the worst fit resulted in a residual location error from 0 to 60 m. The affine transformation was kept to georeference the map, as no offshore reference marks are available on this chart. The affine transformation avoids making large extrapolations in the offshore area. The map has an about 4 km wide sideways overlap with the 1804 map "depuis Ostende jusqu'à Hellevoetsluis" (map 2). The latter map has also offshore reference marks (see next paragraph) and was therefore in the overlap area used as a reference area. In the overlap area, clearly some common depth points and depth contour lines occur. From them, 5 marks were selected and were used as additional control points. This resulted in no increase in the residual location error and certainly improved the quality of the location in the offshore area of the east margin of the map.

The 1804 map "depuis Ostende jusqu'à Hellevoetsluis" (map 2) was georeferenced using all 30 available coordinate crosses. For longitude, 2°20’14.025” was added so as to convert longitude from the Paris meridian to the Greenwich meridian. The lat-long data were then converted using the National Geographic Insitute's cConvert module (available as an online application). Input was set to Datum ED50, ellipsoid Hayford1924, no projection; output to Belgian Datum 72, ellipsoid Hayford1924, projection Lambert 1972. The coordinate marks were used to apply a spline transformation. The six reference marks of the lower edge of the map yielded residual errors, using an affine transformation, of about 200 m while the other marks had a lower error.

After eliminating the marks of the lower map edge, the residual error of the remaining 24 marks was between 10 and 120 m. As the lower edge area also shows the location of church towers, these were additionally used as reference marks (12 towers). The error remained the same. Afterwards, a spline transformation was used, that reduces the error to zero at the reference marks.

All depth points and depth contour lines on both 1804 maps were digitized in the current project. It is clear from the two maps that the depicted depth contour lines were constructed from the depth points that are also shown in the maps. As the number of depth points is limited compared with recent surveys, the depth contour lines are often poorly constrained, resulting in wobbly lines. Where the modern maps show that the large-scale morphology has straight, streamlined features, the wobbly 1804 contour lines were somewhat generalized to better match the modern morphology. In the overlap area between both maps, most contour lines match. Where they deviated, a gradual transition was made through the overlap area from the western to the eastern map. Where the depth points in the overlap do not clearly match, the points of both maps were digitized.

Depth labels on the 1804 charts are in feet. The usual French feet at that time is 0.3248 m (see description of chart above). The depths were converted in metre using this value.

The 1866, 1908 and 1938 maps were georeferenced by Janssen et al. (2012). They made use of all available coordinate reference marks and used the transformation "Adjust". This uses a calculation aimed at obtaining both local and global precision.

The -8 m depth contour and the depth points (Figure 9) had already been digitized by Janssen *et al.* (2012). Clearly, some automated method was used that also caused a few local errors. As an example, sometimes number labels were interpreted as depth contours. This has been corrected. Some depth points are located on wrecks and are shown between brackets. They have been removed, as they are no representation of the bed. The remaining depth contours of the 1866 map were digitized in working year 1 of the MOZES project (Figure 10). The method described there (Dujardin *et al.,* 2023) was followed for the remaining maps. In a few localized cases where large submerged dunes are now known to occur, the intricate course of the contour lines has somewhat been generalized.

A special processing step was applied: the construction of interpreted additional contours (Figure 10). This was thought to be necessary as the number of depth points was relatively small compared with the complex sandbank morphology, so that these large bed features were not optimally described. In addition, in deeper water, no depth contour lines are present on the charts. For instance, the 1938 chart does not contain contours below -10 m. This step proved crucial to produce a realistic seabed morphology model.

Maps using only data in the charts produced often angular TIN surfaces with false interpolations. To overcome this problem, additional contour lines were interpreted for all four charts. In shallow areas, often additional contour lines were interpreted at half depth intervals between the existing contour lines. In deeper water, often no contour lines were present on the charts and sufficient contour lines to describe the large-scale bed morphology were added. The position of the interpreted contour lines was confined by the existing contour lines and by the depth points. By adjusting the distance between the existing contour lines, an interpreted morphology can be added. For instance, a convex sandbank top surface can be created by shifting the intermediate interpreted contour line somewhat towards the deeper of the existing contour lines. Also crest and trough terminations can be better expressed using intermediate depth contours. The style and shape of the interpreted contour lines is inspired by the modern bathymetry, which is available at high resolution and accuracy. The fact that the position of the interpreted contour lines is confined by the contour lines and depth points present on the chart avoids the introduction of a bias imposed by the present-day morphology. Only the shape of the morphology was adopted, where possible, from the modern morphology, as it is sometimes poorly interpreted on the old charts.

In addition, a few additional depth points were added, with an interpreted depth value (Figure 9). This was done where a structure line would otherwise intersect surrounding depth contours.

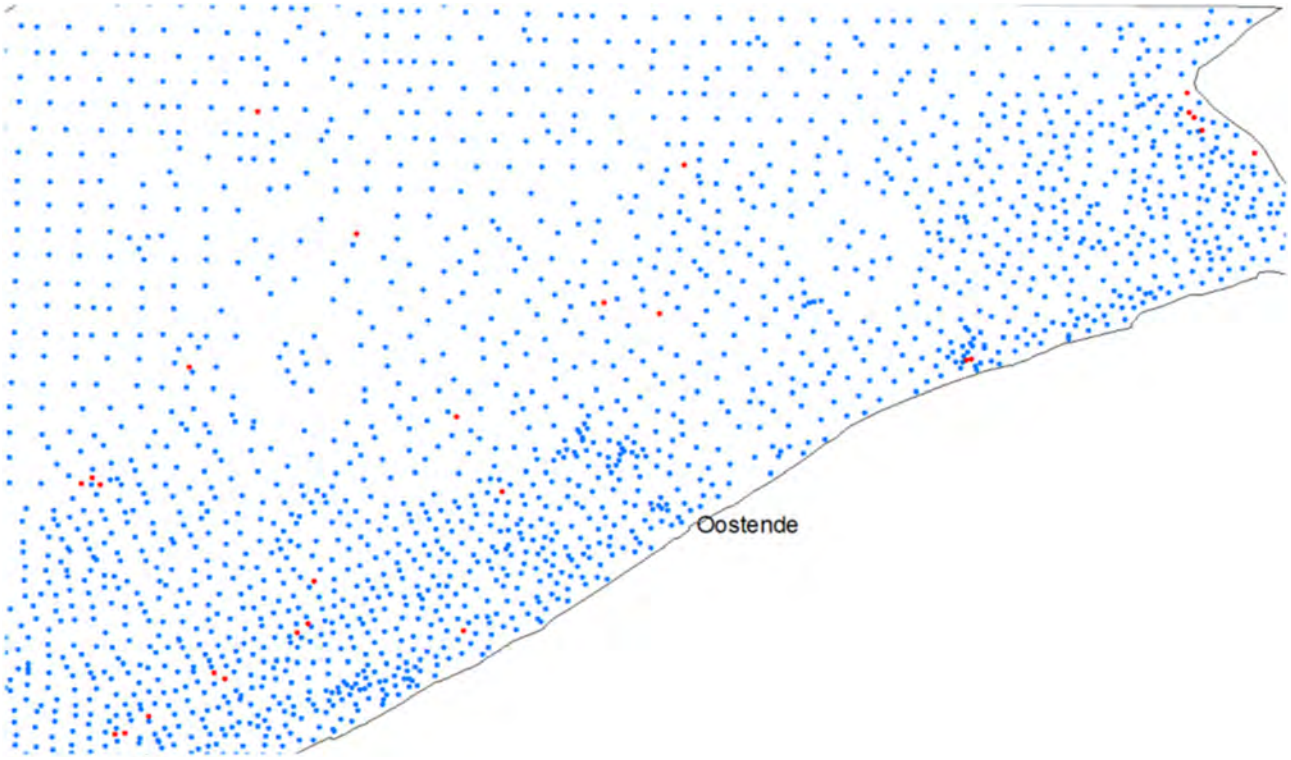

Figure 9 – Depth points of the 1908 chart (blue dots) and a few interpreted depth points (red dots).

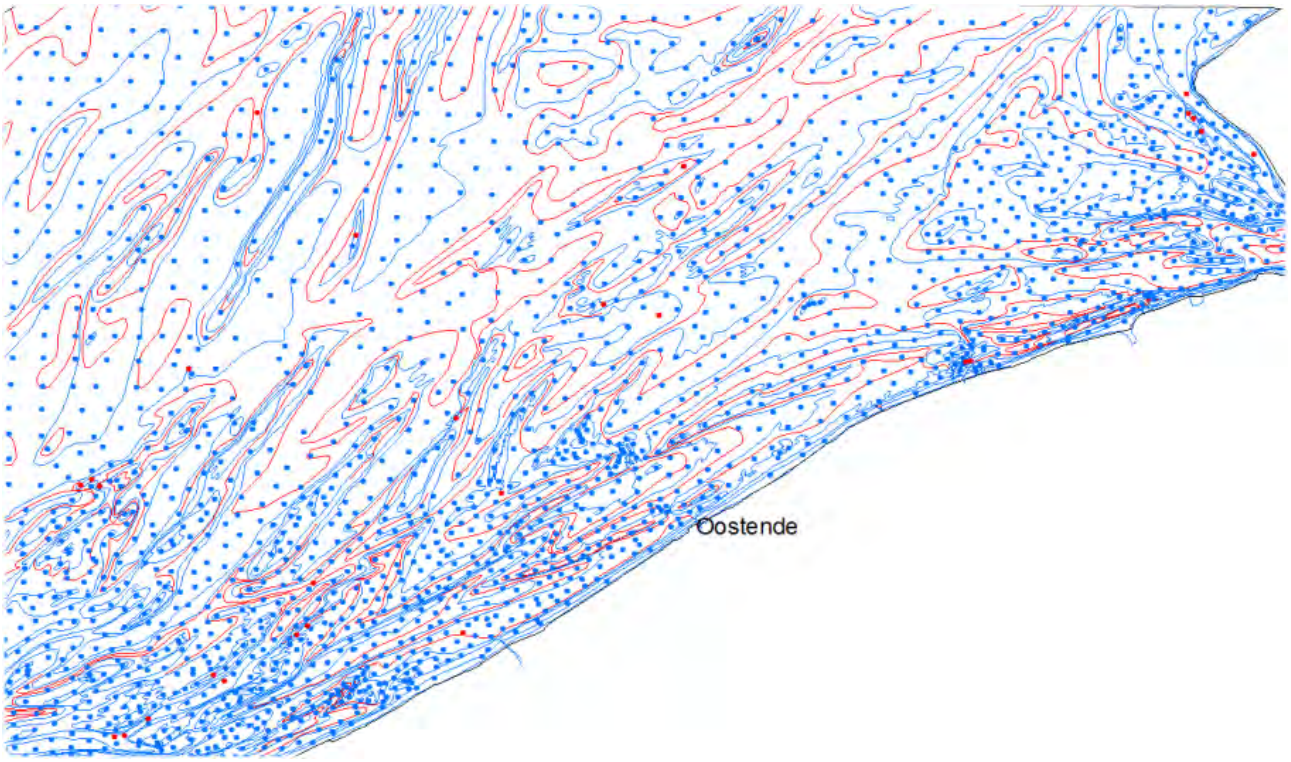

Figure 10 – Depth points and depth contours of the 1908 chart. Red dots and lines: digitized from the chart.
Red dots and lines: interpreted.

After completing the interpreted additional contour lines and depth points, structure lines were added in a separate 2D polyline shapefile (Figure 11). The structure lines represent trough and crest lines and also slope lines where the slope is not evident from the surrounding contour lines. The structure lines are introduced to impose triangle edges during setting up the TIN surface. The structure lines are inserted in the TIN as "hard lines" so that no triangle intersects a structure line. The structure lines are first created as 2D polylines. The polylines are drawn so that vertices are only placed on depth points or at intersections (often vertices) of the depth contour lines. This is necessary to avoid false depth assignments along the line segments of the structure lines.

The structure lines were made 3D features as follows. A temporary TIN was made using the depth points and depth contour lines as input. The latter were inserted as hard structure lines. The 2D polylines of the structure line file were then assigned Z coordinates by using the ArcGIS tool "Interpolate Shape" where the temporary TIN was the Input Surface, and the 2D polylines were the Input Feature Class. Checking "Interpolate Vertices Only" ensured that Z values were only derived at the polyline vertices that lie on data points and lines from the chart. The result of this operation is a 3D polyline file: this contains Z values all along the line segments and they are interpolated linearly between the vertices.

Next, a definitive TIN was made, now using the depth points and contour lines and the structure lines, both as hard lines. On this definitive TIN a 10 m-raster was interpolated (Figure 12).

A final step consisted of converting the raster to TAW. All map values were first converted to metres below chart datum (MLWS) (depths are negative values after conversion). Like in working year 1, it was assumed that the measurements in the chart can be converted using a conversion grid from LAT to NAP (instead of M(L)LWS to NAP) and then adding 2.333 m to convert from NAP to TAW (Dujardin *et al.*, 2023, chapter 1.3.4). The use of the LAT to NAP conversion grid assumed that the error introduced by assuming depth values in LAT instead of MLWS is smaller (maximum 0.15 m at Nieuwpoort) than the possible errors introduced by interpolating several reduction grids. The additional possible error is also much smaller than the estimated error on depth (see below).

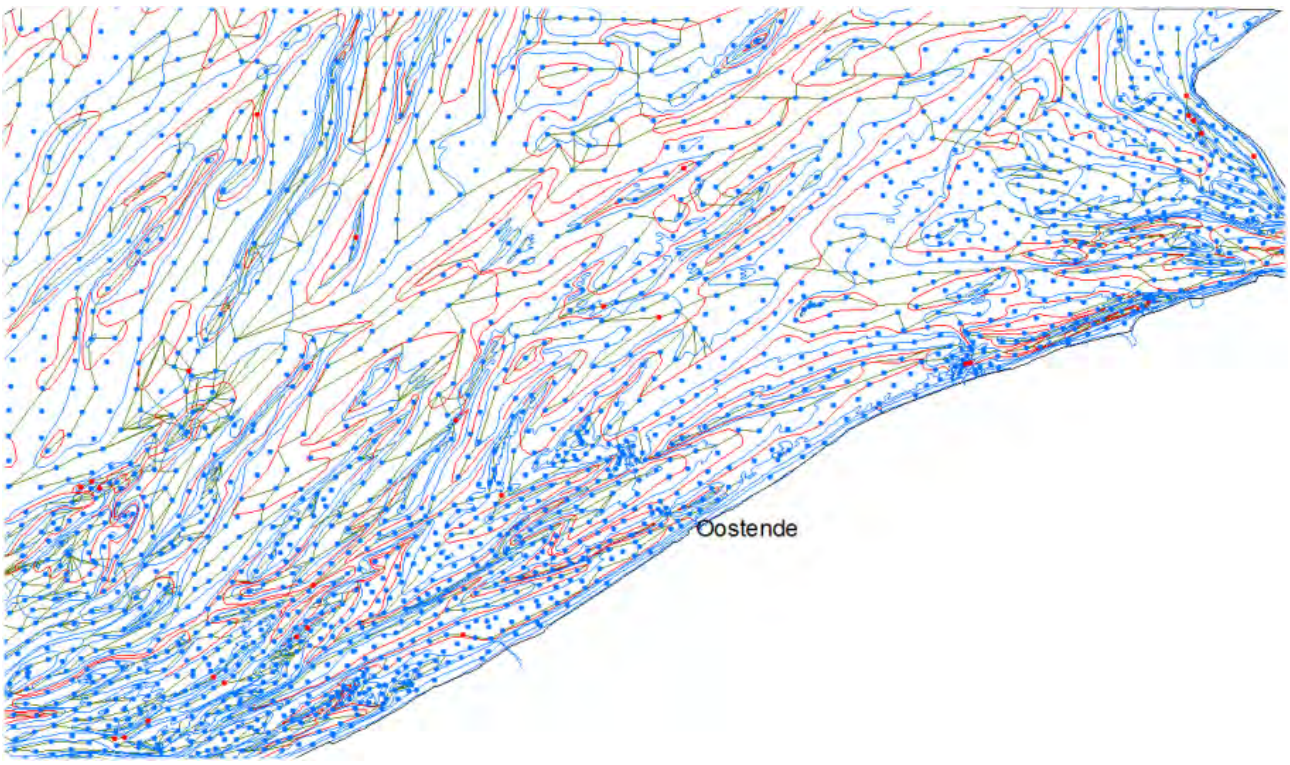

Figure 11 – Crest and trough lines (green lines) added on the data of the 1908 chart.

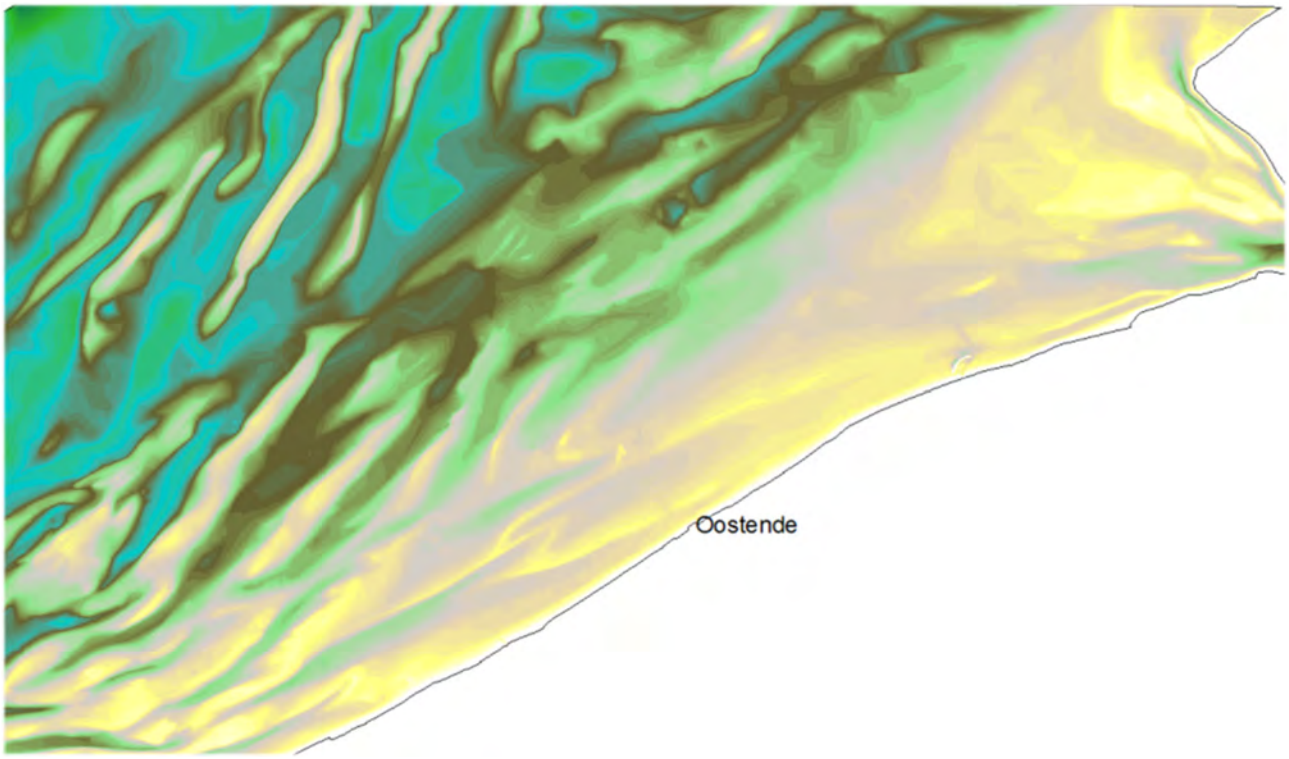

Figure 12 – Resulting elevation model of the 1908 chart.

Produced data sets

These data sets have been produced for the charts of year (YYYY) 1804, 1866, 1908 and 1938:

- depth points: point shapefile YYYY_pt.shp, with attribute "z" containing depth in metres (depths are negative values) and attribute "Source" containing "map" for points digitized from the map and "int" for interpreted depth points
- depth contour lines: 2D polyline shapefile YYYY_pl.shp, with attribute "z" containing depth in metres (depths are negative values) and attribute "Source" containing "map" for contour lines digitized from the map and "int" for interpreted contour lines
- structure lines (crests and troughs): 3D polyline shapefile YYYY_RidgeTroughLines3D.shp. The z coordinate of the vertices of the structure lines are derived from the previous two files
- depth raster (resolution 10 m): G_YYYY_TAW_10

These data sets are located here:

P:\20_079-MorfoInteract\3_Uitvoering\Deeltaak1_DataAcquisition\Kaarten Vlaamse Banken\YYYY

This location also holds the georeferenced image that was processed.

Discussion of error

Location error

Location in the 19th and first half of the 20th century depended on on-board triangulation (Van Cauwenberghe, 1971). Lat-long triangulation based on the sun and the stars was well known. When the coast was visible, high fixed points such as bell towers could be used to do terrestrial triangulation.

No in-depth studies of the error caused by this method is known. As an approximation, when the coast was in sight, the error is estimated at 50 m. When no fixed marks at the coast were available, the error is estimated at 100 m.

Electronic positioning systems have been used since World War II and continued to improve (Van Cauwenberghe, 1971).

Another error may arise from georeferencing the plan scan. As all reference marks are used and an "Adjust" transformation was applied, it is thought that this does not add to the error.

Nevertheless, a visual check was performed on the fit of planimetric element along the coast on recent high-quality maps. Deviations ranging between 0 and 100 m were observed. As the planimetry was probably not always meant to be very detailed, it can be assumed that the error estimated from the match of planimetric elements is about 50 m.

The thickness of the lines on the maps is 15 to 20 m while some fat lines are even 50 m wide. The location of the depth points is not always clear. On the 1938 chart, figures are often 250 m wide and 125 m. Locating the point in the centre of the figure causes an uncertainty of the order of 50 m.

Depth error

Depth measurements were done manually using a lead line. This method was mechanized in the 19th century. The reading had to be reduced to a reference water level. Inshore, the error on this measurement was probably less than 0.5 m, offshore it probably exceeded this value.

On the 1866 chart, depths below -10 m are generally rounded to whole metres. This introduces an additional error of 0.5 m.

Héquette & Aernouts (2010) mention an error range, which includes the error range of the instrument (sounding line in 1911 and single channel echosounder in 1977) as well as errors due to inaccuracy in ship positioning and to tidal correction, estimated at ± 1.0 m in 1911 and ± 0.6 m in 1977, for bathymetric data on hydrographic field sheets of the French Hydrographic Survey in the Calais area.

The reference level is the (lower) low water surface. This was probably well known in the nearshore but no knowledge was available on this surface in the offshore domain. In addition to this, the reference surface must have risen through time along with general sea-level rise. The rate of this rise can be estimated (see §2.2.3).

It can be assumed that all small-scale navigation charts show a selection of local shallowest points. This is common practice to ensure safe navigation. For morphology studies, this selection introduces a depth bias: certainly on sandbanks and in shallow areas, the shallowest points determine the DEM bed values. Often, submerged dunes are present in these areas. The magnitude of the bias depends on the height of the smaller bed features and may vary from a few decimetres to even a few metres on some parts of the Flemish Banks. An a-posteriori correction for this bias cannot be performed, as dune fields are often very mobile.

If a certain location or area shows a consistent depth trend through time, this trend has a higher confidence compared with locations where depth values are scattered through time. The higher the number of available surveys, the better the confidence.

Conclusion

The (standard) error on the pre-1950 bathymetric charts can be evaluated at about 100 m on location and between 0.5 and 1 m on depth. The error increased toward more offshore areas. In morphological studies, sea-level rise and depth point selection bias must be allowed for. If depth at a certain location shows a consistent trend through time, this trend has a higher confidence compared with locations where depth values are scattered through time. The higher the number of available surveys, the better the confidence of the observed trend.

2.2 Morphological analysis of the Belgian inner shelf over 1804-2022

2.2.1 Additional coverage: 2022

Flemish Hydrography

In the MOZES project, use is often made of the recent bathymetry of the inner shelf made available by the Flemish Maritime and Coastal Services department. A 10 m resolution raster was downloaded from https://bathy.agentschapmdk.be/spatialfusionviewer/mapViewer/map.action on 9 September 2022. It contains the date of 2 March 2022. This raster is in ETRS89 UTM31N with depths in LAT. Depths were converted to TAW by subtracting the raster "lattotaw_vb2" using Raster Calculator. In order to allow overlay operations, a projected version in Lambert 72 was produced using ArgGIS tool "Project Raster" and the transformation "Belge_l1972_To_ETRS_1989_2". The result is the 10 m-raster g202203tawl72.

EMODnet

In order to obtain a cover of the neighbouring French and Dutch areas, with a resolution sufficient on the scale of sandbanks and channels, the EMODnet (European Marine Observation and Data Network; https://emodnet.ec.europa.eu/geoviewer/) most recent bathymetric dataset was downloaded on 24 May 2024. The downloaded datasets of tile E4 contain the area of interest of the MOZES project. These datasets were updated until 2022. It has a low resolution. The mean depth is based on a source resolution of 1/16 arc minute (~125 meter). The exported dataset is in WGS_1984 with depth in LAT. Transformed to the Lambert projection, the raster cells are rectangular and about 73 m wide by 115 m high.

The EMODnet 2022 dataset poses some challenges. First, the date of survey depends on the area of concern and varies widely. Second, it covers a very large area and has a relatively low resolution. Finally, it is in geographical coordinates and not projected. A projected dataset in Lambert 72 is however needed for overlay analysis.

Although the dataset carries the time stamp 2022, this is only the date of download. The data are a patchwork of older soundings (Figure 13). The part covering the Belgian Continental Platform contains surveys conducted between 2004 and 2021. The French part is older, using surveys conducted between 1970 and 1990.

Tile E4 contains a wide area down to the Spanish waters. It contains the mouths of the Westerschelde but not the Westerschelde itself. A clip was made of a sufficiently large area containing the MOZES area of interest using ArcGIS tool "Raster Clip".

Projecting the dataset in Lambert 72 not only produced rectangular grid cells, but also some empty cells inside the data area. The cells were populated with an average of the surrounding cell values using the tool Elevation Void Fill. This operation expands the raster with one row of cells. After creating a data contour polygon using the Raster Domain tool and trimming the filled raster on this contour using the Extract by Mask tool, a workable version of the EMODnet bathymetry in Lambert 72 was obtained. It was noted that interference patterns are present in this version. They appear only after zooming in. On the scale of the study area, the result is acceptable.

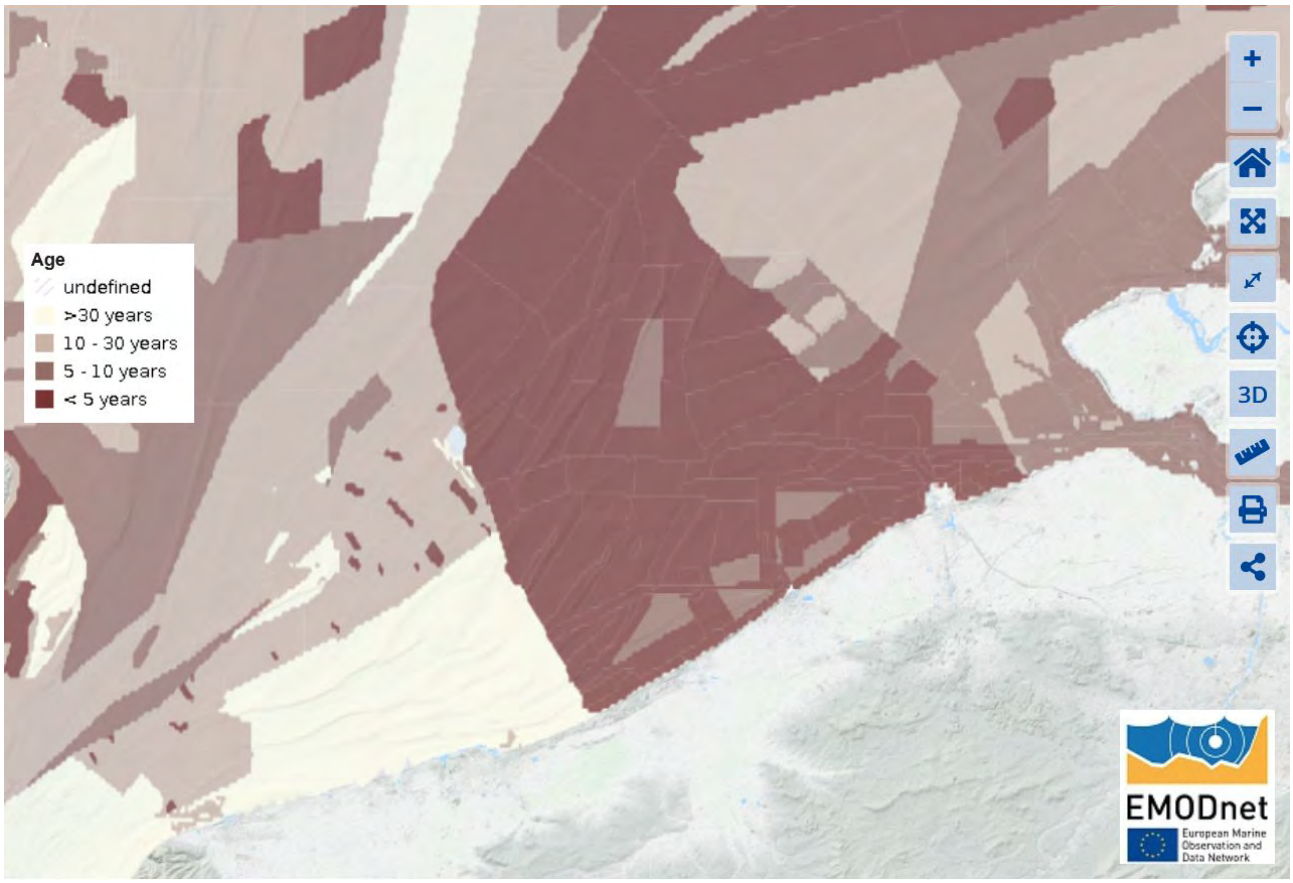

Figure 13 – Age map of the 2022 EMODNET bathymetric dataset.

2.2.2 Depth contour shift

Depth contours were calculated on all inner shelf rasters (1804, 1866, 1908, 1938, 1967 (= averaged date for the 1962 to 1969 inner shelf bathymetry mosaic), 1986 (= averaged date for the 1984 to 1987 inner shelf bathymetry mosaic), 1992 (= averaged date for the 1991 to 1993 inner shelf bathymetry mosaic), 2022 Flemish Hydrography and 2022 EMODnet) using ArcGIS tool "Contour" set to depth interval 1 m. For the current large-scale morphological analysis, only the 0, -2, -5, -8 and -12 m contours were displayed, using a different line type for each selected depth. The lines were displayed using a different colour per bathymetric dataset. The depths are in TAW, and have not been corrected for sea-level rise. It was evaluated that the uncertainty on position exceeds possible shifts in depth contour location due to a sea-level rise correction. In the more quantitative analyses of the next sections, sea-level rise correction was applied.

Figure 14 shows the legend used in the depth contour line shift analysis.

The successive bathymetric rasters were superposed and then shown as a time series. Systematic change or no change was observed and marked using the change marks of Figure 14. Changes back and forth are interpreted to represent no systematic movement. The systematic movements have been quantified over the entire observation period (Figure 14). Displacements are expressed in km, important vertical and systematic change in m. The values in the analysis result maps are a rounded mean of the change in the neighbourhood of the change marker. When a shift in depth contours corresponds to a net displacement of a large-scale morphological feature, the shift arrow is shown in blue. When a contour line shift is accompanied by overall growth of the large-scale morphological feature, the shift arrow is shown in green. When a contour line shift is accompanied by overall decline (volume loss) of the large-scale morphological feature, the shift arrow is shown in red.

It is noted that 1866 is often an outlier where the position of some major banks and channels shifts back and forth compared to 1804 and 1908. Hence, it is concluded that either the geometry of the 1866 chart is of less quality, or the georeferencing introduced a bias, or both.

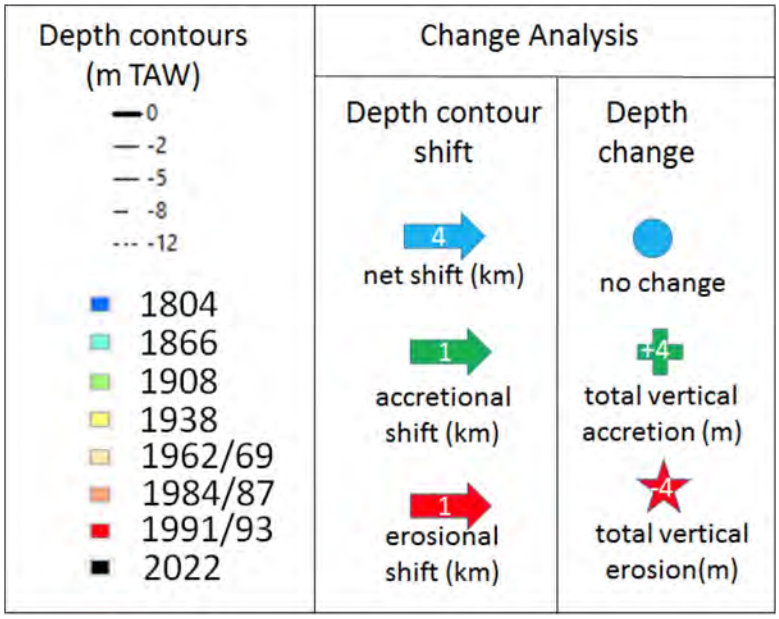

Figure 14 – Legend for the depth contour line change analysis. Change figures quantify change over the entire observation period (displacement in km, vertical change in m).

Flemish Banks, Hinder Banks, Westerschelde outer delta

As the uncertainty on further offshore morphology is larger than for the inner shelf, a separate analysis on a small scale was done for this area (Figure 14). This area is not covered by the inner shelf maps (1967, 1986, 1992).

The Hinder Banks are also not covered by the 1804 survey. Three large sandbanks show a displacement to the east: Westhinder by about 2 km, Oosthinder (just east of Westhinder) and Bligh Bank (just east of Oosthinder) by about 1 km. It is observed that the shift would have occurred between 1908 and 1938. No shift was observed between 1938 and 2022, apart from an about 300 m eastward shift of the northern branch of Westhinder. Noordhinder (just west of Westhinder) is not well captured on the older charts. The southern branch of Fairy Bank is shown on all charts from 1866 on. The crest of this bank shows probably a small shift to the southeast since 1938. The 1866 and 1908 position is between 1938 and 2022.

The results for the Hinder Banks are not well supported by the data. It would appear that the 1908 chart just copied the 1866 contours. As this area is relatively far offshore, the 1866 contours are not certain. It is concluded that, lacking another independent survey, no conclusions can be drawn on change or no change of the Hinder Banks.

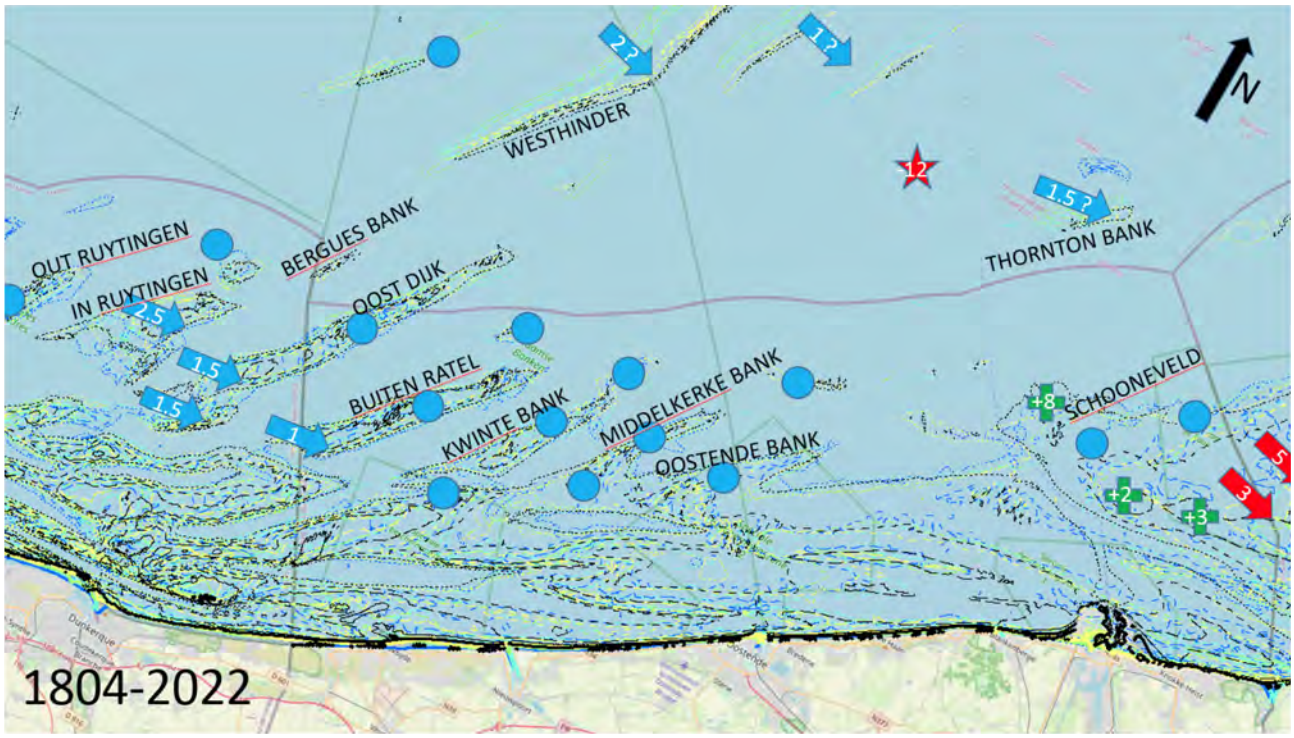

Figure 15 – 1804-2022 contour line and depth change analysis, offshore part of the inner shelf. From Dunkerque to the Westerschelde mouth.

Thornton Bank is represented on the 1804 chart, as a small data outlier. Its position is highly uncertain. The crest area oscillates between 1866 and 2022. Most likely, the sandbank was stable over the observation period. A small area west of Thornton Bank shows a deepening by 12 m since 1866/1938. This is interpreted to be due to a poor rendering of the local bathymetry in this area on both the 1866 and 1938 (copied data?) charts.

The Flemish Banks are present in all shelf charts from 1804. They appear to have remained in the same place. One subarea however does show systematic displacements. This observation concerns the entire In Ruytingen sandbank, the most landward part of Oost Dijk and Buiten Ratel, and the small sandbank landwards of Oost Dijk. The shift in contour lines is considerable and seems to decrease from west to east

inside this subarea. It should be realized that the French part of this subarea has no recent survey in the 2022 EMODnet bathymetry, so the total displacement since 1804 is probably larger than indicated in Figure 15.

The outer part of the Westerschelde ebb tidal delta shows no shift in the deeper contour lines since 1804, whereas the shallower contour lines show an important shift eastwards. Some areas display a considerable vertical accretion. This change occurred mostly between 1938 and 2022 and is likely the result of dredge slurry disposal.

French part west of the Belgian inner shelf

This area is also of importance for Belgium as it may serve as a source area under longitudinal sediment transport. This area has a large reserve of sand as the sandbanks are often wide and are developed high (their crests often emerge at low tide). It is also a morphologically very dynamic area (Figure 15). This area is not covered by the Belgian inner shelf maps (1967, 1986, 1992). Natural dynamics prevail, but land reclaims for the Grand Port Maritime and the construction of Avant-Port Ouest de Dunkerque in 1980 largely influenced the littoral zone. The blocked the littoral drift and the nearshore area here suffers structural erosion (Cartier et al., 2020). Dunkerque Channel requires dredging works by yearly amounts in the order of 0.5 Mm³. New constructions require one-off dredging efforts of several Mm³.

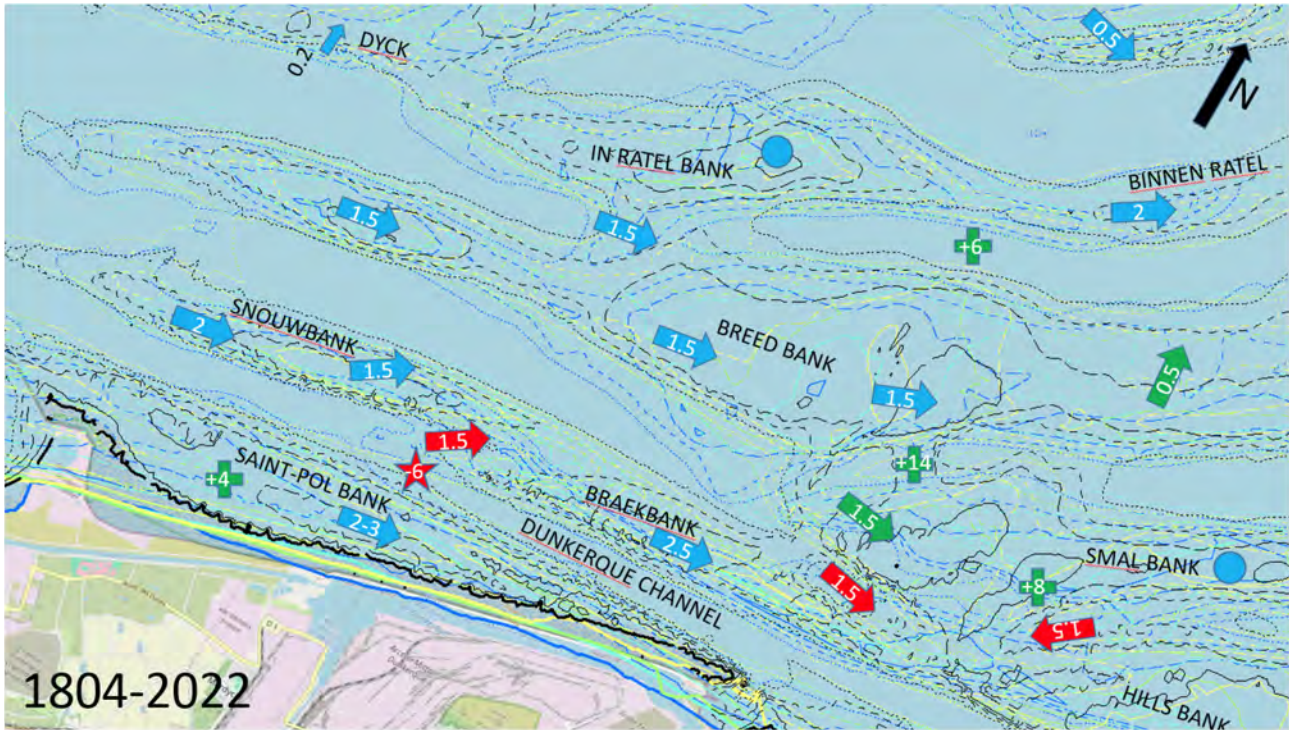

Figure 16 – 1804-2022 contour line and depth change analysis, inner shelf Northern France. From Avant-Port Ouest de Dunkeque to Bray-Dunes.

Proceeding from offshore, Dyck is almost stable and In Ratel Bank crest was largely stable over the observation period. In contrast, Binnen Ratel and all the length of Breed Bank, Snouwbank and Braekbank considerably shifted eastwards (parallel to the coastline). There is a possible trend of larger displacement when going from offshore to inshore. It should be realized that the total movement over 1804-2022 is probably even larger than indicated in Figure 16 as this area has no recent survey in the 2022 EMODnet bathymetry, which would rather represent the 1970-1990 situation.

There is also a large dynamic in the flow channels and especially the passes between the channels. The channel between Binnen Ratel and Breed Bank sanded up by a considerable 6 m. The channel between Breed Bank and Smal Bank practically disappeared. Where on the early charts a flow channel was present, the latter banks were connected by a shallow bridge on the 2022 EMODnet bathymetry.

Possibly, tidal flow was taken over by a new connection between Braekbank and Smal Bank and its extension between Smal Bank and Hills Bank. This recent flow channel is situated more inshore than the abandoned channels. Likewise, the connection between Snouwbank and Braekbank has in the recent decades been cut and a new channel now clearly separates Snouwbank from Braekbank. Near this site, the Dunkerque Channel or Chenal Intermédiaire is now at least 6 m deeper than in the earlier charts. The latter change may however be related to dredging works, as the deepening occurred mainly between 1938 and 2022 (or rather 1970-1990).

Finally, the shoreface west of Saint-Pol Bank accreted, while Saint-Pol Bank itself shifted considerably to the east. The morphological change here mostly occurred after the construction of Dunkerque Avant-Port Ouest (Cartier *et al.*, 2020).

Belgian West Coast

Figure 17 shows the result of the depth contour line shift analysis of the Belgian West Coast from the French border to Middelkerke. It is the area with the strongest imprint of natural morphodynamics.

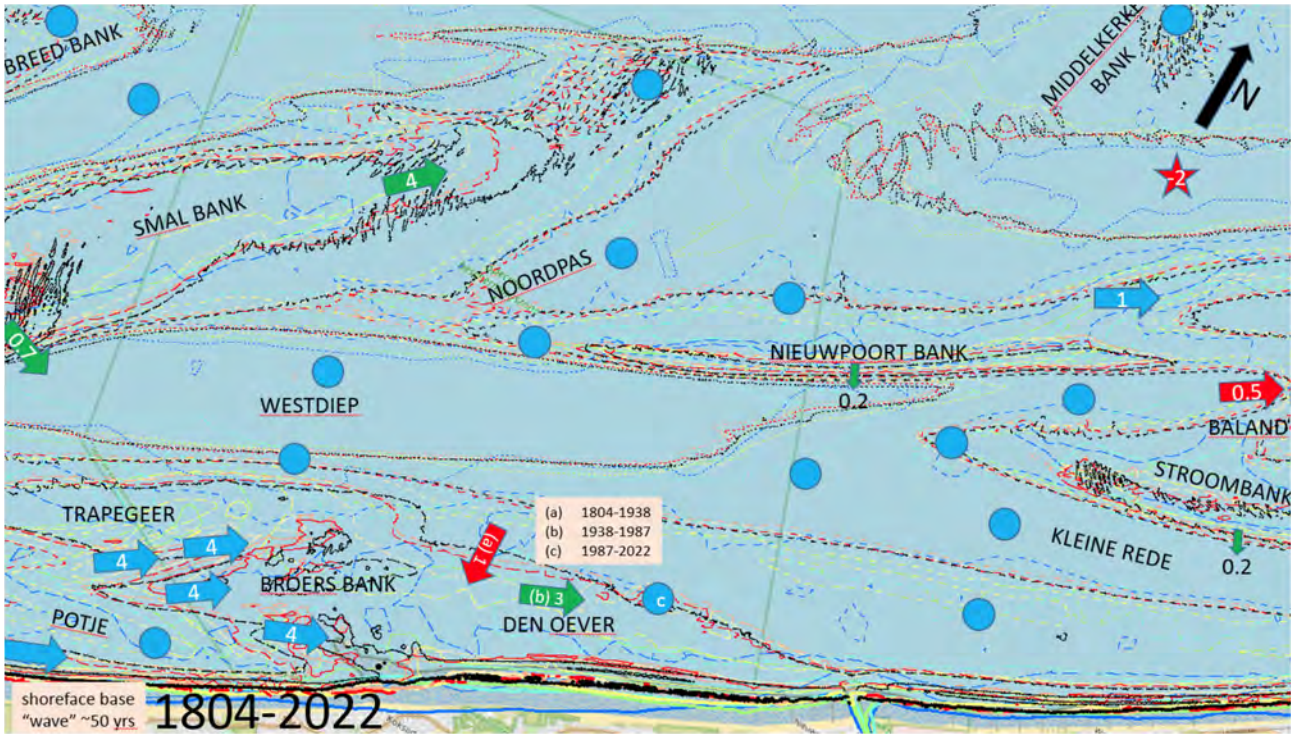

Figure 17 – 1804-2022 contour line and depth change analysis, Belgian West Coast, from De Panne to Middelkerke.

Proceeding from offshore, most of Smal bank, Noordpas, Nieuwpoort Bank, Middelkerke Bank and the flow channels between these bank show no systematic change. A notable exception is a shallow part of Smal Bank, off the resort of Koksijde, where water depths decrease to about -2 m TAW. Here, an important eastward shift of the shallow area is observed. The landward flank of Smal Bank off De Panne and the landward flank of Nieuwpoort Bank show a less intense but systematic landward shift. Finally, the shallow sandbank branching seaward near the NE tip of Nieuwpoort Bank also moves to the east. The channel north of Nieuwpoort Bank deepened.

In the nearshore sandbanks zone, most channels show no systematic change.

The shallow sandbank system Trapegeer – Broers Bank, with its shallowest parts emerging at low tide, is very dynamic. All nearshore parts show a fast movement eastwards in the alongshore direction. Note that the point of attachment of the sandbank system to the coast does not move. Probably, the point of attachment was already at the same place at the time of the foundation of the fishermen's village of Koksijde in the 13th century ("ijde" means a place where ships can be dragged on the beach) (Termote, 1992). Note that also the location and depth of the flow channel Potje have not changed since 1804. A protrusion of the -5 m depth contour presently situated west of De Panne is dynamic. The observation is shown by the text “shoreface base wave” in Figure 17 and its existence needs to be confirmed by more surveys. The change is interpreted as a locally wider and mildly sloping shoreface base that propagates eastwards like a wave with a period of an estimated 50 years.

Den Oever shows a complex morphological evolution. A small sandbank named Broers Bank was situated 3 km from the low-water mark off Oostduinkerke in 1804. In 1866 this sandbank had moved westward by about 750 m towards Koksijde-De Panne. In 1908 it had merged with the shallow sandbank off Koksijde (and its name was transferred to the shoal with which it had merged). The seaward protrusion formed by the merged sandbank had disappeared by 1938. The morphological evolution of Den Oever, the wide shoreface of Oostduinkerke, over 1908-1938-1967 leads to the interpretation that most of the sand of the former small sandbank contributed to making Den Oever shallower and giving it a milder slope. By about 1992, the gain due to this supply mechanism started to be lost again, but at a very slow rate. The morphological changes described here are shown in Figure 17 by three symbols labelled a-b-c.

In the east of this area, off Middelkerke, the flow channel between Nieuwpoort Bank and Baland Bank shifted 0.5 km to the east. The western part of Stroombank does not show an alongshore movement, but a small landward shift of the landward flank is observed.

Belgian Middle Coast

Figure 18 shows the result of the depth contour line shift analysis of the Belgian Middle Coast from Middelkerke to Wenduine. The largest human interference on the inner shelf of this area is the access to and the 2009 expansion of Oostende harbour.

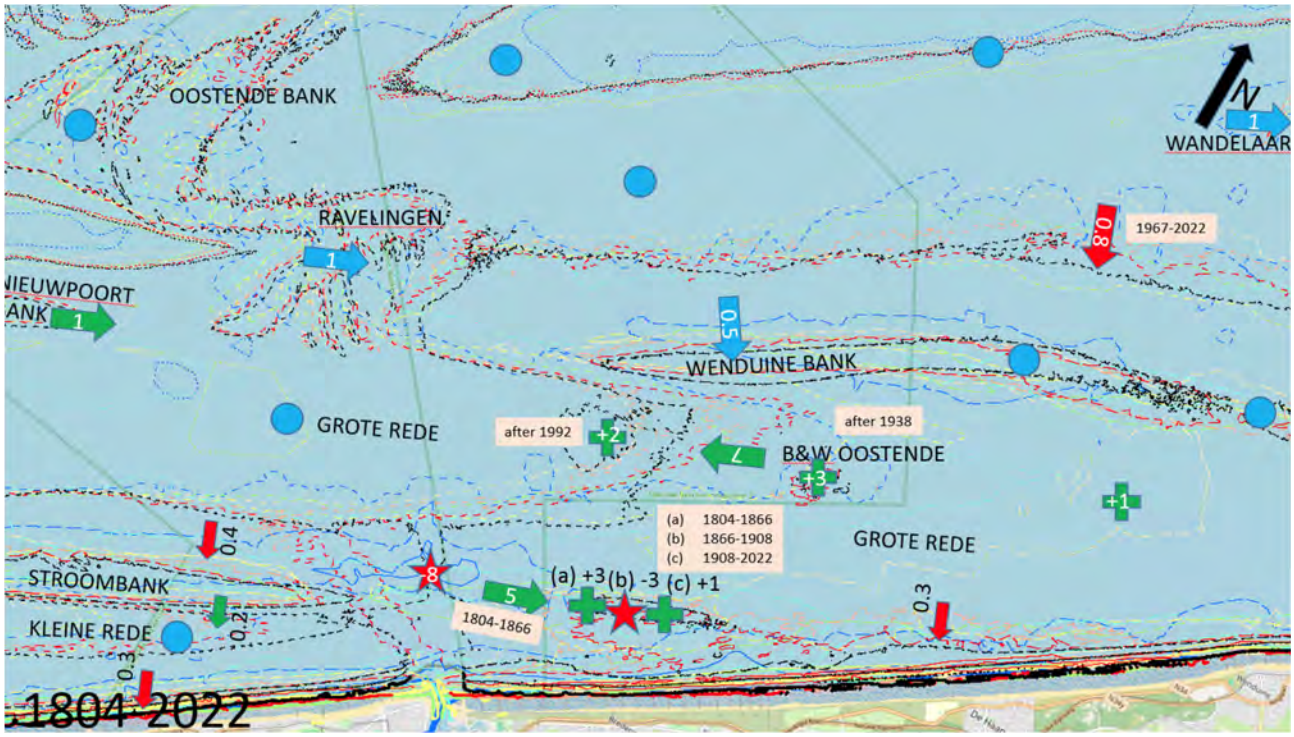

Figure 18 – 1804-2022 contour line and depth change analysis, Belgian Middle Coast, from Middelkerke to Wenduine.

The transition area shows no systematic depth contour line shifts. The eastern end of Nieuwpoort Bank and the dune field of Ravelingen shifted eastwards. Wenduine Bank has a pivot point, indicated by a blue dot in Figure 18. The branch west of this pivot point moved landwards. The branch east of the pivot point did not move in a systematic way. The very mildly sloping seaward flank of Wenduine Bank became slightly steeper. More specifically, the base of the bank moved landward. This movement initiated after 1967 and is likely a morphological response to the dredging operations in the important navigation channel Scheur.

While the western part of the flow channel Grote Rede did not change, the part east of Oostende largely shallowed. The change is related to dredge slurry dumps operated at dump site Bruggen & Wegen Oostende after 1938. The recent accretion (after 1992) by 2 m reflects the changed location of the dump site. The long coast-parallel sandbank that developed east of the first dump site is not visible at this scale, although the +1 m mark off Wenduine is situated on this narrow sandbank.

The landward flank of both Grote Rede and Kleine Rede shows a long-term landward shift. The depth of Kleine Rede shows no change. The section of Stroombank between Middelkerke and Oostende also shifted landwards, like the part near Middelkerke.

The eastern end of Stroombank in the nearshore of Oostende displays important changes that are morphological responses to dredging activities. It is possible that already around 1800 the connection between Stroombank and the shoreface at Bredene was severed due to human interference. The 1804 chart shows a deeper channel near Bredene. The 1866 map shows that the shallow crest area of Stroombank had grown by 5 km towards the coast near Bredene. This evolution could be interpreted as the repair under natural transport after man created the channel off Bredene around 1800. It was reasoned earlier that Stroombank must have connected to the shore in the centuries before 1800 (Houthuys *et al.,* 2021). A man-made channel severing Stroombank from the coast and dug around 1800 is however hypothetical.

A first navigation channel crosscutting the sandbank near Oostende was already present in 1908. It has been maintained by dredging ever since. This channel dates from shortly after 1880 (Devos *et al.,* 2014). As it was made to provide a direct access to the harbour, it was named "Rechtstreekse Kil". Note that around the same time, the connection between Stroombank and the shoreline east of Bredene was (a second time?) opened by dredging, to promote flow currents to clear the navigation channel Kleine Rede near Oostende. This artificial channel was named "Oostpas". While the maintenance of Oostpas appears to have been abandoned by 1938, Rechtstreekse Kil was well kept and later widened and deepened. In 2009, a new navigation channel with a deeper bottom was dredged to Oostende harbour (see section 2.3.1). This explains the -8 m change at that location.

Due to the successive interventions, the evolution of the eastern part of Stroombank (east of Oostende) is complex. Between 1804 and 1866, the bank crest gained 3 m vertically while it extended 5 km so that the connection to Bredene shoreface was repaired. Between 1866 and 1908, it had lowered by 3 m. It is thought to be the morphological response of the creation of the first navigation channel that crosscut Stroombank. While a navigation channel to Oostende was maintained ever since, a partial recovery by 1 m vertically was probably the result of suspended sand bypassing the navigation channel.

Belgian East Coast

The Belgian East Coast from Blankenberge to Cadzand is strongly affected by the expansion of Zeebrugge Harbour in 1979-1986. Therefore, the geographic change analysis is reported in two maps, the first until 1967, before the named Zeebrugge Harbour expansion (Figure 19), and the second from 1967, after the expansion (Figure 20). The resulting evolution over the entire period is shown in Figure 21.

While the Westerschelde ebb tidal delta top (Vlakte van de Raan) shows no change at the Belgian-Dutch border (grey line), two areas north of the navigation channel Wielingen-Scheur did shallow by about 2 m. The eastern one accreted earlier than the area at S2. S2 is a dredged slurry dump site presently in use; the other site is probably a former dump site.

Almost every erosional change (red markers in Figure 21 in the area offshore of Zeebrugge) occurred after 1967 (Figure 20) and is related to dredging works to create and maintain the navigation channels to the Westerschelde and to Zeebrugge, and the morphological response of the environment. Indeed, dredging is only effected in the navigation channels Scheur and Pas van 't Zand. Nevertheless, these works apparently ultimately deplete the surrounding flat seabed areas near Wandelaar, north of Wenduine Bank and near Bol van Heist. The areas at the offshore side of Zeebrugge Harbour dams are subject to stronger currents since the construction of the dams. The morphological response to the stronger currents is local scour of the seabed.

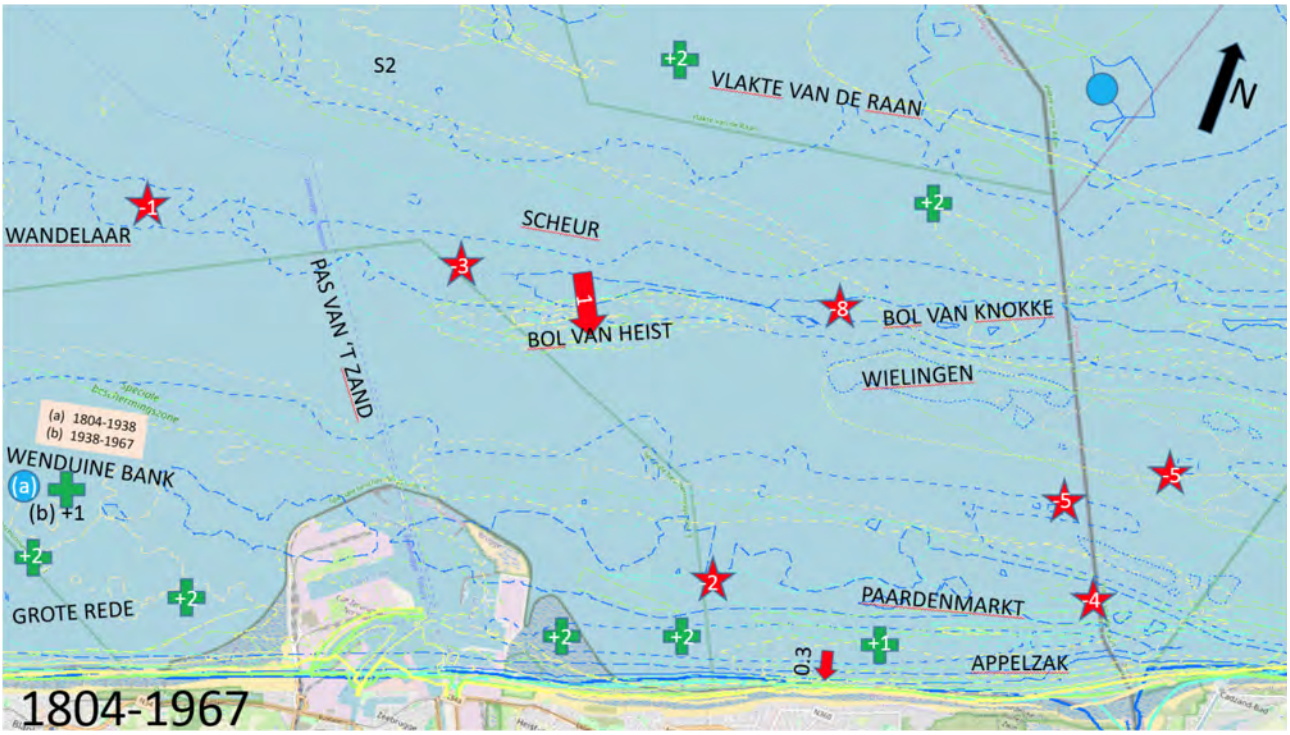

Figure 19 – 1804-1967 contour line and depth change analysis, Belgian East Coast, from Blankenberge to Cadzand.

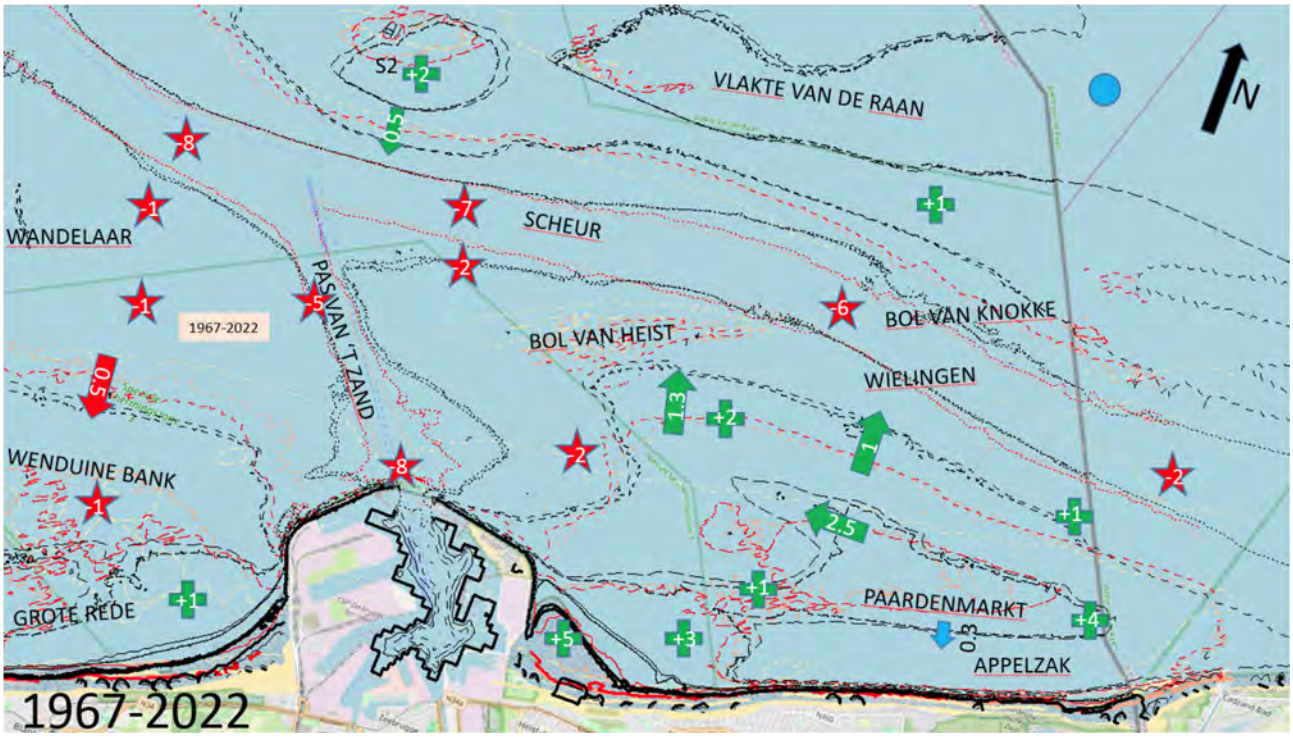

Figure 20 – 1967-2022 contour line and depth change analysis, Belgian East Coast, from Blankenberge to Cadzand.

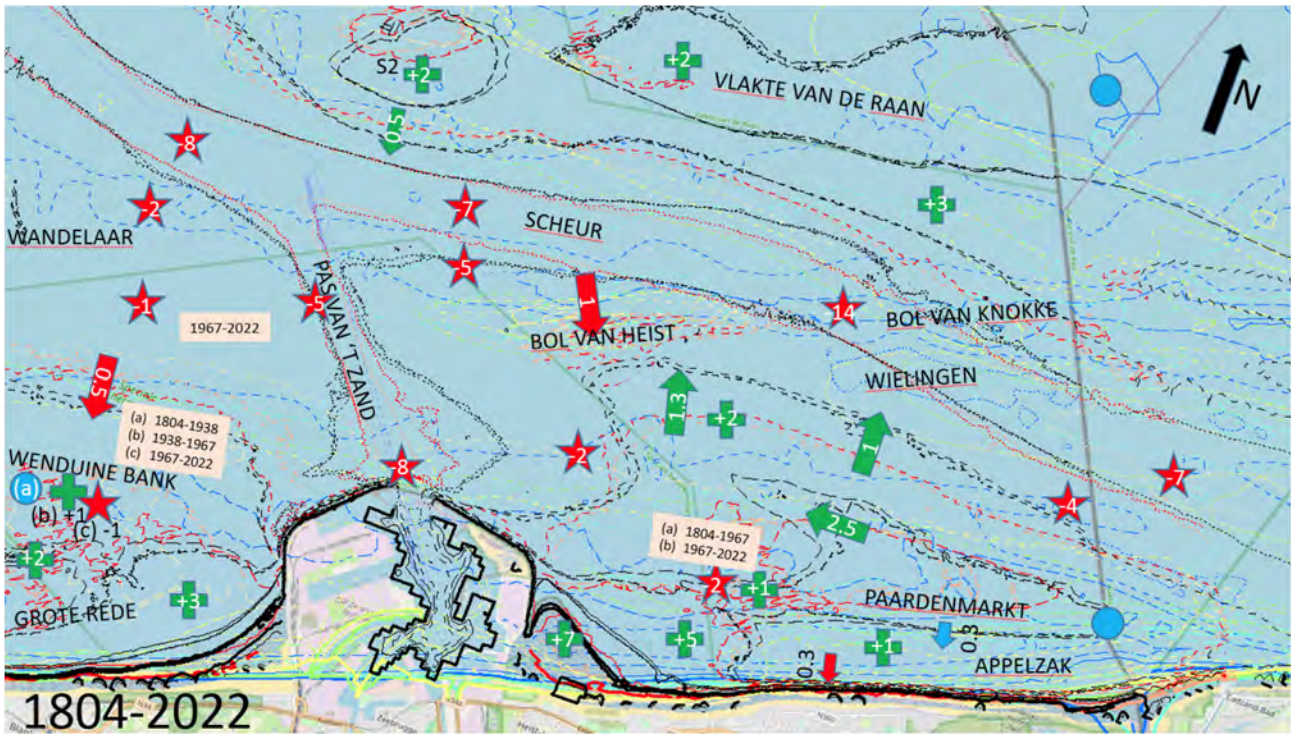

Figure 21 – 1804-2022 contour line and depth change analysis, Belgian East Coast, from Blankenberge to Cadzand.

Scheur was connected to Wielingen by means of dredging. This work resulted in the disappearance of Bol van Knokke (Figure 19). The main navigation route was thus shifted from a channel north of Bol van Knokke called Wielingen in 1804 to a channel called French Pass in 1804 and presently called Wielingen. Names also change in the course of time.

Another important adaptation is seaward accretion at the wide, gently sloping north flank of Paardenmarkt, especially off Heist and Knokke. It is thought that the deepening of Scheur-Wielingen accommodated more of the tidal discharge entering and leaving Westerschelde. Therefore, some sedimentation space was created landward of the main shipping lane. This is a post-1967 change.

As to the area of the shoreface-connected ridges, Wenduine Bank and Paardenmarkt were connected in 1804 and 1866. On older maps, this long sandbank was named Hard Zand (Houthuys *et al.,* 2021). It connected to the Zeeland-Flemish coast just east of Zwin (present-day Cadzand-Bad). The Leopold II Dam in Zeebrugge was constructed in 1899. This dam protrudes over 1 km seawards from the low-water mark and affected the currents. A first erosion trough north of the dam appears on the 1908 chart. The part of Hard Zand that was not affected by erosion was crosscut by a dredged navigation channel called "Passe du Zand" on the 1908 chart that also mentions "dragages en cours". This work sealed the fate of the shoreface-connected ridge; it was severed into two parts: Wenduine Bank at the west and Paardenmarkt at the east.

The remnant of Wenduine Bank west of Zeebrugge remained stable between 1804 and 1938. The wide shoreface of Wenduine-Blankenberge, including the eastward termination of Grote Rede and the crest area of Wenduine Bank, sanded up between 1938 and 1967 (Figure 19). It is interpreted to be a far-field morphological response to the construction around 1900 of Leopold II Dam in Zeebrugge. Immediately following the 1979-1986 construction of Zeebrugge Outer Harbour, the seaward part of the area lost sediment. This goes on until today (Figure 20). The inner nearshore, sheltered by Leopold II Dam and later the new Outer Harbour, gained 2 to 3 m vertically (Figure 21) thus filling the eastern termination of Grote Rede.

At the east side of Zeebrugge, the Paardenmarkt crest area deepened by 2 m between 1804 and 1967 after which it recovered by 1 m. More to the east, the Paardenmarkt crest between Knokke and Zwin was highly dynamic, but the 2022 situation there now resembles again the 1804 situation. The only systematic change is a landward approach by 0.3 km. In addition, Appelzak channel shows large morphodynamics, and in spite of the deepening trend of the last decades, its floor is in 2022 still 1 m shallower than in 1804. It can be inferred that after the construction of the Leopold II dam, flow currents were lower in this channel, which as a result shallowed up.

The beach between Wenduine and Heist must have suffered erosion in the first decades of the 19th century. Groynes are present along this part of the coast on the Dutch 1828 dune map (Quant, 1828), while there are no groynes on the 1804 map. The construction of the Leopold II dam just before 1900 may have been the trigger of more erosion, now also in Knokke-Zoute. Beach erosion there was studied in 1938-1940 by the newly founded Flanders Hydraulics Institute in its "Model 41" report that proposes a progressive subsidence ("un abaissement progressif") of the ground surface as the ultimate cause of coastal erosion between Zeebrugge and the Dutch border. However, using the present knowledge, it can be put forward that the beach and shoreface drift was blocked by the Leopold II dam, resulting in sand depletion at Knokke. Erosion has ever since been observed there, and also after the large beach 1977-1979 nourishment. Blocking of alongshore sand transport has even been greater after the seaward expansion of Zeebrugge in 1979-1986 (Houthuys et al., 2022). Over the past two centuries, the landward flank of Appelzak channel, which is also the shoreface, shifted about 0.3 km landward.

Opposed to the beach evolution, the wide shoreface area of Heist and Duinbergen shallowed by 5 to 7 m since 1804. Most of the sedimentation here occurred after the construction of Zeebrugge Outer Harbour. Sedimentation still continues here today.

Summary

Generally, the offshore part of the inner shelf (Flemish Banks) shows no systematic morphological movement over the last two centuries. In the more nearshore zone of the shoreface-connected ridges, significant movements of the sandbanks to the east, in the alongshore direction, are observed. The movements are largest in the area of the French-Belgian border and there, the magnitude of the alongshore movement increases in the onshore direction. Furthermore, most shoreface-connected ridges also show an onshore movement component, but at rates that are only 1/5th or less than the alongshore movement rates. Some passes between the nearshore sandbanks disappear (they are filled up by sediment) while other new passes are created. This is seen in the North-French part of the study area. The new passes are more landward than the abandoned ones. The attachment points of the shoreface-connected ridges to the coast did not shift, probably since the late Middle Ages. The shoreface tends to move landwards at rates comparable to the landward shift rate of the shoreface-connected ridges. The depth of the flow channels in general does not change. The entire Westerschelde ebb tidal delta shifts landwards, towards the Westerschelde estuary.

It is thought that the ongoing sea-level rise is the ultimate driving force of the described natural cross-shore movements. The residual west-to-east sediment transport is the ultimate driving force of the described natural alongshore movements.

Human interference also triggered important morphological changes. The creation of navigation channels cross-cutting the nearshore sandbanks depleted the downdrift (eastward) part of the affected sandbanks. In the neighbourhood of important dredged fairways, also the surrounding seabed lost sediment. Due to flow constriction, scour channels developed at the seaward side of the new harbour dams that protrude in the nearshore area. At the same time, sedimentation occurs updrift and downdrift of the new harbour dams. Most nearshore shallowing is observed at the downdrift (east) side of the outer harbours. Finally, dumping of dredge spoils creates long-lasting positive bed changes. At Bruggen & Wegen Oostende, even a new, 10 km long low sandbank developed downdrift of the dump site.

2.2.3 Taking sea-level rise into account

All historic maps contain depths in (lower) low water spring. It can reasonably be assumed that the present rate of sea-level rise persisted over the last two centuries. It can thus be reasoned that the reference levels were lower in the past, by about the number of years before 2022 x sea level rate. The quantitative analysis in the following two sections takes sea-level rise of the reference datum into account. Thus, bed levels were corrected towards the reference level of 2022. Also, volume differences were obtained that allow for rising sea level.

Ozer *et al.* (2019) report a mean sea level rise of 1.7 mm/year over 1936-2016 and 2.4 mm/year over 1972-2016 at Oostende. Huybrechts *et al.* (2023) report 2.3 mm/year over 1900-2020 at Vlissingen and 1.6 mm/year over 1960-2020 in Dunkerque and a value in between of about 1.8 mm/year at Oostende over 1936-2020. Wahl *et al.* (2013) report 2.1 mm/year over 1950-2011, 2.5 mm/year over 1980-2011 and 3.5 mm/year over 1993-2011 for Oostende. To accommodate at the same time the possibly somewhat lower rates before the start of the measurements and the fact that the 2022 mosaic (both from Flemish Hydrography as EMODnet) was assembled from recent and older surveys, a rate of 2 mm/year is adopted here.

So for the corrected bed levels and volume differences per box, the following correction was applied on the depth levels such as mentioned on the original maps:

- 1804: 218 * 0.002 = -0.436
- 1866: 156 * 0.002 = -0.312
- 1908: 114 * 0.002 = -0.228
- 1938: 84 * 0.002 = -0.168
- 1967: 55 * 0.002 = -0.110
- 1986: 36 * 0.002 = -0.072
- 1992: 30 * 0.002 = -0.060

2.2.4 Evolution of sandbank height and channel depth

As theoretical models (Nnafie et al., 2014-1) describing the development of shoreface-connected ridges under natural hydrodynamic conditions show growth of ridge crests, oriented oblique to the shoreline, at the expense of the surrounding seafloor that is deepened into channels, it was decided to examine the evolution of the height of the nearshore-connected ridges in the Belgian inner shelf.

A set of 22 locations was selected (Figure 22) to represent the three major zones near the Belgian coast: 1-8 are on the shoreface-connected ridges (SFCR) (7 is on the newly formed sandbank downdrift of Oostende dredge dump); 9-18 are in the transition zone and 17-22 are in the zone of the tidal sand ridges (TSR).

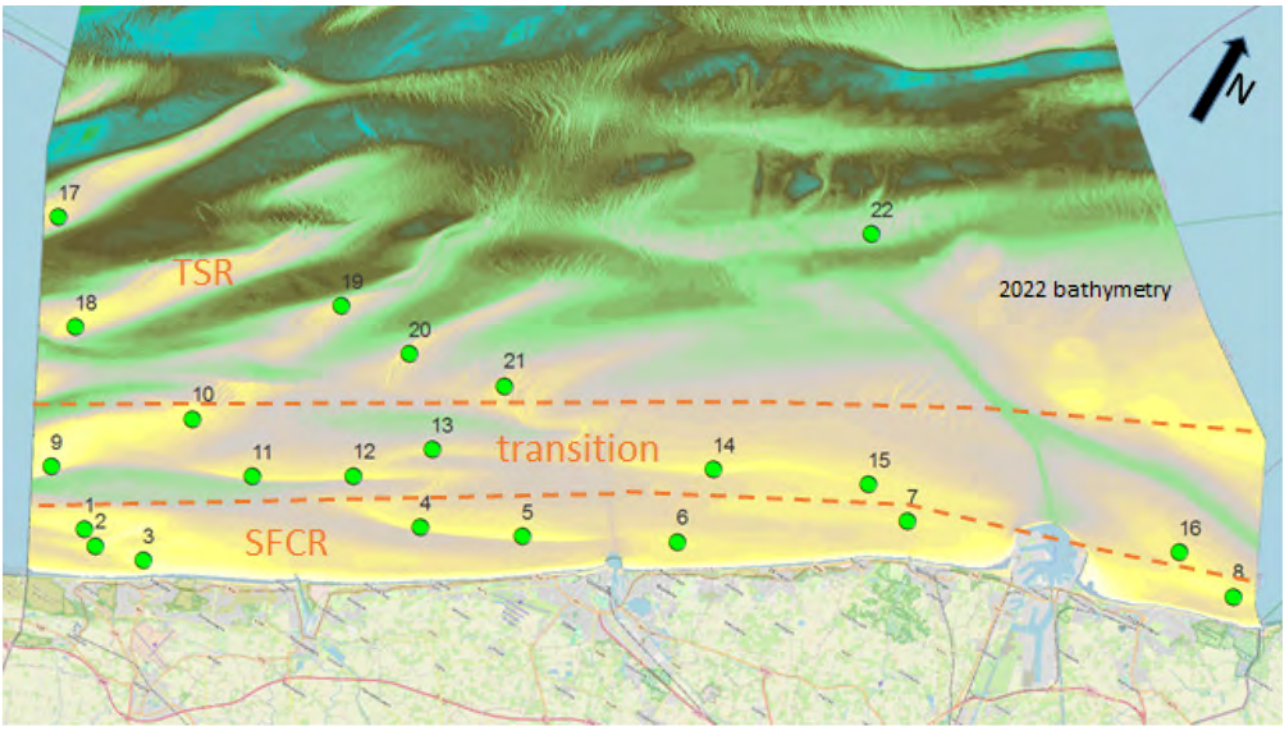

Figure 22 – Belgian inner shelf, 2022 bathymetry. Selected points for the 1804-2022 evolution of sandbank height.

Using the point files containing the vectorised depth points of the scanned maps spanning 1804-2022, the shallowest and deepest point was recorded in about a 1 km radius around each research location. In the case where significant systematic movements of the large-scale bedforms are observed (see previous section), the search area for the shallowest and deepest point was extended so that the actual movement of the large-scale bedform is followed. The deepest point was systematically recorded from the channel landward of the sandbank crest. The 1804 depths were converted into metres. Next, the depths were converted to 2022 bed levels by applying the correction like explained in the previous section.

The results are plotted in Figure 23 to Figure 25. The figures contain grouped points per zone. The vertical scale expresses depth (like shown in the charts) in m. The evolution of the bank crest and trough elevation at each individual point is shown by two line graphs, with a different colour per point. ,The upper curve in each colour connects the sandbank crest points and the lower curve the corresponding trough points. In order to evaluate the evolution of the sandbank height at a given location, one should isolate the top and bottom curve of the same colour in the figures.

There is a general tendency for sandbank crests in the SFCR zone to rise through time, and so do the corresponding deep points in the channels (Figure 23). If sea-level rise is taken into account, this tendency is even stronger. The strongest tendency to rise is seen in Broers Bank and Paardenmarkt. Point 6 at the eastern end of Stroombank is influenced by dredging works for the navigation to Oostende. After 1938, the upper and lower curves meet (Figure 23) expressing the fact that the sandbank disappeared. Point 7 ("Spoorbank", the trace downdrift of the dredge dump site) only developed after 1992.

The height of the sandbanks (distance between the upper and lower same colour curves) does not increase, it rather tends to diminish.

The crest heights and corresponding channel depths in the transition zone (Figure 24) also rise, but at lower rates than in the SFCR zone. The rate is a little bit higher when sea-level rise is taken into account. Again, the height (difference between crest and channel point depth) does not change at the observation time.

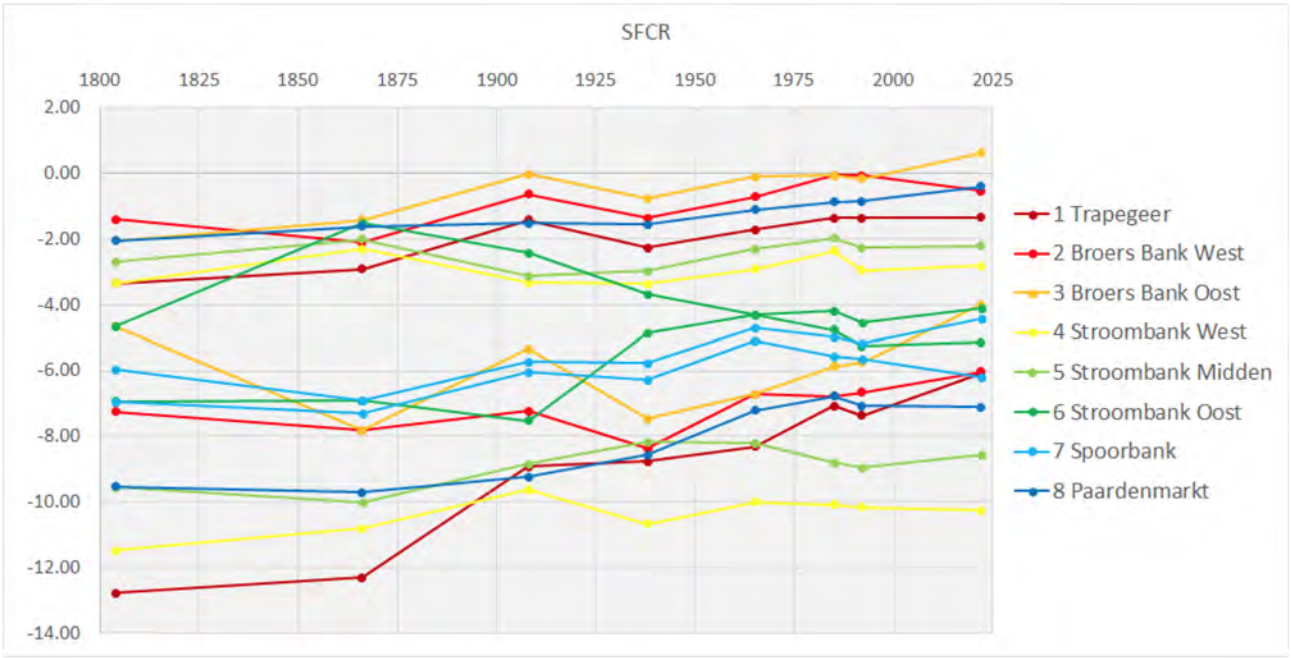

Figure 23 – Evolution of crest level and corresponding channel level of some selected sandbank locations in the SFCR zone.

Colours represent the different locations. Per location, the upper line represents the level evolution of the ridge crest, while the lower line represents the level evolution of the nearby trough. The evolution of the ridge height can be appreciated by the distance between the two corresponding lines.

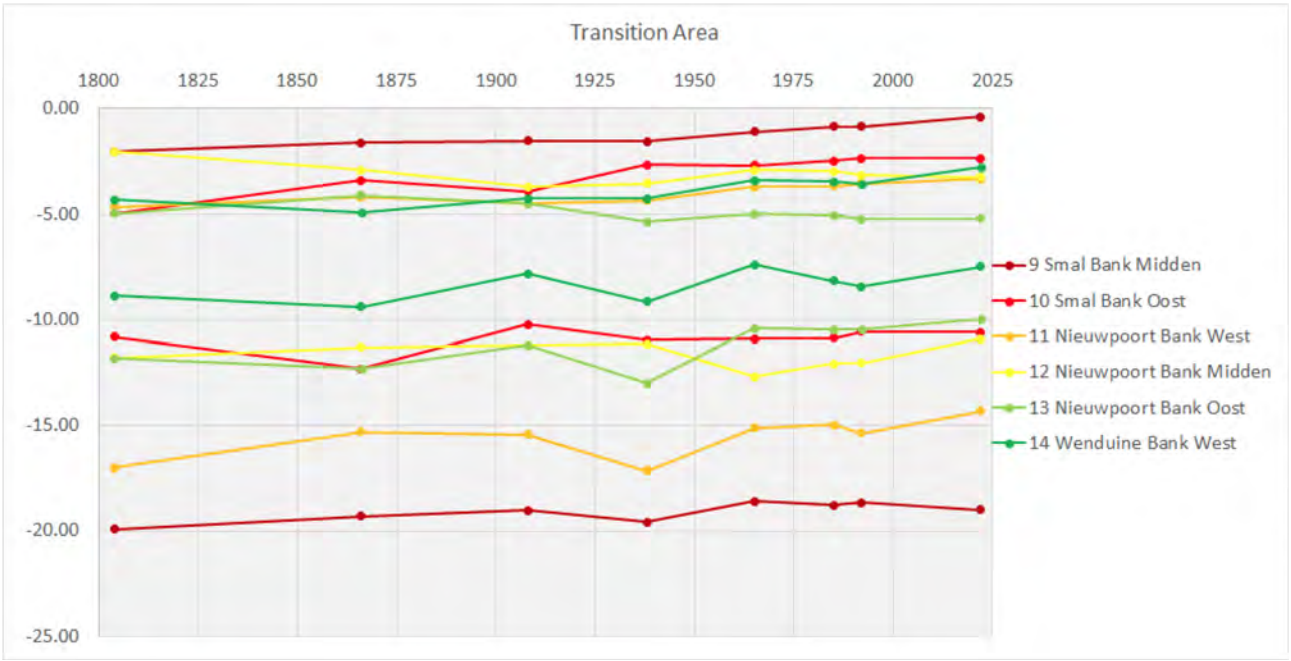

Figure 24 – Evolution of crest level and corresponding channel level of some selected sandbank locations in the transition zone.

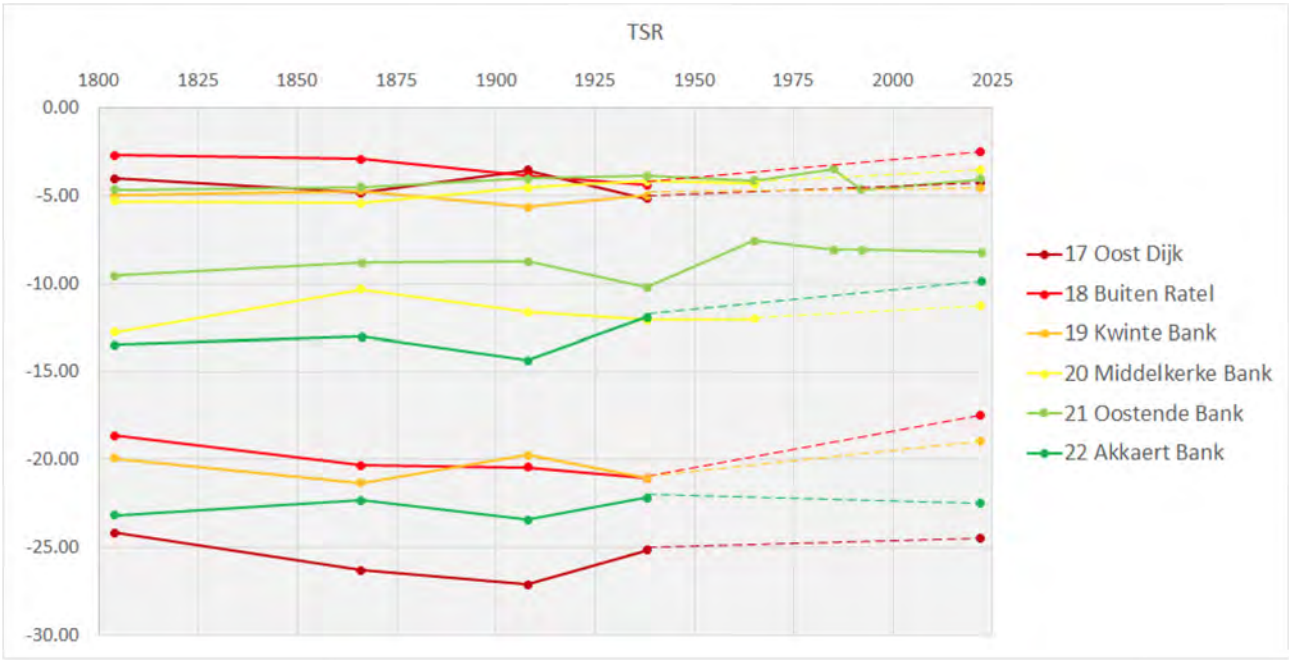

Figure 25 – Evolution of crest level and corresponding channel level of some selected sandbank locations in the TSR zone.

The dashed line segments connect points in the graph where no 1960s-1990s survey is available.

The change in crest and channel depth is small to absent in the TSR zone. Point 22 (Akkaert Bank) seems the exception. However, the crest area contains large dunes and was probably less well captured in the older charts. Most likely, here also, there is no change.

When allowing for depth selection bias, like explained in §2.1.2, the "no change" trend of the tidal sand ridges and the "general shallowing" trend of the shoreface-connected ridges is even more confirmed.

In conclusion, the sandbanks and channels in the SFCR zone have risen, those in the transition zone too, but at a lower rate, and in the TSR zone, there is no change. More specifically, the relative height of all sandbanks, expressed by the bed level difference between the sandbank crest and the corresponding channel, did not change in the observation period.

2.2.5 Volumetric analysis

In spite of the relatively large uncertainty on location and depth of the historic chart data, it is thought that a large-scale volume balance of the seabed can be attempted. This is approached by computing volume differences in a few large rectangular areas or boxes.

As the results above indicate a different large-scale morphological behaviour in the inshore and offshore area, boxes were defined in three coast-parallel rows: the most inshore one contains the nearshore ridges, the middle one is the transition area and the most offshore one contains the tidal current ridges. It must be realized that the most offshore row is not completely covered in each survey.

In the alongshore direction, 5 columns of boxes were created. The three middle ones coincide with the Belgian part of the North Sea, where good-quality recent bathymetry is available from Flemish Hydrography. The westernmost boxes are in French territorial waters and the easternmost in Dutch waters (Figure 26). As the bathymetric rasters do not cover the intertidal beach, the inner boxes were bounded at about the low-tide mark. There is no change of the position of the low-water mark at this small scale, except around the harbours.

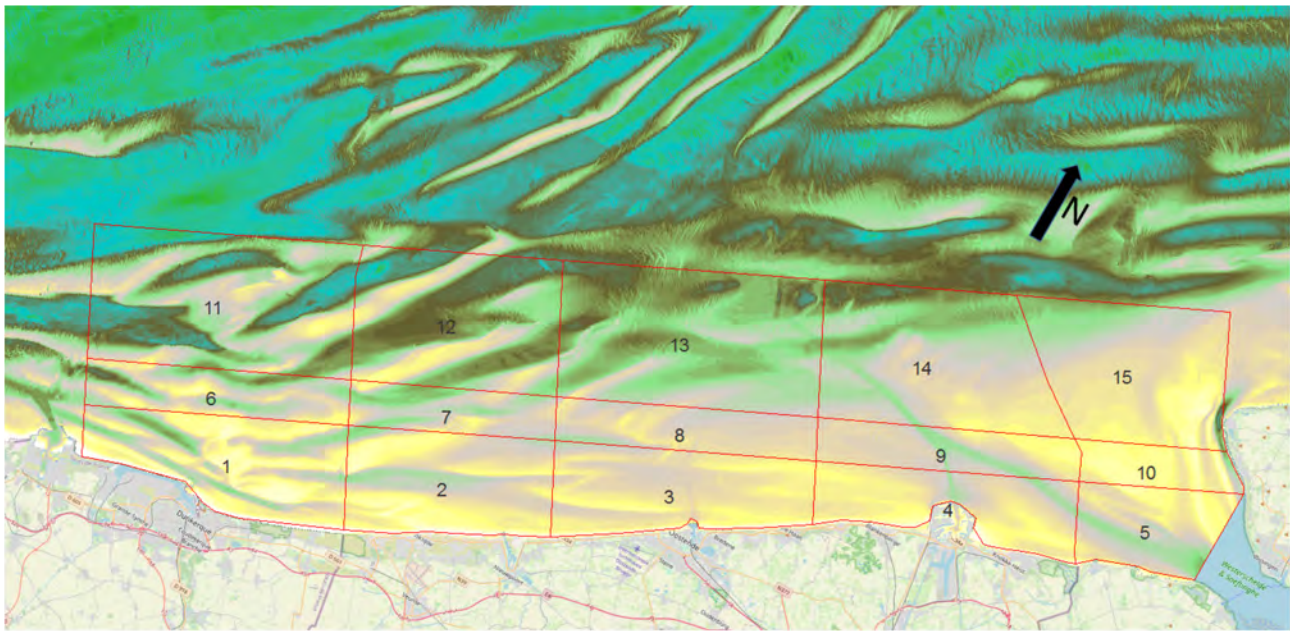

Figure 26 – Definition of large boxes (fine red lines) for the analysis of the large-scele long-term sediment budget. Background is 2022 bathymetry.

As the 2022 survey has the best quality, volume differences were calculated for each historic chart to the 2022 survey. For the boxes on Belgian territory, the 2022 Flemish Hydrography survey (projected to Lambert 72 like described in §2.2.1) served as a reference. In order to extend the analysis to the wider environment, in a second series of calculations the EMODnet 2022 survey (projected to Lambert 72 like described in §2.2.1) was taken as a reference. For boxes 1, 5, 6, 10, 11 and 15, this provided the only available volume difference values.

In practice, it does not matter whether sea bed difference maps are made using rasters in MLLWS or TAW as the same operation ([raster in MLLWS] – [conversion raster LAT to NAP] + 2.333 [constant difference between NAP and TAW]) has been applied to convert the MLLWS rasters to TAW. Therefore, sea bed difference rasters are created using the raster expression: [2022 raster in TAW] – ([YYYY raster in TAW] – (0.002 x number of years 2022 - YYYY)). As a result, the bottom height difference is increased by an amount supposed to be the real sea level rise over the difference period, as described before.

The sea-level rise corrected bed difference rasters are named:

- VH2022-YYYYSR: rasters with reference to Vlaamse Hydrografie (VH) 2022 bathymetry, used for boxes 2-4, 7-9, 12-14
- E2022-YYYYSLR: rasters with reference to EMODnet 2022 bathymetry; used for boxes 1, 5, 6, 10, 11, 15. The boxes 2-4, 7-9, 12-14 have also been calculated but the result is inferior to the previous

S(L)R (sea level rise) is added in the name to remind the user that the raster was shifted to compensate for sea level rise. The rasters are stored here:

P:\20_079-MorfoInteract\3_Uitvoering\Deeltaak1_DataAcquisition\MorphAnalysis

They are 10 m-resolution rasters in Lambert 72. The rasters with reference to the EMODnet 2022 bathymetry have interference effects, caused by interpolating the raster from geographical coordinates to Lambert 72. At the scale of the boxes, the interference effects are thought to cancel each other across the box.

Dividing the computed volume difference per box by the box area yields the mean bed level difference per box, corrected for sea-level rise.

The results of the volume calculations are presented in Table 3 to Table 6 and in Figure 27 and Figure 28. Some general guidelines to consult these tables and graphs:

- For the Belgian part of the continental shelf, more surveys were available, i.e. the vectorised 1962-1969 survey (abbreviated in the tables and graphs to 1967), the vectorised 1984-1987 survey (abbreviated to 1986) and the vectorised 1991-1993 survey (abbreviated to 1992).
- These extra surveys covered most of the inshore and transition boxes, but only a small part of the offshore boxes. Therefore, the volume difference for the additional surveys is not relevant in the offshore boxes.
- Table 3 and Table 5 present the volume and bed level differences per box. Table 4 and Table 6 present longshore sums over the nearshore, transition and offshore boxes, as well as the sum over the entire area.
- The graphs display time plots of the average bed level difference, as this is a quantity that can be compared across the boxes. The partial plots are arranged like the place of the boxes in Figure 26
- All graphs start in 1804 and end in 2022. The distance between the vertical grid lines is 100 years
- The horizontal (time) axis in all graphs is at average bed level difference 0. The distance between the horizontal grid lines is 1 m (depth difference)
- All graphs show average bottom height difference with respect to the reference survey, 2022. The value at 2022 is always 0

Table 3 – Volume difference and average bed level difference in the boxes on Belgian territory, relative to the Flemish Hydrography 2022 survey. Results per box. Average bed level difference to 2022 with and without correction for sea level rise.

Box	Year	SLR correction	Common area	Common area % of box area	Volume diff. (SLR corrected)	Average depth diff. (SLR corr.)	Average depth diff. (no SLR corr.)
n°		[m]	[ha]	%	[m³]	[m]	[m]
2	1804	0.436	16390	100	-109 060 000	-0.67	-0.23
2	1866	0.312	16390	100	-89 720 000	-0.55	-0.24
2	1908	0.228	16390	100	-113 150 000	-0.69	-0.46
2	1938	0.168	16390	100	-147 090 000	-0.90	-0.73
2	1967	0.110	16243	99	-26 470 000	-0.16	-0.05
2	1986	0.072	16236	99	12 750 000	0.08	0.15
2	1992	0.060	16256	99	-8 580 000	-0.05	0.01
2	2022	0.000	16390	100	0	0.00	0.00
3	1804	0.436	16303	100	-8 320 000	-0.05	0.38
3	1866	0.312	16303	100	-62 690 000	-0.38	-0.07
3	1908	0.228	16303	100	-15 400 000	-0.09	0.13
3	1938	0.168	16303	100	-62 700 000	-0.38	-0.22
3	1967	0.110	16175	99	79 720 000	0.49	0.60
3	1986	0.072	16210	99	37 670 000	0.23	0.30

3	1992	0.060	16248	100	6 380 000	0.04	0.10
3	2022	0.000	16303	100	0	0.00	0.00
4	1804	0.436	12518	100	2 660 000	0.02	0.46
4	1866	0.312	12552	100	-34 140 000	-0.27	0.04
4	1908	0.228	12556	100	-18 330 000	-0.15	0.08
4	1938	0.168	12556	100	-50 180 000	-0.40	-0.23
4	1967	0.110	12230	97	47 250 000	0.39	0.50
4	1986	0.072	12155	97	44 290 000	0.36	0.44
4	1992	0.060	12501	100	13 980 000	0.11	0.17
4	2022	0.000	12556	100	0	0.00	0.00
7	1804	0.436	7288	100	32 870 000	0.45	0.89
7	1866	0.312	7288	100	29 390 000	0.40	0.72
7	1908	0.228	7288	100	-38 210 000	-0.52	-0.30
7	1938	0.168	7288	100	-46 210 000	-0.63	-0.47
7	1967	0.110	6790	93	-17 160 000	-0.25	-0.14
7	1986	0.072	4411	61	6 690 000	0.15	0.22
7	1992	0.060	4398	60	-6 740 000	-0.15	-0.09
7	2022	0.000	7288	100	0	0.00	0.00
8	1804	0.436	9068	100	1 560 000	0.02	0.45
8	1866	0.312	9068	100	-22 710 000	-0.25	0.06
8	1908	0.228	9068	100	-39 200 000	-0.43	-0.20
8	1938	0.168	9068	100	-56 810 000	-0.63	-0.46
8	1967	0.110	9068	100	26 920 000	0.30	0.41
8	1986	0.072	8329	92	540 000	0.01	0.08
8	1992	0.060	8549	94	-9 810 000	-0.11	-0.05
8	2022	0.000	9068	100	0	0.00	0.00
9	1804	0.436	8911	100	84 770 000	0.95	1.39
9	1866	0.312	8911	100	108 070 000	1.21	1.52
9	1908	0.228	8911	100	91 490 000	1.03	1.25

9	1938	0.168	8911	100	63 280 000	0.71	0.88
9	1967	0.110	7495	84	116 310 000	1.55	1.66
9	1986	0.072	7766	87	59 170 000	0.76	0.83
9	1992	0.060	7880	88	31 470 000	0.40	0.46
9	2022	0.000	8911	100	0	0.00	0.00
12	1804	0.436	18831	86	266 720 000	1.42	1.85
12	1866	0.312	21964	100	437 150 000	1.99	2.30
12	1908	0.228	21964	100	-34 940 000	-0.16	0.07
12	1938	0.168	21964	100	31 990 000	0.15	0.31
12	2022	0.000	21964	100	0	0.00	0.00
13	1804	0.436	23932	85	102 660 000	0.43	0.86
13	1866	0.312	28163	100	174 730 000	0.62	0.93
13	1908	0.228	28163	100	-115 470 000	-0.41	-0.18
13	1938	0.168	28163	100	110 100 000	0.39	0.56
13	2022	0.000	28163	100	0	0.00	0.00
14	1804	0.436	19692	82	-35 360 000	-0.18	0.26
14	1866	0.312	24032	100	-71 200 000	-0.30	0.02
14	1908	0.228	24032	100	-158 000 000	-0.66	-0.43
14	1938	0.168	24032	100	-4 670 000	-0.02	0.15
14	2022	0.000	24032	100	0	0.00	0.00

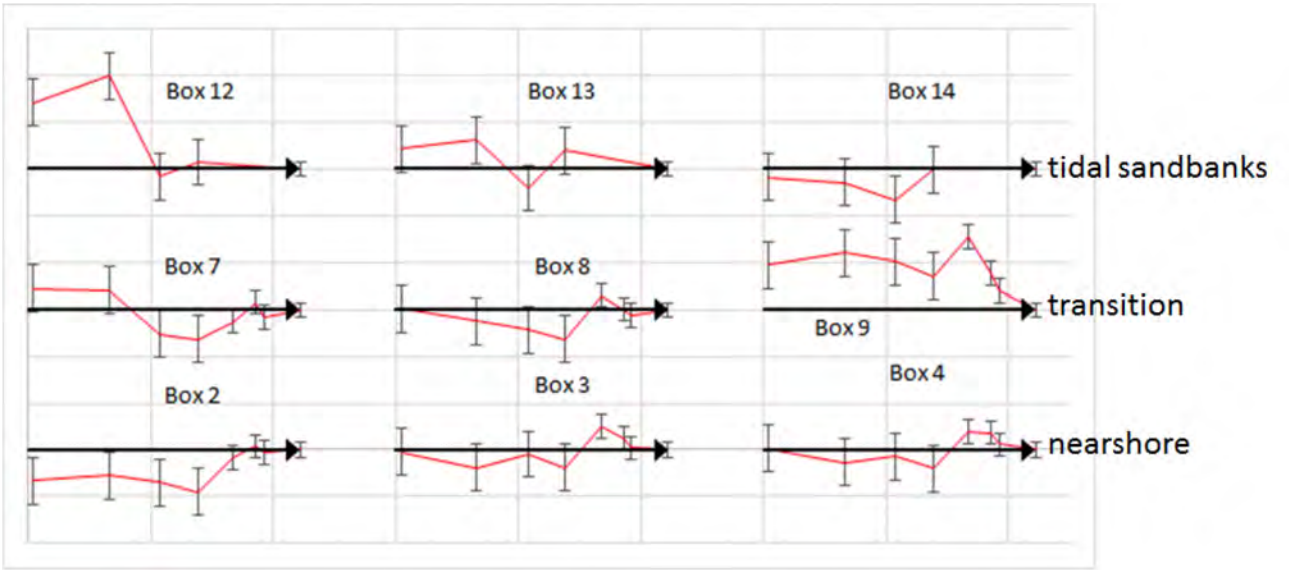

Figure 27 – Time series of average bottom height difference in the boxes on Belgian territory , relative to the Flemish Hydrograpy 2022 survey. Results per box. Average bottom height was corrected for sea level rise. The vertical bars indicate uncertainty.

Table 4 – Volume difference and average bed level difference in the boxes on Belgian territory , relative to the Flemish Hydrography 2022 survey. Results summed over the box rows and the entire area. Average bed level difference to 2022 with and without correction for sea level rise.

Box	Year	SLR correction	Common area	Common area % of box area	Volume diff. (SLR corrected)	Average depth diff. (SLR corr.)	Average depth diff. (no SLR corr.)
n°		[m]	[ha]	%	[m³]	[m]	[m]
2-4	1804	0.436	45211	100	-114 720 000	-0.25	0.18
2-4	1866	0.312	45245	100	-186 550 000	-0.41	-0.10
2-4	1908	0.228	45249	100	-146 880 000	-0.32	-0.10
2-4	1938	0.168	45249	100	-259 970 000	-0.57	-0.41
2-4	1967	0.110	44648	99	100 500 000	0.23	0.34
2-4	1986	0.072	44600	99	94 710 000	0.21	0.28
2-4	1992	0.060	45005	99	11 780 000	0.03	0.09
2-4	2022	0.000	45249	100	0	0.00	0.00
7-9	1804	0.436	25267	100	119 200 000	0.47	0.91
7-9	1866	0.312	25267	100	114 750 000	0.45	0.77
7-9	1908	0.228	25267	100	14 080 000	0.06	0.28
7-9	1938	0.168	25267	100	-39 740 000	-0.16	0.01
7-9	1967	0.110	23354	92	126 070 000	0.54	0.65
7-9	1986	0.072	20505	81	66 400 000	0.32	0.40
7-9	1992	0.060	20826	82	14 920 000	0.07	0.13
7-9	2022	0.000	25267	100	0	0.00	0.00
12-14	1804	0.436	62455	84	334 020 000	0.53	0.97
12-14	1866	0.312	74160	100	540 680 000	0.73	1.04
12-14	1908	0.228	74160	100	-308 410 000	-0.42	-0.19
12-14	1938	0.168	74160	100	137 420 000	0.19	0.35
12-14	2022	0.000	74160	100	0	0.00	0.00
2-4, 7-9, 12-14	1804	0.436	132933	92	338 500 000	0.25	0.69
2-4, 7-9, 12-14	1866	0.312	144672	100	468 880 000	0.32	0.64

2-4, 7-9, 12-14	1908	0.228	144675	100	-441 210 000	-0.30	-0.08
2-4, 7-9, 12-14	1938	0.168	144675	100	-162 290 000	-0.11	0.06
2-4, 7-9, 12-14	2022	0.000	144675	100	0	0.00	0.00

Table 5 – Volume difference and average bed level difference in all boxes, relative to the EMODnet 2022 bathymetry. Results per box. Average bed level difference to 2022 with and without correction for sea level rise.

Box	Year	SLR correction	Common area	Common area % of box area	Volume diff. (SLR corrected)	Average depth diff. (SLR corr.)	Average depth diff. (no SLR corr.)
n°		[m]	[ha]	%	[m³]	[m]	[m]
1	1804	0.436	17381	100	-98 090 000	-0.56	-0.13
1	1866	0.312	17371	100	-136 650 000	-0.79	-0.47
1	1908	0.228	17382	100	-122 590 000	-0.71	-0.48
1	1938	0.168	17372	100	-109 670 000	-0.63	-0.46
1	2022	0.000	17382	100	0	0.00	0.00
2	1804	0.436	16401	100	-119 290 000	-0.73	-0.29
2	1866	0.312	16401	100	-100 110 000	-0.61	-0.30
2	1908	0.228	16401	100	-123 700 000	-0.75	-0.53
2	1938	0.168	16401	100	-157 640 000	-0.96	-0.79
2	2022	0.000	16401	100	0	0.00	0.00
3	1804	0.436	16317	100	-17 010 000	-0.10	0.33
3	1866	0.312	16317	100	-71 550 000	-0.44	-0.13
3	1908	0.228	16317	100	-24 100 000	-0.15	0.08
3	1938	0.168	16317	100	-71 360 000	-0.44	-0.27
3	2022	0.000	16317	100	0	0.00	0.00
4	1804	0.436	12525	100	-4 940 000	-0.04	0.40
4	1866	0.312	12559	100	-41 740 000	-0.33	-0.02
4	1908	0.228	12560	100	-26 390 000	-0.21	0.02
4	1938	0.168	12560	100	-58 110 000	-0.46	-0.29
4	2022	0.000	12560	100	0	0.00	0.00

5	1804	0.436	9397	100	12 620 000	0.13	0.57
5	1866	0.312	9397	100	38 710 000	0.41	0.72
5	1908	0.228	9397	100	-10 720 000	-0.11	0.11
5	1938	0.168	9397	100	18 180 000	0.19	0.36
5	2022	0.000	9397	100	0	0.00	0.00
6	1804	0.436	9556	100	19 050 000	0.20	0.64
6	1866	0.312	9556	100	-34 880 000	-0.36	-0.05
6	1908	0.228	9517	100	-59 500 000	-0.63	-0.40
6	1938	0.168	9556	100	31 650 000	0.33	0.50
6	2022	0.000	9556	100	0	0.00	0.00
7	1804	0.436	7294	100	27 600 000	0.38	0.81
7	1866	0.312	7294	100	24 010 000	0.33	0.64
7	1908	0.228	7294	100	-43 620 000	-0.60	-0.37
7	1938	0.168	7294	100	-51 640 000	-0.71	-0.54
7	2022	0.000	7294	100	0	0.00	0.00
8	1804	0.436	9076	100	-4 980 000	-0.05	0.38
8	1866	0.312	9076	100	-29 170 000	-0.32	-0.01
8	1908	0.228	9076	100	-45 630 000	-0.50	-0.27
8	1938	0.168	9076	100	-63 310 000	-0.70	-0.53
8	2022	0.000	9076	100	0	0.00	0.00
9	1804	0.436	8919	100	81 940 000	0.92	1.35
9	1866	0.312	8919	100	105 230 000	1.18	1.49
9	1908	0.228	8919	100	88 970 000	1.00	1.23
9	1938	0.168	8919	100	60 640 000	0.68	0.85
9	2022	0.000	8919	100	0	0.00	0.00
10	1804	0.436	5196	100	-66 310 000	-1.28	-0.84
10	1866	0.312	5196	100	-48 050 000	-0.92	-0.61
10	1908	0.228	5196	100	-27 520 000	-0.53	-0.30

10	1938	0.168	5196	100	6 600 000	0.13	0.30
10	2022	0.000	5196	100	0	0.00	0.00
11	1804	0.436	23298	83	327 960 000	1.41	1.84
11	1866	0.312	28004	100	389 450 000	1.39	1.70
11	1908	0.228	23395	83	-72 420 000	-0.31	-0.08
11	1938	0.168	28078	100	322 920 000	1.15	1.32
11	2022	0.000	28078	100	0	0.00	0.00
12	1804	0.436	18837	86	248 070 000	1.32	1.75
12	1866	0.312	21983	100	415 420 000	1.89	2.20
12	1908	0.228	21983	100	-57 210 000	-0.26	-0.03
12	1938	0.168	21983	100	9 870 000	0.04	0.21
12	2022	0.000	21983	100	0	0.00	0.00
13	1804	0.436	23945	85	86 320 000	0.36	0.80
13	1866	0.312	28189	100	155 510 000	0.55	0.86
13	1908	0.228	28189	100	-135 190 000	-0.48	-0.25
13	1938	0.168	28189	100	90 620 000	0.32	0.49
13	2022	0.000	28189	100	0	0.00	0.00
14	1804	0.436	19702	82	-52 510 000	-0.27	0.17
14	1866	0.312	24057	100	-93 210 000	-0.39	-0.08
14	1908	0.228	24057	100	-180 230 000	-0.75	-0.52
14	1938	0.168	24057	100	-26 680 000	-0.11	0.06
14	2022	0.000	24057	100	0	0.00	0.00
15	1804	0.436	12865	65	95 810 000	0.74	1.18
15	1866	0.312	19832	100	15 750 000	0.08	0.39
15	1908	0.228	18729	94	-5 660 000	-0.03	0.20
15	1938	0.168	19832	100	37 740 000	0.19	0.36
15	2022	0.000	19832	100	0	0.00	0.00

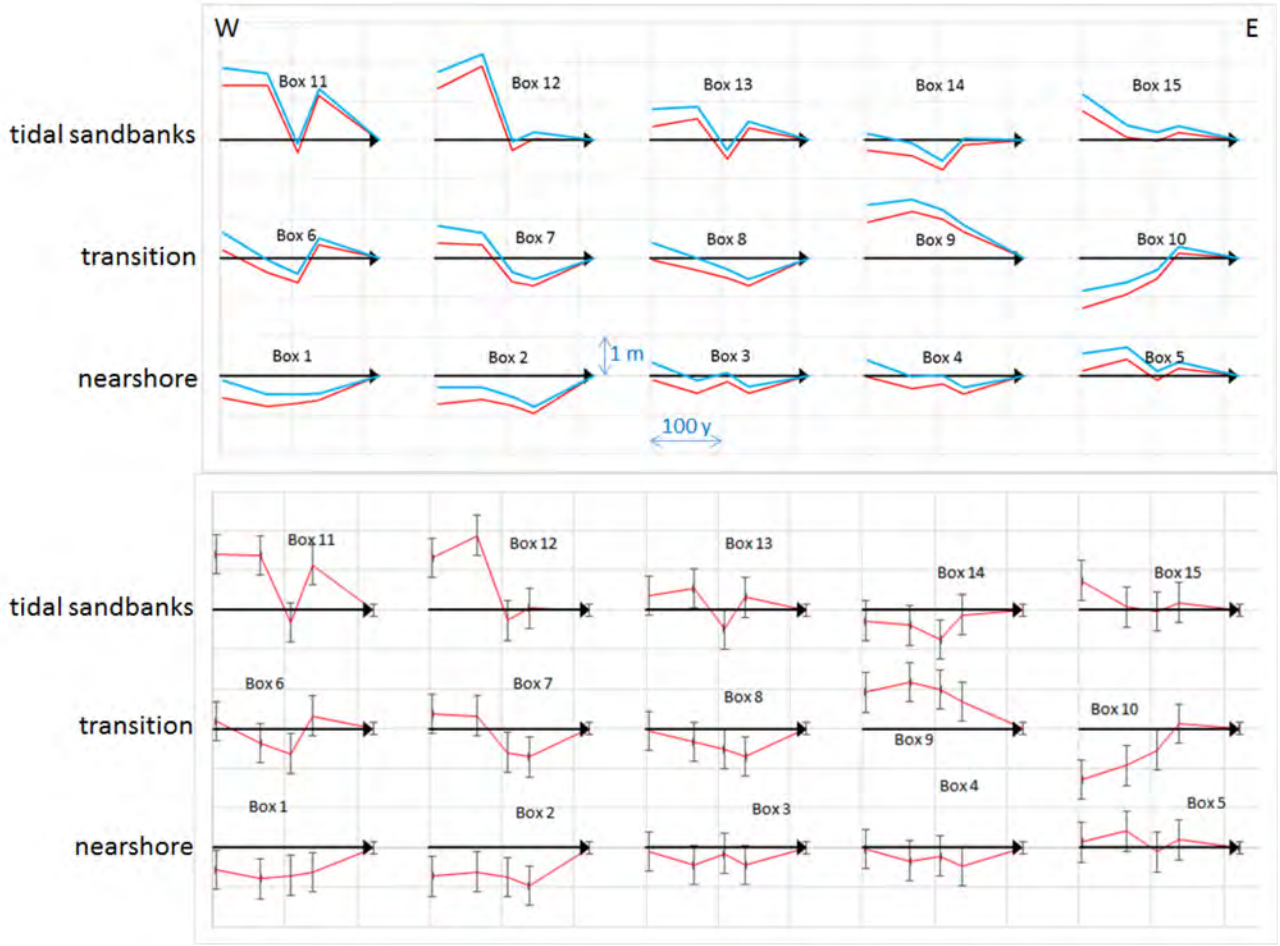

Figure 28 – Time series of volume difference and average bed level difference in all boxes, relative to the EMODnet 2022 bathymetry. Results per box. Average depth corrected for sea level rise. The vertical bars indicate uncertainty.

Table 6 – Volume difference and average bed level difference in all boxes , relative to the EMODnet 2022 bathymetry. Results summed over the box rows and the entire area. Average bed level difference to 2022 with and without correction for sea level rise.

Box	Year	SLR correction	Common area	Common area % of box area	Volume diff. (SLR corrected)	Average depth diff. (SLR corr.)	Average depth diff. (no SLR corr.)
n°		[m]	[ha]	%	[m³]	[m]	[m]
1-5	1804	0.436	72021	100	-226 710 000	-0.31	0.12
1-5	1866	0.312	72045	100	-311 340 000	-0.43	-0.12
1-5	1908	0.228	72056	100	-307 500 000	-0.43	-0.20
1-5	1938	0.168	72047	100	-378 600 000	-0.53	-0.36
1-5	2022	0.000	72057	100	0	0.00	0.00
6-10	1804	0.436	40041	100	57 300 000	0.14	0.58
6-10	1866	0.312	40041	100	17 140 000	0.04	0.35

6-10	1908	0.228	40002	100	-87 300 000	-0.22	0.01
6-10	1938	0.168	40041	100	-16 060 000	-0.04	0.13
6-10	2022	0.000	40041	100	0	0.00	0.00
11-15	1804	0.436	98648	81	705 650 000	0.72	1.15
11-15	1866	0.312	122065	100	882 920 000	0.72	1.04
11-15	1908	0.228	116353	95	-450 710 000	-0.39	-0.16
11-15	1938	0.168	122138	100	434 470 000	0.36	0.52
11-15	2022	0.000	122138	100	0	0.00	0.00
1-15	1804	0.436	210710	90	536 240 000	0.25	0.69
1-15	1866	0.312	234151	100	588 720 000	0.25	0.56
1-15	1908	0.228	228411	98	-845 510 000	-0.37	-0.14
1-15	1938	0.168	234227	100	39 810 000	0.02	0.18
1-15	2022	0.000	234237	100	0	0.00	0.00

Where the boxes have about the same cover by the bed level difference map, the results when using 2022 Flemish Hydrography or 2022 EMODnet as a reference are very similar. The results relative to Flemish Hydrography have more surveys in the nearshore and transition boxes.

Regarding the sea-level rise corrected mean bed level differences, the main findings are listed below:

- Most average bed level differences per box are smaller than 1 metre across all boxes and surveys since 1804. This is almost everywhere within the uncertainty of bed level difference, which can be estimated at $\sqrt{(0.5\ m)^2 + (0.15\ m)^2}$ = 0.52 m ≅ 0.5 m.
- In the nearshore Boxes 1 and 2, in Northern France and at the Belgian West Coast, the bed shallowed up by almost 1 metre. The transition Boxes 6 and 7 have no average depth change while the offshore Boxes 11 and 12 gained over a metre in depth.
- The nearshore Boxes 3-5 at the Belgian Middle and East Coast and the Zeeland-Flemish coast show no trend in depth change.
- The depth increase by about 1 m on average in Box 9 (Transition area, Belgian East Coast) since the 1960s is mainly caused by deepening the navigation channel to the Westerschelde. The offshore Box 14 shallowed by a few decimetres, likely due to dumping of dredge slurry.
- The offshore Boxes 13 (Belgian Middle Coast) and 15 (outer Westerschelde ebb tidal delta) lost sediment, and average depth increased by less than 0.5 m.
- The transition Box 10 (top of Westerschelde ebb tidal delta) accreted by more than a metre. This change is likely related to the natural shift of the ebb tidal delta towards the Westerschelde estuary.

From the results including and disregarding sea-level rise correction, included in the tables, the contribution of sea-level rise correction in the findings can be estimated. Sea-level rise correction enhances the growth magnitudes in the boxes that show shallowing of the sea bed and reduces sand loss in the boxes that undergo erosion (or sediment loss due to dredging). The boxes with the strongest trends remain showing this trend, also when no correction for sea-level rise is applied.

Generalising for the entire analysis area, the main findings are presented below:

- The total change across two centuries is slightly negative (cf. 0.25 m in Table 6) (i.e., taking see level rise correction into account, there was a small loss of sediment), but the change is smaller than the order of magnitude of the uncertainty on the depth soundings (especially the older ones).
- In the western most boxes and in the boxes containing the Westerschelde ebb tidal delta, there is a hint of a systematic trend when going onshore. The most offshore boxes lost sediment, the transition boxes show no change while the nearshore boxes mostly show growth. The offshore loss of sediment however exceeds the onshore gains.

The latter finding can be interpreted as an expression of the seabed adaptation under rising sea level: sediment is pushed onshore. This is not a purely cross-shore shift. The analysis of the contour line movements show a large longshore component in the movement of large-scale bed features, that probably exceeds the cross-shore component.

2.2.6 Discussion

Chapter 2.7 of Dujardin *et al.* (2024) presented the results of a contour line analysis spanning the 1980s to 2022 and only the nearshore area. The main findings were:

- The low-water mark moved tens of metres seawards. This represents natural beach growth at the Belgian West Coast, beach growth around a few newly constructed long groynes and mostly nourishment elsewhere.
- Nourishment is repeated to compensate losses by erosion.
- The lower shoreface (i.e. the shoreface foot area) retreats at most places
- Downdrift and updrift of the outer harbours of Oostende and Zeebrugge, the beach and the upper shoreface expanded seawards by hundreds of metres. Much of the elsewhere eroded sand is caught here. In the western lee, both shoreface and beaches expanded. At the eastern lee, it is primarily the shoreface that accretes. Looking at the large scale, it can be put forward that most of the nourished sand ultimately remains in the active zone.
- Apart from the previous, the sandbank Paardenmarkt off Knokke-Zoute shows landward and eastward accretion.

The analysis presented now expands both the analysis area and the observation period, as inner shelf maps since 1804 have been used.

It was found that in an offshore zone, containing the tidal sand ridges, no systematic movement of the large bedforms has been observed, while in general, this zone may have lost sediment. The loss is of the same order or just exceeds the uncertainty on the data. On the other hand, in an about 7 km wide nearshore zone, containing the shoreface-connected ridges, large and systematic movements of the large-scale bedforms to the east, smaller and systematic onshore movements, and general shallowing, albeit in the order of the data uncertainty, occur. Between the nearshore and the offshore zone, there is an about 4 km wide transition zone where the offshore trends gradually transition into the nearshore trends. In this zone, also the offshore eastwards widening of the sandbank-to-shore distance changes to eastwards nearing. The transition zone shows no systematic change in sand volume.

The alongshore movements of entire sandbanks in the nearshore zone reach up to 5 km over two centuries in the area straddling the French-Belgian border and even 5 km in 60 years when only a thinner segment of the sandbank is involved (Stroombank near Oostende between 1804 and 1866). Furthermore, most shoreface-connected ridges also show an onshore movement component, but at rates that are only 1/5th or less than the alongshore movement rates.

The attachment points of the shoreface-connected ridges to the coast did not shift, probably so since the historic times. Houthuys at al. (2021) put forward the hypothesis that the attachment point of the shoreface-connected ridges may be the point of entry of offshore sand supply to the coast-dune system. A long strip of young coastal dunes, such as at Bray-Dunes – De Panne – Koksijde – Oostduinkerke could thus testify to an alongshore migration of the attachment point of Broers Bank. However, probably since the late Middle Ages, the location of the attachment point seems to have been where it is also now.

There is a weak indication that alongshore and cross-shore movements of large bedforms in the transition and nearshore shore increase in the onshore direction.

Over the two-century observation period, the height of all sand ridges, expressed by the bed level difference between the sandbank crest and the corresponding channel, did not change. Theoretically, starting from a flat bottom shoreface-connected ridges grow in height at the expense of the surrounding channel beds (Nnafie *et al.*, 2014). Such a growth was not observed since 1804. The large-scale bedforms may represent a morphological equilibrium state.

When allowing for sea-level rise and the fact that the charts' reference surface has risen along with it, and also allowing for depth selection bias in the older charts, the observed large-scale volume trends per zone are preserved, but the offshore volume decrease trend is somewhat weakened while the nearshore volume increase trend is in the same degree reinforced. As a result, the amounts of sand loss in the offshore zone become nearly equal to the amounts of sand gain in the nearshore zone.

It is thought that the described 1804-2022 large-scale morphological changes represent natural change, driven by natural hydrodynamic processes combined with the ongoing sea-level rise. A generalised response to sea-level rise seems to be the piling up of sand towards the coast. Such large-scale transfer is widely observed worldwide, also during earlier sea-level cycles documented in geological sediments (Catuneanu, 2006). In the case of the Belgian inner shelf, this is clearly not a purely cross-shore transfer, as the alongshore large-scale bedform movements are even larger than the cross-shore movements.

The receiving area, i.e. the nearshore zone, would under completely natural conditions have migrated inland, i.e. transgression would take place (Catuneanu, 2006). Since the 16th century, the coastline was about at its present position (Houthuys *et al.,* 2021). This is the result of seawalls and groynes stabilising the beach, and embankments protecting the inland lowlands so that they did no longer inundate and sediment was no longer be transferred to the inland part of the coastal plain. The effort to fixate the coastline culminated the last decades in nourishing the beaches, so that overall they even prograded by tens of metres, locally up to 100 m. As a result, accommodation is lost in the nearshore area. Combined with the shoreward long-term movement of sandbanks, this may lead to channel deepening. Channel deepening has effectively been observed in the recent 10-20 years (Houthuys *et al.,* 2022).

Channel deepening may be a temporary stage. If sediment supply from offshore continues, combined with continued nourishments of beaches and shoreface, a stage may be reached where current erosion is outpaced by sediment supply. Then a general sanding up of the nearshore may set in. The volume and time scale of this flipping point is unknown. Idealised and numerical models may give indications of the amounts of time and sediment needed to cause such a large-scale morphological flip.

The large-scale landward shift of Westerschelde's ebb tidal delta, towards the estuary, is also thought to be a response to sea-level rise. The trend reported here to have existed during the last two centuries is probably partly captured in Elias *et al.*'s (2016) subarea k, Vlakte van de Raan, of the Westerschelde. They report erosion in the order of 1 m at the seaward side and sedimentation in the (smaller) landward part, locally exceeding 2 m, between 1964 and 2011. In SW-Netherlands, it was observed that closure of the sea inlets changed the hydrodynamic regime from mixed to wave dominated. The outer delta moved both landwards (i.e. towards the Westerschelde Estuary) and alongshore, northwards. The total volume present in the wide area did not change significantly during the last 50 years. The change in hydrodynamic regime can however not have played at the Westerschelde mouth. Therefore, the large-scale shift reported here is thought to reflect a response to gradual and ongoing sea-level rise.

The human activities near the harbours have a huge impact on the seabed in the wide environment of the activities.

Man has ever tried to improve nautical access. Already around 1804, Stroombank was disconnected from the shoreface at Bredene, probably by dredging. The impact on the beach then is not known. The recovery of Stroombank by 1866 was spectacular. The shallow crest area was extended over a distance of 5 km towards the coast near Bredene, testifying to the large longshore transport. Since the dredging of a new navigation channel, this time crosscutting Stroombank perpendicular to the coast, the shoreface connection area of the sandbank was again and definitively depleted. This may be an important cause of beach erosion in the 20th century in Bredene and De Haan (De Moor, 1991; Houthuys *et al.,* 2022).

The impact of harbour construction and dredging at Zeebrugge is even more far-reaching. It is thought that the first harbour dam constructed around 1900 entailed widespread shallowing of the eastern part of Grote Rede, off Wenduine and Blankenberge, by about 1 m. A scour channel was already present in 1908 at the seaside of the dam, and it had expanded alongshore by 1938. The navigation channel Pas van 't Zand was created across Hard Zand, the local name of the sandbank linking Wenduine Bank to Paardenmarkt, before 1908. Its floor was at least 3 m below the crest of the sandbank. As a result, the crest of Paardenmarkt suffered depletion and was lowered by 2 m between 1908 and 1967.

Even larger-scale change was observed after 1967. It is caused by Zeebrugge Outer Harbour, constructed in 1979-1986, and the deepening of Pas van 't Zand and Wielingen-Scheur by dredging. These works apparently ultimately depleted the surrounding flat seabed areas near Wandelaar, north of Wenduine Bank and near Bol van Heist, where a wide surrounding area deepening by 1 to 2 m, locally near the channels even up to 5 m. The areas at the offshore side of Zeebrugge Harbour dams are subject to stronger currents since the construction of the dams. The morphological adaptation is scour of the seabed. At the same time, seaward accretion was observed at the wide, gently sloping north flank of Paardenmarkt, especially off Heist and Knokke. It is believed that the deepening of Scheur-Wielingen accommodated more of the tidal discharge entering and leaving Westerschelde. Therefore, some sedimentation space was created landward of the main shipping lane. As a result, also Paardenmarkt was restored off Knokke and Zwin to its 1804 (equilibrium) height.

The present results can be further supported by adding a recent bathymetry of the French and Dutch part of the analysis area; by adding intermediate bathymetries, like the nearshore bathymetry of the 1970s and another step around 2000-2010. The evolution of the emerging part of the shore can be included by obtaining the position of the low and high-water mark on 19th and 20th century maps. Furthermore, information of historic dredging work can confirm some hypotheses and changes could be made more quantitative by involving gross dredged volume figures.

2.2.7 Conclusions

The large-scale inner shelf bed morphological evolution of the Belgian inner shelf and the surrounding parts of the French and Dutch territorial waters was studied using the bathymetry of the area charted from 1804 on.

In the offshore part of the inner shelf, containing the tidal current ridges, no systematic movement of the large bedforms has been observed, while in general, this zone may have lost sediment. The loss is of the same order of, or just exceeds, the uncertainty on the data. On the other hand, in an about 7 km wide nearshore zone, containing the shoreface-connected ridges, but excluding the beach, large and systematic movements of the large-scale bedforms to the east, smaller and systematic onshore movements, and general shallowing, albeit in the order of the data uncertainty, occur. Between the nearshore and the offshore zone, there is an about 4 km wide transition zone where the offshore trends grade into the nearshore trends

The attachment points of the shoreface-connected ridges to the coast did not shift, probably so since the historic times. The shoreface base tends to move landwards at rates comparable to the landward shift rate of the shoreface-connected ridges. The height of the nearshore sandbanks did not change, though often both crest and channel appear to have risen over the past two centuries. The entire Westerschelde ebb tidal delta shifted landwards, towards the Westerschelde.

It is thought that the described 1804-2022 large-scale morphological changes represent natural change, driven by natural hydrodynamic processes combined with the ongoing sea-level rise. This would imply that the observed piling up of sand towards the coast would represent a generalised response to sea-level rise .

The receiving area, i.e. the nearshore zone, is not allowed to migrate inland. As a result, accommodation is lost in the nearshore area. Combined with the shoreward long-term movement of sandbanks, this may lead to channel deepening. If sediment piling up near the coast would continue, a tipping point might be reached where general sanding up of the nearshore may set in. The volume and time scale of this tipping point is unknown.

Human interference also triggered important morphological changes. The creation of navigation channels cross-cutting the nearshore sandbanks depleted the downdrift (eastward) part of the affected sandbanks, thus probably also depriving the downdrift beach of sand supply. In the neighbourhood of Wielingen-Scheur and Pas van 't Zand, a wide surrounding area deepened after the 1960s survey by 1 to 2 m, demonstrating the fact that large-scale dredging below the generalised seabed depth also affects the environment. Due to flow constriction, scour channels developed at the seaward side of the new harbour dams that protrude in the nearshore area. At the same time, sedimentation occurs updrift and downdrift of the new harbour dams. Combined nearshore and beach accretion is observed at the updrift (west) side of the outer harbours, while accretion at the downdrift (east) side is also important but only affects the nearshore.

2.3 Estimation of the longitudinal bed transport based on the sanding up of the old navigation channel to Oostende

2.3.1 Introduction

In 2009-2010, a new and deeper navigation channel to Oostende harbour was created by dredging. This "Pas van Stroombank" crosscuts the Stroombank and Kleine Rede channel. Its floor is 1 to 2 m deeper than the Kleine Rede channel floor (Figure 29). The morphological evolution of this channel, at the transition through Stroombank, in relation to the construction and maintenance dredging work was used in MOZES working year 2 to estimate the magnitude of longshore sand transport at that location (Dujardin *et al.*, 2024). In addition, the sanding up after 2009 of the old navigation channel "Rechtstreekse Kil" in the part contained in the yearly nearshore surveys was used to derive a second estimate.

Now, this research is completed by tracking the morphological recovery of Stroombank by the natural transport processes after the old navigation channel "Rechtstreekse Kil" was abandoned. Up to 2009, also Rechtstreekse Kil was maintained as a navigation channel by dredging.

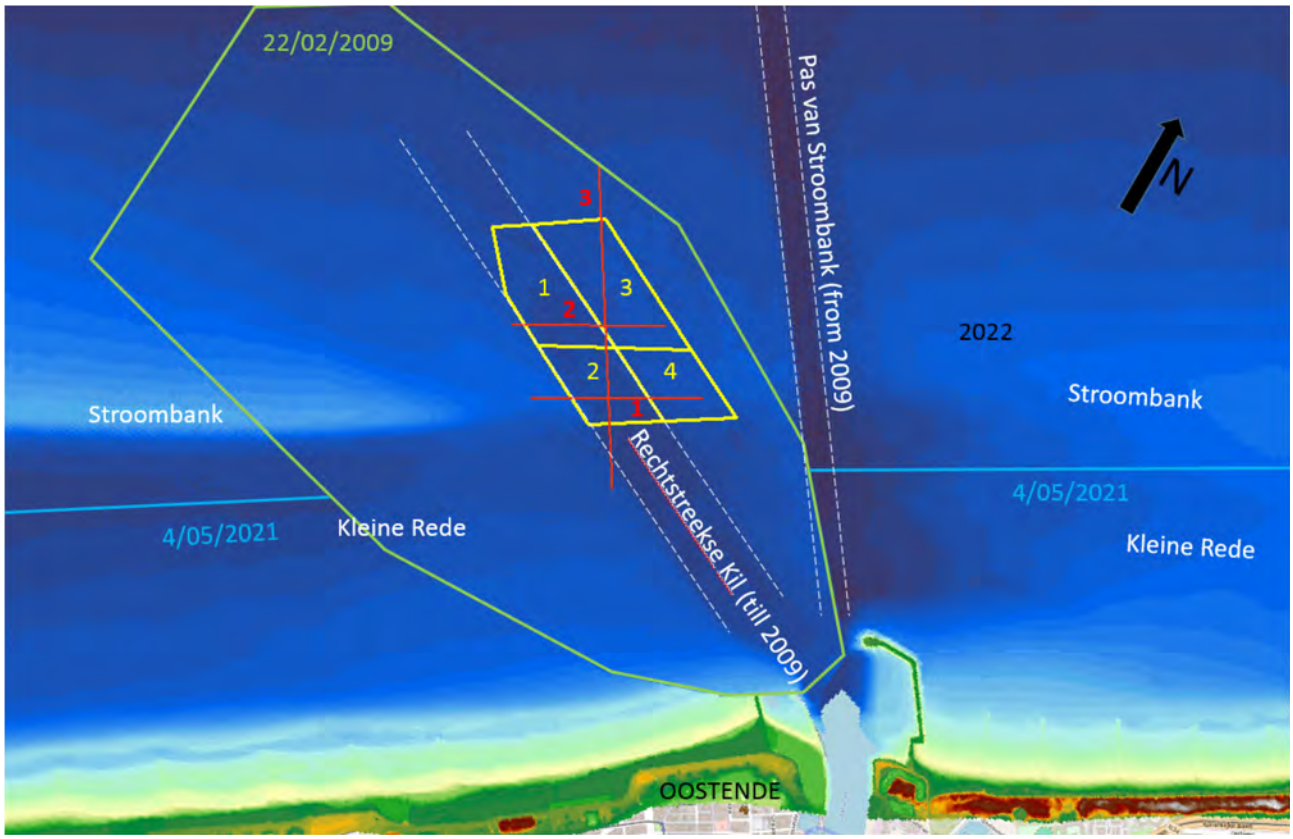

Figure 29 – Locaton of the old navigation channel Rechtstreekse Kil and the new Pas van Stroombank , created in 2009-2010.

Background is 2022 bathymetry (northern part). Nearshore bathymetry from 4/05/2021. The background is covered by the 22/02/2009 bathymetry, inside the green polygon. White dashed lines show the navigation channels. Yellow boxes are areas of volume difference calculation, namely the areas of largest morphological change. Red lines are cross profiles.

2.3.2 Data used

The following surveys are available and were kindly put at our disposal by Flemish Hydrography (Table 7). Like requested, the points were projected to Lambert 72 and the depths converted to TAW.

The depths were converted to elevations in TAW (depth negative). The rasters are available in the project folder P:\20_079-MorfoInteract\3_Uitvoering\Deeltaak1_DataAcquisition\MorphAnalysis.

More DEMs were available from the study of the longshore transport in work year 2: 15/02/2014, 15/10/2014, 30/06/2024 (all three also 1 m rasters) and also the 2022 10 m raster from the Flemish Hydrography mosaic was used.

Table 7 – Surveys used in the analysis.

Data file name	Survey period	Name of 1 m raster
090200_RO_MB_300_TAW.txt	20/02/2009 – 24/02/2009	G_090222_RO
090000_RO_MB_300_TAW.txt	29/05/2009 – 13/06/2009	G_090608_RO
091000_RO_MB_300_TAW.txt	22/10/2009 – 28/10/2009	G_091025_RO

091200_RO_MB_300_TAW.txt	09/12/2009 – 15/12/2009	G_091212_RO
100500_RO_MB_300_TAW.txt	13/05/2010 – 21/05/2010	G_100517_RO
110500_RO_MB_300_TAW.txt	08/05/2011 – 19/05/2011	G_110513_RO
110800_RO_MB_300_TAW.txt	15/08/2011 – 17/08/2011	G_110816_RO
120200_RO_MB_300_TAW.txt	06/02/2012 – 11/02/2012	G_120209_RO
121100_RO_MB_300_TAW.txt	07/11/2012 – 15/11/2012	G_121111_RO

2.3.3 Analysis

Visual analysis of successive bathymetries

The abandoned channel "Rechtstreekse Kil" was filled fast, during the first months after abandonment, but only partially, i.e. until the bed level of the surrounding flow channels. Stroombank rebuilded much slower; this took several years. Up to 2017, a slight depression was visible in the crest of Stroombank.

The crest part of Stroombank situated between the former Rechtstreekse Kil and the new Pas van Stroombank accreted to a depth comparable to the crest west of the abandoned navigation channel, but lowered again afterwards. It is thought that sediment is dragged into the new, deeper Pas van Stroombank and removed there by dredging.

Longshore transport estimate from volumetric analysis

Four delimited areas (boxes) were defined to study the volume and depth change, as proxies for longitudinal sediment transport (Figure 29). Box 1 and Box 2 are segments of the former navigation channel "Rechtstreekse Kil". Box 1 is on the intersection of Rechtstreekse Kil with the seaward flank of Stroombank. Box 2 is at the intersection of Rechtstreekse Kil with the crest area of Stroombank. Box 3 is east of Box 1, with about the same alongshore length. This area might recuperate if box 1 is completely sedimented up. Box 4 is east of Box 2, with also about the same alongshore length. In addition, the former crest area might morphologically recover if Box 2 is full.

In Figure 30 and Table 8, the volume, mean depth and derived alongshore transport are shown over time starting in 2009, the year of the shut-down of dredging maintenance work in the old channel.

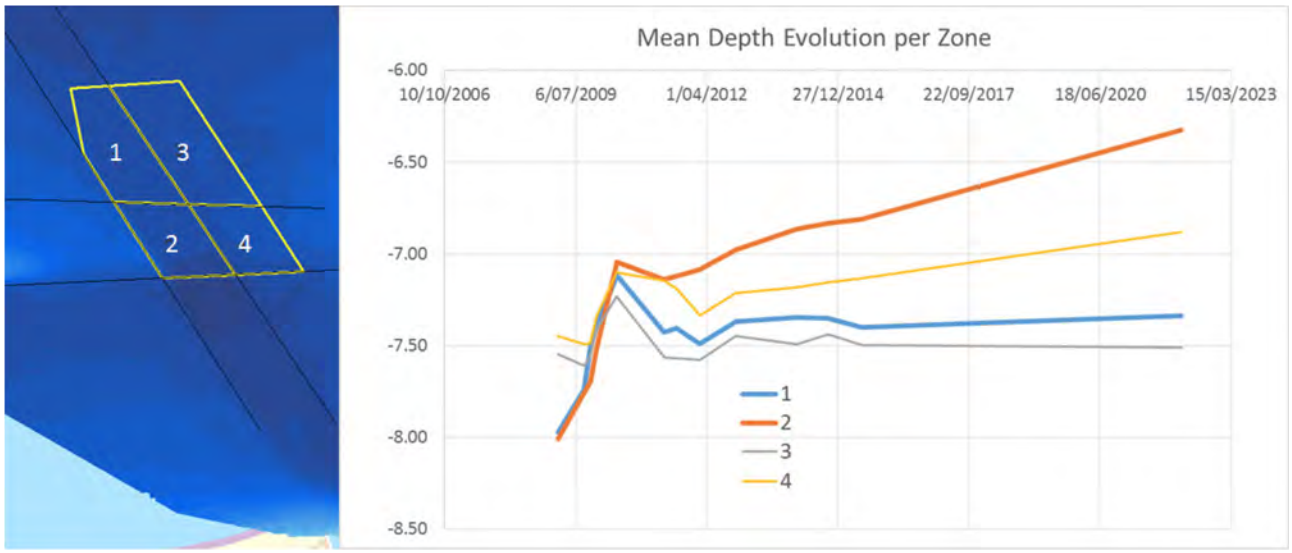

Figure 30 – Plot of mean depth versus time, per box.

The volumes and mean depths in Boxes 1 and 2 reached a temporary maximum in May 2010, only 15 months after the first survey. In box 1, the depth increased afterwards by about 0.4 m. This is explained by two events: in May 2010, a medium dune field passed through Box 1, resulting in a temporary supply of sand. Around that time, intensive dredging took place to create and deepen the new Pas van Stroombank. The creation of accommodation space likely has attracted sediment from the environment, explaining the increase in depth seen in all boxes at that time. It can be concluded that the old channel was already filled within 15 months after the first survey. When taking the across-shore width of Boxes 1 and 2 into account (Table 8), the alongshore the overall sedimentation rate over this period can be estimated: 226 (Box 1) to 285 (Box 2) $m^3/m/yr$. Afterwards, from 2011 to 2022, a slow accretion rate persisted in Box 2: 28 $m^3/m/yr$. This corresponds to the slow but continuing rebuilding of Stroombank's crest area. Possibly, this process will continue after 2022. A similar evolution is observed in Box 4, but at an even lower rate: 11 $m^3/m/yr$. From Box 4, possibly some sediment is attracted into the space of the new Pas van Stroombank.

The initial quick fill of Box 2, by 285 $m^3/m/yr$, is interpreted to reflect trapping of the net longshore transport. Theoretically, the fill can also have trapped longshore transport from the east. However, due to the presence of the new and deeper Pas van Stroombank, it is believed that this channel trapped most of the east-originated longshore transport, also back then. The value is furthermore considered to reflect the net eastwards longshore transport over Stroombank, as the old channel floor was between 0 and 0.5 m above the floor of Kleine Rede, so that an influx of fluid mud from Kleine Rede into this area is unlikely.

Table 8 – Volume trends per box. Note different calculation period per box. Box 3 has mostly no change.

	From	To	Trend [m/yr]	Error on trend [m/yr]	Trend [m³/yr]	Box across-shore width [m]	Along-shore trend]m³/m/yr]	Box area [m²]	Error on volume [m³]	Error on along-shore trend [m³/m/yr]
box 1	22/02/2009	17/05/2010	0.72	0.09	124280	550	226	172652	36257	54
box 2	22/02/2009	17/05/2010	0.77	0.13	99818	350	285	129485	27192	63
box 2	13/05/2011	2/03/2022	0.08	0.00	9728	350	28	129485	27192	7
box 4	13/05/2011	2/03/2022	0.03	0.01	3639	330	11	115536	24263	7

The error on bed level difference is the standard error on bathymetric depth (0.15 m) x square root of 2 = 0.21 m. The error on volume difference is this value times the box area.

Longshore transport estimate from profiles

Three profiles were created to study in more depth the volume and depth change, as proxies for longitudinal sediment transport (Figure 29). Profile 1 is coast-parallel and crosses the old navigation channel "Rechtstreekse Kil" at the crest of Stroombank. Profile 2 is also coast-parallel but it crosses Rechtstreekse Kil at the north flank of Stroombank. Profile 3 is coast-normal and allows visualizing the recovery of Stroombank after the abandonment of Rechtstreekse Kil.

Profile 1 (Figure 31) shows the overall Stroombank crest slope down towards the east. The overall change is a long-term adaptation of the sandbank's shape in response to the dredged navigation channels, first Rechtstreekse Kil, then, from 2009 on, Pas van Stroombank (a few 100 metres east of the profile). The floor of Rechtstreekse Kil was about 1.5 m lower than the crest of Stroombank at the west side of the channel, and about 1 m lower at the east side. The profile shows a fast shallowing of the channel, by about 1 m, between 22/02/2009 and 17/05/2022. The unit volume accretion over the 532 m wide channel is 354 m³ in 1.23 year or 288 m³/yr $\pm$ 112 m³/yr (the error estimation uses the error on bed level difference of 0.21 m).

The further evolution shows dynamic beds: all surveys display medium dunes. They are the morphological expression of active bed transport. As the dunes' steepest slope is at their east side, they travel from west to east, towards Pas van Stroombank. Note that the 2022 profile was derived from a 10 m raster that probably smoothed the dunes out.

Profile 2 (Figure 32) shows the old channel to be 1 m deeper than Stroombank's north flank at the west and 0.5 m at the east. The profile underwent very fast fill between 22/02/2009 and 17/05/2010. The latter survey is the shallowest bed observed here. The unit volume accretion over the 400 m wide channel is 417 m³ in 1.23 year or 339 m³/yr $\pm$ 84 m³/yr. The May 2010 profile has a peculiar shape. A medium-dune field passed by over the area during that survey. Afterwards, the area lost sediment, likely towards Pas van Stroombank due to the construction and maintenance dredging going on there. The estimate of 339 m³/yr is likely an overestimation of the longshore transport as the May 2010 bed was never reached again afterwards.

Interpreting both results, it is concluded that both at the seaward flank and at the crest of Stroombank, the longshore near-bed sediment transport can be estimated at 280 $\pm$ 80 m³/m/yr during the initial abandonment stage of Rechtstreekse Kil. The profiles also demonstrate that most (or all) of the sediment that moves through the area is sourced in the west. This is in agreement with the fact that the new and deeper Pas van Stroombank, located east of Rechtstreekse Kil, probably traps most (or all) of the east-sourced longshore transport. It can thus be assumed that the 2009-2010 derived fill rater of the abandoned channel provides a reliable estimate of the net (west to east) longshore transport.

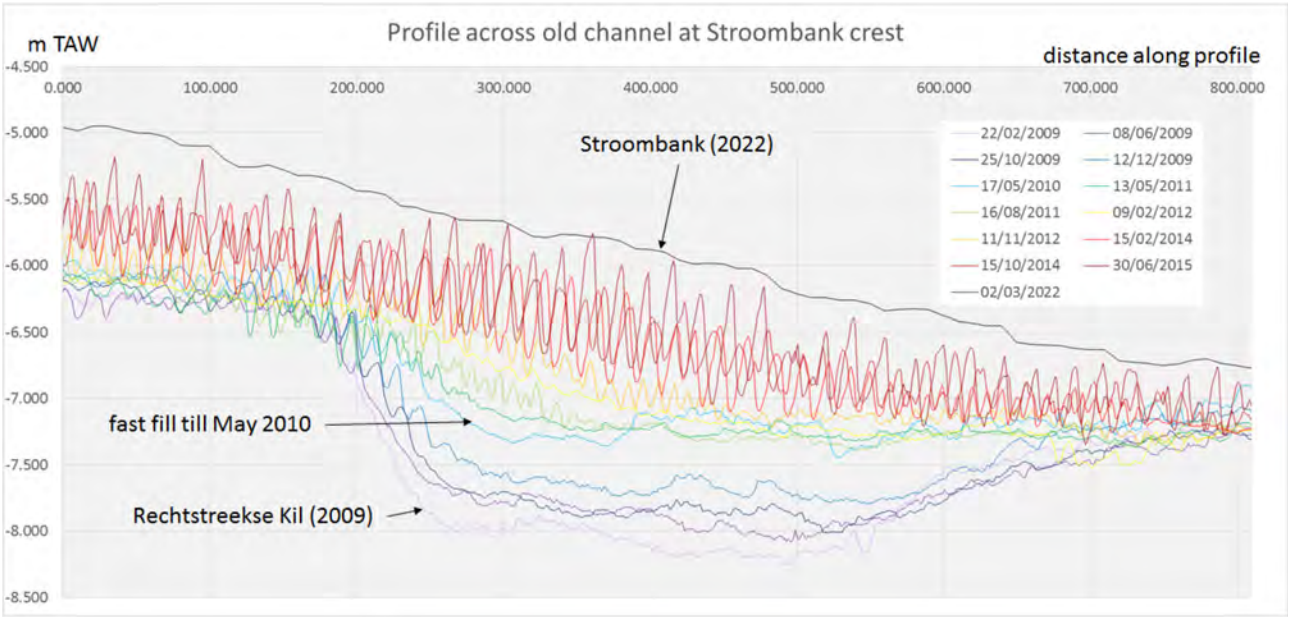

Figure 31 – 2009-2022 bed profiles of Profile 1, across Rechtstreekse Kil at crest of Stroombank (west is left).

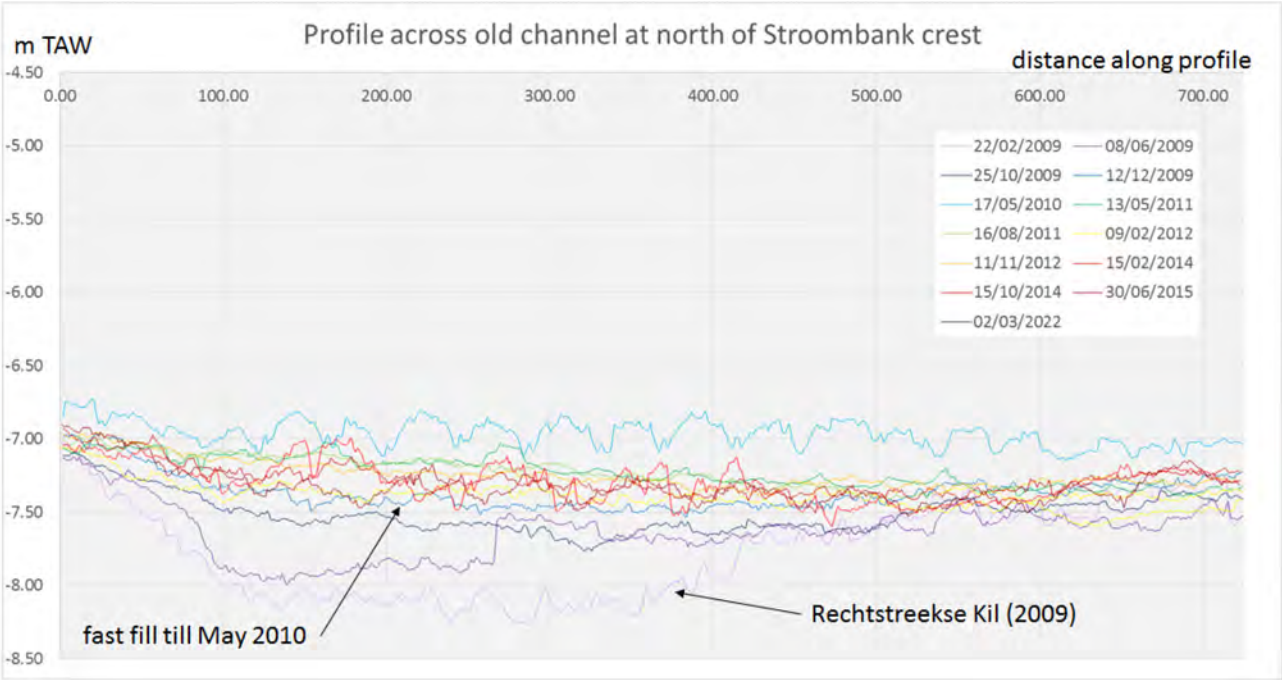

Figure 32 – 2009-2022 bed profiles of Profile 2, across Rechtstreekse Kil at north flank of Stroombank (west is left).

Profile 3 (Figure 33) illustrates the recovery of Stroombank in a coast-normal profile. This profile cannot be used for longshore sediment estimates, but it shows clearly some important morphological features:

- the fast initial fill of the abandoned channel
- the bed anomaly on the north flank of Stroombank at the May 2010 survey
- the subsequent recovery of Stroombank as a positive bed feature. The rebuilding had a stage of medium to large dunes. There is a time gap between 2015 and 2022, but it can be assumed that recovery has been going on steadily over this period.

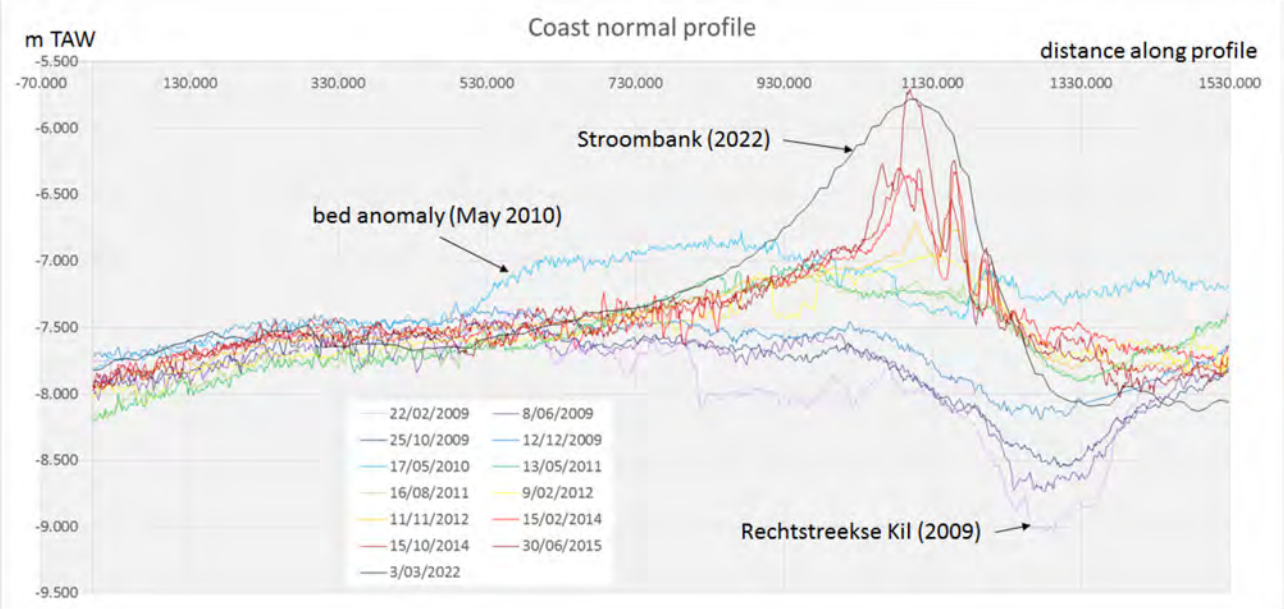

Figure 33 – 2009-2022 bed profiles of Profile 3, perpendicular to the coast (north is left) showing the recovery of Stroombank.

2.3.4 Discussion and comparison with previous estimates

The present study showed that both at the seaward flank and at the crest of Stroombank, the total longshore near-bed sediment transport can be estimated at 280 $\pm$ 80 m³/m/yr during the initial abandonment stage of Rechtstreekse Kil, when it can be assumed that most bed transport is trapped in the abandoned channel. As explained above, the 2009-2010 fill of Rechtstreekse Kil in Box 2 is argued to be almost exclusively sourced from the west, along the crest of Stroombank. Therefore, the fill rate is thought to be a good estimate of the nest west-to-east longshore transport.

In the previous working year, an estimate of the longshore sediment transport was carried out at two sites (Dujardin *et al.,* 2024).

The first site used the frequent bathymetric surveys in relation to the construction and maintenance dredging work of the new navigation channel Pas van Stroombank at the crossing of Stroombank. The transport was estimated at about 100 m³/m/year using a first 9-month period. Another value was obtained over a later 7-month interval and was about 75 m³/m/year. These estimates were obtained from observations from 2014 and 2015.

The second site was the abandoned crossing of Rechtstreekse Kil through the tidal channel Kleine Rede. The fast fill in 2009 to 2010 yielded an estimate of the longitudinal bed transport in Kleine Rede of about 300 to 500 m³/m/year. The large value may contain a contribution of (fluid) mud, while the transport on Stroombank is thought to be fully sand.

Modelled results are in the same order of magnitude as the results derived in the previous working year. Transport rates at the Stroombank crossing are about 70 to 145 m³/m/year in Scaldis-Coast and 95 m³/m/year in Flemco. Calculations in Kleine Rede are about 120 m³/m/year in Scaldis-Coast and 185 m³/m/year in FlemCo.

At the level of Stroombank crest, a gradient in longshore transport is observed (Figure 34). After analysis of the morphological evolution of the repair of Stroombank at the ancient crossing of Rechtstreekse Kil, where it appeared that repair of Stroombank crest continued at least until 2022, and thus intercepted part of the longshore transport over Stroombank crest that can in this period of repair not have contributed to the sand volumes trapped in Pas van Stroombank, the estimates found there in 2014 to 2015 must be interpreted as underestimations.

To put the estimation in a wider perspective: under the assumption that the estimate is valid for a 1500 m wide, coast-normal transect, the values of 280 to 500 m³/m/year would result in a total trapped near-bed longshore transport of 4.2 to 7.5 10^5 m³/year.

It can be concluded that both values found for the fast 2009 to 2010 fill of Rechtstreekse Kil, both in the deepest part of the Kleine Rede crossing as at the crossing of Stroombank crest, are realistic estimates of the longshore transport (Figure 34). These are roughly double the order of magnitudes found in the transport models.

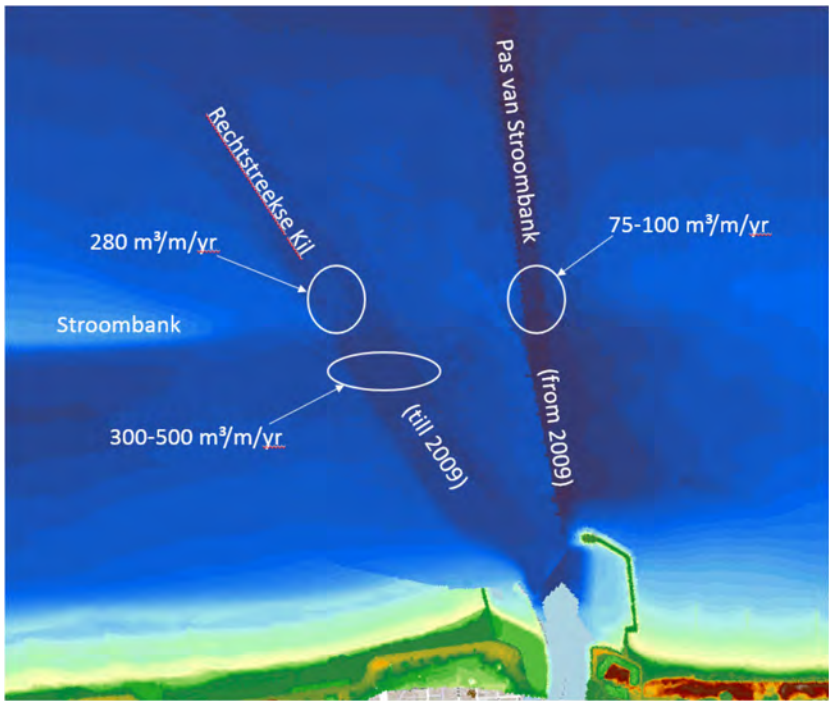

Figure 34 – Schematic map of longshore transport estimates (same bathymetry as in Figure 26).

2.4 Conclusion

Vectorisation of old topo-bathymetric maps continued in the 3rd working year. An additional inner shelf cover for 1974-1978 has been realised. The Spring 1992 beach maps were finalised to produce a complete cover of the Belgian coast. In addition, the Autumn 1989 and March 1990 nearshore bathymetry of the eastern part of the Belgian nearshore was vectorised, as well as the corresponding part of the Autumn 1989 beach topography.

Bathymetric rasters of the Belgian inner shelf and the surrounding parts of the French and Dutch territorial waters were also vectorised from 1804, 1866, 1908 and 1938 small-scale navigation maps. The sometimes-

sparse data were modelled taking knowledge of the present bed morphology into account. This data set, complemented with the 1960s, 1980s and 1990s inner shelf bathymetries, allow to study the large-scale seabed evolution over the last two centuries.

In the offshore part of the inner shelf, containing the tidal sand ridges, no systematic movement of the large bedforms has been observed, while in general, this zone may have lost sediment. The loss is of the same order or just exceeds the uncertainty on the data. On the other hand, in an about 7 km wide nearshore zone, containing the shoreface-connected ridges, large and systematic movements of the large-scale bedforms to the east, smaller and systematic onshore movements, and general shallowing, albeit in the order of the data uncertainty, occur. Between the nearshore and the offshore zone, there is an about 4 km wide transition zone where the offshore trends gradually transition into the nearshore trends

The attachment points of the shoreface-connected ridges to the coast did not shift, probably so since the historic times. The shoreface tends to move landwards at rates comparable to the landward shift rate of the shoreface-connected ridges. The height of the nearshore sandbanks did not change, though often both crest and channel appear to have risen over the past two centuries. The entire Westerschelde ebb tidal delta shifted landwards, towards the Westerschelde.

It is thought that the described 1804-2022 large-scale morphological changes represent natural change, driven by natural hydrodynamic processes combined with the ongoing sea-level rise. A generalised response to sea-level rise seems to be the piling up of sand towards the coast.

The receiving area, i.e. the nearshore zone, is not allowed to migrate inland. As a result, accommodation is lost in the nearshore area. Combined with the shoreward long-term movement of sandbanks, this may lead to channel deepening. If sediment piling up near the coast would continue, a flipping point might be attained where general sanding up of the nearshore may set in. The volume and time scale of this flipping point is unknown.

Human interference also triggered important morphological changes. The creation of navigation channels cross cutting the nearshore sandbanks depleted the downdrift (eastward) part of the affected sandbanks, thus probably also depriving the downdrift beach of sand supply. In the neighbourhood of Wielingen-Scheur and Pas van 't Zand, a wide surrounding area deepened after the 1960s survey by 1 to 2 m, demonstrating the fact that large-scale dredging below the generalised seabed depth also affects the environment. Due to flow constriction, scour channels developed at the seaward side of the new harbour dams that protrude in the nearshore area. At the same time, sedimentation occurs updrift and downdrift of the new harbour dams. Combined nearshore and beach accretion is observed at the updrift (west) side of the outer harbours, while accretion at the downdrift (east) side is also important but only affects the nearshore.

The abandonment of the old navigation channel to Oostende crosscutting Stroombank in 2009 allowed to obtain another measure for the average longshore sediment transport at the intersection of the channel with Stroombank crest. An estimate of 280 $\pm$ 80 m³/m/yr was obtained. It is thought to be a better estimate of the net longshore transport than 75 to 100 m³/m/yr found earlier based on morphological change in 2014-2015 in the new navigation channel Pas van Stroombank, as it appeared that repair of Stroombank crest continued at least until 2022, and thus intercepted part of the longshore transport over Stroombank crest. The result also compares well to the earlier estimate of 300 to 500 m³/m/yr at the crossing of Kleine Rede.

3 Numerical modelling

3.1 Coupled shelf-shoreline model morphodynamics: idealized model study (WP2)

3.1.1 Introduction

Shelf ridges

The inner shelf of Belgium features a field of large-scale rhythmic sand ridges, known as shoreface-connected sand ridges (hereafter referred to as sfcr). These ridges are highly oblique to the shoreline, with their seaward ends displaced several kilometres southwest relative to their landward ends (Figure 35a, refer also to Chapter 1). Sfcr have spacings of 10-20 km between successive ridges, lengths of 15-30 km long, widths of 2-5 km, heights of 5-10 m and they migrate alongshore at speeds of several meters per year in the northeast direction. Similar ridges are also observed on other sandy inner shelves that are frequently impacted by storms, such as along the Dutch coast (Van de Meene et al., 1996), the German coast (Antia 1996), the East Coast of the United States (Duane et al. 1972; Swift and Freeland, 1978), and in Argentina (Parker et al., 1982). The typical orientation of sfcr is related with the direction of storm-driven currents, which, on the Belgian shelf, are directed predominantly to the northeast. This suggests that sfcr evolve during storms, when high waves and strong storm-driven currents cause significant erosion and transport of sand (Swift et al. 1978).

Further offshore on the Belgian outer shelf are tidal sand ridges (tsr). Although these ridges share similar horizontal dimensions with sfcr, they differ in orientation: their seaward ends are displaced several kilometres northeast relative to their landward ends (Figure 35a). These ridges are typically found on outer shelves characterised by meso- and macro-tidal conditions, such as those of the East China Sea (Li et al. 2001; Liu et al. 2007) and the Celtic Sea (Belderson et al., 1986). The alignment of tsr relative to the shoreline is related the direction of the dominant tidal current, which on the Belgian shelf is directed alongshore. This alignment is such that ridge crests and channels are rotated counter-clockwise (clockwise) relative to the tidal current in the Northern (Southern) Hemisphere (Huthnance 1982; Dyer and Huntley 1999; Swart and Yuan 2019). Other differences between tsr and sfcr are that the former ridges hardly migrate on the shelf (see Chapter 1) and that they are much higher (up to 20 m). Figure 35a further shows that on the Belgium shelf other sand ridges are present between sfcr and tsr, which are oriented nearly parallel to the shoreline. These ridges deviate from the typical orientation of sfcr and tsr described earlier.

The formation mechanism of sfcr was first explained by Trowbridge (1995) (see the review by Ribas et al., 2015). According to this mechanism, a ridge aligned up-current relative to the alongshore storm-driven flow induces an offshore deflection of this flow due to mass conservation. The sloping seabed leads to sediment convergence over the ridge, promoting ridge growth. Huthnance (1982) was the first to provide a physical explanation of the initial formation of tsr. He argued that the crucial aspect for the formation of tsr is the deflection of the tidal current over the ridges, allowing net sediment accumulation above the crests. This deflection results from the combined effect of the background tidal current and a residual current generated by tide-topography interaction (Zimmerman 1980). The sources of the residual current are frictional and Coriolis torques (see the review by Swart and Yuan, 2019).

Studies so far (see the review by Ribas et al., 2015) have indicated that mainly waves and storm-driven currents are primarily responsible for the morphodynamic evolution of sfcr. Previous literature focus on sfcr in micro-tidal conditions, thus neglecting the effects of tides. Since the Belgian shelf is characterised by meso- to marco-tidal conditions, tidal impact on the morphodynamic evolution of sfcr remains unexplored.

Impact of shelf ridges on shoreline morphodynamics

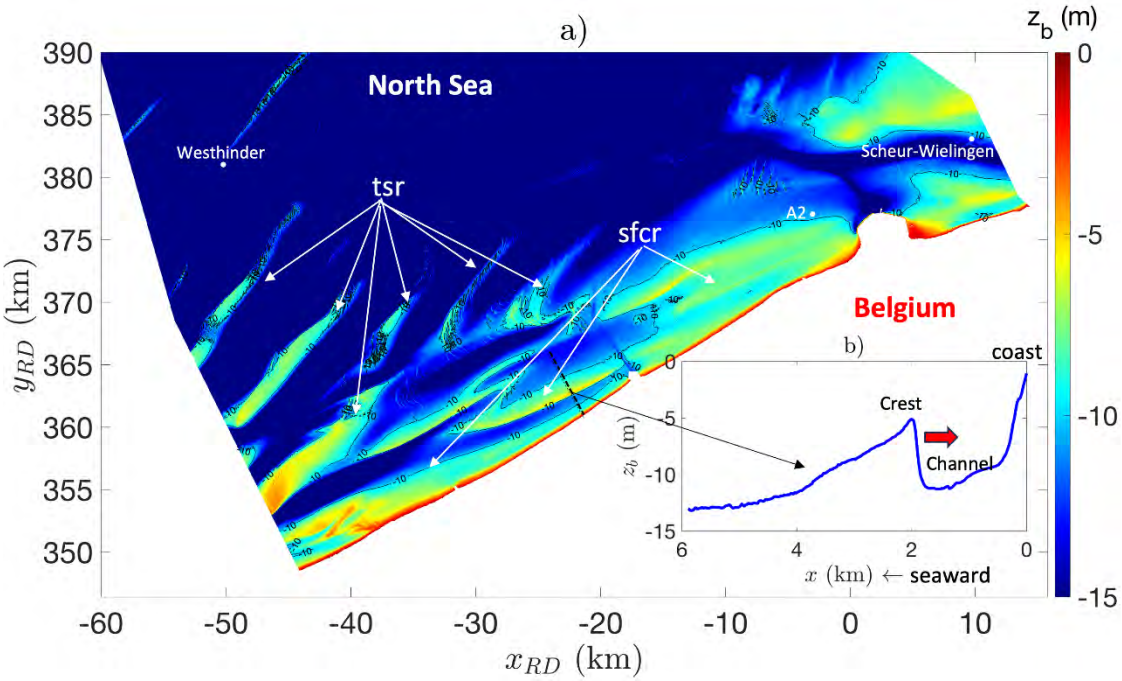

Figure 35 –a) Bathymetric map (in m with respect to mean sea level, MSL), showing fields of shoreface-connected sand ridges (sfcr) and the more offshore located tidal sand ridges (tsr). White dots denote the locations of measuring stations ("Westhinder", "A2" and "Scheur-Wielingen") used to derive wave, wind and tide forcing data. b) Bathymetric profile along the transect depicted in panel a (dashed black line). The transect crosses a ridge known as "Stroombank". The thick red arrow highlights the observed onshore migration of this ridge and its neighbouring channel.

Previous modelling studies (Xu 2015; Safak et al. 2017; Nnafie et al. 2021) have indicated that sfcr act as a forcing template for shoreline morphodynamics: the ridges influence onshore wave propagation, creating alongshore gradients in the sediment transport within the nearshore zone and consequently impacting the decadal shoreline evolution. Verwaest et al. (2022) and Dujardin et al. (2023) analysed bathymetric data spanning several decades in the Belgian coastal zone and reported that shoreline progradation predominantly occurs near the crests of the landward ends of the sfcr, while retreat is observed near the channels between the ridges and the coast (Figure 35b).

Furthermore, the analysis of the historical bathymetric maps presented in Chapter 1, revealed that, besides an alongshore migration, sfcr are also migrating landward, at rates of about 1 meter per year. This onshore migration raises concerns about the potential for increased impact on the decadal evolution of the Belgian shoreline in the proximity of these ridges and channels. Additionally, the growing demand for sand extraction from shelf ridges in recent decades (Van Lancker et al. 2010), along with the expansion of coastal infrastructures, coastal protection works, and the construction or deepening of navigation channels, may further amplify this impact on Belgian shoreline morphodynamics.

To quantify potential impacts of onshore and alongshore migrating sfcr on the decadal evolution of the Belgian shoreline, a coupled shelf-shoreline model is being developed within the MOZES project.

This coupled model integrates a shelf model (Delft3D+SWAN) with a shoreline evolution model (Arriaga et al. 2017). In the first two years of the MOZES project, this coupled model was applied to the Belgian coast, where a synthetic field of morphostatic sfcr (i.e., the ridges and the shelf bathymetry did not evolve during the simulation) was placed on the shelf (Dujardin et al. 2023). Simulations with this model suggested that the observed onshore movement of ridges on the Belgian shelf is likely to enhance shoreline retreat near the channels and progradation near the ridge crests. A key limitation in that model, however, was the exclusion of tidal sand ridges on the shelf, which might also impact shoreline evolution on decadal scales. Another limitation was the assumption of a morphostatic shelf model, where the sfcr remained "frozen" during the simulation. This assumption implies a one-way coupling between the shelf and nearshore models, meaning that the shelf morphology influences the bed level of the nearshore zone and the shoreline, but not the other way around. Finally, another limitation was the use of a single sfcr on the shelf, whereas on the Belgian shelf, three sfcr are located (Figure 35, see also Chapter 1). The use of more sfcr might induce non-linear interactions between the shoreline undulations induced by the individual ridges.

Study aims

The considerations outlined above motivated the specific objectives of year 3 within Workpackage 2 (WP2) of the MOZES project, which are divided among activities 1 and 2 (Figure 36). The overall objective in Activity 1 is to further refine the coupled shelf-shoreline model by implementing a ridge configuration resembling that of the Belgian shelf, whereby multiple sfcr and tsr are present on the shelf. The specific objectives are threefold: the first is to investigate the extent to which sfcr and tsr act as a forcing template for the decadal morphodynamic evolution of the nearby shoreline. The second is to assess the relative impacts of sfcr and tsr on this evolution. Finally, the third objective is to quantify how shoreline undulations depend on the position of the shelf ridges relative to the shoreline.

In Activity 2, the overall objective is to further develop the morphodynamic shelf model. The specific objectives are to 1) incorporate a wind climate more representative for the Belgian shelf and 2) to include tides in the shelf model.

It is important to emphasise that the goal of this study is not to reconstruct the morphodynamic evolution of the sfcr and tsr on Belgian shelf and the adjacent shoreline over recent decades, but rather to gain fundamental insights into the effects of onshore migrating sfcr on the shoreline and the influence of tides on the shelf ridges. To achieve this, an idealised modelling approach is employed, in which the tides, waves, bathymetry and ridge configuration are schematised and serve as first-order approximations of reality.

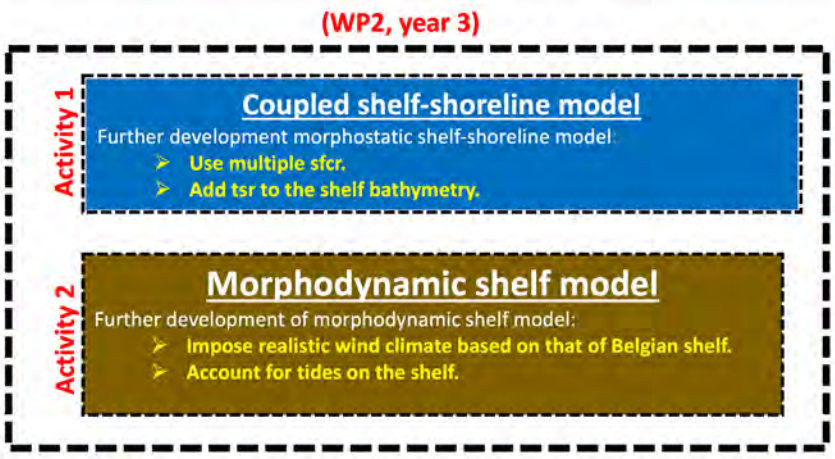

Figure 36 – Block diagram showing the steps toward the improvements of the existing coupled shelf-shoreline morphodynamic model (Activity 1) and the morphodynamic shelf model (Activity 2) to be used in the Mozes project. The activities within Work Package 2 (WP2) in the third year of the Mozes project are also shown (indicated by yellow text).

3.1.2 Schematising wind and tide

Wind

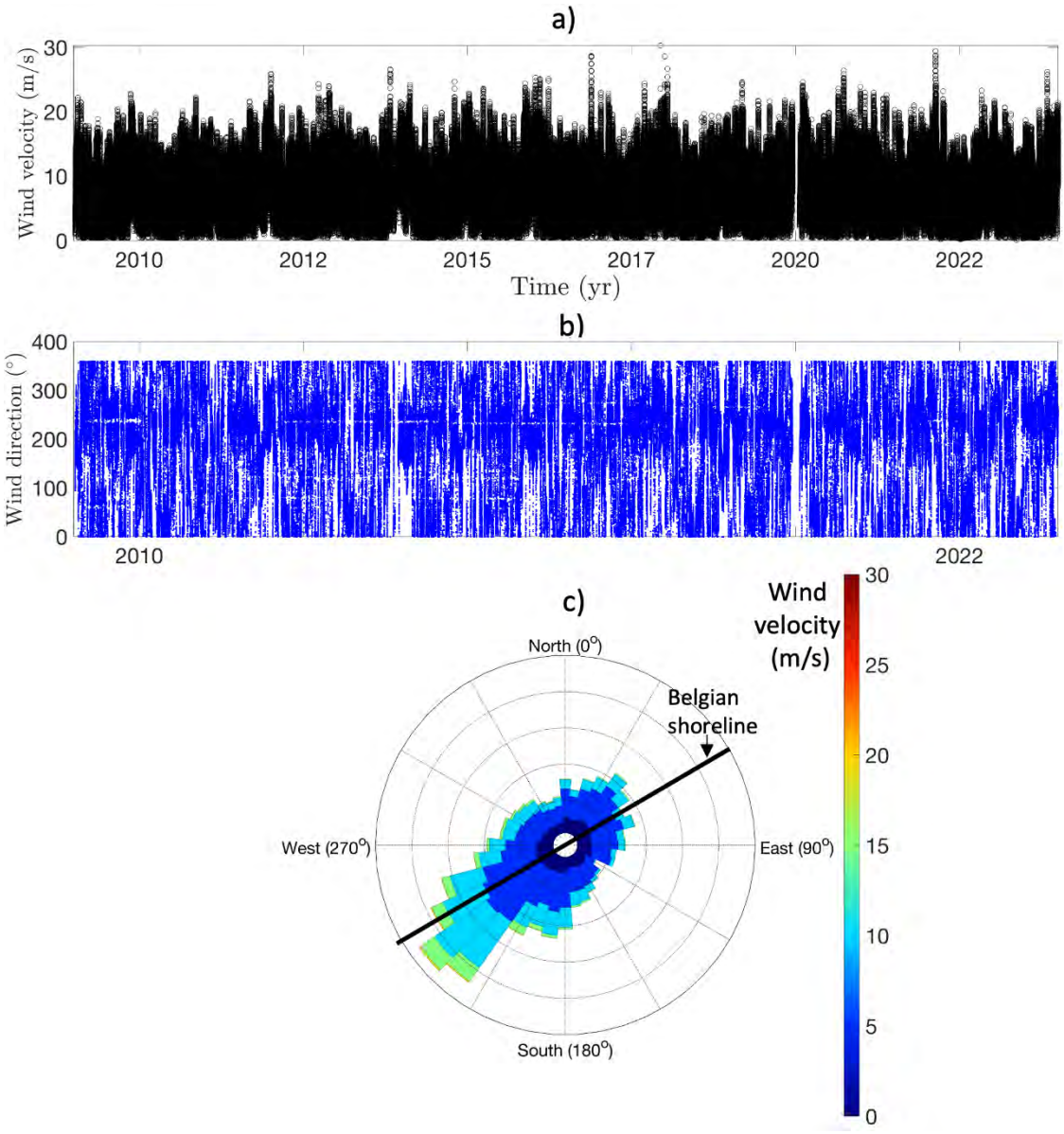

Figure 37 – Wind climate on the Belgian shelf, showing a) wind velocities (m/s), b) wind directions (°) with respect to geographic north (positive clockwise) and c) the corresponding wind rose. The thick black line in panel c indicates the orientation of the Belgian shoreline (Strypsteen, Houthuys, and Rauwoens 2019). These data, collected from 2009 to 2023 at the "Westhinder" buoy (location shown in Figure 35a), were obtained from the "Meetnet Vlaamse Banken", accessible at https://meetnetvlaamsebanken.be/.

To derive a representative wind climate to force the morphodynamic shelf model (Activity 2), time series of wind conditions over a period between 2009 and 2023 at the "Westhinder" buoy are analysed. Results are shown in Figure 37, which depicts wind velocities (b), wind directions (b) and the corresponding wind rose (c). This analysis clearly indicates that winds from the southwest are the most frequent, occurring 43% of the time, and align almost parallel to the shoreline (indicated by the thick black line). The majority of stormy conditions also originate from the southwest. Other wind conditions and their corresponding probabilities of occurrence are summarised in Table 9.

Utilizing these time series, synthetic wind time series of V_w and Φ_w are constructed following the same methodology used by to generate synthetic time series for waves. First, the probability of occurrence (in %) of wind events belonging to distinct classes of wind velocities V_w and wind angles Φ_w was computed. Results are shown in Table 9. This wind climate classification was then employed to create a 2000-year long synthetic time series of randomly occurring wind events. Specifically, the probabilities of occurrence for various wind classes determined the number of days each class of wind events would occur within the 2000-year simulation period (maximum duration of the experiments). The assumption made here was that each wind event lasts for one day. Each wind event was assigned the mean values of its corresponding wind class. To mimic the stochastic nature of a realistic wind climate, all the wind events were randomly distributed across the 2000-year interval, assuming no correlation between individual wind events. The resulting synthetic time series is presented in Figure 38. The wind events in these time series follow a specific sequence of appearance, meaning that this synthetic time forcing represents just one possible realization among numerous potential scenarios in a realistic wind climate. Ideally, this process should be repeated for a significant number of different realizations (i.e., distinct orderings of wind events), followed by averaging the results across these realizations. Currently, simulations are restricted to a single realization, but future studies will explore multiple realizations.

Table 9 – Overview of probability of occurrence p (in %) per wind velocity/direction class at "Westhinder" station (location shown in Figure 35a). Wind velocity (V_w) and wind direction (Φ_w) are sorted in 3 and 4 classes, respectively.

	p (%)	p (%)	p (%)	p (%)	Total
v_w (m/s))/Φ_w	[0-90]°	[90-180]°	[180-270]°	[270-360]°	(%)
0-10	18.5	12.8	25.9	13.1	70.3
10-20	4.2	2.8	17.1	5.2	29.3
> 20	0.01	0.0	0.3	0.1	0.4
Total (%)	22.7	15.6	43.2	18.3	100

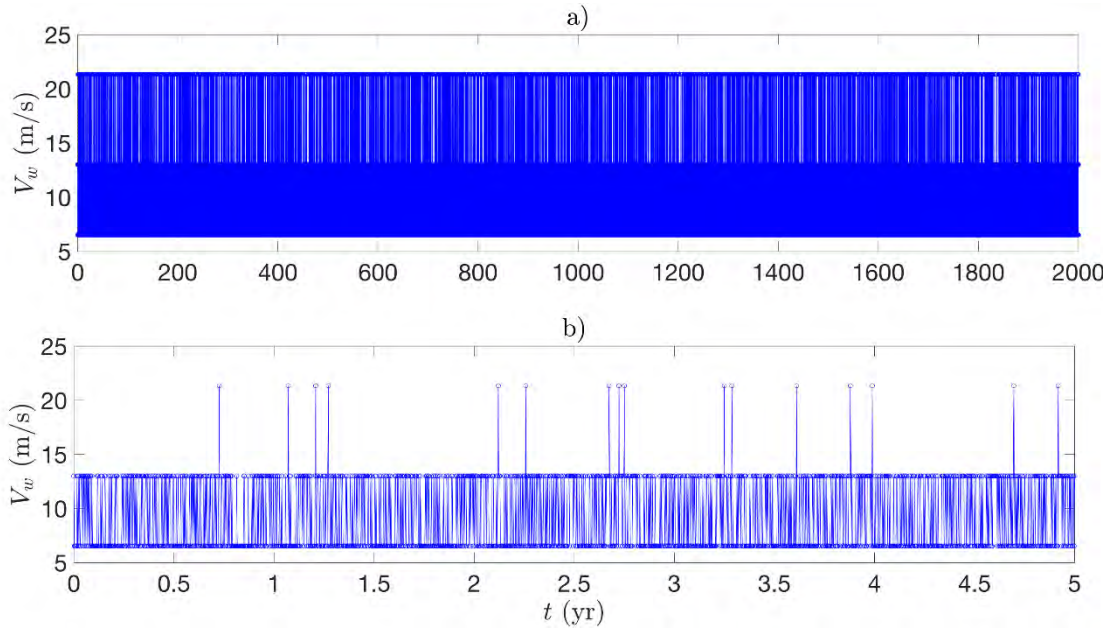

Figure 38 – Artificial wave forcing used in the model , which was constructed based on wave time series collected at different wave buoys offshore the Belgian coast. a) Artificial time series of H_{s0} (a), (b) peak period T_{p0} and (c) wave angle of incidence θ_0, which are prescribed at the seaward boundaries in the shelf model. Note that, due to the difference in the shoreline orientation in the model (S-N) compared to that of the Belgium shoreline (NE-SW), the wave angle of incidence in the model was rotated 60° counter-clockwise.

Tide

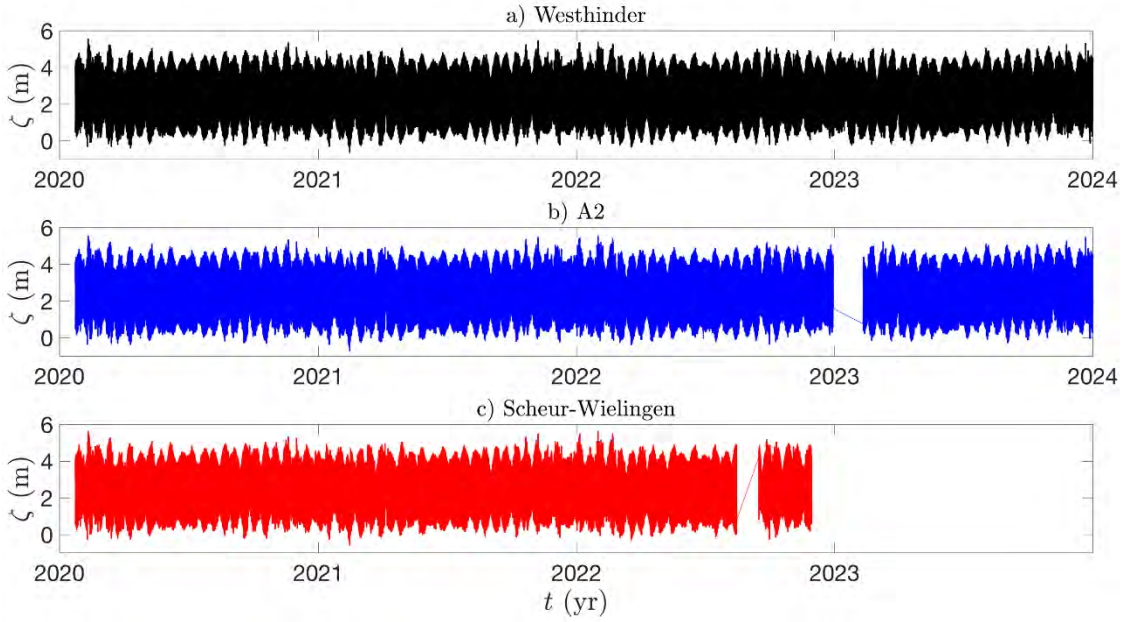

Figure 39 – Time series of water level ζ (in m relative to TAW) on the Belgium shelf in the period 2020-2023, measured at three tide gauge stations: "Westhinder", "A2" and "Scheur-Wielingen" (locations shown in Figure 35a). Note that the time series contain some data gaps. Data were downloaded from the "Meetnet Vlaamse Banken", accessible at https://meetnetvlaamsebanken.be/.

Table 10 – Amplitudes ($\hat{\zeta}_2$, $\hat{\zeta}_4$) and phases (ϕ_2, ϕ_4) of the M_2 and M_4 tidal constituents at tide gauge stations "Westhinder", "A2" and "Scheur-Wielingen" (locations shown in Figure 35a).

Tide gauge	$\hat{\zeta}_2$ (m)	ϕ_2 (°)	$\hat{\zeta}_4$ (m)	ϕ_4 (°)
Westhinder	1.67	73	0.09	94
A2	1.63	89	0.09	161
Scheur-Wielingen	1.58	96	0.1	187

Figure 39 presents time series of water level ζ (in meters relative to TAW) on the Belgian shelf for the period 2020-2023, measured at three tide gauge stations: "Westhinder", "A2" and "Scheur-Wielingen" (locations shown inFigure 35a). The tidal range (difference between high and low waters) at these sites varies between approximately 2.5 m during neap tides and 5 m during spring tides. The amplitudes and phases of the various constituents of the tidal signal are computed using T_tide harmonic analysis program (Pawlowicz et al., 2002). Since tidal constituents M_2 and M_4 are important for sediment transport, this analysis focuses only on these constituents. The results are summarised in Table 10.

3.1.3 Coupled shelf-shoreline model

Model description

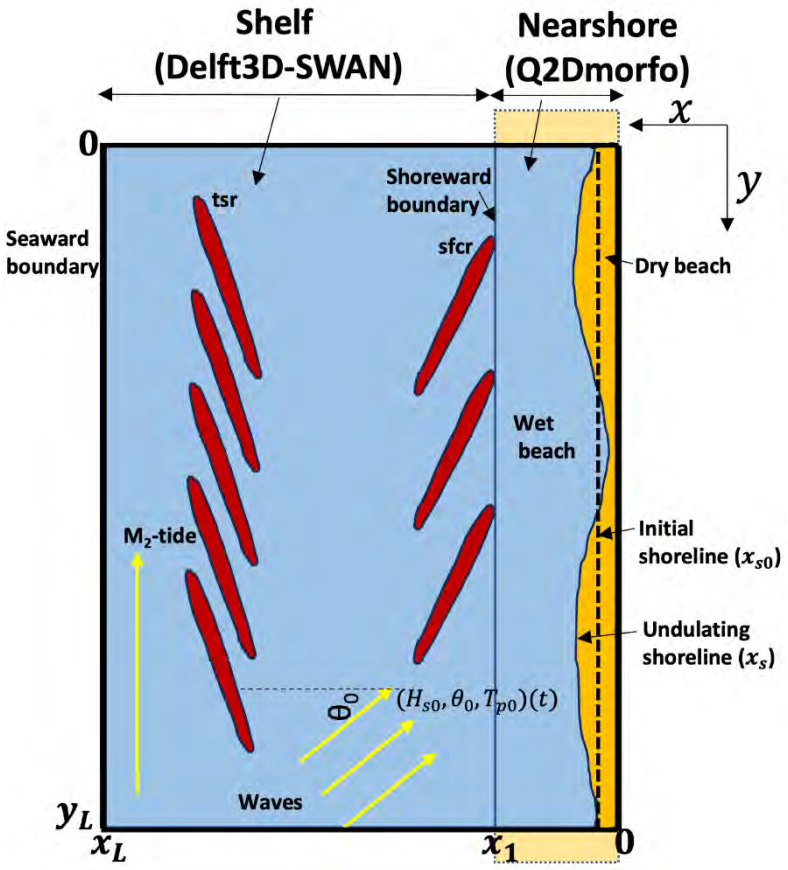

Figure 40 – Domains of the shelf model ($x_1 \leq x \leq x_L$, $0 \leq y \leq y_L$) and nearshore model ($0 \leq x \leq x_1$, $0 \leq y \leq y_L$), with x,y pointing in, respectively, the cross-shore and alongshore directions. Shoreline position $x_s(y,t)$ marks the border between the dry ($z_b > 0$) and the wet beach ($z_b \leq 0$). Here, z_b is the bed level, which is defined with respect to the mean sea level $z = 0$ (MSL), with z the vertical coordinate (positive upward). Tidal forcing is imposed at the seaward boundary of the shelf (x_L) as an M_2 wave that propagates from south to north along the coast. Furthermore, a time-varying wave forcing with a significant wave height $H_{s0}(t)$, peak period $T_{p0}(t)$ and wave direction $\theta_0(t)$ (relative to the shore-normal, positive counter-clockwise) is prescribed at the seaward boundary. Wave parameters $H_{s1}(t)$, $T_{p1}(t)$, $\theta_1(t)$, computed by the shelf model at the shoreward boundary (x_1), are subsequently used as a wave forcing for the nearshore model. The orange rectangles at the lateral boundaries of the nearshore model domain indicate the extensions used to compute the waves near these boundaries. The red areas on the shelf are sketches of tsr and sfcr.

The work conducted within Activity 1, using the coupled shelf-shoreline model, is currently in the process of being published in the Journal of Geophysical Research-Earth Surface (Nnafie et al. 2024). This report highlights the key outcomes obtained within this activity, which are presented in this section. Further details and results are available in Nnafie et al. (2024).

The model comprises a shelf model (Delft3D+SWAN) that is coupled to a reduced-complexity nearshore model known as Q2Dmorfo (hereafter referred to as nearshore model). The model has dimensions $x_L \times y_L$, featuring a rectangular shelf ($x_1 \leq x \leq x_L$, $0 \leq y \leq y_L$) and a nearshore domain ($0 \leq x \leq x_1$, $0 \leq y \leq y_L$), where x,y represent the cross-shore and alongshore directions, respectively (Figure 40). Furthermore, x_1 is the transition between the shelf and nearshore models. Shoreline position $x_s(y,t)$ is defined as the border between the dry ($z_b > 0$) and wet beaches ($z_b \leq 0$). Here, z_b is the bed level, which is defined with respect to the mean sea level $z = 0$ (MSL), with z the vertical coordinate (positive upward). A brief description of this coupled model system is provided below, with additional information available in Nnafie et al. (2024).

Morphostatic shelf model

On the shelf, depth-averaged currents, waves and their interactions are computed with the Delft3D and SWAN models. The bed level in the shelf model is kept fixed (morphostatic) during the simulations, meaning only the FLOW module of Delft3D is used (Lesser *et al.,* 2004; Deltares 2022). Module FLOW computes the water level and currents on the shelf, which are described by the non-linear depth-averaged shallow water equations. This module is forced with sea-level variations at the seaward ($x = x_L$) and lateral ($y = 0,\ y_L$) boundaries, which mimic a semi-diurnal lunar M_2 tidal wave that propagates in the negative y-direction (Figure 40). This tidal wave, characterised by an amplitude $\hat{\zeta}_2$, exhibits a linearly increasing phase from $y = 0$ to $y = L_y$, resulting in a phase difference $\Delta\phi_2$ between the two boundaries. Since the equations of motion are nonlinear, the response to this forcing is an asymmetric tidal motion: it contains the primary constituent (M_2), but also overtides (M_4, M_6,..), as well as a tidal residual.

The SWAN model simulates the wave propagation on the shelf by solving the spectral wave action balance, which is applied in stationary mode (Holthuijsen 2007; Delft 2024). The default settings are used, as they have been successfully applied by previous studies on coastal morphodynamics (Ridderinkhof *et al.,* 2016; Nnafie et al., 2020). Specifically, dissipation due to whitecapping, depth-induced wave breaking, and bottom friction are considered, utilising the formulations of, respectively, Komen and Hasselmann (1984), Battjes and Janssen (1978) and Hasselmann et al. (1973). Nonlinear wave-wave interactions, as well as wave growth by wind are neglected. JONSWAP wave spectra are prescribed at the offshore boundaries, with a peak enhancement factor of $\hat{p}$ and directional spreading of $\Delta\theta$.

The waves have a time-varying significant wave height $H_{s0}(t)$, a time-varying peak period $T_{p0}(t)$, and a time-varying wave direction $\theta_0(t)$. Additionally, to avoid the formation of shadow zones (i.e., a strong decrease in H_s) near the lateral boundaries ($y = 0, L_y$), periodic boundary conditions are applied at these boundaries.

Waves influence currents in the FLOW module by introducing additional shear stress at the bed (Soulsby, 1997) and causing a momentum flux through divergence of radiation stresses (Longuet-Higgins and Stewart, 1964). Currents, in turn, affect waves through frequency shifting, refraction and sea level variations. The computed wave time series ($H_{s1}(t)$, $T_{p1}(t)$, $\theta_1(t)$) at the shoreward boundary of the shelf model ($x = x_1$, Figure 40) are used as input to drive the nearshore model.

Nearshore model

In the nearshore area, comprising of the dry and wet beaches (Figure 40), the reduced-complexity nearshore model Q2Dmorfo (Arriaga et al. 2017) is used, which simulates the morphodynamic evolution of the nearshore and the changes of its shoreline position $x_s(y,t)$. This model does not explicitly resolve the current field, but it uses empirical formulations to compute the sediment transport directly from the wave field. The model consists of three modules: WAVES, TRANSP and BED.

Module WAVES, forced with waves (H_{s1}, T_{p1}, θ_1) at the seaward boundary ($x = x_1$, Figure 40), applies the geometrical optics approximation, i.e., linear dispersion relation, irrotationality of the wave vector (also known as the generalised Snell law) and conservation of wave energy, to simulate the wave propagation in the interior of the domain (Arriaga et al. 2017). To define the boundary condition at the up-waves lateral boundary (i.e., the lateral boundary at which wave rays enter) the bathymetry at this boundary is alongshore uniformly extended for a certain alongshore distance (orange rectangle in Figure 40). The wave transformation is done in this extended domain, and the transformed waves are then assumed to incide through the lateral boundary.

Module TRANSP calculates the sediment transport vector $\vec{q}_{tot}$ in the nearshore, derived directly from the wave field through empirical formulations, without explicitly resolving the flow field. To accommodate the curvature of the shoreline represented by $x_s(y,t)$, $\vec{q}_{tot}$ is expressed in a local coordinate system defined by x' and y'. In this system, x' points outward in the direction normal to the local shoreline $x_s(y,t)$, while y' points tangentially along the shoreline. Transport $\vec{q}_{tot}$ is separated into three contributions:

$$\vec{q}_{tot} = \vec{q}_L + \vec{q}_C + \vec{q}_D. \qquad (1)$$

The first contribution ($\vec{q}_L$) is the longshore transport vector caused by breaking waves, which is evaluated as a parametrised cross-shore distribution of the total transport rate given by the CERC formula (with coefficient μ that controls the magnitude of this alongshore transport, Komar, 1998). The second contribution ($\vec{q}_C$) represents the cross-shore transport, which is computed as being proportional to the departure of the local bed slope with respect to the slope of an equilibrium profile $z_{b,e}$. Cross-shore sediment transport is the result of several complex processes, mainly including wave nonlinearities, undertow and gravity, which makes it difficult to accurately evaluate this transport. The parametrisation of $\vec{q}_C$ in the model is based on the assumption that, over long time scales (on the order of years to decades), the cross-shore profile of the actual bed level z_b in the nearshore adjusts to the used equilibrium profile $z_{b,e}$. This is consistent with many observations both in nature and in wave flumes. Finally, the third contribution ($\vec{q}_D$) is a bed-slope induced sediment transport. Details on boundary conditions in this module can be found in Arriaga et al. (2017).

The evolution of nearshore bed level z_b is computed in module BED, as a result of the divergence of the sediment transport:

$$\frac{\partial z_b}{\partial t} = -\frac{1}{1-p}\vec{\nabla}\cdot\vec{q}_{tot}, \qquad (2)$$

with p the porosity of the bed. The dry beach ($0 \leq x \leq x_s(y,t)$) is part of the computational domain of the nearshore model, meaning that it also experiences erosion and accretion during the simulation. The position of shoreline $x_s(y,t)$ is determined by applying a linear interpolation between the cross-shore locations of the last dry cell and the first wet cell of the nearshore domain.

Methodology

Model configuration

Dimensions of the coupled model domain, bathymetry, tides and waves are based on field data of the Belgian coast, using the "Meetnet Vlaamse Banken" and "Flemish Hydrography" data portals, accessible at https://www.agentschapmdk.be/en. Other parameter values are adopted from the work by Arriaga et al. (2017) and Nnafie et al. (2021). A list of all the values of model parameters is provided in Table 11. The coupled model domain covers a total area $x_L \times y_L = 50 \times 75$ km. The nearshore zone spans from $x = 0$ and $x = x_1 = 1.5$ km, while the shelf area is between $1.5 < x \leq 50$ km (Figure 40).

Table 11 – Overview of the physical and numerical parameters of the coupled shelf-nearshore model.

Parameter	Value	Description
Model		
Geometry/bathymetry		
$x_L \times y_L$	50×75 km^2	Dimensions shelf-nearshore system.
x_{s0}	500 m	Initial shoreline position.
x_1	1500 m	Transition between nearshore and shelf.
$[H_c, w, \alpha]$	[8.2 m, 300 m, -5.23×10^{-4}]	Parameters bathymetric profile (Eqs. 3 and 4).
Shelf model		
$[f, C]$	[1.43× 10^{-4} s^{-1}, 65 m$^{1/2}$ s^{-1}]	Coriolis and Chézy coefficients.
ν	1 m^2 s^{-1}	Viscosity coefficient.
$[\hat{\eta}_2, \Delta\psi_2]$	[1.8 m, 31.5°]	M_2-tidal forcing.

Parameter	Value	Description
σ	1.405× 10^{-4} s^{-1}	Angular frequency M_2 tide.
$[\hat{p}, \Delta\theta]$	[3.3, 25°]	Peak enhancement factor and directional spreading JONSWAP.
Nearshore model		
γ_b	0.5	Breaker index.
d_{50}	0.2 mm	Grain size.
μ	0.06 $m^{1/2}$ s^{-1}	Coefficient CERC formula.
L_2	10 m	Width swash zone.
D_c	8 m	Depth of closure.
Numerics shelf model		
Δt	2 min	Time step (in minutes).
$[\Delta x, \Delta y]$	[250, 250] m	Size grid cells.
Numerics nearshore model		
Δt	0.005 d	Time step (in days).
$[\Delta x, \Delta y]$	[15, 250] m	Size grid cells.
Numerics coupling		
Δt_c	10 days	Coupling time shelf-nearshore model.

Bathymetry

The bathymetric map depicted in Figure 35a serves as the basis for deriving a representative bathymetry within the model, which is assumed alongshore uniform. In the shelf domain, the following linear bed level profile is used (Figure 41, panel a):

$$z_b = \alpha(x - x_1) - H_c, \qquad (3)$$

where $\alpha = -5.23 \times 10^{-4}$ is the shelf slope, and $H_c = 8.2$ m is the depth (relative to MSL) at the transition between the nearshore and shelf areas ($x_1 = 1.5$ km). In the nearshore domain (panel b), the bed level profile is approximated by the following (modified) hyperbolic tangent function:

$$z_b = -H_c \left[\frac{\exp(\tilde{x}) - \frac{b}{H_c}\exp(-\tilde{x})}{\exp(\tilde{x}) + \exp(-\tilde{x})} \right], \qquad \tilde{x} = \frac{x - \epsilon x_{s0}}{w}. \qquad (4)$$

Here, $b = 1$ m is the maximum height of the (dry) beach, which is located at the landward boundary of the nearshore domain ($x = 0$), $w = 300$ m is a characteristic nearshore width and $\epsilon = 1.36$ is a tuning parameter used to smoothly connect the nearshore bathymetry with the shelf bathymetry at the transition x_1. Furthermore, $x_{s0} = 0.5$ km is the initial shoreline position (vertical dashed line in panel b), which divides the dry beach ($x \leq 0.5$ km, with an onshore increasing height to $b = 1$ m at $x = 0$) and the wet beach ($0.5 < x \leq 1.5$ km). The profile defined in Equation (4) is assumed to be an equilibrium profile $z_{b,e}$, which is needed for calculating the cross-shore sediment transport in the nearshore model.

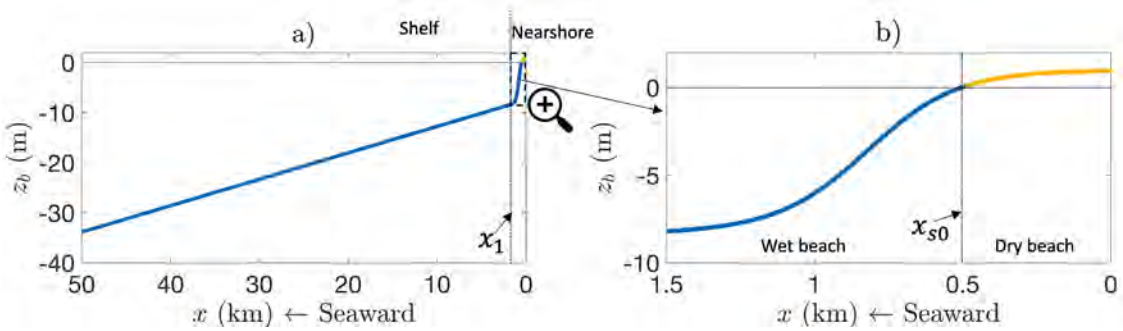

Figure 41 – Model bathymetry.a) Shelf and nearshore initial bathymetric profiles used in the model (Eqs. [eq:bathymetry_shelf]-[eq:bathymetry nearshore]). b) A zoom-in view of the bathymetric profile in the nearshore area, which is used as the equilibrium profile $z_{b,e}$. The vertical dashed line in this inset denotes the position of the shoreline ($x = 0.5$ km, $z_b = 0$ MSL), which distinguishes between the dry beach (with an onshore increasing height to 1 m) and the wet beach.

Tides

In the shelf model, a semi-diurnal lunar M_2 tide forcing (period 12 h 25 min) is applied at the seaward boundary ($x = x_L$), featuring an amplitude $\hat{\eta}_2 = 1.8$ m and a phase difference of $\Delta\psi_2 = 31.5^o$ between the lateral boundaries, $y = 0, y_L$. This prescribed tidal forcing simulates a propagating M_2-tidal wave in the negative y-direction. Tides are not considered in the nearshore model.

Wave climate

To derive a representative wave climate to force the model, time series of significant wave height (H_s, in m), wave direction (θ, in degrees with respect to North) and peak wave period (T_p, in s) collected at the "Westhinder" wave buoy are used (Figure 35). These time series cover the period from 1990 to 2019. Since these wave time series are not long enough to be used as a forcing in the 100-year model experiments, and given the presence of several data gaps, an alternative wave forcing is derived by constructing synthetic wave time series of H_{s0}, T_{p0} and θ_0. Further details are provided in Nnafie et al. (2024).

Finally, coefficient μ, which controls the magnitude of the alongshore sediment transport in the nearshore model is set to 0.06 $m^{1/2}$ s^{-1}. Using this value yields a total average transport (i.e., integrated over the cross-shore direction and averaged over 10 years) of about 1.1×10^5 m^3/yr, which is of the same order of magnitude as those found from FlemCo and ScaldisCoast complex models (Section 3.2).

Numerical aspects

The computation grids (for both wave and flow computations) have sizes of 250 m in the cross- and alongshore directions. The hydrodynamic time step is set at 2 minutes. The alongshore grid size in the nearshore model matches that of the shelf model. However, to capture nearshore processes (e.g., wave refraction and shoaling), the cross-shore grid size is considerably smaller ($= 15$ m). A time step of 0.005 days is used.

Coupling aspects

Since the shelf model is morphostatic, a one-way coupling between the shelf and nearshore models is applied, i.e., the bathymetry of the shelf model influences the waves and consequently the evolving bathymetry and the shoreline in the nearshore model, while changes in the latter do not feed back to the shelf morphology. This one-way coupling between the shelf and nearshore models is executed as follows. The two models run separately within time intervals $[t_n, t_{n+1}]$, where $t_n = n\Delta t_c$, $n = 0,1,2,\ldots$, and Δt_c is the coupling time. During these intervals, the wave forcing of the nearshore model is kept fixed. Only at the end of each interval, this forcing is updated by new wave data (H_{s1}, T_{p1}, θ_1) computed by the shelf model. A coupling time Δt_c of 10 days is used. Test experiments show that, compared with smaller coupling times, a 10-days coupling time yields accurate results, while maintaining reasonable computation durations.

Model experiments

The bathymetries of the shelf and nearshore domains in the cross-shore direction used in the experiments are given by Equations (3) and (4), respectively, while remaining uniform in the alongshore direction (Figure 42). The nearshore zone features an initially straight shoreline situated at $x_s = 0.5$ km.

To address the first and second objectives within Activity 1, four experiments are conducted (Series S1 in Table 12). In the first experiment (referred to as "sfcr+tsr (Ref)"), which serves as a reference experiment, synthetic fields of tsr and sfcr are imposed onto the shelf bathymetry (Figure 42, panel a). The dimensions, alongshore spacings, and orientations (relative to the shoreline) of these ridges, as well as their heights (crest-to-channel distances), are based on field data of the Belgian shelf (Chapter 1). There are three sfcr with alongshore spacings of 15 km and heights of 6 m, which have landward endings positioned at a distance $d_0 = 2$ km from the initially straight shoreline. At approximately 15 km away from the shoreline, five tsr are located, with alongshore spacings of 10 km and heights of 14 m. In the second experiment ("NoRidges", panel b) all ridges are removed. In the third experiment ("sfcr only", panel c), only the sfcr are introduced onto the shelf, while in the fourth experiment ("tsr only", panel d), the shelf features only tsr.

Impacts of onshore and alongshore displacements of the ridges on the shoreline (third objective) are addressed by executing three additional series of experiments (S2, S3 and S4 in Table 12 and depicted in Figure 43). These series simulate the observed onshore and alongshore migrations of the ridges. In all these series, only the sfcr are displaced on the shelf. The tsr are kept fixed, which is supported by the observations presented in Chapter 1.

The four experiments of Series S2 are similar to the reference experiment (Figure 43, panel a), with the difference that the sfcr are positioned closer to and farther from the shoreline: $d_1 = 1.5$ km in experiment "Onshore-1" (panel b), $d_2 = 1$ km in experiment "Onshore-2" (panel c), $d_3 = 2.5$ km in experiment "Offshore-1" (panel d) and $d_4 = 3$ km in experiment "Offshore-2" (panel e). In Series S3, besides a shoreward displacement, the sfcr are shifted alongshore to the north by 1000 m ("OnshoreAlong-1", panel f) and by 2000 m ("OnshoreAlong-2", panel g). This northward shift mimics the migration direction of the sfcr on the Belgian shelf.

In reality, the onshore and alongshore displacement of the sfcr is a continuous process, during which sfcr positions change over time. To investigate how existing shoreline profiles respond to these dynamic changes, two additional experiments are carried out: "OnshoreAlong-1-50yrRef" and "OnshoreAlong-2-50yrOA1" (Series S4). These two experiments are similar to experiments "OnshoreAlong-1" and "OnshoreAlong-2", respectively, with the difference that they begin with shoreline profiles obtained at $t = 50$ yr in the reference and "OnshoreAlong-1" cases.

In each experiment, a simulation time of 100 years is used, which is relatively short compared to the time scale over which ridges evolve (Dyer and Huntley 1999), but long compared to that of the shoreline undulations (van den Berg et al., 2012). The experiments are executed on an intel Xeon 2.80 GHz Linux computer, with each experiment requiring approximately 15 days to complete.

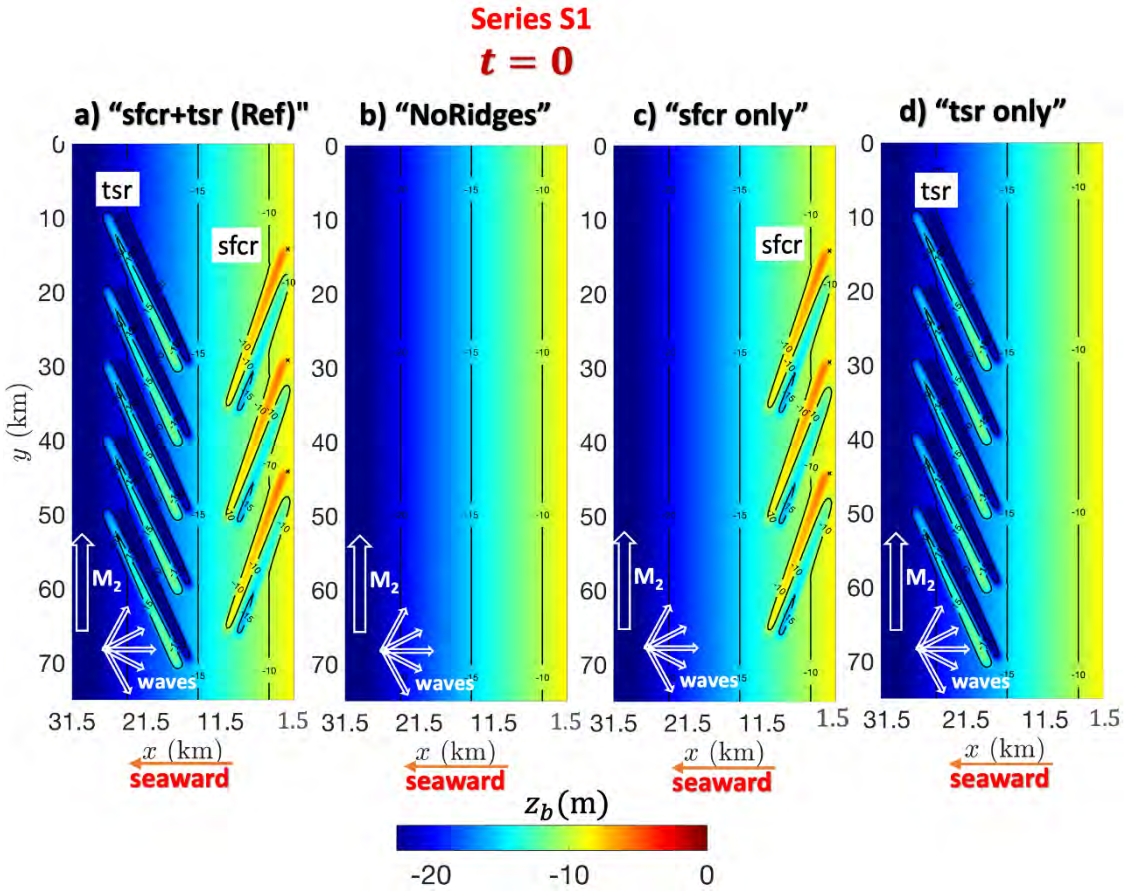

Figure 42 – The bathymetric configuration on the shelf used in the experiments of Series S1: Initial bathymetry a) with superimposed fields of synthetic sfcr and tsr (reference experiment, referred to as "sfcr+tsr (Ref)"), b) without ridges on the shelf ("NoRidges"), c) with a field of synthetic sfcr ("sfcr only") and d) a field of synthetic tsr "tsr only". The dimensions (width, length and orientation), as well as the distance of the ridges to the shoreline, are based on field data of the Belgian shelf (Fig. 1) and the bathymetric map of shown in Fig. A1 in the SI. Arrows indicate directions of the forcings prescribed at the offshore boundaries (M_2 tidal water level and waves). Note that, for clarity, only a portion of the cross-shore shelf domain is shown ($1.5 \leq x \leq 31.5$ km).

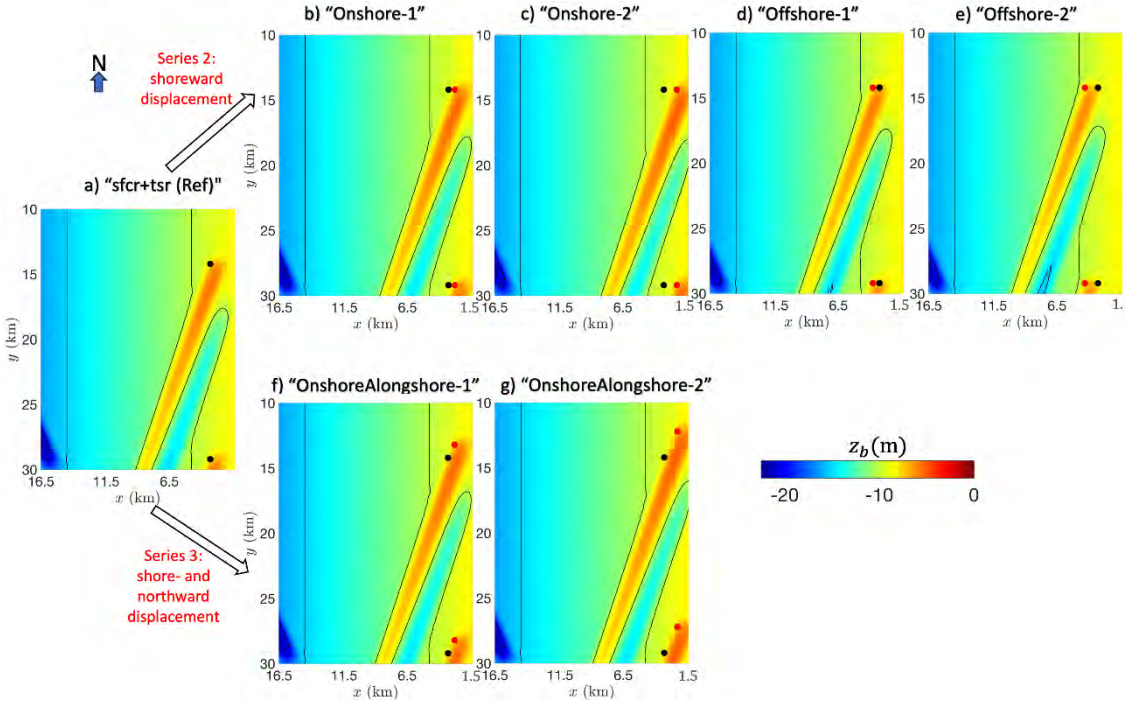

Figure 43 – The bathymetric configuration used in the experiments of Series S2 and S3. For clarity, only zoom-ins on the northern-located ridge (indicated by the black rectangle in Figure 42a) are displayed for each case. In Series S2, the sfcr are displaced with respect to their locations in the reference experiment (panel a): 500 m shoreward in "Onshore-1" (b), 1000 m shoreward in "Onshore-2" (c), 500 m seaward in "Offshore-1" (d) and 1000 m seaward in "Offshore-2" (d). In the experiments of Series S3, besides a shoreward displacement, the sfcr are displaced 1000 m northward in experiment "OnshoreAlong-1" (g) and 2000 m in "OnshoreAlong-2"(g). As a reference, black dots pinpoint the offshore location of the landward ends of the ridge crests in the reference case at $y = [14.2,29.2]$ km, while red dots denote their corresponding locations in the other cases. In all cases, the tsr (not visible in the panels) are located offshore.

Table 12 – List of model experiments, organised into four different series: S1, S2, S3 and S4.

Name experiments	Description
S1: "sfcr+tsr (Ref)"	Reference experiment: Both sfcr and tsr present on shelf. Sfcr positioned 2 km from shoreline.
S1: "NoRidges"	No ridges are present on shelf.
S1: "sfcr only"	Only sfcr are present on shelf.
S1: "tsr only"	Only tsr are present on shelf.
S2: "Onshore-1"	As in "sfcr+tsr (Ref), but sfcr are shifted 500 m shoreward.
S2: "Onshore-2"	As in "sfcr+tsr (Ref), but sfcr are shifted 1000 m shoreward.
S2: "Offshore-1"	As in "sfcr+tsr (Ref), but sfcr are shifted 500 m offshore.
S2: "Offshore-2"	As in "sfcr+tsr (Ref), but sfcr are shifted 1000 m offshore.
S3: "OnshoreAlong-1"	As in "sfcr+tsr (Ref)", but sfcr are shifted 500 m shoreward and 1000 m northward.
S3: "OnshoreAlong-2"	As in "sfcr+tsr (Ref)", but sfcr are shifted 1000 m shoreward and 2000 m northward.
S4: "OnshoreAlong-1-50yrRef"	As in "OnshoreAlong-1", but starting from shoreline profile at $t =$ 50 yr of "sfcr+tsr (Ref)".

Name experiments	Description
S4: ”OnshoreAlong-2-50yrOA1”	As in ”OnshoreAlong-2”, but starting from shoreline profile at $t =$ 50 yr of ”OnshoreAlong-1”.

Analysis of results

The assessment of the influence of the presence of shelf ridges on the decadal evolution of the nearshore and shoreline involves: 1) identifying areas of progradation and retreat along the shoreline, and 2) evaluating the magnitude of these shoreline undulations. This influence of the ridges are assessed relative to the experiment without ridges ("NoRidges").

The identification of areas of progradation and retreat along the shoreline includes assessing the relative positions of these areas in relation to the adjacent ridge crest and channel between the ridge and the coast. The magnitude of these shoreline undulations is quantified by two quantities: the rate of shoreline change $\partial x_s / \partial t$ (in meters per year) at fixed locations in the proximity of the landward ends of ridge crests and channels; and the root-mean-square (rms) amplitude $\sigma_{x'_s}$ of shoreline undulations, denoted as $x'_s = x_s - \langle x_s \rangle$, where brackets $\langle\ \rangle$ represent alongshore averaging over length y_L.

Results

Impact of sfcr versus tsr on shoreline dynamics

The outcomes of the full set of experiments of Series S1 are presented in Figure 44. Blue, red and green lines denote those of the reference experiment (both tsr and sfcr present), the case with only sfcr, and the case with only tsr, respectively.

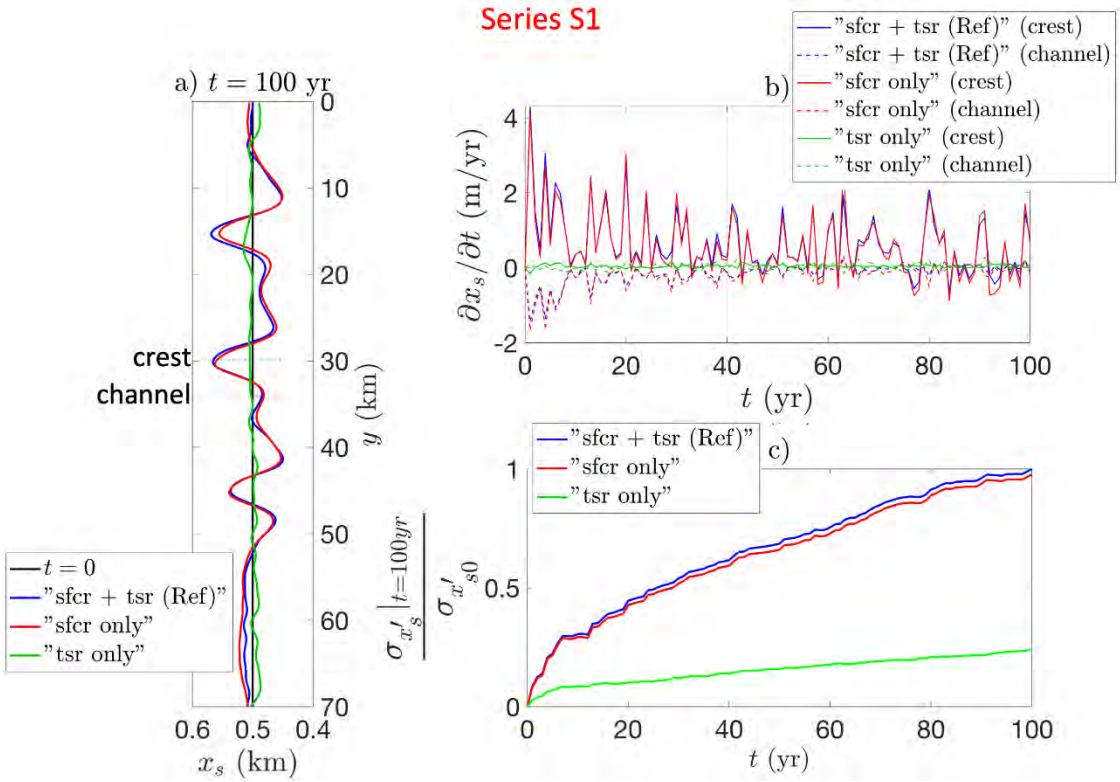

Figure 44 – Results from Series S1. a) Simulated shoreline profiles at $t = 100$ yr in the experiments "sfcr+tsr (Ref)" (blue line), "sfcr only" (red line) and "tsr only" (green line). b) Rate of shoreline change ($\partial x_s/\partial t$) versus time near the crest of the middle sfcr (at $y =$ 30 km) and near its channel (at $y = 34$ km) in the three cases. c) Root-mean square amplitude $\sigma_{x'_s}$ of shoreline undulations (normalised by its corresponding value at $t = 100$ yr in the reference case, $\sigma_{x'_{s0}}$) versus time in the three cases.

In all three cases, the presence of shelf ridges induces undulations along the shoreline. When only tsr are present, shoreline undulations are weaker ($\sigma_{x'_s} \sim 6$ m after 100 years) compared to the "sfcr+tsr (Ref)" and "sfcr only" cases, with an rms amplitude $\sigma_{x'_s}$ that is about 24% of that in the reference case. Moreover, unlike the "sfcr only" and "sfcr+tsr" cases, there is no apparent correlation between the locations of tsr and those of shoreline undulations in the "tsr only" case. Furthermore, Figure 44 (panel c) shows that the rms amplitude $\sigma_{x'_s}$ of the reference case is approximately 98% of the value in the reference case, indicating that the difference in amplitude between the two cases is smaller than what might be expected based on the sum of $\sigma_{x'_s}$ values from the separate sfcr and tsr cases. This aspect is further discussed in Nnafie et al. (2024). Finally, note the fluctuations in the temporal evolution of the rate of shoreline change ($\partial x_s/\partial t$, panel b), which is caused by alternating stormy and fair wave events whitin the synthetic wave time series.

Different locations of the sfcr

Cross-shore displacement

Figure 45 shows the results of the experiments in which the sfcr are placed at different cross-shore positions on the shelf (Series S2). An animation showing the temporal evolution of bed levels and shoreline positions x_s between $t = 0$ and $t = 100$ yr in the "Onshore-2" case can be found in Nnafie et al. (2024) (Movie A2).

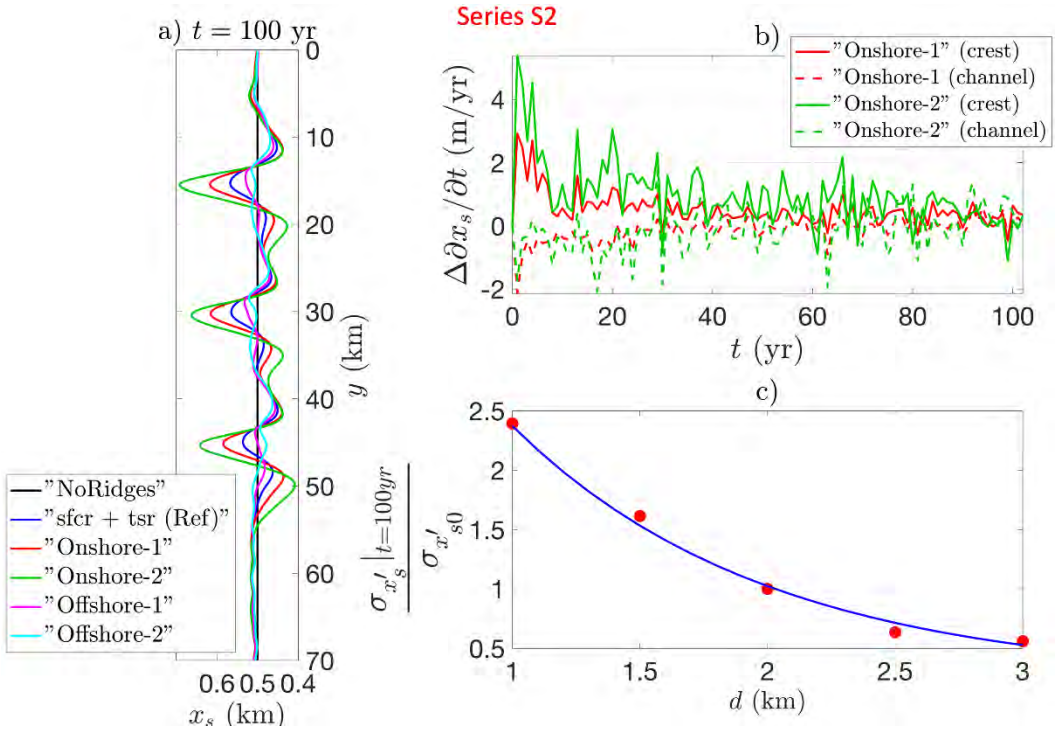

Figure 45 – Results of the experiments of Series S2 , featuring sfcr with different positions with respect to the shoreline. a) Simulated shoreline profiles at $t = 100$ yr in the different cases (see legend). b) Difference in rate of shoreline change ($\Delta\partial x_s/\partial t$) at fixed locations between the reference case and the "Onshore-1" and "Onshore-2" cases. For the sake of clarity, other cases are omitted. Rates $\partial x_s/\partial t$ are computed near the crest of the landward end of the middle sfcr (at $y = 30$ km) and near its adjacent channel ($y = 34$ km). c) Rms amplitude $\sigma_{x'_s}|_{t=100\text{yr}}$ of shoreline undulations at $t = 100$ yr (normalised by $\sigma_{x'_{s0}}$) versus distance d of the sfcr in the experiments of Series S2. The blue curve represents a fit $\sigma_{\text{fit}} = \sigma_{\text{tsr}} + 5.8exp(-2d/d_0)$ through the data, with σ_{tsr} (~ 0.24) the normalised $\sigma_{x'_s}|_{t=100\text{yr}}$ in the case that only tsr are present on the shelf.

From Figure 45 (panel a) it is seen that, as the sfcr are positioned more onshore (offshore), shoreline progradation and retreat near, respectively, the crests of the landward ends of all three sfcr and the channels between the ridges and the coast become stronger (weaker). This is also evident from panel b, which depicts the time development of the rate of shoreline change $\partial x_s/\partial t$ in the proximity of the crest and channel of the middle sfcr. These rates are initially large, after which they reduce over time. In all cases, shoreline progradation in the proximity of sfcr crests generally exceeds shoreline retreat near the channels (panel a).

In the "Onshore-1" and "Onshore-2" cases, the shoreline extends seaward at average rates $\partial x_s / \partial t$ (averaged over the simulation period) of about 1 m/yr and 1.5 m/yr in the proximity of the crests of the landward ends of the sfcr (0.6 m/yr in the reference case), respectively. Meanwhile, near the channels, the shoreline retreats at average rates of approximately 0.5 m/yr and 0.8 m/yr, respectively (0.2 m/yr in the reference case). When the sfcr are displaced further offshore, in the "Offshore-1" case, the shoreline extends seaward (landward) at average rates of about 0.3 m/yr (0.05 m/yr) near the crests (channels). In the "Offshore-2" case, the sfcr still impact the shoreline evolution. However, the manifestation of either progradation or retreat in the proximity of sfcr crests and channels is less evident, indicating that the ridges are situated too far for a notable correlation to emerge between the locations of their landward ends and those of shoreline undulations. Overall, the areas adjacent to all three sfcr undergo qualitatively similar changes in their shoreline. However, in some cases (e.g., "Onshore-2" and "Offshore-1"), rates of progradation and retreat differ quantitatively among these areas.

Panel c of Figure 45 shows the rms amplitude $\sigma_{x'_s}|_{t=100\text{yr}}$ of shoreline undulations at $t = 100$ yr (normalised by $\sigma_{x'_{s0}}$) versus distance d of the sfcr. The blue curve represents a fit $\sigma_{\text{fit}} = \sigma_{\text{tsr}} + 5.8\exp(-2d/d_0)$ through the data, with σ_{tsr} the normalised $\sigma_{x'_s}|_{t=100\text{yr}}$ in the case that only tsr are present on the shelf (experiment "tsr only"). This panel reveals that $\sigma_{x'_s}$ decreases exponentially with distance d from the shoreline. When the sfcr are located far offshore, the influence of the much higher tsr (about 14 m) becomes more significant, with $\sigma_{x'_s}$ approaching $\sigma_{\text{tsr}} = 0.24$.

Shoreward and alongshore displacement

Results from experiments in which the sfcr are positioned more shoreward and northward (Series S3, Figure 46) closely resemble those obtained from experiments "Onshore-1" and "Onshore-2" of Series S2. In addition to the observed reinforcement of the shoreline undulations when the sfcr are situated closer to the shoreline, these undulations shift the same distance northward as that of the sfcr (panels a-b).

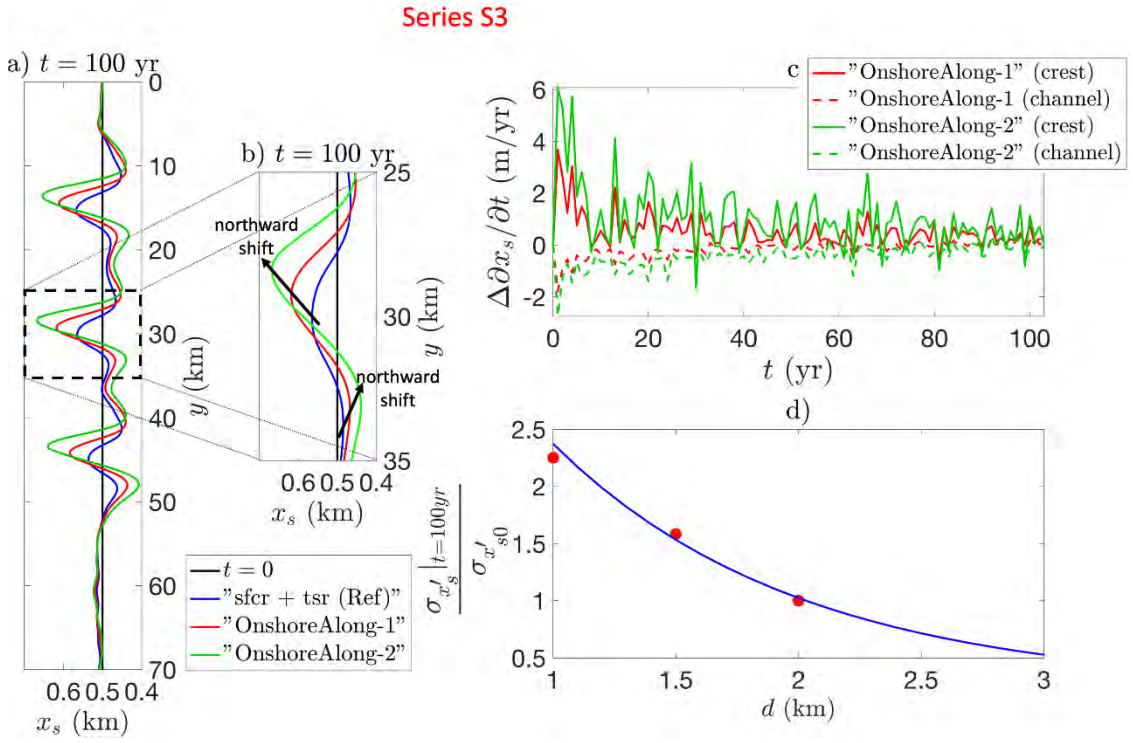

Figure 46 – Results of the experiments of Series S3. As in Figure 45, but for the experiments of Series S3, where the sfcr are positioned more shore- and northward. A zoom-in on the middle sfcr is also provided (panel b). The thick black arrows indicate the northward shifts of shoreline retreat and progradation areas.

The rates of shoreline progradation and retreat in the "OnshoreAlong-1" and "OnshoreAlong-2" cases are the same as those in the "Onshore-1" and "Onshore-2" cases, respectively. Specifically, the shoreline progrades seaward at an average rate of $\partial x_s / \partial t \sim 1$ m/yr and 1.5 m/yr in the proximity of the crest of landward ends of the ridges in the cases of "OnshoreAlong-1" and "OnshoreAlong-2", respectively. Near the landward ends of the channels, the shoreline retreats at average rates of about 0.5 m/yr and 0.8 m/yr, respectively. Initially, the rate of shoreline change is large, after which it reduces over time (panel c). Similar to the experiments of Series S2, the rms amplitude of the shoreline undulations increases exponentially with decreasing distance of the sfcr to the shoreline (panels d).

Finally, results from experiments of Series S4 (not shown), indicate that, irrespective of whether starting from an initially straight or a pre-existing shoreline profile, the shoreline profiles that eventually develop are nearly identical. Further details are available in Nnafie et al. (2024).

Discussion

Novelty of this study

The novelty of this study is that, for the first time, a coupled shelf-shoreline model was used, which considers the joint effect of tsr and sfcr on decadal shoreline dynamics. The model outcomes demonstrate that the presence of sfcr on the shelf notably impacts decadal shoreline development, with this impact becoming stronger with decreasing distance of the sfcr to the shoreline. Compared to sfcr, the impact of tsr on the shoreline development turned out to be weaker but non-negligible, consistent with the findings by Nnafie *et al.* (2021), who obtained similar outcomes when they used conditions of time-varying wave forcing.

Comparison with observations

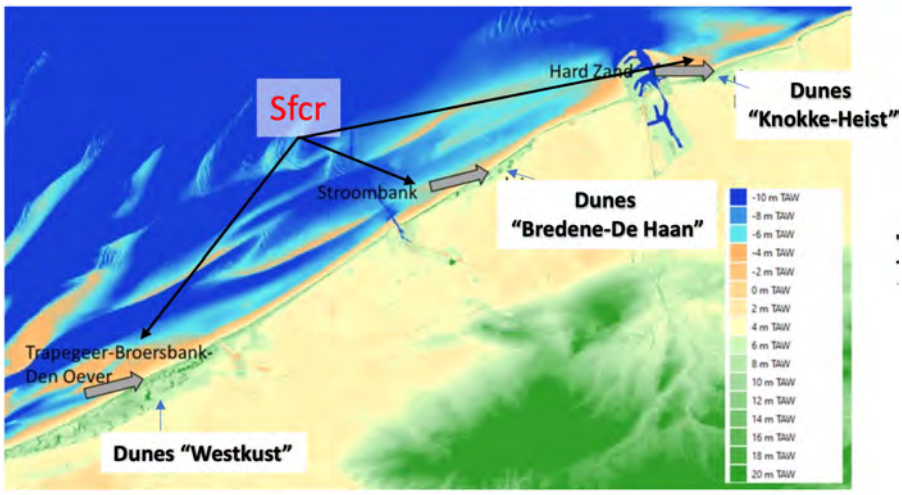

Figure 47 – Bathymetric map of the Belgian coastal zone, showing the development of extensive dune areas (green colour) near three offshore located sfcr , as indicated by the black arrows. Figure adapted and modified from the work by Verwaest et al. (2022)

Figure 47, which depicts a bathymetric map of the Belgian coastal zone including locations of dunes, shows that three extensive (aeolian) dunes (green areas) have developed on the upper beach and backshore near three offshore located sfcr (indicated by the black arrows), which suggest that shoreline progradation took place in these areas. Verwaest et al. (2022), who analysed topographic data for the Belgian west coast between 2000 and 2020, reported the existence of a natural sediment feeding from offshore to the coastline, likely contributing to the growth of dune "Westkust". This natural sediment supply was attributed to the presence of the crest of the offshore located sfcr.

Beach nourishments have been executed in the proximity of the channel between these ridges and the coast, implying that the shoreline tends to erode at these locations (Dujardin *et al.,* 2023). Similar trends in the shoreline development at decadal time scales were observed by Héquette and Aernouts (2010), who linked the shoreline evolution in the northern coast of France near Calais during the 20th century to offshore changes in bathymetry. They found that eroding (accreting) shorelines generally correspond to areas adjacent to channels (sfcr crests).

The results of the present study seem to agree with these observations. However, the Belgian coast zone has experienced intense human activities over the past two centuries, including beach nourishments, construction of groins, harbours, navigation channels and hard coastal protection measures. Whether human activities have also contributed to the observed shoreline progradation and dune growth near the sfcr (Figure 47) remains unclear. In particular, the "Knokke-Heist" coastal area has experienced an extensive expansion of the Zeebrugge harbour between 1970 and 1985, which might have impacted the shoreline evolution in this area. Additionally, the "Knokke-Heist" area may have been significantly influenced by the human activities in the Scheldt estuary and its mouth (e.g., channel deepening, land reclamations), which further complicates the quantification of the relative impact of the shelf ridges on shoreline evolution compared with human-induced evolution.

In addition to shoreline retreat near channels, model results suggest a retreat to the north of ridge crests, as can be seen from, e.g., Figure 44a. However, whether such a retreat occurred in the field is currently unknown. Furthermore, observations in the Belgian coastal area show that, besides an onshore migration, sfcr also migrate alongshore (Chapter 1). Based on the model results, it is expected that the zones of shoreline progradation (retreat) will intensify near ridge crests (channels), with these shoreline changes moving alongshore with the alongshore movement of the ridges.

Physical interpretation

The emergence of shoreline undulations in the present study is attributed to the forcing template established through the influence of the shelf ridges on the wave propagation towards the shoreline. The basic ingredient of the underlying physical mechanism is wave refraction by the ridges. This gives rise to distinct zones of strong and weak wave energy, as wave energy is focused over the crests of the sfcr and defocused in the channels between them (Safak et al. 2017). The zones of strong and weak wave energy generate high and low sediment transport in the nearshore zone, resulting in significant gradients along the shoreline. Tsr modify the wave energy as well, but the corresponding spatial variations in wave energy density are considerably smaller than those induced by sfcr. When the sfcr are situated more onshore, focusing or defocusing of wave energy over the sfcr crests or in the channels becomes stronger. Consequently, larger alongshore gradients in the total sediment transport along the shoreline are created, leading to enhanced shoreline undulations. Further discussion can found in Nnafie *et al.* (2024).

Model limitations and potential model improvements

It is important to stress that this model was not designed to perform a reconstruction of the morphodynamic evolution of the Belgian shoreline over recent decades, but rather to gain basic understanding of the effects of onshore migrating ridges towards the shoreline. Therefore, this model was highly idealised, incorporating several simplifications, which are discussed below.

Morphostatic shelf model

The bathymetry of the shelf model, including the tsr and sfcr, was kept fixed during the simulations. This "freezing" of the shelf bathymetry was done because current existing models (including the present one) are not (yet) capable of self-developing sfcr and tsr through the self-organisation mechanism. The assumption of a morphostatic shelf model implies a one-way coupling between the shelf and nearshore models, meaning that the shelf morphology influences the bed level of the nearshore and its shoreline, but not the other way around. In the present study, amplitudes of shoreline undulations are typically of order 10 to 100 meters, which is much smaller than the width of the nearshore zone (1 km).

For these small amplitudes, the one-way approach is considered reasonable. However, in the "Onshore-2" case, where the amplitude of shoreline undulations reached up to 250 m, the validity of the assumption of a morphostatic shelf becomes questionable. In that case, a morphodynamic shelf model where self-developing tsr and sfcr occur is necessary to account for the impact of shoreline changes on the shelf evolution. Developing such a morphodynamic shelf model is the topic of the current research within Activity 2 (Section 3.1.4).

Wave climate

To mimic the stochastic nature of a realistic wave climate, all the wave events in the applied wave forcing were randomly distributed across the 100-year interval. Only a single realisation of the wave climate was used in the model experiments. Ideally, numerous realisations of the wave events should be considered, followed by averaging the ensemble across these realisations. However, due to the long computation times, this approach was not feasible for this study. To explore the sensitivity of model results to the chosen wave climate realisation, two additional experiments were conducted using the setting of the reference experiment, each with a different realisation of the synthetic wave climate. Results (not shown) were nearly identical to those of the reference case, supporting the fact that the choice of a specific realisation of the wave events does not significantly impact the evolution of the shoreline. However, the wave events within these realisations were treated as statistically independent, while in reality, time series of wave parameters exhibit some degree of correlation, which is linked to the wind. Implementing a correlated wave time series would be a next step, which is considered a topic of future research

Role of tides

Tides in the shelf model are forced by a progressive M_2 tidal wave at the seaward boundary of the shelf. Due to tide-topography interaction, both a tidal residual and higher harmonics of the M_2 constituent are generated, so tidal motion in the domain is asymmetric. Additional tidal asymmetry would result from adding e.g. an M_4 component in the tidal forcing.

The morphodynamics in the nearshore model is only indirectly influenced by tides, in the sense that they only modify the wave motion on the shelf and thereby the wave forcing of and sediment transport in the nearshore zone. This is because the topography of the shelf is kept fixed (morphostatic) and sediment transport in the nearshore model is computed with a bulk transport formula that contains only waves as input. The assumption of a morphostatic shelf is reasonable, as the timescale of shoreline undulations (years to decades) is much shorter (van den Berg et al., 2012) than that of the ridges, which typically evolve on centennial and millennia time scales (Dyer and Huntley 1999). Southgate (1989) and Anthony and Orford (2002) showed that strong interactions between waves and tides occur in the nearshore zone of macro-tidal shelves. More recently, Nnafie et al. (2021) demonstrated that the inclusion of tidal sea-surface variations in the nearshore zone somewhat weakens shoreline undulations, yet the overall trend remains unchanged. However, their results should be interpreted with caution, since they did not consider tidal velocities. Incorporating tides in nearshore modelling is recognized as an important topic of future research.

Role of onshore sediment transport

Analysis of sediment budgets in the Belgian (Verwaest *et al.,* 2022) and northern French coasts (Battiau-Queney *et al.,* 2003), as well as in the Fire Island coastal area (Schwab *et al.,* 2013) indicates the existence of sediment transport from the sfcr towards the shoreline. This suggests that sfcr supply sediment to the nearshore. Especially in the case of sfcr located in relatively shallower waters, as studied in the present work, these ridges can contribute substantial amounts of sediment to the beach through shoreward-directed wave asymmetry-induced transport or other mechanisms (Anthony and Aagaard 2020). Héquette and Aernouts (2010) argued that wave-related transport significantly contributed to the formation of the shoreline progradation observed near the ridge in the Calais coastal area, northern France. Similarly, Schwab et al. (2013) provided evidence for the existence of onshore directed sediment transport from the sfcr towards the adjacent shoreline of Fire Island, USA. In the present study, an onshore-directed sediment transport is anticipated to further enhance shoreline progradation in the proximity of the ridge crest, particularly in the case of sfcr located close to the shoreline.

Investigation of ways to incorporate onshore-directed sediment transport is considered a key topic for future model improvements.

Migrating vs displacing sfcr

In the present study, sfcr were displaced cross- and alongshore on the shelf. In reality, however, the sfcr migrate on the shelf, leading to continuous adjustments of the shoreline over time. Model results indicated that regardless of whether starting from an initially straight or a pre-existing shoreline profile (run series S3 and S4 in Table 12), the shoreline goes towards the same equilibrium shoreline profile. Therefore, the static positioning of the sfcr on the shelf in this study, rather than applying a dynamic movement, is not expected to change the outcomes of this study.

Relevance of model results

As the time scale for the evolution of shelf ridges is similar to that of sea level changes, sea level rise might have caused the observed onshore migration of sfcr in the Belgian coastal area (Chapter 1). Given the reported acceleration of sea level rise in these coastal areas over recent decades (Wahl et al., 2013; Steffelbauer *et al.* 2022), this onshore migration could intensify, potentially amplifying shoreline changes near these ridges. Furthermore, the increasing demand for sand extraction from shelf ridges and construction or deepening of navigation channels (Van Lancker *et al.* 2010; Wyns *et al.* 2021) could significantly impact ridge evolution, potentially leading to additional changes along the adjacent shoreline. Continuous monitoring of bathymetric changes and shoreline evolution in these areas is therefore essential to determine whether the onshore movement of shelf ridges and the associated shoreline changes are accelerating.

Summary and Conclusions

The model results show that sfcr and tsr on the Belgian shelf act as a forcing template for the decadal evolution of the shoreline. This template is established through wave refraction over sfcr crests and channels between the ridges and the shoreline. This creates gradients in wave energy density, which induce spatial variations in the longshore sediment transport in the nearshore zone. Consequently, shoreline progradation occurs in the proximity of crests of landward ends of the sfcr, while shoreline retreat appears adjacent to the channels in between the ridges Compared to sfcr, the impact of tsr on the shoreline development turns out to be smaller, but significantWhen the sfcr are positioned more onshore, both shoreline progradation and retreat become stronger. The root-mean square amplitude after 100 years of simulation time of these shoreline undulations appears to strongly increase with decreasing distance of the sfcr to the shoreline. These shoreline undulations shift in conjunction with the alongshore displacement of the sfcr. Based on these outcomes, it is expected that the observed onshore migration of sfcr on the Belgian continental shelf will lead to increased shoreline retreat near the channels and progradation near the crests of the sfcr, with these changes moving with the alongshore movement of the ridges.

Finally, not that model results suggest that a meandering Belgian shoreline should be observed, whereas this meandering is not clearly visible in the present-day shoreline, which is attributed to shoreline fixation. Whether a meandering shoreline existed prior to human interventions would be an interesting subject for further research.

3.1.4 Morphodynamic shelf model

The shelf model in the coupled shelf-shoreline modelling system used in Activity 1 (Section 3.1.3) was morphostatic, i.e., the shelf bathymetry (including the synthetic tsr and sfcr) was kept fixed during the simulations. This "freezing" of the shelf bathymetry was done because the coupled shelf-shoreline model is not (yet) capable of self-developing sfcr and tsr through the self-organisation mechanism. The assumption of a morphostatic shelf model implies a one-way coupling between the shelf and nearshore models, meaning that the shelf morphology influences the bed level of the nearshore and its shoreline, but not the other way around. The amplitudes of shoreline undulations were found to be typically of order 10 to 100 meters, which were much smaller than the width of the nearshore zone (1 km). For these small amplitudes, the one-way approach is considered reasonable. However, in the "Onshore-2" case, where the amplitude of shoreline undulations reached up to 250 m, the validity of the assumption of a morphostatic shelf becomes questionable. In that case, a morphodynamic shelf model where self-developing tsr and sfcr occur would be necessary to account for the impact of shoreline changes on the shelf evolution. The overall objective of Activity 2 is to develop such a morphodynamic shelf model. This model will account for waves, wind and tides. This section presents results obtained so far with this model.

Model description

The morphostatic shelf model used in Activity 1 (Section 3.1.3) is extended into a morphodynamic version by incorporating sediment transport and bed level update. The shelf model assumes a rectangular shelf with dimensions $L_x \times L_y$, where the x and y represent the cross- and alongshore directions, respectively (Figure 48a). Coordinate z denotes a vertical position, while $z_b(x,y,t)$ (defined with respect to the undisturbed water level $z = 0$) marks the position of the bed level, positive upward. Perturbations in bed-level $z_b(x,y,t)$ with respect to its initial value ($z_b(x,y,0)$) are represented by h (positive upward), i.e., $h(x,y,t) = z_b(x,y,t) - z_b(x,y,0)$.

Sediment transport, assumed to be non-cohesive and characterized by a spatially uniform d_{50}, is calculated according to the formulations of Van Rijn (1993). These formulations included both bedload and suspended load transport under the joint action of waves and currents. The time evolution of the shelf bed level ($\partial z_b / \partial t$) is determined by the net exchange of sediment between the water column and the bed, as well as the spatial gradients in the bedload sediment transport vector $\vec{q}_b$. Further details are available in Appendix A.

A view of the structure of the new morphodynamic shelf model is depicted in Figure 48b. Waves exert a shear stress at the bottom, thereby eroding sediments from this bottom. Subsequently, these sediments are transported by current $\vec{v}$, which is induced by wind and tide. The divergence or convergence of sediment transport $\vec{q}_{tot}$ determines changes in bed-level z_b, which influence the current and the waves. Waves affects also the currents and vice versa. At the offshore boundary, obliquely incoming waves and a wind forcing pointing in the negative y-direction are prescribed. The waves are characterized by a significant wave height H_{s0}, angle of wave incidence θ_0 (with respect to the negative x-axis, positive counter-clockwise) and peak period T_{p0}. These waves are assumed to have a JONSWAN shape.

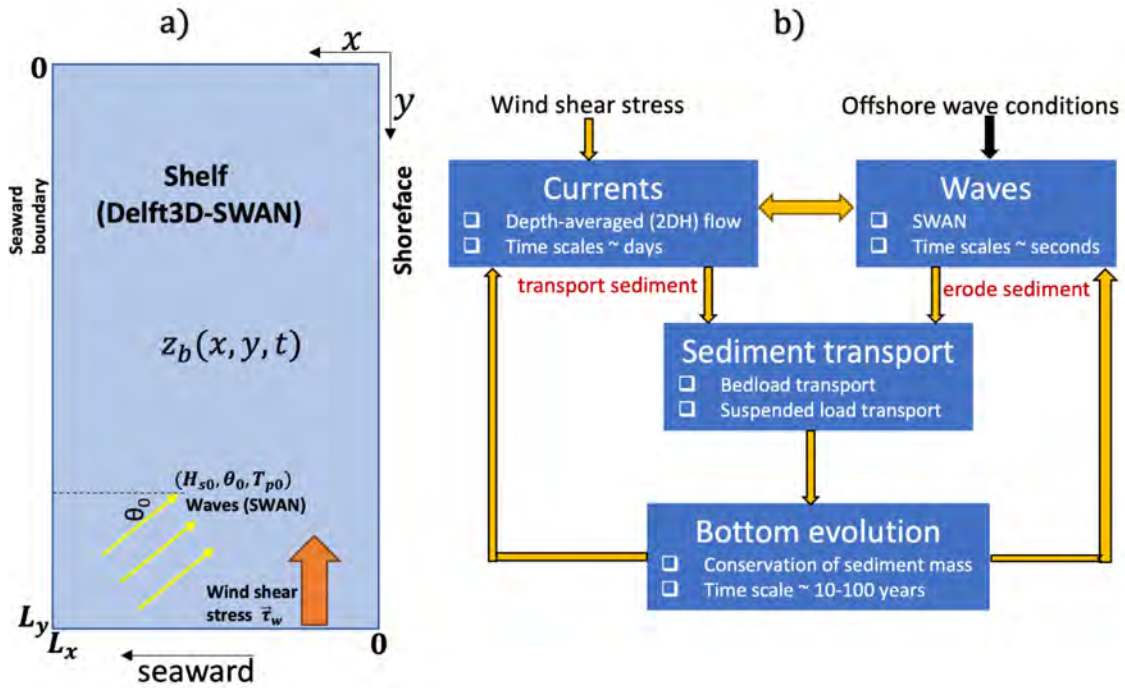

Figure 48 – Schematisation of the morphodynamic shelf model. a)Top view of the rectangular model domain, with dimensions $L_x \times L_y$, where the x and y represent the cross- and alongshore directions, respectively. The model, comprising of a coupled Delft3D-SWAN modelling system, is driven by time-varying wave and wind forcings. Currents and sediment transport and resulting bed level changes are simulated using Delft3D, while waves are computed using SWAN. Waves are characterized by a time-varying significant wave height $H_{s0}(t)$, angle of wave incidence $\theta_0(t)$ (with respect to the negative x-axis, positive counter-clockwise), and peak period T_{p0}. These waves are assumed to have a JONSWAP shape. Wind forcing is represented by a time-varying wind stress $\vec{\tau}_w$ directed alongshore the negative y-axis. b) Structure of the morphodynamic shelf model: Waves erode sediment from the seabed, which is subsequently transported by wind-induced currents. Divergence or convergence of sediment transport leads to bed level changes, which, in turn, influence both currents and waves. Additionally, waves affect currents and vice versa, creating a dynamic feedback loop.

Methodology

The morphodynamic shelf model has the same dimensions as the morphostatic shelf model in the coupled shelf-shoreline modelling system. Tidal forcing, comprising M_2 and M_4 components, are prescribed at the seaward boundary ($x = x_L$). Amplitudes and phases of these components are derived from the harmonic analysis described in Section 3.1.2 (see also Table 10). Specifically, at the southern boundary ($y = 0$), the M_2 and M_4 tidal components have amplitudes $\hat{\eta}_2 = 1.67$ m and $\hat{\eta}_4 = 0.1$ m, with phase differences of $\phi_2 = 73°$ and $\phi_2 = 94°$. At the northern boundary (y_L), the amplitudes remain the same, but the phase differences are $\phi_2 = 96°$ and $\phi_2 = 187°$. This prescribed tidal forcing simulates a tidal wave moving in the negative y-direction. As a first step, southwesterly stormy waves are considered, which are assumed to remain constant during the model simulations, with $H_s = 3.5$ m, $T_p = 11$ s and $\phi_w = 110°$. A wind forcing is prescribed, having the time-varying wind velocity depicted in Figure 38. Since wind blows predominantly from the southwest (almost parallel to the Belgian shoreline, Figure 37c), the wind forcing imposed in the model is directed in the negative y-axis (Figure 48a).

To address the first objective within Activity 2, two experiments are carried out: one with a constant wind velocity of $V_w = 20$ m/s (experiment "ConstantWavesWind_NoTides", Table 13) and another with a time-varying wind velocity using the time series depicted in Figure 38 ("Time-varying wind"). In both experiments, the waves, with $H_s = 3.5$ m, $T_p = 11$ s and $\phi_w = 110°$, represent stormy conditions.

For the second objective, which examines the effects of tides on ridge evolution on the shelf, two additional experiments are conducted: "OnlyTide" and ""TideWavesWind". In "OnlyTide", the model is forced with tides only (M_2 and M_4), excluding waves and wind. In "TideWavesWind", the model forcing is similar to that in the "Time-varying wind" experiment, with the difference that tides are included in the model forcing. Note that, as a first exploration, the waves ($H_s = 3.5$ m, $T_p = 11$ s and $\phi_w = 110°$) represent stormy conditions.

The simulations start from small-scale random bottom perturbations (with a root-mean square height of 10 cm) superimposed on the bathymetry. The idea here is these perturbations contain all kinds of patterns with different length scales. The formation mechanisms of (sfcr) and (tsr) will subsequently cause the bottom pattern that initially has the fastest growth rates to dominate after some time. After that stage, when ridges have attained considerable height, they will nonlinearly interact with each other and typically saturated towards finite heights. To reduce computation time, a morphological amplification factor of 400 is used. This is justified because the morphodynamic timescale is much longer (order of years) than the hydrodynamic timescale (order of hours to days). Test experiments confirm that using smaller amplification factors does not alter the model outcomes. Experiments were conducted for a maximum duration of 2000 years. The characteristics of the simulated bedforms are analysed in terms of their average height H_{av} (crest-to-trough distance), global migration speed V_m and their longshore dominant spacing λ. Migration V_m and spacing λ are defined as follows:

$$V_m = -\frac{1}{\overline{\left(\frac{\partial h}{\partial y}\right)^2}}\overline{\frac{\partial h}{\partial y}\frac{\partial h}{\partial t}}. \qquad (5)$$

In these expressions, the overbar indicates averaging over the entire model domain, i.e., $\frac{1}{L_x L_y}\int_0^{L_y}\int_0^{L_x}\cdot\ dxdy$.

The longshore dominant spacing of the sand ridges (λ_d) is computed using the discrete Fourier transform of the bottom perturbations h at the longshore section $x = 2.2$ km. This dominant spacing is defined as the longshore spacing between ridges for which the modulus of the Fourier coefficients is maximum:

$$F(x_t, k_l, t) = \sum_{j=1}^{N_y} h\left(x_t, y_j\right) e^{-i\frac{2\pi}{N_y}(j-1)(l-1)}, k_l = \frac{2\pi(l-1)}{L_y},\ \ l = 1{:}\,N_y,\ \ y_j = j\Delta y. \qquad (6)$$

Here, $F(x_t, k_l, t)$ is the Fourier coefficient that corresponds to the topographic wavenumber k_l and N_y is the number of grid points in the longshore direction (y). The wavenumber for which the modulus of the Fourier coefficient ($|F(x_t, k_l, t)|$) is maximum for a given time t and longshore position x_t defines the dominant mode, which is used to compute the longshore dominant spacing λ_d.

Table 13 – List of model experiments conducted within Activity 2.

Name experiments	Description
"ConstantWavesWind_NoTides"	Reference experiment: Constant waves and wind (stormy conditions), no tide.
"Time-varying wind"	Constant (stormy) waves and time-varying wind velocity, no tide.
"OnlyTide"	Only tides (M_2 and M_4), no waves and wind.
"TideWavesWind"	Tides (M_2 and M_4), constant (stormy) waves and time-varying wind velocity.

Results and discussion

Reference case: only waves and wind

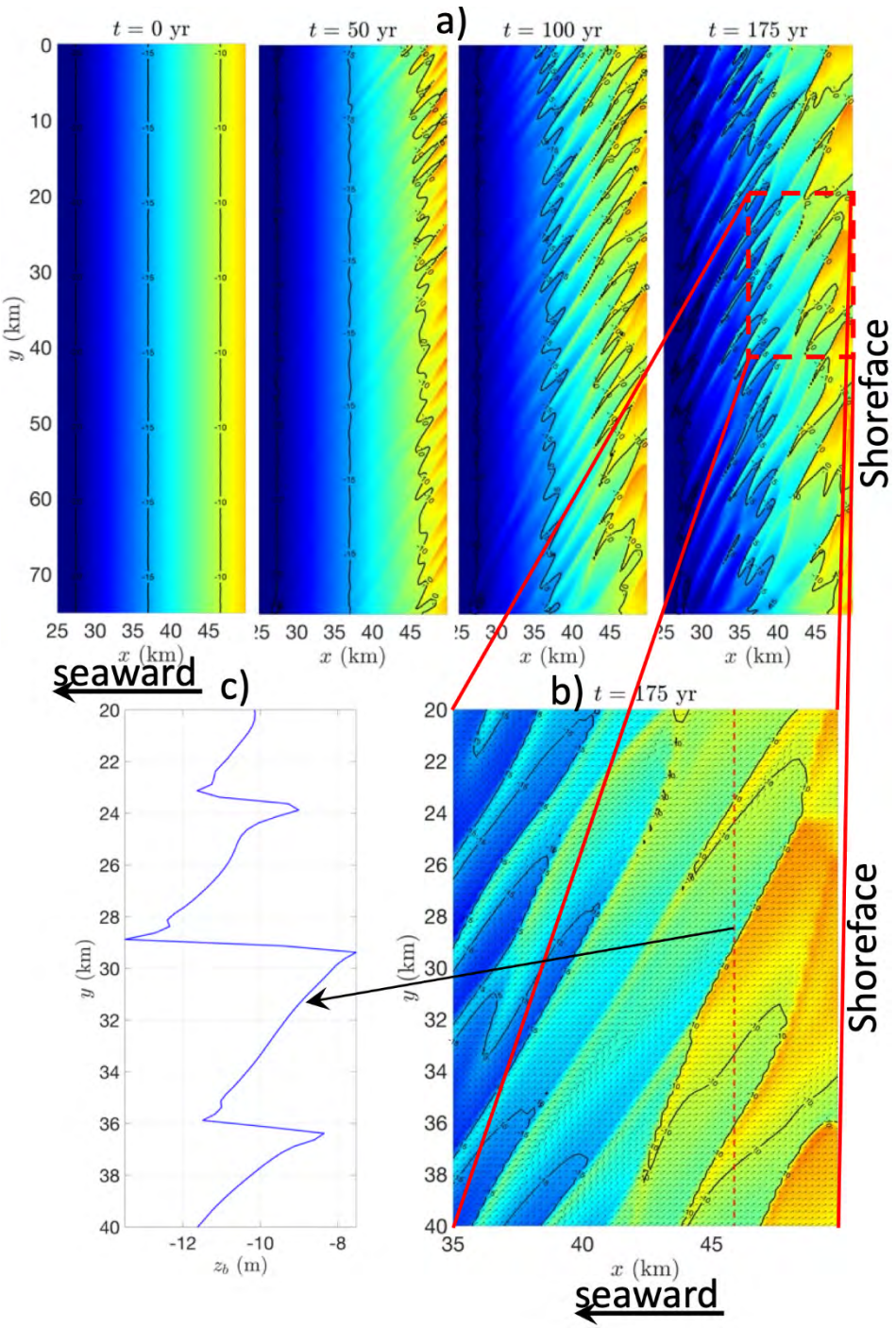

Figure 49 – Morphodynamic shelf model results. a) Snapshots of the simulated bed level z_b at times $t = 0$ yr, $t = 50$ yr, $t = 100$ yr and $t = 175$ yr. A zoom-in at $t = 175$ yr is displayed in panel b, while panel c shows the bed level profile along the alongshore transect depicted in panel b (dashed red line).

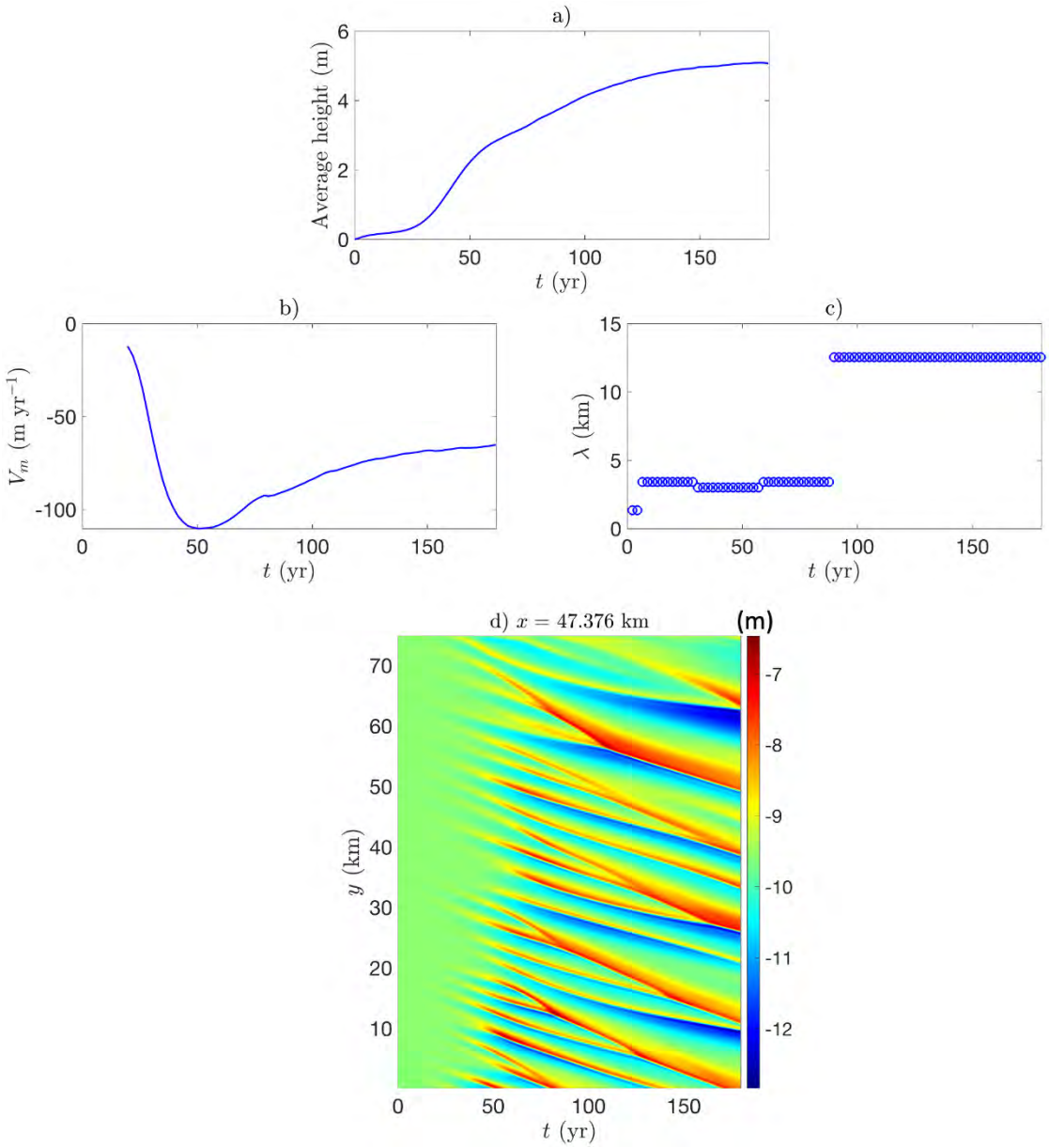

Figure 50 – Average height of the ridges H_{av} (a), their migration speed V_m (b) and their dominant longshore spacings λ_b versus time.

Figure 49 (panel a) shows snapshots of the simulated bed level z_b at different points in times ($t = 0$ yr, $t = 50$ yr, $t = 100$ yr and $t = 175$ yr) in the case that only waves and wind are considered ("ConstantWavesWind_NoTides" experiment). These snapshots illustrate the evolution of randomly imposed bottom perturbations on the initial bathymetry over time, which evolve into large-scale, elongated, and oblique ridges on the shelf. Initially, a mode scale selection process takes place, where the bottom mode with the most-preferred topographic wavelength (alongshore spacing) grows over time, while other modes decay. Over time, coast-oblique ridges resembling shoreface-connected sand ridges (sfcr) manifest on the shelf, maintaining a connection to the shoreface. These sfcr originate close to the shoreface and gradually extend offshore. Eventually, these sfcr exhibit widths of approximately 5 km, with lengths spanning between 15 and 25 km (panel b). From Figure 49c and Figure 50, it is seen that 1) the sfcr attain heights of about 5 m over time (panel a), 2) they migrate downstream (negative y direction) at rates V_m of roughly -55 myr^{-1},

as a result of the storm-driven currents (Figure 50, panel b), and 3) they have alongshore spacings of roughly ∼ 12 km (panel c). Initially, ridge height grows exponentially, eventually saturating towards the end of the simulation period (panel a).

Furthermore, Figure 50 (panel d), which displays the time evolution of the bed level along the alongshore transect depicted in panel b of Figure 49 (red dashed line), reveals that as the ridges develop on the shelf, smaller ridges gradually merge into larger-scale bedforms with larger alongshore spacings. This merging causes the jumps in wavelength that are seen in panel c.

The height, dimensions (width and length) and alongshore spacing of the simulated sfcr described above are similar to those observed on the Belgian shelf (Figure 35, see also Chapter 1). However, a notable difference is that the observed ridges on the Belgian shelf are more oblique than the simulated ones. This discrepancy in ridge orientation may arise from the absence of tides and the use of constant wave and wind forcing in this experiment. Another notable difference is the migration rate of the ridges: the simulated ridges migrate significantly faster than the observed ones, which migrate at approximately 10 to 20 m/yr alongshore in the northeastern direction (Chapter 1). This discrepancy is attributed to imposing continuous stormy conditions in the reference experiment, whereas in reality, the wind climate alternates between fair and stormy conditions. When a time-varying wind velocity that alternate between these conditions is prescribed, as is the case in the "Time-varying wind" experiment, the (average) migration rate is reduced by a factor of ∼ 2, as shown in Figure 51 (panel c). Note the fluctuating migration rate between larger and smaller values, reflecting the time-varying wind velocity. Figure 51 further demonstrates that incorporating a time-varying wind velocity significantly reduces the growth rate of the ridges (panels a and b). The use of a time-varying wave climate is expected to further reduce the growth and migration rates of the ridges, which is a topic of future research.

Finally, we would like to highlight an important novelty of this study: for the first time, a morphodynamic model is established in which sfcr develop on the shelf in the case of using a sediment formulation other than the traditional formulations employed in previous models (see the review by Ribas et al., 2015). Specifically, this study uses the formulations of Van Rijn (1993) (see Appendix A), in contrast to the widely used Bailard (1981) sediment formulations. Results from additional experiments (not shown) show that, besides the Van Rijn (1993) formulations, sfcr also develop when using other transport formulations, such as the Soulsby-van Rijn (Soulsby 1997) and Van Rijn (2007) formulations. Thus, the occurrence of sfcr on the shelf is not limited by the type of sediment transport formulation employed in the model, unlike in previous studies (Calvete et al. 2001; Vis-Star et al., 2007; Nnafie et al. 2014). The reason why sfcr develop on the shelf, irrespective of the type of transport formulation used, is believed to be due to the presence of directional wave spreading in the SWAN wave modell. Notably, previous modelling studies on sfcr, which were based on linear wave theory, did not account for directional wave spreading.

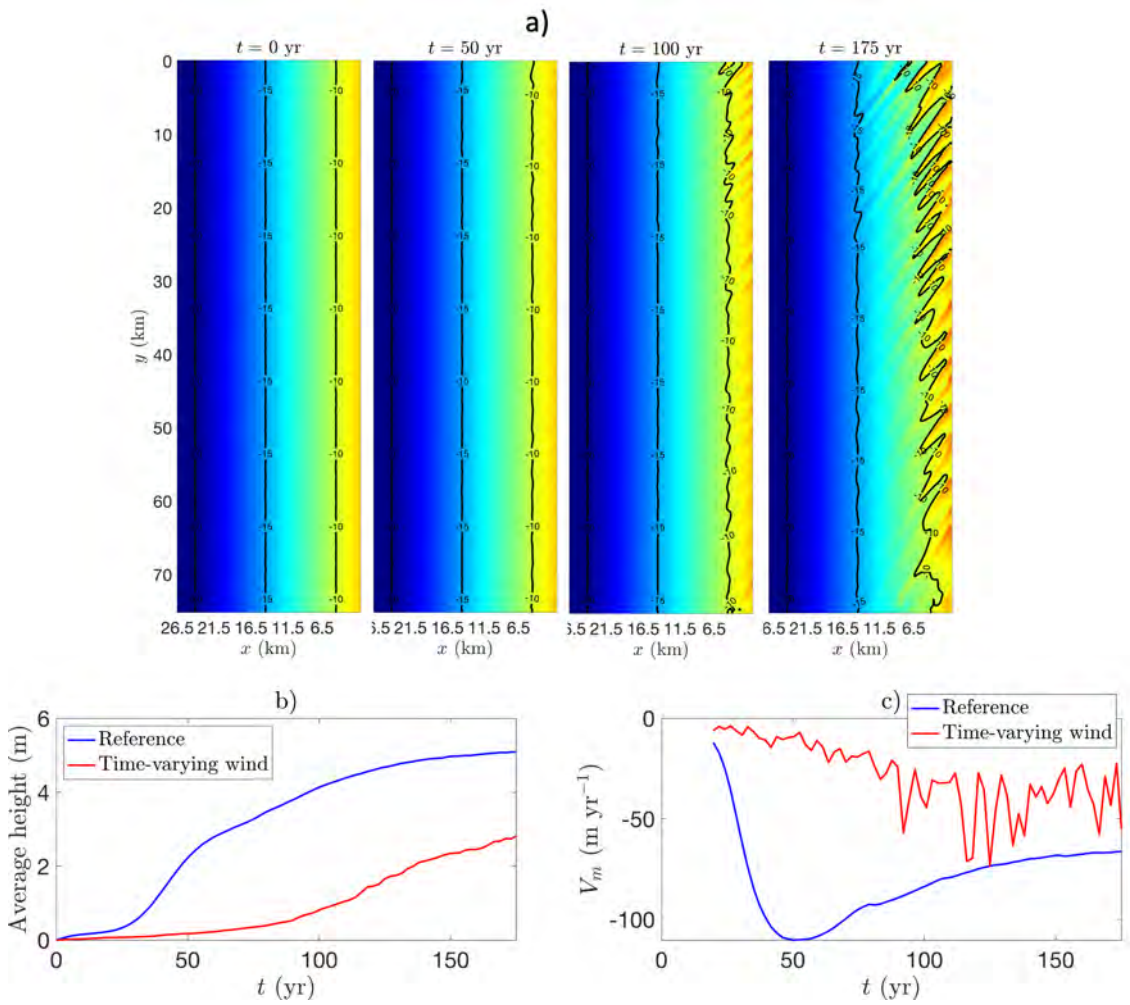

Figure 51 - Snapshots of the simulated bed level z_b at times $t = 0$ yr, $t = 50$ yr, $t = 100$ yr and $t = 175$ yr in the "Time-varying wind" case. b-c) Average height of the ridges H_{av} (b) and their migration speed V_m (c) versus time in the "ConstantWavesWind_NoTides" and "Time-varying wind" cases (blue and red lines, respectively)

Only tides

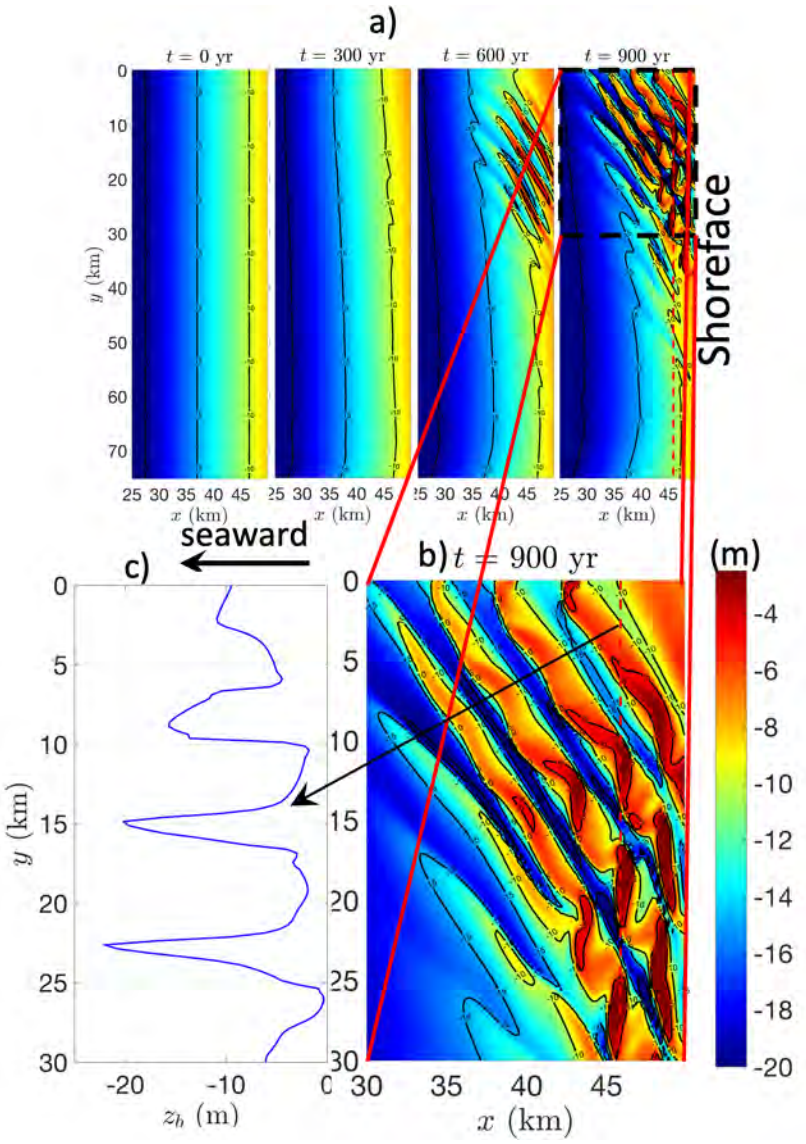

Figure 52 – Morphodynamic shelf model; results for only tides. a) Snapshots of the simulated bed level z_b at times $t = 0$ yr, $t = 300$ yr, $t = 600$ yr and $t = 900$ yr in the case of only tides (no waves and wind). A zoom-in at $t = 900$ yr is displayed in panel b, while panel c shows the bed level profile along the alongshore transect depicted in panel b (dashed red line).

Figure 52 presents snapshots of the simulated bed level z_b at times $t = 0$ yr, $t = 300$ yr, $t = 600$ yr and $t = 900$ yr (panel a) in the case that the shelf model is forced only by tides (so no waves and wind forcing, experiment "OnlyTide"). A zoom-in at $t = 300$ yr is displayed in panel b, while panel c shows the bed level profile along the alongshore transect indicated by the dashed red line in panel b. From the snapshots in panel a it appears that the random bottom perturbations imposed on the initial bathymetry evolve on a centennial time scale into large-scale elongated bedforms on the shelf. These bedforms initially form close to the shoreward boundary and gradually extend to the offshore area. Panel c shows that the ridges reach heights (crest-to-trough distances) up to 25 m, with lengths on the order of tens of kilometres, and wavelengths of about 6 km. Crests of the ridges are rotated counterclockwise by up to 30° relative to the main south–north direction of the tidal current. These bottom patterns resemble tidal sand ridges observed on the Belgian shelf (Figure 35).

Waves, wind and tide

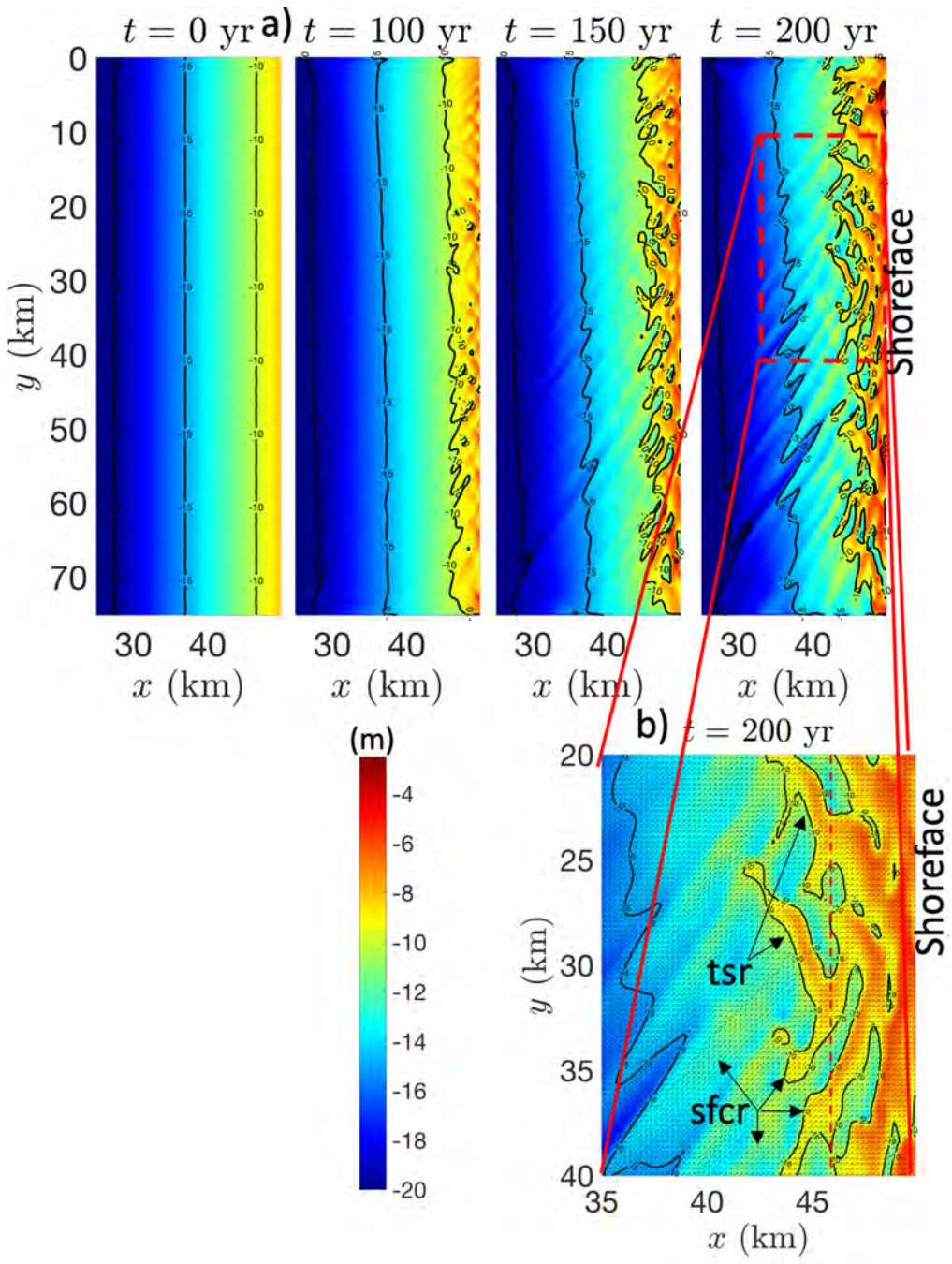

Figure 53 – Morphodynamic shelf model; experiment “WavesWindTides” a) Snapshots of the simulated bed level z_b at times $t =$ 0 yr, $t = 100$ yr, $t = 150$ yr and $t = 200$ yr in the case of constant (stormy) waves, time-varying wind velocities and tides (experiment "WavesWindTides"). A zoom-in at $t = 200$ yr is displayed in panel b..

Results in the case that all three forcings (waves, wind and tides, experiment "WavesWindTides") are imposed in the shelf model are presented in Figure 53, which shows Snapshots of the simulated bed level z_b at times $t = 0$ yr, $t = 100$ yr, $t = 150$ yr and $t = 200$ yr in the case of constant (stormy) waves, time-varying wind velocities and tides (experiment "WavesWindTides"). A zoom-in at $t = 200$ yr is displayed in panel b. From panel a it is seen that a complex bottom pattern develop on the shelf over time, comprising of a mix of ridges that resemble sfcr and tsr (indicated in panel b).

These results indicate that the formation mechanisms of sfcr and tsr proposed by, respectively, Trowbridge (1995) and Huthnance (1982) are both active on the shelf. Results from additional experiments (not shown) reveal that reducing

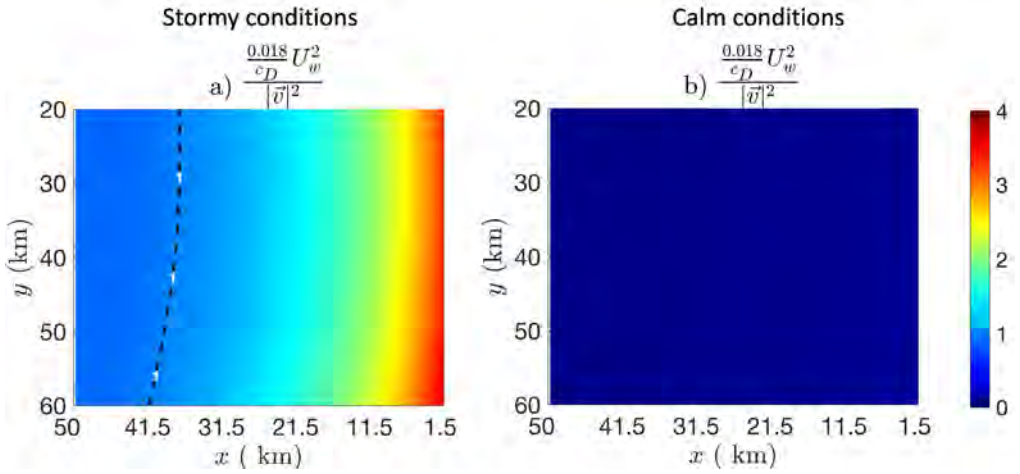

Figure 54 – Ratio R of the bottom shear stresses related with waves ($\sim \frac{0.018}{c_D} U_w^2$) and currents ($\sim |\vec{v}|^2$) according to the Soulsby-van Rijn sediment formulation (Soulsby 1997) in the cases of stormy (a) and calm conditions (b). In these expressions, c_D ($= 4$ mm) is a morphodynamic drag coefficient, typically ranging from 1 to 10 mm (Damgaard et al. 2002), U_w represents the magnitude of the near-bed peak wave orbital velocity (computed by SWAN) and $|\vec{v}|$ is the magnitude of current velocities resulting from tide and wind. For stormy conditions, the wave and wind forcings of the "ConstantWavesWind_NoTides" experiment are applied, while for calm conditions, values $H_s = 0.5$ m and $V_w = 5$ m/s are used.

the significant wave height weakens the growth of sfcr. Under fair weather wave conditions ($H_s < 1$ m), the sfcr do not develop, while tsr dominate on the shelf. Results from these additional experiments also show that decreasing tidal amplitude weakens the formation of tsr. When tidal currents are too weak, only sfcr form on the shelf. This competition between the formation mechanisms of sfcr and tsr can be characterised by the ratio R of bottom shear stresses related with waves ($\sim \frac{0.018}{c_D} U_w^2$) and currents ($\sim |\vec{v}|^2$) according to the Soulsby-van Rijn sediment formulation (Soulsby 1997). In these expressions, c_D ($= 4$ mm) is a morphodynamic drag coefficient, typically ranging from 1 to 10 mm (Damgaard et al. 2002), U_w represents the magnitude of the near-bed peak wave orbital velocity (computed by SWAN) and $|\vec{v}|$ is the magnitude of current velocities resulting from tide and wind. By plotting ratio $R = \frac{\frac{0.018}{c_D} U_w^2}{|\vec{v}|^2}$, it appears that the wave related shear stress dominate ($R \geq 1$) during stormy conditions (Figure 54, panel a). Under calm conditions, the current related shear stress dominate $R << 1$ (panel b).

A notable difference between model results and observations the location of tsr on the Belgian shelf. Observations indicate that the tsr are situated further offshore, while the sfcr are located on the shoreward part of the shelf (Figure 35). In contrast, the tsr and sfcr that form in the model are both located on the shoreward part of the shelf (Figure 53). This difference in tsr location between model results and observations may be caused by the use of constant (stormy) waves in experiment "WavesWindTides". Incorporating tides along with alternating stormy and fair wave conditions is anticipated to cause the tsr to form further offshore, as reported in the study by Walgreen et al. (2002). Investigating the effects of alternating fair and stormy wave conditions on the evolution of the shelf ridge evolution remains a topic of future research.

Summary and Conclusions

In Activity 2, efforts were concentrated on further developing the morphodynamic shelf model by 1) incorporating a wind climate more representative for the Belgian shelf and 2) including tides in the model.

The morphodynamic shelf model successfully simulate sfcr with characteristics (height, width, length and alongshore spacings) similar to those observed on the Belgian shelf. However, the observed sfcr on the Belgian shelf are more oblique and their migration rates are slower than the simulated ridges. Incorporating a time-varying wind velocity alternating between stormy and fair weather reduces both migration rates and sfcr growth. Further reduction is expected by including a time-varying wave climate, a focus of year 4 of the MOZES project.

When only tides are included, large-scale, elongated, counterclockwise-rotated bedforms resembling tsr evolve. With waves, wind and tides active, a complex mix of sfcr and tsr emerges on the shelf, indicating that both formation mechanisms of these ridges are active on the shelf. A key discrepancy is the tsr location: observed tsr occur offshore, while modelled tsr are situated more shoreward. This mismatch likely stems from the use of stormy waves and the absence of sea level rise in the model, aspects that will be addressed in year 4 of the MOZES project.

Furthermore, we would like to highlight the novelty of this study: the morphodynamic shelf model is the first to simulate sfcr on the shelf using sediment formulations (Van Rijn 1993; 2007; Soulsby 1999) other than those used in traditional models. This is attributed to the presence of directional wave spreading in the SWAN wave model, unlike in earlier modelling studies where directional spreading was absent. These results demonstrate that sfcr formation is not constrained by a specific sediment transport formulation, unlike in earlier studies.

3.2 2DH models development for Knokke-Heist area

3.2.1 Introduction

Research conducted in working year 2 of the MOZES-project revealed that both the Scaldis-Coast (openTELEMAC-suite) and FlemCo (Delft3D Flexible Mesh) models predict comparable longshore sediment transport along the Belgian coast for an idealised setup, where

- the same wave model settings (as far as possible, given the different applied wave modelling software),
- constant wave and wind boundary conditions and
- no groynes in the FlemCo model are applied (Dujardin *et al*., 2024).

However, when the models are used with their calibrated settings (see Grasmeijer *et al*., 2020 and Röbke *et al.,* 2000 for FlemCo and Kolokythas *et al*., 2023 for Scaldis-Coast) and realistic boundary timeseries, the FlemCo model systematically predicts lower longshore sediment transport for the Belgian coast than the Scaldis-Coast model (Dujardin *et al*., 2024).

Sensitivity simulation runs performed with the two models based on different forcing combinations (tide, waves and wind) revealed that it is mainly the wave related longshore sediment transport that differs between the two models, while the tide related transports show a closer match. The observed discrepancies of the predicted waves between models is – apart from the different wave models used by Scaldis-Coast and FlemCo (TOMAWAC/SWAN) – related to

- different settings used in the two wave models, especially the applied bed friction coefficient (lower in Scaldis-Coast) and breaker index (higher in Scaldis-Coast),
- the fact that groynes in the Scaldis-Coast model are clearly smaller in dimension (interpolated as bathymetry on the computational grid) in the FlemCo model (fixed weirs with specified elevations), and therefore block the wave-induced longshore current to a smaller degree than in the FlemCo model,
- less directional spreading of waves in the nearshore zone in the Scaldis-Coast model resulting in more dominant wave directions and stronger wave-induced longshore currents than in the FlemCo model.

This altogether favours higher wave energy and/or more pronounced wave-induced longshore currents in the nearshore zone and by this higher longshore transport in the Scaldis-Coast than in the FlemCo model. In the absence of sufficient wave validation data for the applied simulation periods, the wave models could not yet been sufficiently calibrated and validated for the nearshore zone of Knokke-Heist, where tides in the Appelzak gully appear to have an important effect on wave direction.

In the current study, both the Scaldis-Coast and FlemCo models are therefore applied for a different, more recent simulation period that allows for a more detailed calibration and validation of the wave models in the nearshore zone between Zeebrugge harbour and the Belgian-Dutch border, especially with regard to the predicted wave directions and wave heights.

Furthermore for the coastal zone between Zeebrugge harbour and the Belgian-Dutch border, the exact crest height and length of the groynes was examined. For the position above the low water mark a long-term dataset LiDar flights was used. To define the underwater part two multibeam soundings – executed by DEME within the framework of the 2023 – 2024 shoreface nourishment – and scans of the design plans were used. The derived crest heights and (underwater) length of the groynes were then implemented into the Scaldis-Coast model.

3.2.2 Wave model calibration and validation

Methodology

Figure 55 shows the locations of the wave buoys in the area of the Scaldis-Coast and FlemCo model domains, for which wave direction measurements are generally available. The so-called *Meetpalen* buoys are taking measurements since several decades (e.g. MP7 – Wandelaar and MP3 – Bol van Heist since 1995). The buoys, located further offshore are operating since ca. 10 years. Recently (since 2021), several nearshore buoys have been added to the monitoring network, for which, however, the data availability is more scarce and scattered in time.

The primary zone of interest for WP4 (see Section 3.3) is the Belgian east coast. Locations with directional wave data at the Belgian east coast are shown in Figure 56. However, it seems good practice to study the wave propagation in the models as a whole, and also to take into account more offshore locations in deeper water.

Because of the primary interest for the Belgian east coast, the choice for a new simulation period should be based on the data availability of directional wave data for MP2 – Appelzak (Figure 57). Three measurement periods can be distinguished:

- 25 March 2020 – 20/12/2022: numerous data gaps, especially of the wave direction parameters;
- 16 June 2023 – 16 October 2023: no wave direction data because of incomplete installation of the Radac;
- 8 December 2023 – today: complete data set
- Therefore, the period from 8 December 2023 to 22 February 2024 (= start of this study) was chosen as the new calibration/validation period. For this period, corresponding wave measurements are available for MP7 – Westhinder buoy, which were used to force the wave models of both Scaldis-Coast and FlemCo. Several small data gaps of the MP7 – Westhinder measurements were filled by corresponding data measured at Thorntonbank Zuid buoy. For the wave model forcing, we used the measured significant wave height H_{m0}, the peak period T_P and the wave direction *Th0* associated with the maximum wave energy. The wind forcing of the wave (and flow) models of Scaldis-Coast and FlemCo is based on the wind measurements in 10 m above NAP at Vlakte van de Raan buoy.

The calibration and validation of the wave models was based on measurements taken at the following wave buoys (from offshore to the coast; see also Figure 55 and Figure 60):

- MP7 – Westhinder
- Thorntonbank Zuid
- Akkaert Zuid
- Deurlo
- MP3 – Bol van Heist
- A2-Boei
- Blankenberge
- MP2 – Appelzak.

One should note that all measurement locations show a bi-directional wave rose, except for MP2 – Appelzak (Figure 58) where waves propagating from the west are blocked by the breakwaters of Zeebrugge. Figure 59 also illustrates the change in wave directions from offshore to the coast due to refraction.

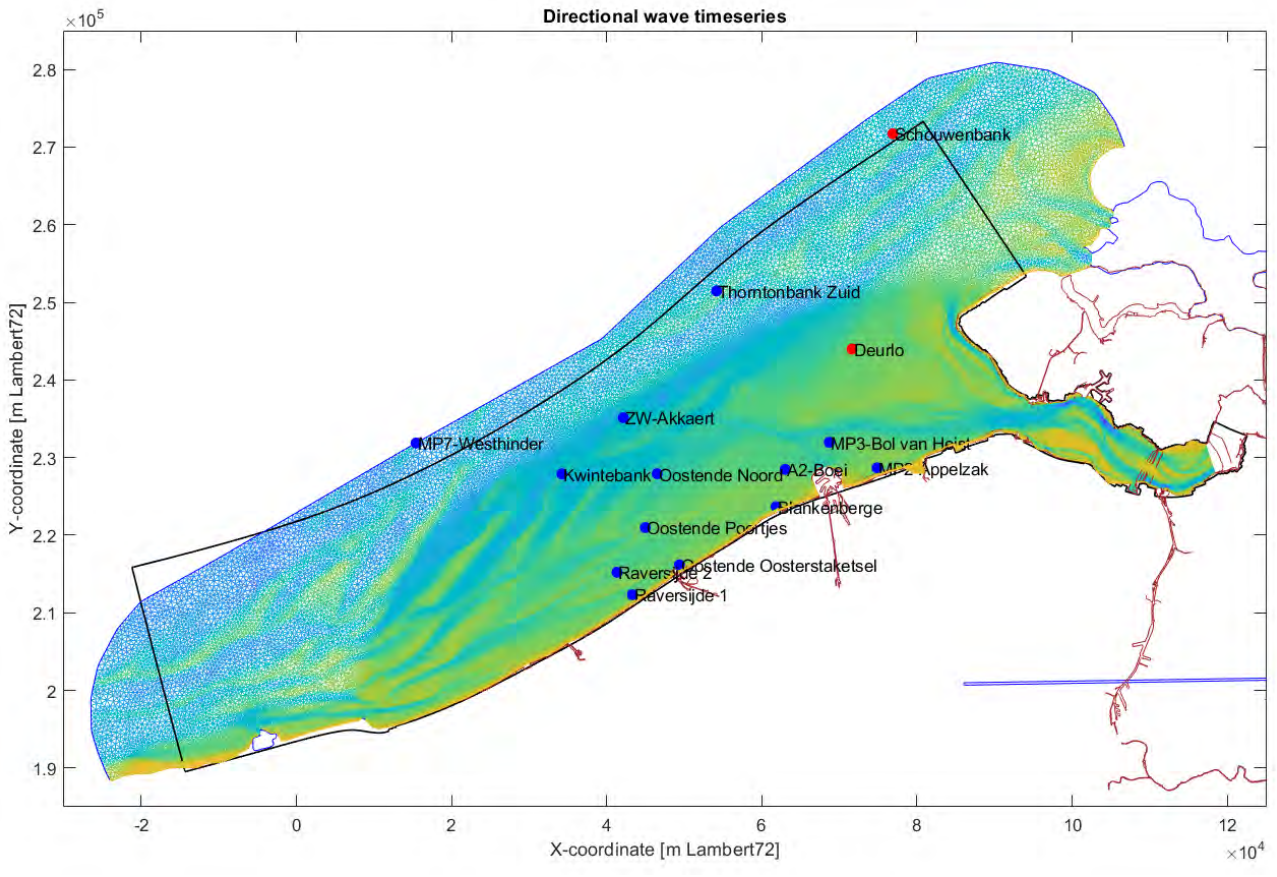

Figure 55 – Location of directional wave buoys from Meetnet Vlaamse Banken (blue dots) and Rijkswaterstaat (red dots) in respect to FlemCo model contour (black line) and Scaldis-Coasts wave mesh (coloured mesh) and current mesh contour (blue line).

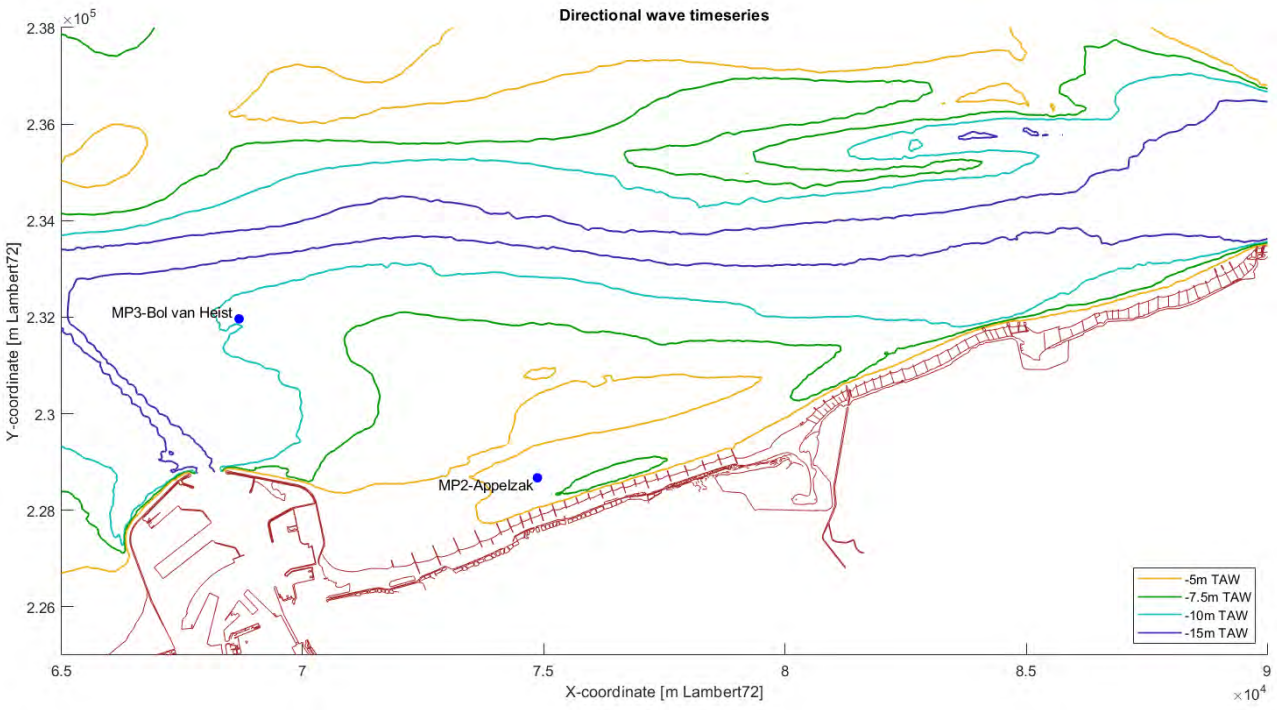

Figure 56 – Location of directional wave buoys MP2 – Appelzak and MP3 – Bol van Heist from Meetnet Vlaamse Banken (blue dots)

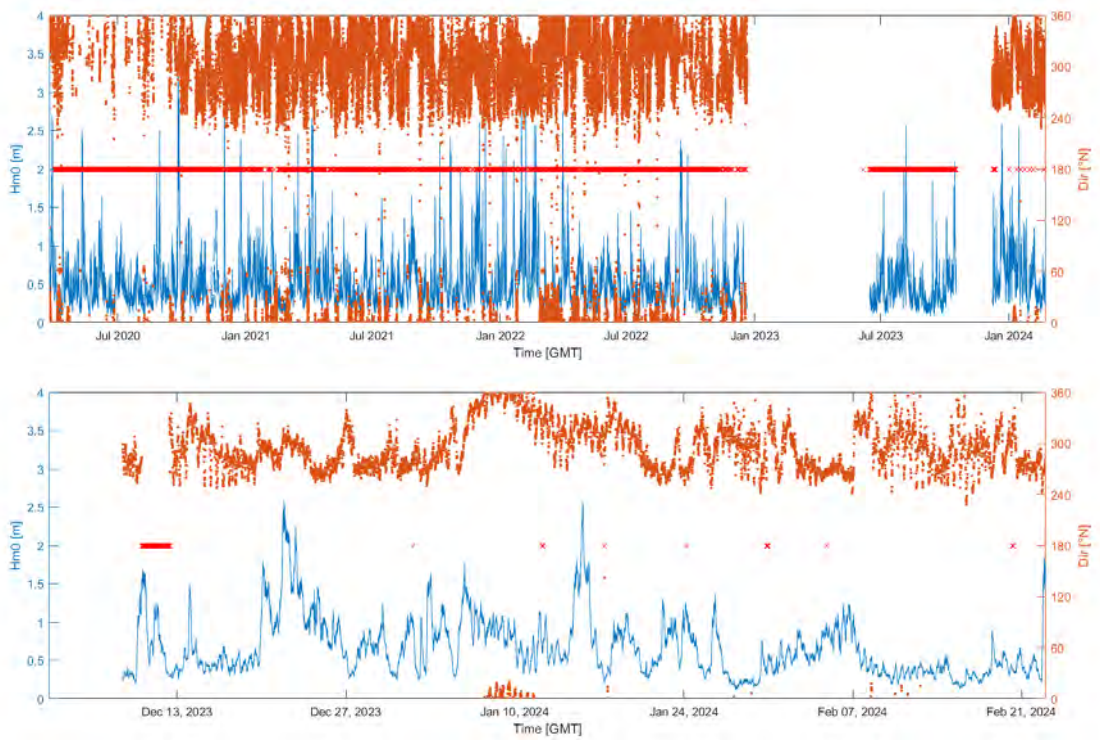

Figure 57 – Data availability for MP2: Radac Appelzak - Bol van Knokke. Top panel: full measurement period from 25/03/2020 – 23/02/2024; bottom panel: zoom on 8/12/2023 – 23/02/2024. Blue line: Hm0; brown dots: mean direction of the 30 – 500 mHz frequency waves; red crosses: directional data is missing.

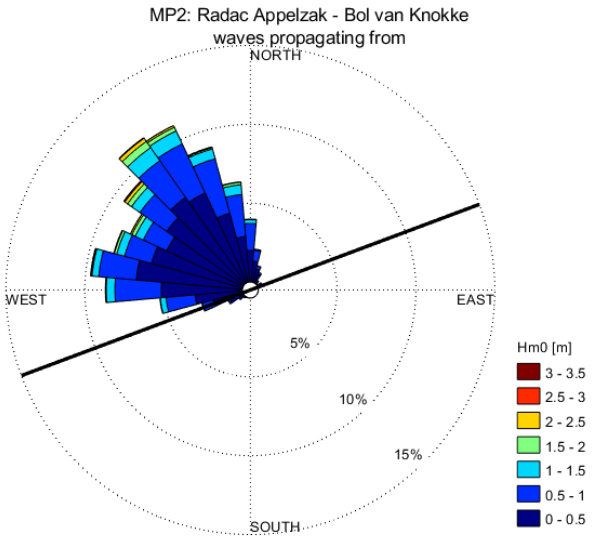

Figure 58 – Wave rose for MP2: Radac Appelzak - Bol van Knokke. Full measurement period from 25/03/2020 – 23/02/2024, only valid Hm0 – Dir data-couples are taken into account.

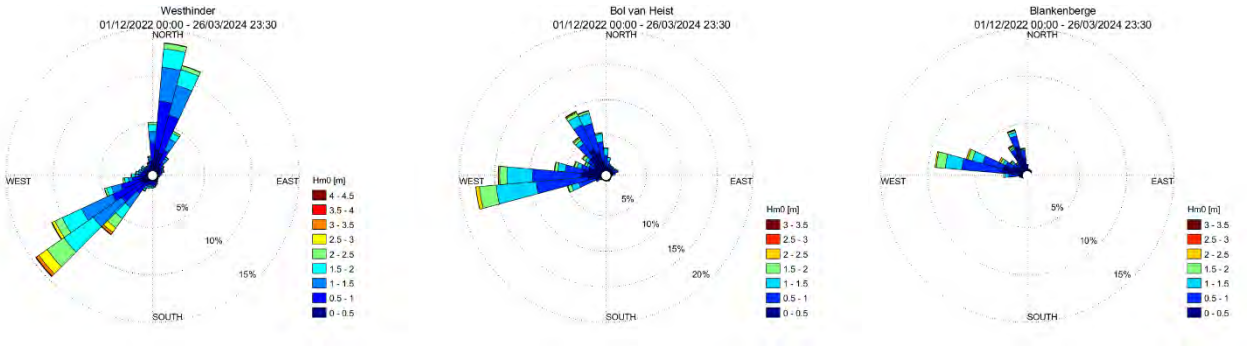

Figure 59 – Observed wave directions for locations Westhinder, MP3 – Bol van Heist and Blankenberge.

With both the Scaldis-Coast and the FlemCo model, several sensitivity runs were performed in order to investigate the effects of various model parameters on the wave predictions for the above mentioned locations and to increase the accuracy of the models with respect to the measurements. Owing to the differences between the applied wave modelling software (TOMAWAC/SWAN), a different set of sensitivity runs has been performed per model.

With the Scaldis-Coast model, particularly the effects of

- the directional spreading parameter,
- the bed friction coefficient,
- the break gamma index (ratio between the wave height and water depth at breaking) and
- the wind forcing (Vlakte van de Raan versus MP7 – Westhinder measured time series)

were studied (see Table 14). Other wave setting for the Scaldis-Coast model (coupling period, wind drag coefficient, white capping dissipation, …) were kept as advised in Wang *et al.* (2021) and Wang *et al.* (2025). The sensitivity runs revealed that both the significant wave height and the wave directions were highly sensitive to the applied wind timeseries (the MP7 – Westhinder time series resulted in a clear overestimation of the wave height and less accurate wave directions nearshore). In contrast, changes of the other parameters had comparatively small impact on the accuracy of the simulated wave height and direction.

The FlemCo model sensitivity runs focussed on

- the simulation mode (non-stationary versus stationary),
- the coupling of flow velocities with the wave model (i.e. the effects of flow on the waves),
- the maximum number of wave computation iterations,
- the directional spreading parameter,
- the bed friction coefficent,
- the break gamma index (ratio between the wave height and water depth at breaking),
- the wind forcing (Vlakte van de Raan versus MP7 – Westhinder measured time series; Table 15).

Also in the case of the FlemCo model, the significant wave height and the wave directions were highly sensitive to the applied wind forcing (the MP7 – Westhinder time series resulted in a clear overestimation of the wave height and less accurate wave directions nearshore). Moreover, the usage of flow velocities in the wave model lead to more accurate wave direction predictions and slightly improved the prediction of the wave height. The remaining parameters had a comparatively small impact, as was found for the Scaldis-Coast model.

In the following three sections, we present the simulated significant wave heights, wave directions and wave roses based on the reference runs of the Scaldis-Coast (Run MO6_207) and FlemCo models (Run 35), which show the best match with the measurements.

Table 14 – Overview of selected wave sensitivity runs of the Telemac Scaldis-Coast model performed for the current study.

Run ID	Simulation mode	Dir. spreading	Bed fric. coef.	Break Gamma	Wind forcing
MO6_200	Non-stationary	4	0.038	0.8	MP7 - Westhinder
MO6_201	Non-stationary	4	0.038	0.5	MP7 - Westhinder
MO6_202	Non-stationary	4	0.067	0.8	MP7 - Westhinder
MO6_203	Non-stationary	4	0.067	0.5	MP7 - Westhinder
MO6_204	Non-stationary	10	0.038	0.8	MP7 - Westhinder
MO6_205	Non-stationary	2	0.038	0.8	MP7 - Westhinder
MO6_206	Non-stationary	3	0.038	0.8	MP7 - Westhinder
MO6_207 (Ref.)	Non-stationary	3	0.038	0.8	Vlakte van de Raan

Table 15 – Overview of selected wave sensitivity runs of the Delft3D Flexible Mesh FlemCo model performed for the current study.

Run ID	Simulation mode	Effects of flow on waves	Max. iterations	Dir. spreading	Bed fric. coef.	Break Gamma	Wind forcing
Run 34	Non-stationary	Yes	15	4	0.067	0.73	MP7 - Westhinder
Run 35 (Ref.)	Non-stationary	Yes	15	4	0.067	0.73	Vlakte van de Raan
Run 36	Stationary	Yes	15	4	0.067	0.73	Vlakte van de Raan
Run 37	Non-stationary	No	15	4	0.067	0.73	Vlakte van de Raan
Run 39	Non-stationary	Yes	50	4	0.067	0.73	Vlakte van de Raan
Run 40	Non-stationary	Yes	15	9	0.067	0.73	Vlakte van de Raan
Run 42	Non-stationary	Yes	15	4	0.075	0.73	Vlakte van de Raan
Run 43	Non-stationary	Yes	15	4	0.067	0.5	Vlakte van de Raan

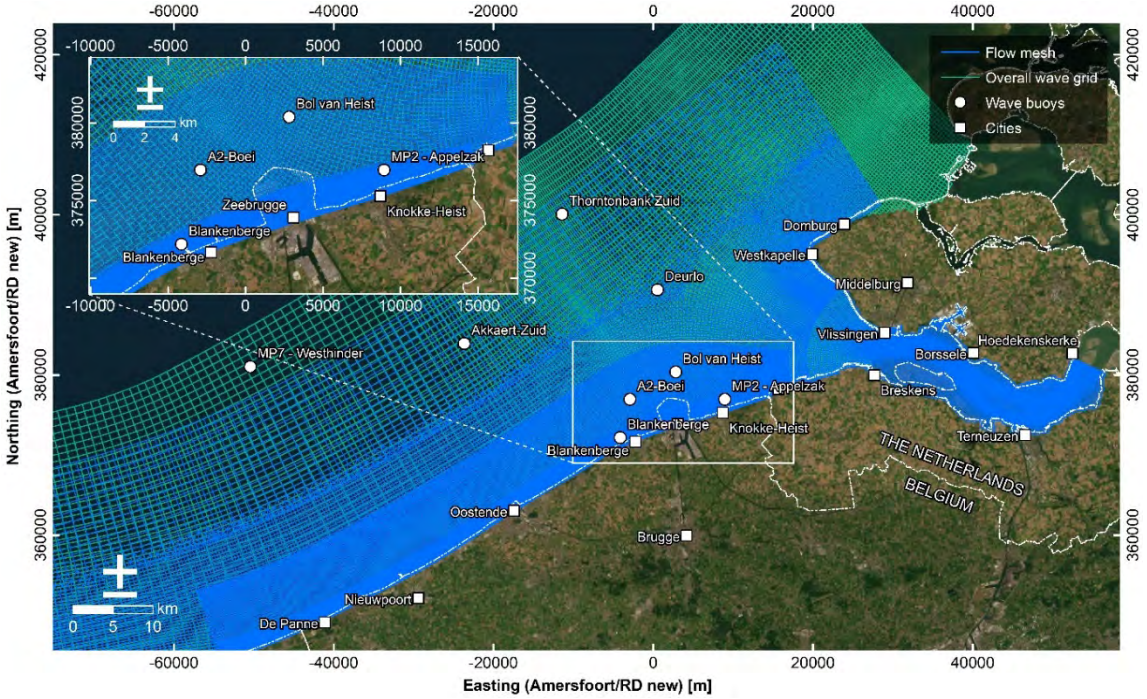

Figure 60 – Map of the study area showing the wave buoys located at the Flemish Coast, for which measured and simulated significant wave heights and wave directions (direction associated with highest wave energy) are compared based on the Telemac Scaldis coast model and the Delft3D Flexible Mesh FlemCo model. The blue and green lines indicate the FlemCo model flow and wave grids.

Validation of the simulated significant wave height

Figure 61 shows the significant wave height at MP7 – Westhinder buoy according to the measurements and the Scaldis-Coast and FlemCo models. The measured wave height strongly varies over time with a minimum value of about 0.3 m, a maximum value of almost 4 m and an average of ca. 1.47 m. Both models generally reproduce the measured wave height time series. While the average wave height according to Scaldis-Coast almost coincides with the average measured wave height, the average wave height simulated with FlemCo is slightly higher (ca. 4 cm). Both models underestimate several wave height peaks despite the fact that the measured MP7 – Westhinder time series is used for the wave forcing of the models. Wang *et al*. (2025) report a better fit between modelled and measured waves at Westhinder for the Scaldis-Coast model. Since Scaldis-Coast model parameter settings were kept identical for the runs presented here, the discrepancy can only be explained by either the different time period modelled and/or the different measurement location of the applied wind time series: Vlakte van de Raan in this report vs. Westhinder in Wang *et al.* (2021).

The wave height time series measured at the other offshore buoy, Thorntonbank Zuid (Figure A 1), is very similar to the time series of MP7 – Westhinder. Also at this location, the simulated wave heights of both models show a good match with the measurements. While the Scaldis-Coast model slightly underestimates the average wave height (by ca. 3 cm), the FlemCo model slightly overestimates it (by ca. 4 cm).

The buoys Akkaert Zuid (Figure A 2) and Deurlo (Figure A 3), which are several kilometres closer to the coast, show a very similar measured wave height time series, although the wave heights are larger at Akkaert Zuid than at Deurlo due to the larger water depth. At both locations, the two models generally reproduce the measured wave heights, although Scaldis-Coast slightly underestimates and FlemCo slightly overestimates the average wave height, as was observed for Thortonbank Zuid buoy.

A2-Boei (Figure A 4) and Bol van Heist (Figure 62) are both located relatively close to Zeebrugge Harbour at a comparable distance to the coast and at a similar water depth. As a result, the measured wave height closely agrees between both locations. Both the Scaldis-Coast and the FlemCo model show a close match with the measured wave heights. At Bol van Heist, the Scaldis-Coast model tend to overestimate several wave height peaks, while it accurately reproduces the average wave height. The FlemCo model slightly overestimates the average wave height at Bol van Heist.

At MP2 – Appelzak buoy (Figure 63), the measured wave heights are clearly smaller compared to the locations described so far, due to the relatively shallow water depths near the coast. Both models accurately reproduce the measured wave height time series, although the FlemCo model shows a slight overestimation of the average wave height by about 5 cm.

Finally, the conclusions regarding the measured and simulated MP2 – Appelzak wave heights also hold true for the Blankenberge buoy (Figure A 5), which is located in similar water depth and distance to the coast. Nevertheless, both models slightly underestimate the average measured wave height at this location.

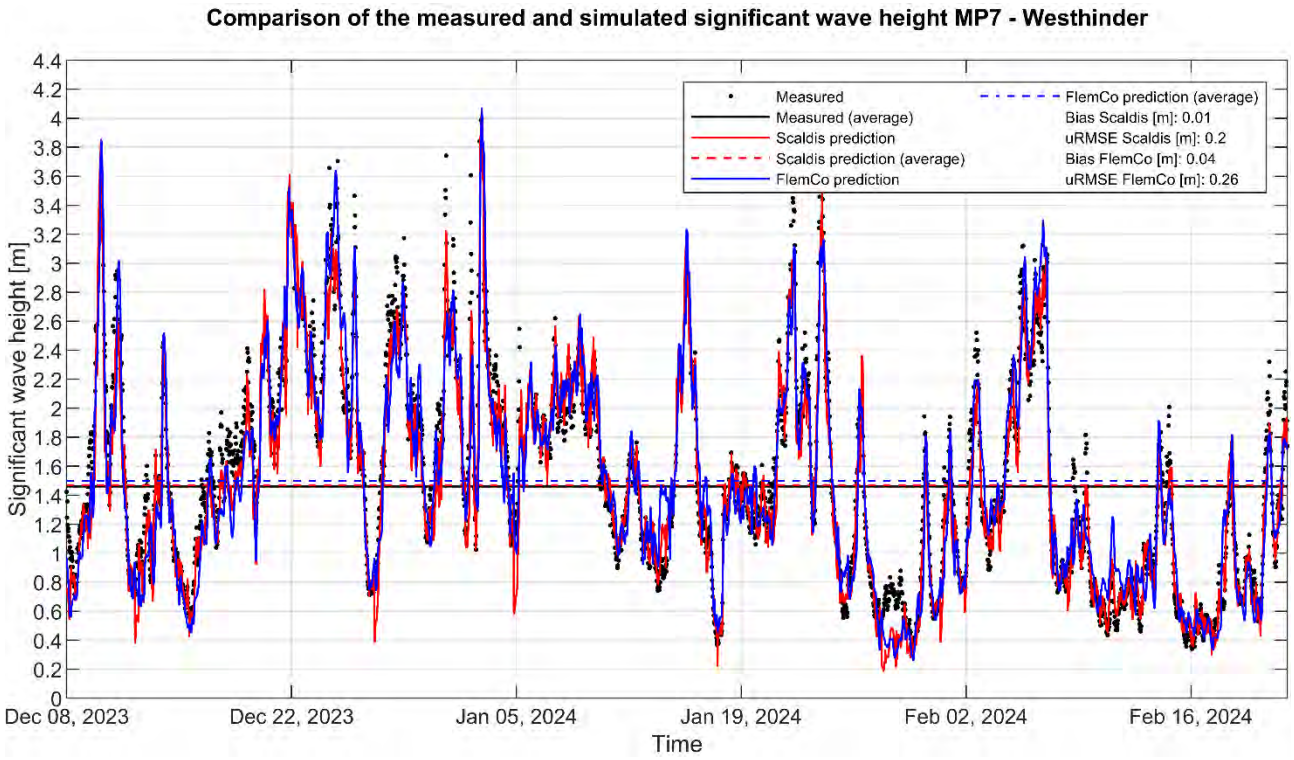

Figure 61 – Comparison of the measured and simulated significant wave height at wave buoy MP7 – Westhinder based on Scaldis-Coast model reference Run MO6_207 and FlemCo model reference Run 35. The measured significant wave height is derived from Meetnet Vlaamse Banken (2024).

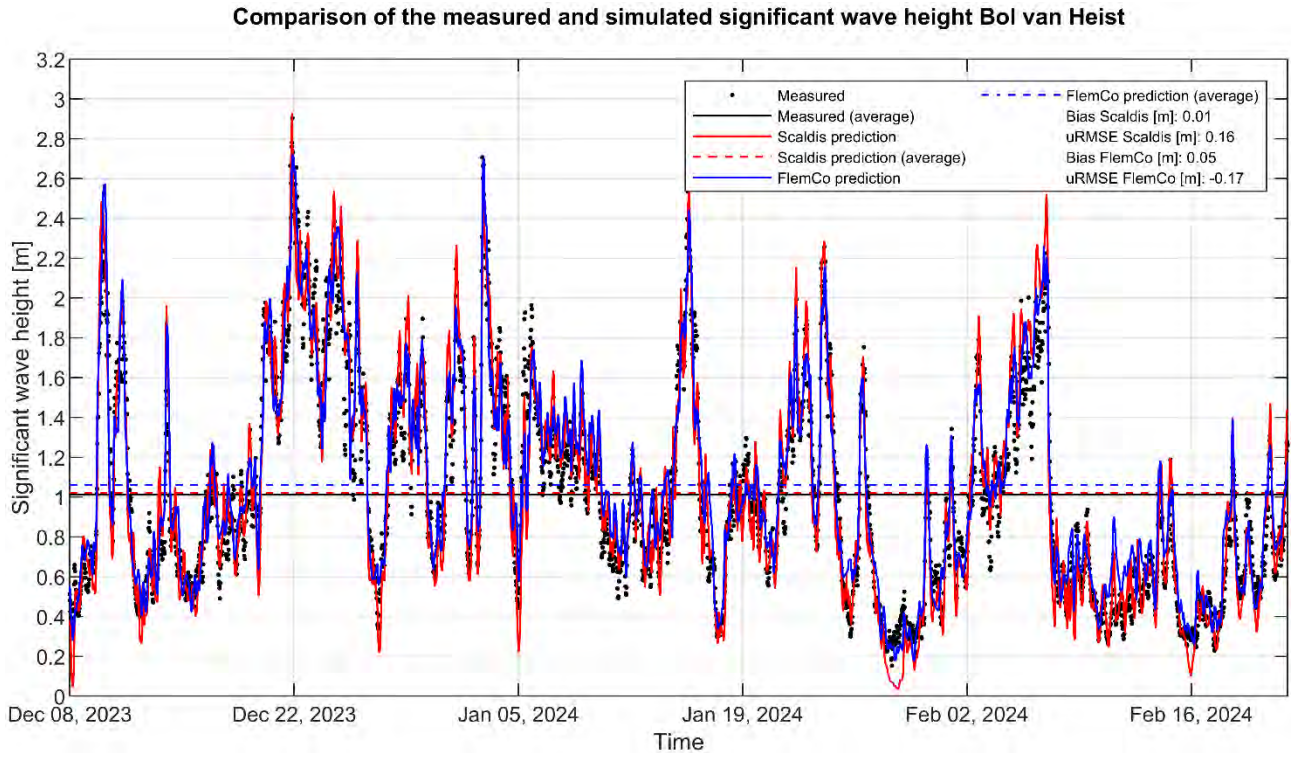

Figure 62 – Comparison of the measured and simulated significant wave height at wave buoy Bol van Heist, based on Scaldis-Coast model reference Run MO6_207 and on FlemCo model reference Run 35. The measured significant wave height is derived from Meetnet Vlaamse Banken (2024).

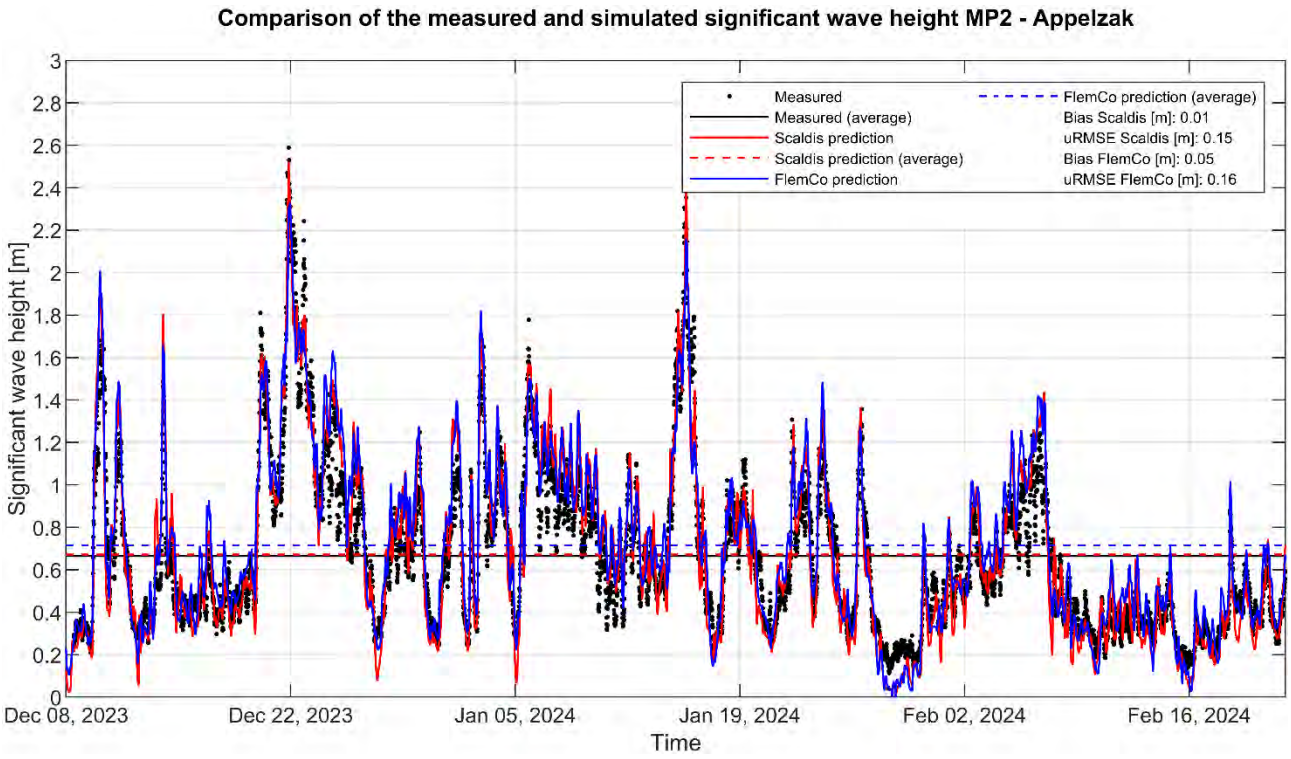

Figure 63 – Comparison of the measured and simulated significant wave height at wave buoy MP2 – Appelzak, based on Scaldis-Coast model reference Run MO6_207 and on FlemCo model reference Run 35. The measured significant wave height is derived from Meetnet Vlaamse Banken (2024).

Validation of the simulated wave direction

Figure 64 to Figure 66 and Figure A 6 to Figure A 10 in Appendix Bshow the measured and the simulated wave directions (associated with the maximum wave energy) based on the Scaldis-Coast and FlemCo model reference runs for all eight buoy locations. According to the measurements, the dominant wave directions during the study period are west-southwest (offshore) to west-northwest (nearshore). The time varying wave directions are generally reproduced by the Scaldis-Coast and the FlemCo models, although short-term fluctuations of the wave directions are mostly not well captured by both models.

Especially at the nearshore locations like MP2 – Appelzak (average waterdepth < 7 m) an influence of the vertical and horizontal tide (water level and tidal current) on the wave height and wave direction is observed (Figure 67). Wave height clearly decreases with decreasing water depth (either by wave breaking or sheltering by the Paardemarkt sand ridge). The flood current (west to east) seems to deflect the wave directions clockwise, while the ebb current (east to west) deflects wave directions counter clockwise. The change in wave angle can be as much as 45° in the measured data, but is never more than 30° in the output of the Scaldis-Coast model. Most of the time the tide driven change in wave angle is only a few degrees in the Scaldis-Coast model and seems absent in the FlemCo model. Data-analysis of a more data series could be done in a follow-up research in order to obtain a better insight in this phenomenon (tidal modulation of wave direction). These modulations are observed all along the coast, including at sites of greater depth (MP1 Bol van Heist, Oostende Poortjes). Closer to the coast they do seem more pronounced (Raversijde, Blankenberge, MP2 – Appelzak).

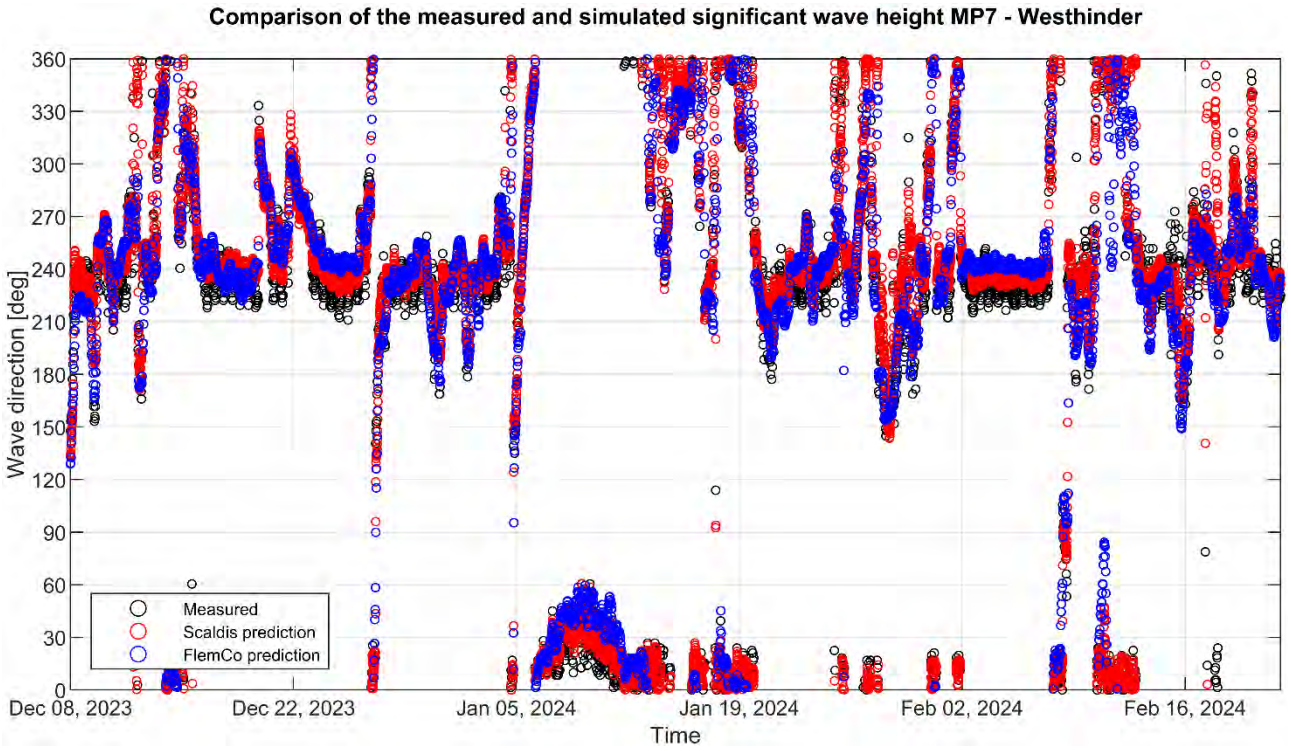

Figure 64 – Comparison of the measured and simulated wave direction (= direction associated with the maximum wave energy) at wave buoy MP7 – Westhinder based on Scaldis-Coast model reference Run MO6_207 and on FlemCo model reference Run 35. The measured wave direction is derived from Meetnet Vlaamse Banken (2024).

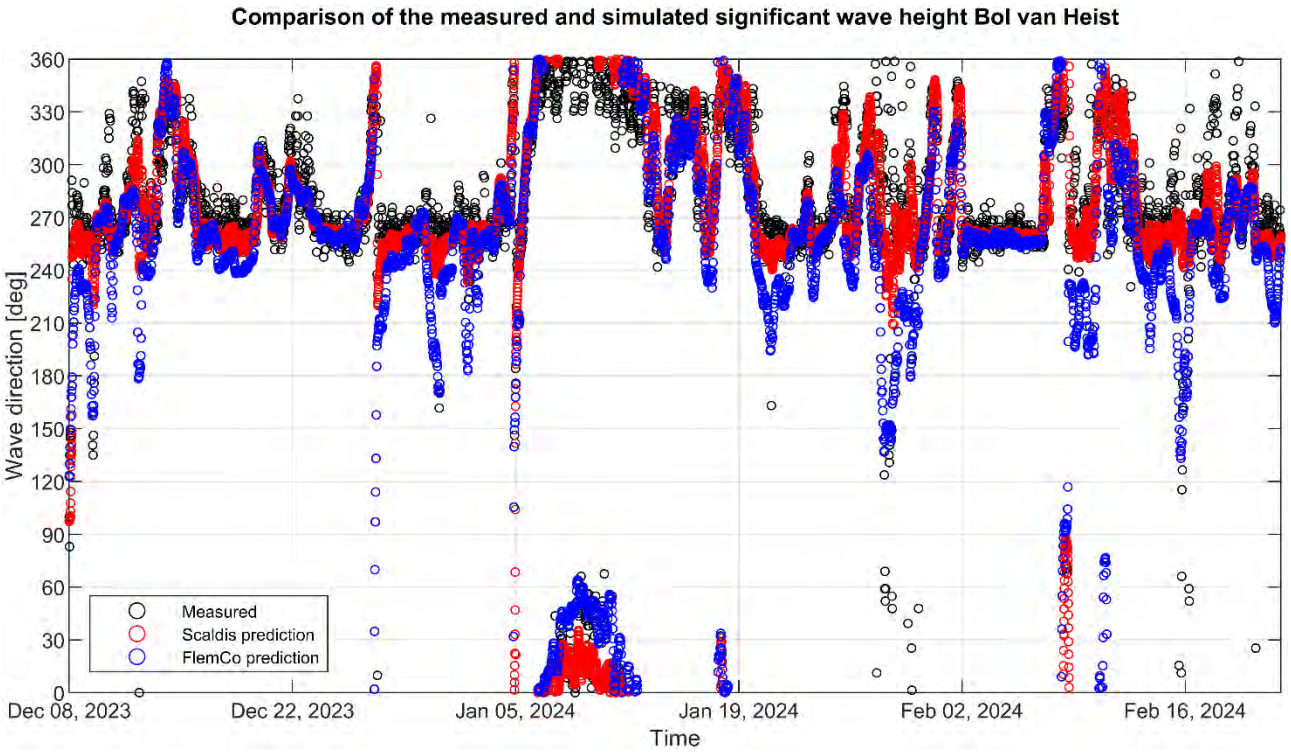

Figure 65 – Comparison of the measured and simulated wave direction (= direction associated with the maximum wave energy) at wave buoy Bol van Heist based on Scaldis-Coast model reference Run MO6_207 and on FlemCo model reference Run 35. The measured wave direction is derived from Meetnet Vlaamse Banken (2024).

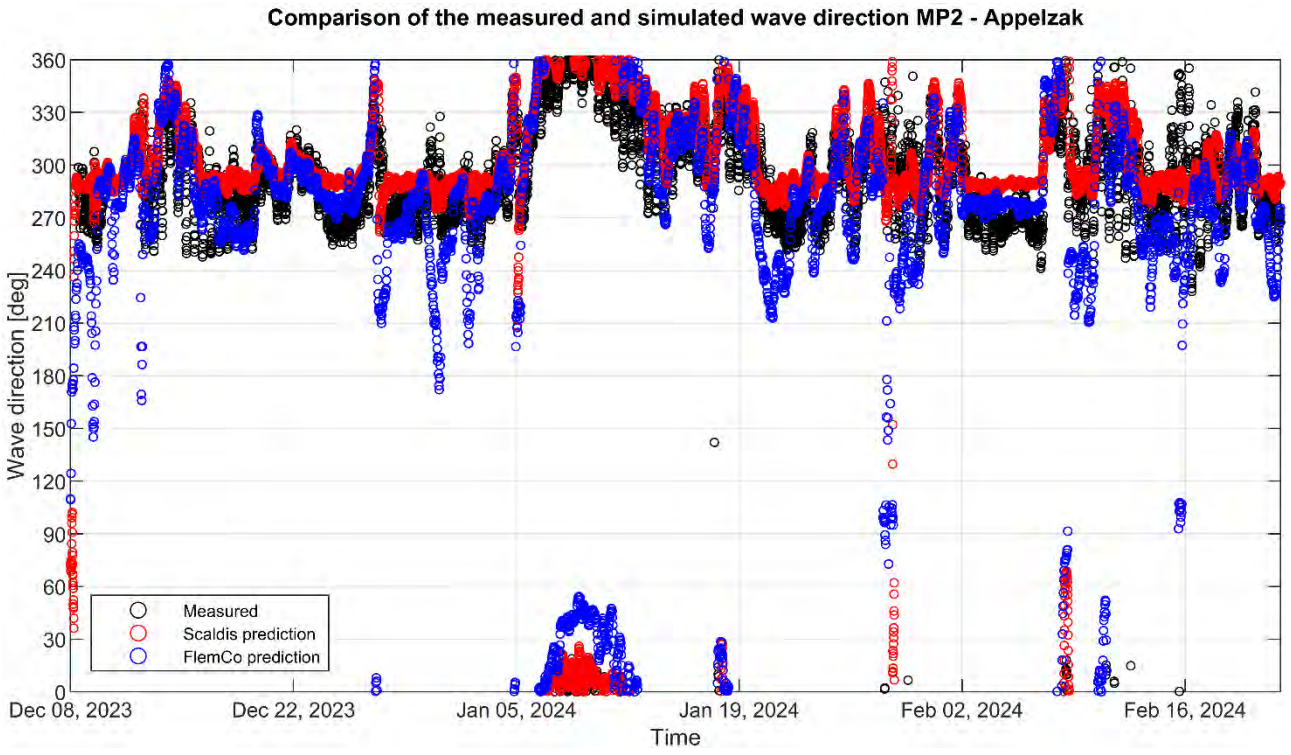

Figure 66 – Comparison of the measured and simulated wave direction (= direction associated with the maximum wave energy) at wave buoy MP2 – Appelzak based on Scaldis-Coast model reference Run MO6_207 and on FlemCo model reference Run 35. The measured wave direction is derived from Meetnet Vlaamse Banken (2024).

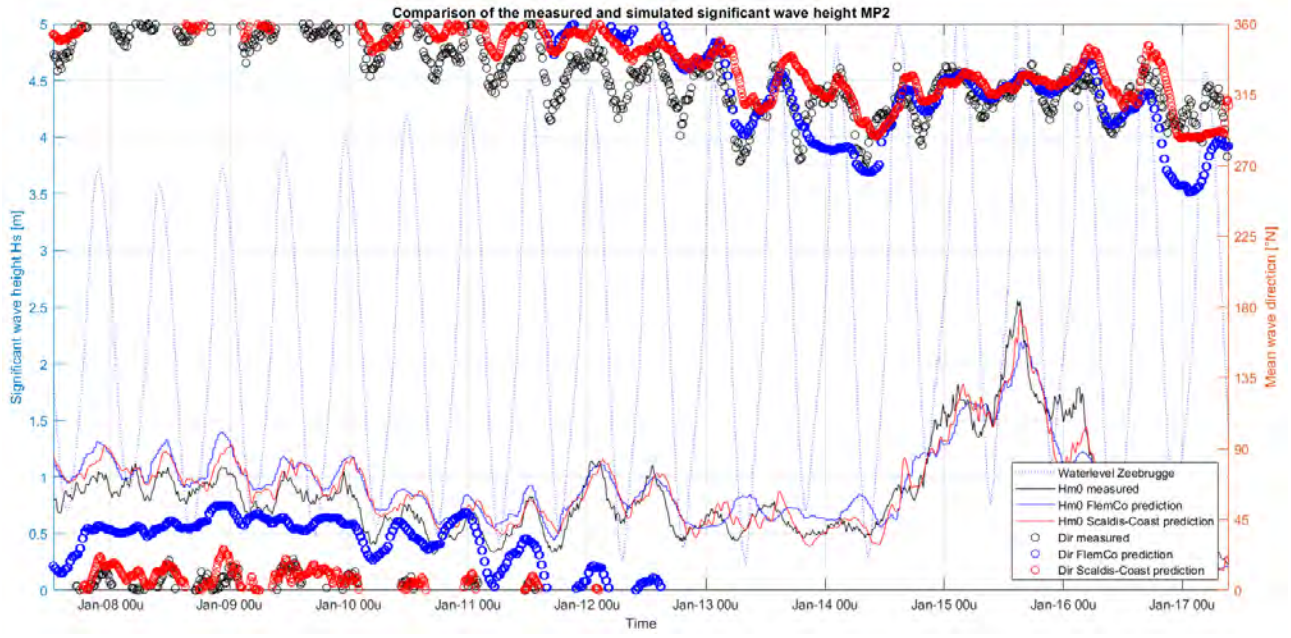

Figure 67 – Comparison of the measured and simulated wave heigth and direction at wave buoy MP2 – Appelzak based on Scaldis-Coast model reference Run MO6_207 and on FlemCo model reference Run 35. The measured wave and water level timeseries are derived from Meetnet Vlaamse Banken (2024).

Validation of the wave roses

The wave roses depicted in Figure 68 show the relation between the significant wave height and the wave direction (associated with the maximum wave energy) at the two offshore buoy locations MP7 – Westhinder and Thorntonbank Zuid according to the measurements and the Scaldis-Coast and FlemCo models. At both locations, the measurements indicate two dominant wave directions, i.e. the primary directions southwest/west-southwest, which are associated with the largest wave heights, and the secondary directions north-northeast/north-northwest. The Scaldis-Coast model shows a good match with these dominant directions and associated wave heights, although the western directions are overestimated while the northern directions are underestimated. In the FlemCo model, both the western and the northern directions are underestimated and the wave roses generally show a stronger directional spreading of the wave directions than measured and the Scaldis-Coast model.

Being situated closer to the coast, the dominant wave directions at buoy locations Akkaert Zuid and Deurlo become west-southwest to west and a stronger spreading of the directions can be observed (Figure 69). Only at Akkaert Zuid, a second although smaller peak can be found for waves from the north. The dominant west-southwestern to western wave directions and associated wave heights are well predicted by both models, although the Scaldis-Coast model overestimates and the FlemCo model underestimates these directions. The observed second peak for waves from the north at Akkaert Zuid is hardly captured by both models. Again, the FlemCo model shows a stronger directional spreading of waves than the Scaldis-Coast model. While this stronger spreading is mostly in line with the spreading according to the measurements at Deurlo, the spreading is overestimated at Akkaert Zuid.

At the A2-Boei and Bol van Heist buoy locations, the primary wave direction is west, followed by waves from the north-northwest (Figure 70). Also the models reproduce the dominant western directions and associated wave heights, although the Scaldis-coast model shows an overestimation and the FlemCo model an underestimation. The northern waves are clearly underestimated by both models. As observed before, the FlemCo model predicts a stronger directional spreading of the waves compared to the Scaldis-coast model and the measurements.

Finally, Figure 71 shows the wave roses for the two nearshore buoy locations MP2 – Appelzak and Blankenberg. At MP2 – Appelzak, waves from western to north-western directions are dominant and show a relatively pronounced spreading within this sector. This spreading is well captured by the FlemCo model, while the Scaldis-Coast model predicts a significant single peak for waves from the north-west. The same observation can be made at Blankenberge, where the Scaldis-Coast underestimates the direction spreading of the waves, although to a smaller degree compared to MP2 – Appelzak.

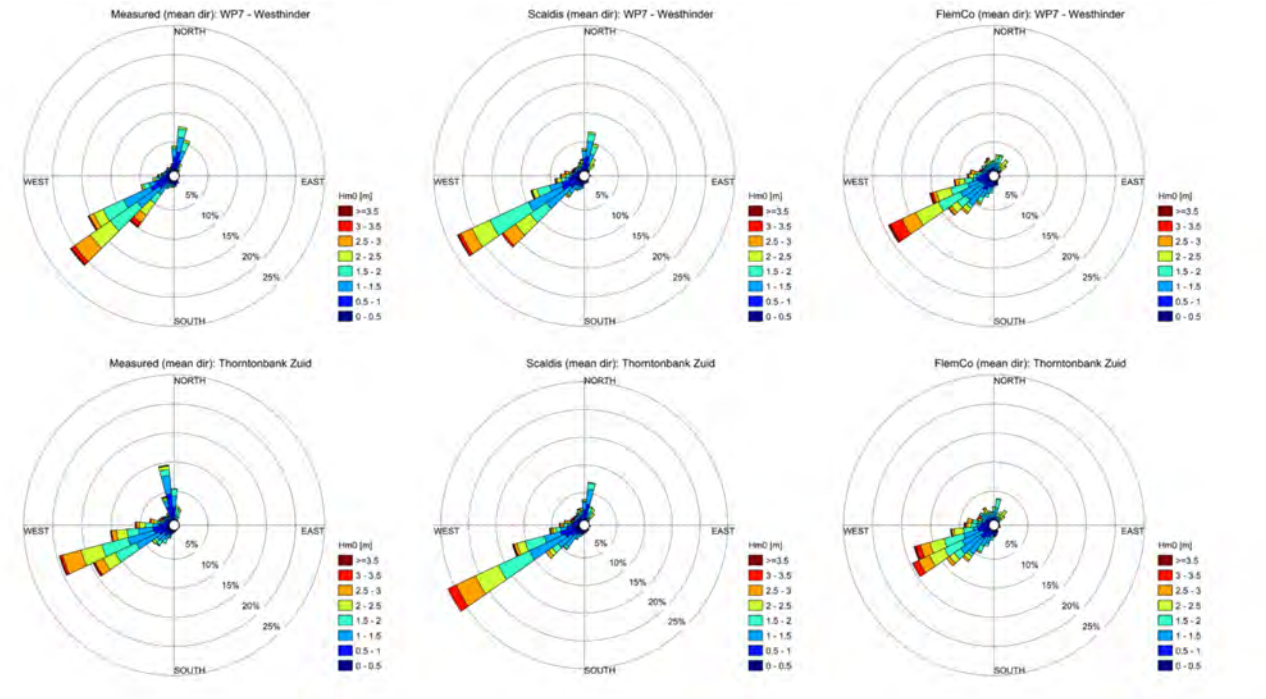

Figure 68 – Wave roses of the measured (left) and simulated Scaldis (centre) and FlemCo (right) significant wave height and wave direction (= direction associated with the maximum wave energy) at wave buoys MP7 – Westhinder and Thorntonbank Zuid based on Scaldis-Coast model reference Run MO6_207 and on FlemCo model reference Run 35. The measured significant wave height and wave direction is derived from Meetnet Vlaamse Banken (2024).

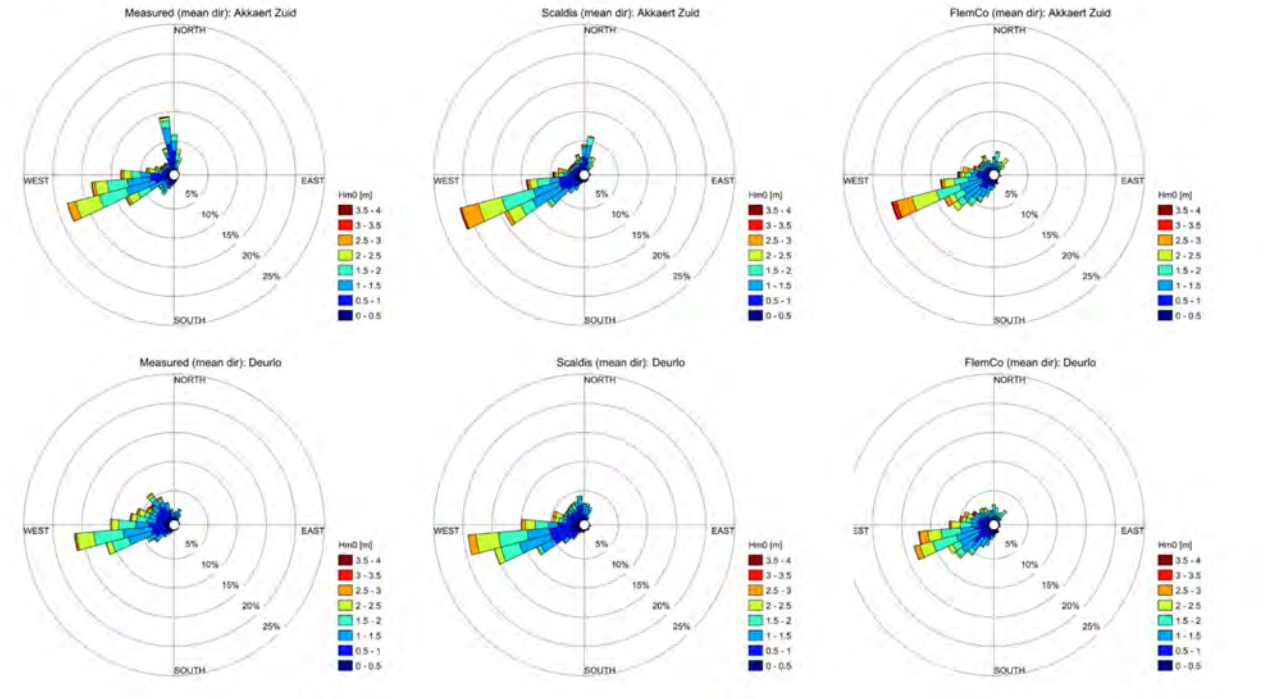

Figure 69 – Wave roses of the measured (left) and simulated Scaldis (centre) and FlemCo (right) significant wave height and wave direction (= direction associated with the maximum wave energy) at wave buoys Akkaert Zuid and Deurlo based on Scaldis-Coast model reference Run MO6_207 and on FlemCo model reference Run 35. The measured significant wave height and wave direction is derived from Meetnet Vlaamse Banken (2024).

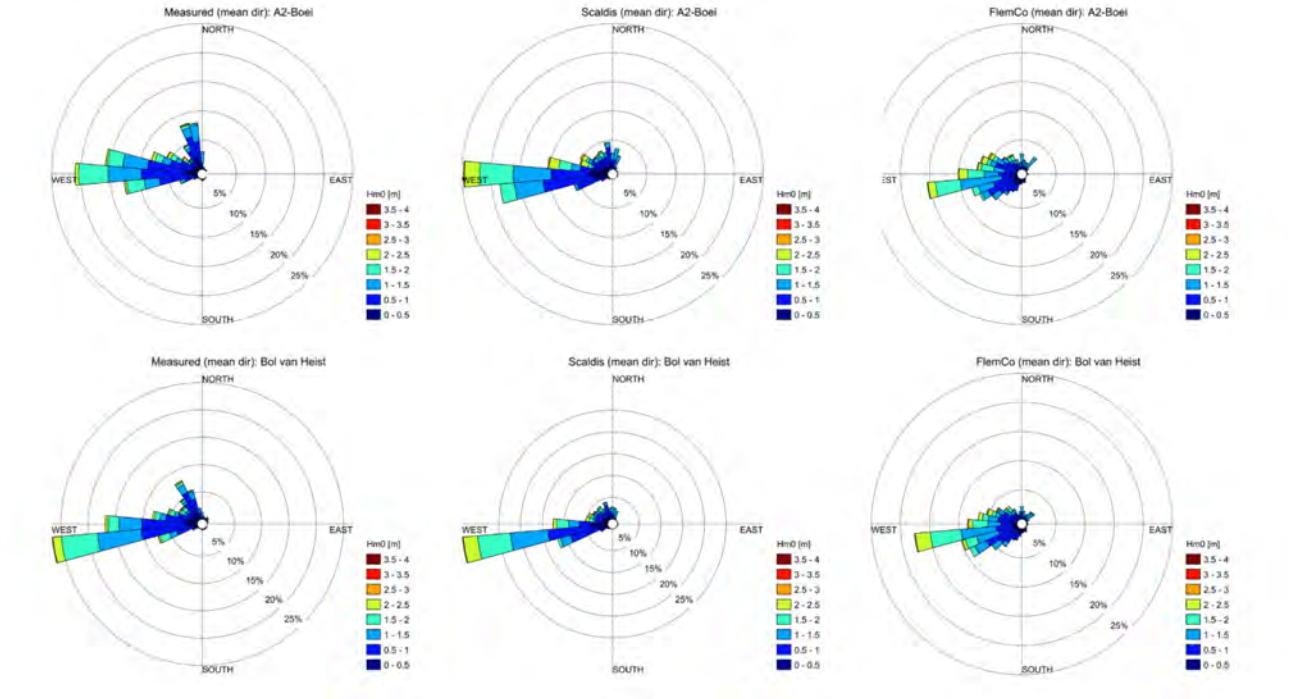

Figure 70 – Wave roses of the measured (left) and simulated Scaldis (centre) and FlemCo (right) significant wave height and wave direction (= direction associated with the maximum wave energy) at wave buoys A2-Boei and Bol van Heist based on Scaldis-Coast model reference Run MO6_207 and on FlemCo model reference Run 35. The measured significant wave height and wave direction is derived from Meetnet Vlaamse Banken (2024).

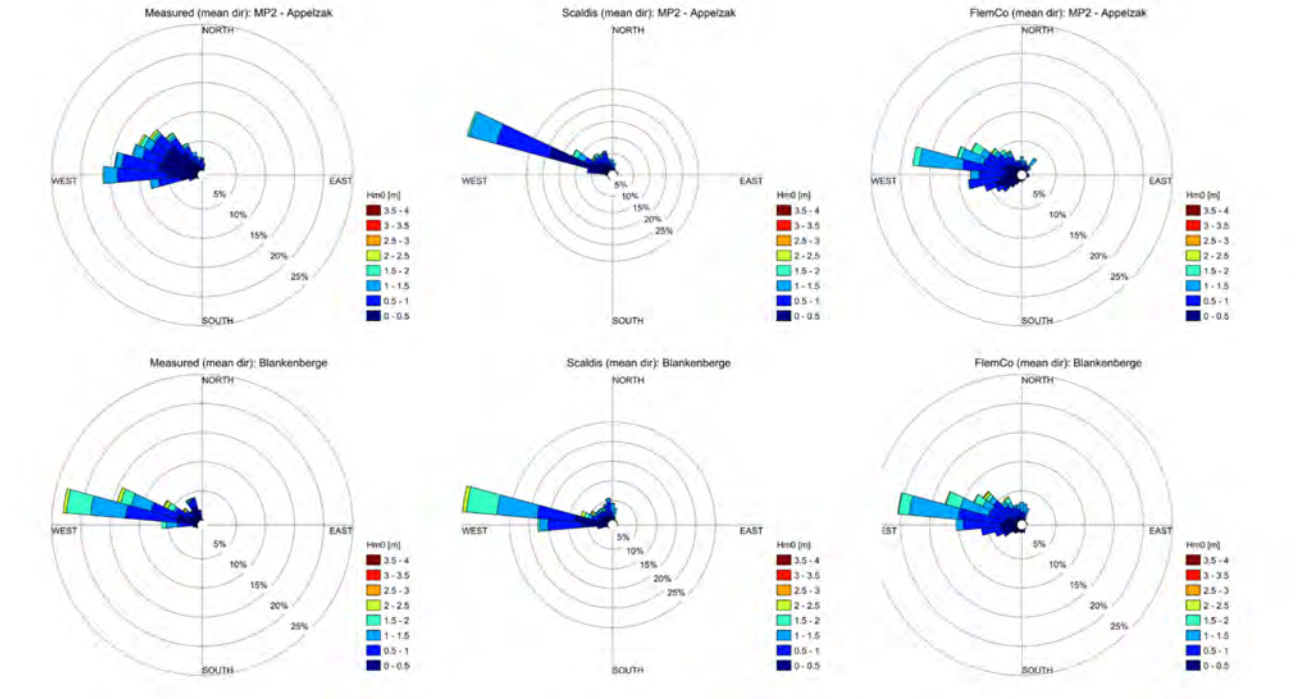

Figure 71 – Wave roses of the measured (left) and simulated Scaldis (centre) and FlemCo (right) significant wave height and wave direction (= direction associated with the maximum wave energy) at wave buoys MP2 – Appelzak and Blankenberge based on Scaldis-Coast model reference Run MO6_207 and on FlemCo model reference Run 35. The measured significant wave height and wave direction is derived from Meetnet Vlaamse Banken (2024).

3.2.3 Implementation of groynes in Scaldis-Coast

In the previous working year of the MOZES project, it was observed that, the groynes as implemented in the Scaldis-Coast model are lacking in length and/or crest height (Figure 72). This section handles the lay-out and implementation of groynes east of Zeebrugge.

Computational mesh

Special attention was paid to the implementation of groynes into the computational meshes of both hydrodynamic and wave modules of the Scaldis-Coast model. Based on DEM's from 2018 and 2011, contour lines were generated (mails Wouter D'Haese to Gerasimos Kolokythas, December 2019). These contours were used in the model to (a) delimit non-erodible layers and (b) define the grid resolution around the groynes (Figure 73).

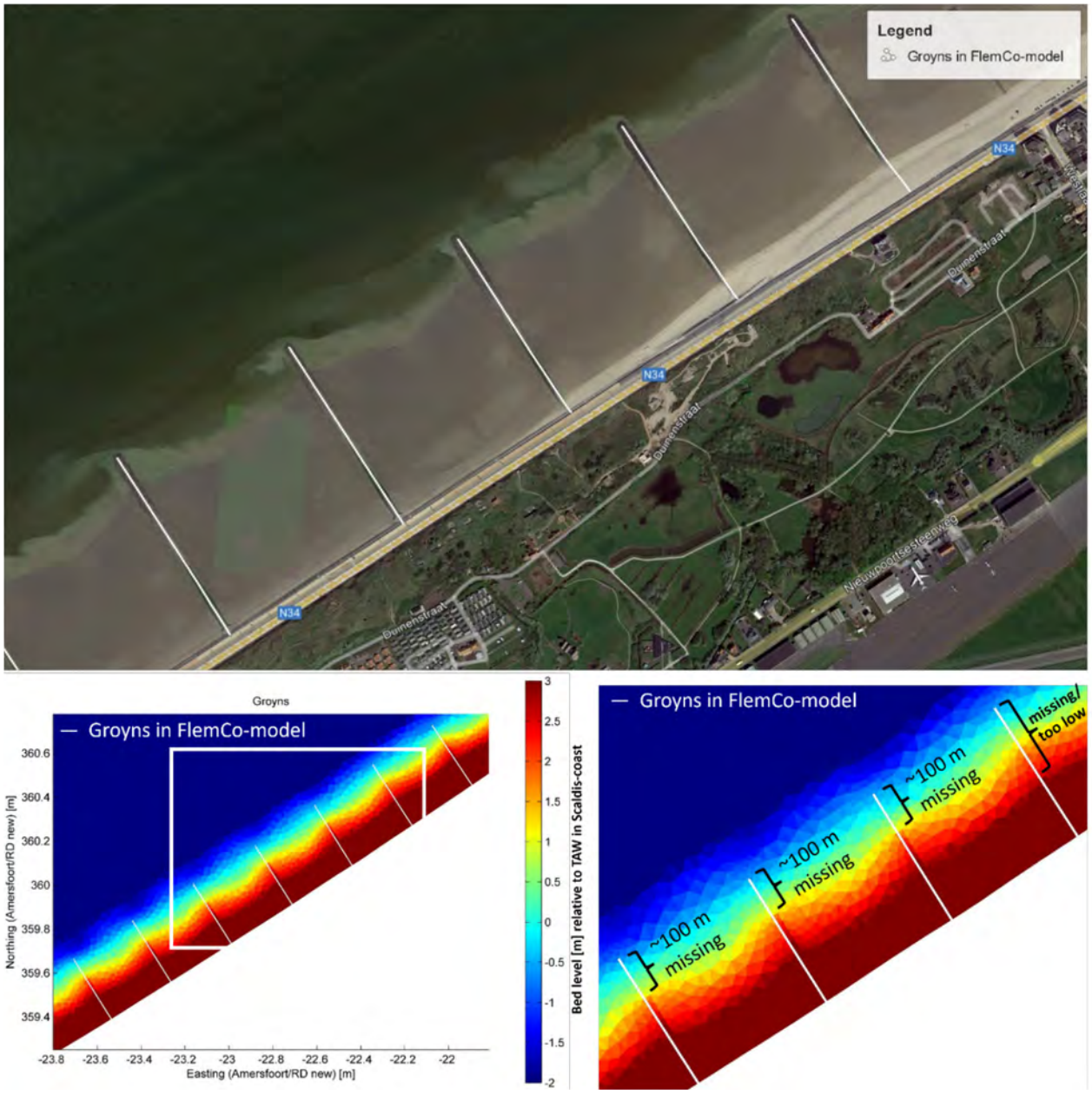

Figure 72 – Comparison of the dimensions of groynes as implemented in the Scaldis-Coast and in the FlemCo models.

The contour lines were used as soft lines in the mesh generator (GMSH), to assure mesh nodes were placed freely at a pre-defined distance along them. Figure 73 shows how the groynes are mapped identically in both the TELEMAC2D and TOMAWAC mesh, even though the latter is coarser in the area between the groynes. Where the groyne contour is relatively wider, the mesh generator connects (some of) the mesh nodes along the groynes crest line. Unfortunately this is not the case for parts that are not as wide, here

- mesh nodes inside the groyne contour are not interconnected (to avoid obtuse triangles), and
- mesh nodes on the western and eastern side of the groyne contour are connected directly to each other

Both these features can result to the height of the crest line of the groyne not being interpolated accurately, as the lower lying topography of the beach and shoreface on both sides of the groyne might be interpolated over the crest of the groyne.

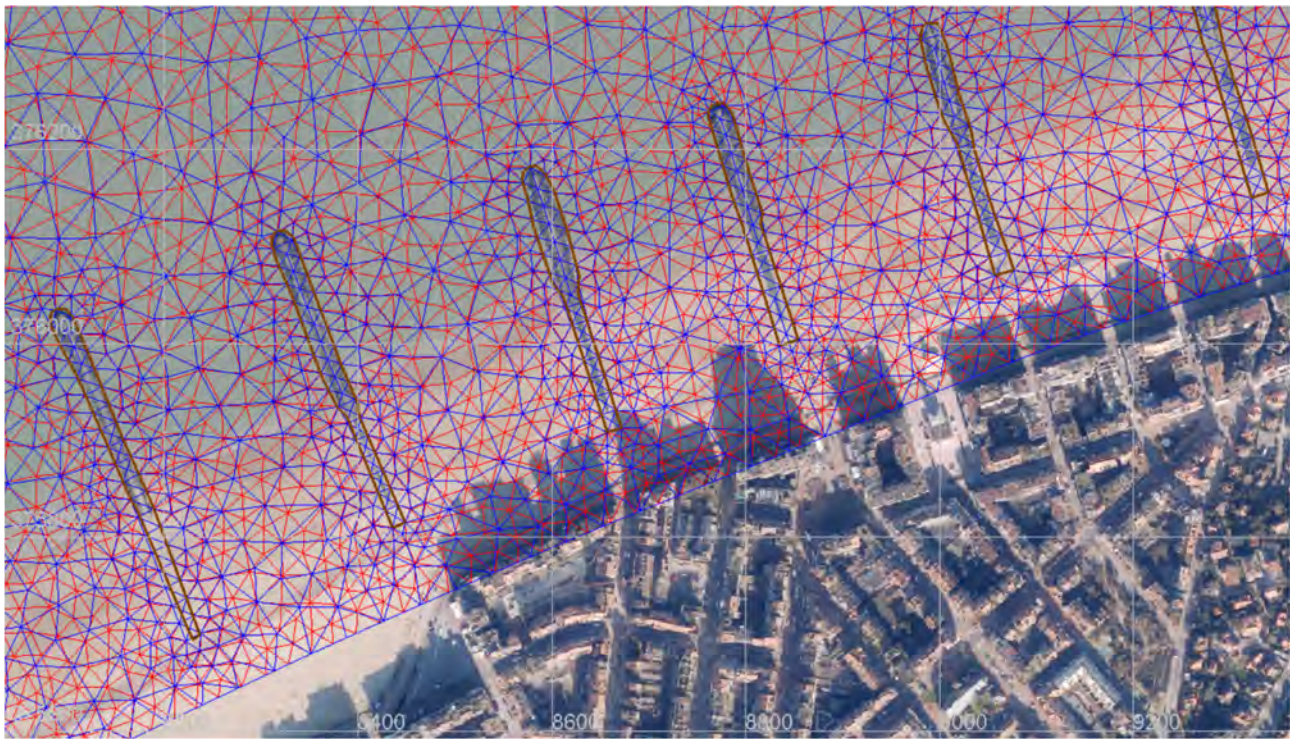

Figure 73 – Computational mesh for TELEMAC2D (red) and TOMAWAC (blue) around the groynes (brown contour lines) at Knokke-Heist.

Topo-Bathymetry

Since the late 1990's, early year 2000 the topo-bathymetry of the coastal area is typically monitored by (semi-)annual LiDar flights and single beam soundings. To get as much spatial coverage as possible LiDar flights should be conducted at low water and the bathymetry surveys at high water. However, currents and waves cannot be too strong/high to obtain reliable bathymetric results, and because of safety reasons the survey vessels do not come close to the groynes. So usually there still remains a data-gap around the underwater toe of the groynes.

Within the framework of the 2023 – 2024 beach nourishment at Knokke-Zoute additional pre- and post-nourishment multibeam soundings and topographic drone flights were conducted by DEME (pre- and post-nourishment respectively in October 2023 and March 2024). The swath beam of the multibeam echosounder allows to get a wider coverage and to get closer to the underwater toe of the groynes. This is illustrated in Figure 74: a highly detailed image is achieved of the seabed and the revetments at the most seaward part of the groyne. Above low water, the revetments, and the lower lying centre line of the groyne are captured by the drone image. At the upper shoreface between the groynes there still remains a data gap between the multi-beam sounding and the drone image; here the interpolation between the two datasets creates the large triangular surfaces with a uniform slope, clearly visible in Figure 74.

The position of both the survey vessel and the drone is defined by an onboard RTK GPS-system. The vertical position (depth measurement) of the multibeam sounding is ground truthed on a concrete plate at known depth near the harbour of Vlissingen. The topography obtained by the drone was subsequently calibrated by using the z-values in the overlapping area of both datasets (personal communication Kris Van De Velde, DEME, d.d. 08-Oct-2024).

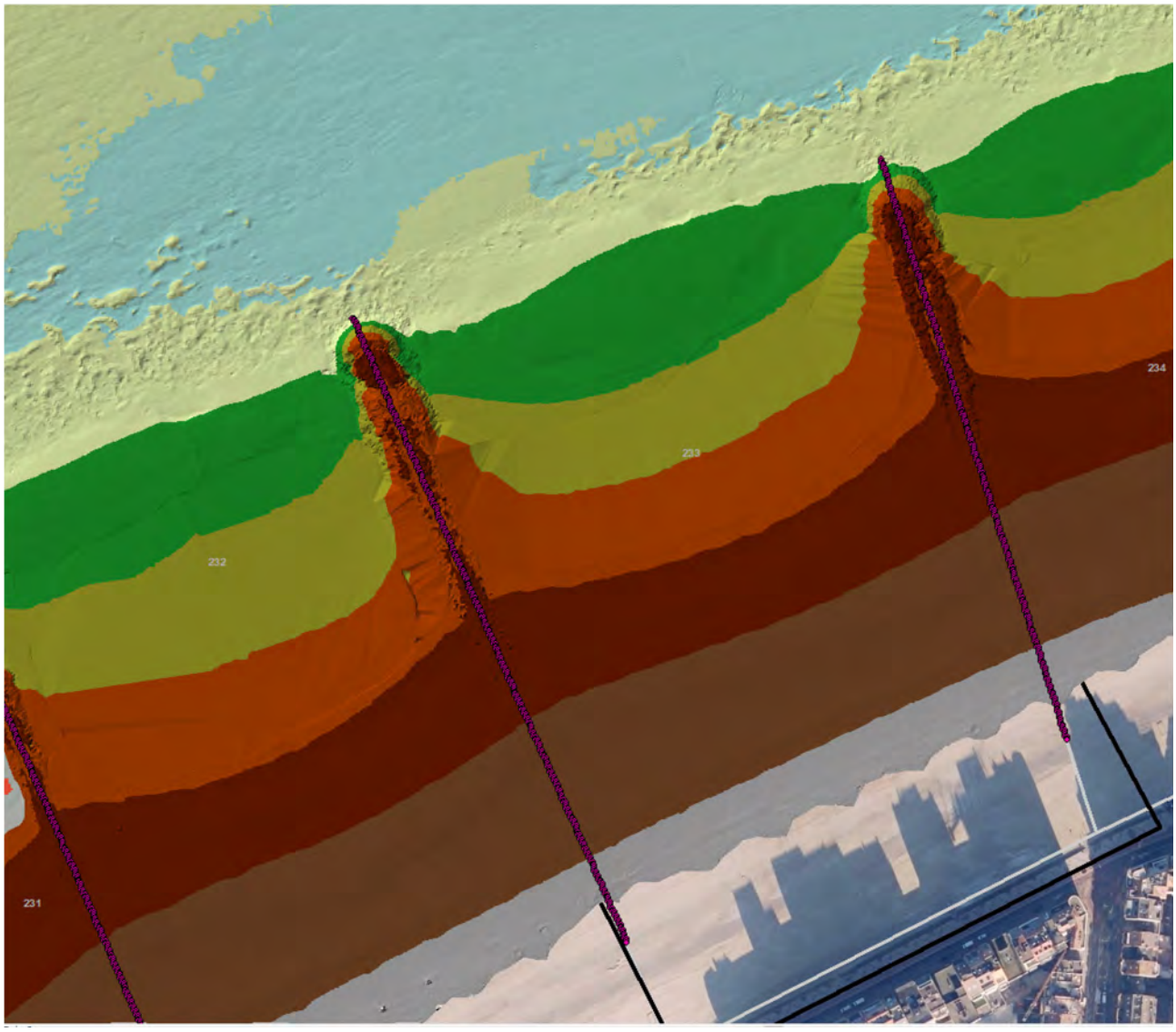

Figure 74 – Zoom on the multi-beam sounding of the shoreface and topographic drone flight of the beach performed by DEME between Knokke-Heist and Knokke-Zoute.

Determination of the crest height and length of the groynes

To get a better knowledge on the crest height of the groynes, and to get an estimate of the error margin of the obtained height, the two datasets from DEME and all available semi-annual LiDar sets were interpolated on the centre line of the groynes (Appendix C, Groyne crest height). Generally there's good agreement between all measured datasets and the design plans. For some older LiDar flights however, the water surface was not filtered out properly.

Based on the profiles and building plans of the groynes, three types of groynes can be distinguished:

- The groynes in the coastal sections of Heist and Duinbergen were lengthened and heightened in the 1970's. They extend 400 to 628 m seawards from the crest of the dike and have a flat crest at their seaward end at a height of approximately 0.8 m TAW (0.9 m Z).
- Groynes Duinbergen 4 and Duinbergen 8 are exceptions here. They are short (340 m) and have a sloping crest, which is topped by a row of wooden poles. Most of the time these two groynes are completely buried, but sometimes the poles stick out of the beach sand and the revetment can be seen near the low water line.
- The groynes in the coastal section of Knokke are typically shorter and lower than those in Duinbergen. They extend 325 to 400 m seawards from the dike and have a flat crest at their seaward end at a height of approximately 0.6 m TAW (0.7 m Z). The Appelzak tidal gully is located directly seawards of the tip of these groynes.

The groyne Heist 51 was demolished only in 2009. It's profile was included in this research because it needs to be incorporated into the models for the 1999 – 2003 hindcast (see §3.3)

Additionally profiles were derived on 6 profiles alongshore (see Appendix C, Alongshore profiles). In these profiles the groynes clearly stick out, unless they are buried (either naturally or by recent beach nourishments). A zoom on groyne level (Figure 75 bottom panel) shows that a 2x2 m raster of the LiDar data is still detailed enough to catch the revetments and lower center line of the groyne. Not only do the groynes stick out of the topo-bathmetry, also in the standard deviation the groynes are visible as a downward spike. Therefore it is assumed that the error in height is less than 10 cm.

Implementation in Scaldis-Coast

To test the influence of the groyne heights on the simulated longshore sediment transport in Scaldis-Coast the groyne crest heights and lengths were implemented in the bathymetry of the model only. To rule out any interpolation of the beach topography over the groynes, it was ensured that for each groyne the crest height was applied at least 3 nodes wide in the alongshore direction. Figure 76 shows the height difference between the new bathymetry (simulation MO6_213) and the original bathymetry (simulation MO6_212). In the deep blue areas the bathymetry is unaltered. Almost all groynes have been heightened and made longer in their seaward part.

Simulation results and conclusion

Figure 77 shows the annual longshore sediment transport as calculated in simulations MO6_212 (reference) and the MO6_213 with more realistic groyne crest height and length. Near the location of the Knokke-Heist and Knokke-Zoute groyne fields, the sediment transport has decreased (as should be expected when increasing the groyne height and length).

The decrease in longshore sediment transport however is not so important that it would necessitate a remapping of the models' computational mesh in order to get a better representation of these structures.

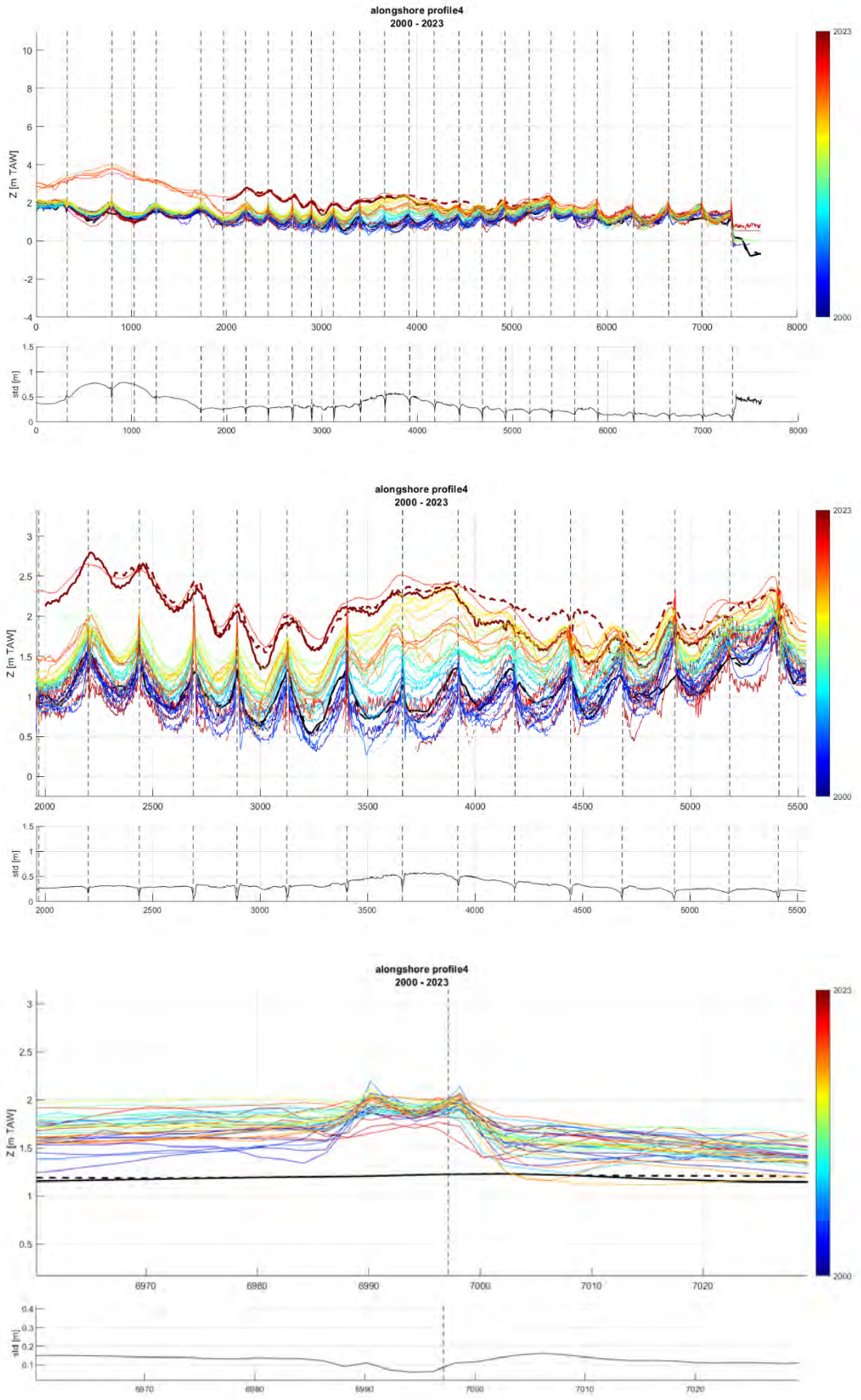

Figure 75 – Alongshore topographic profile for the beach east of Zeebrugge at different zoom levels.

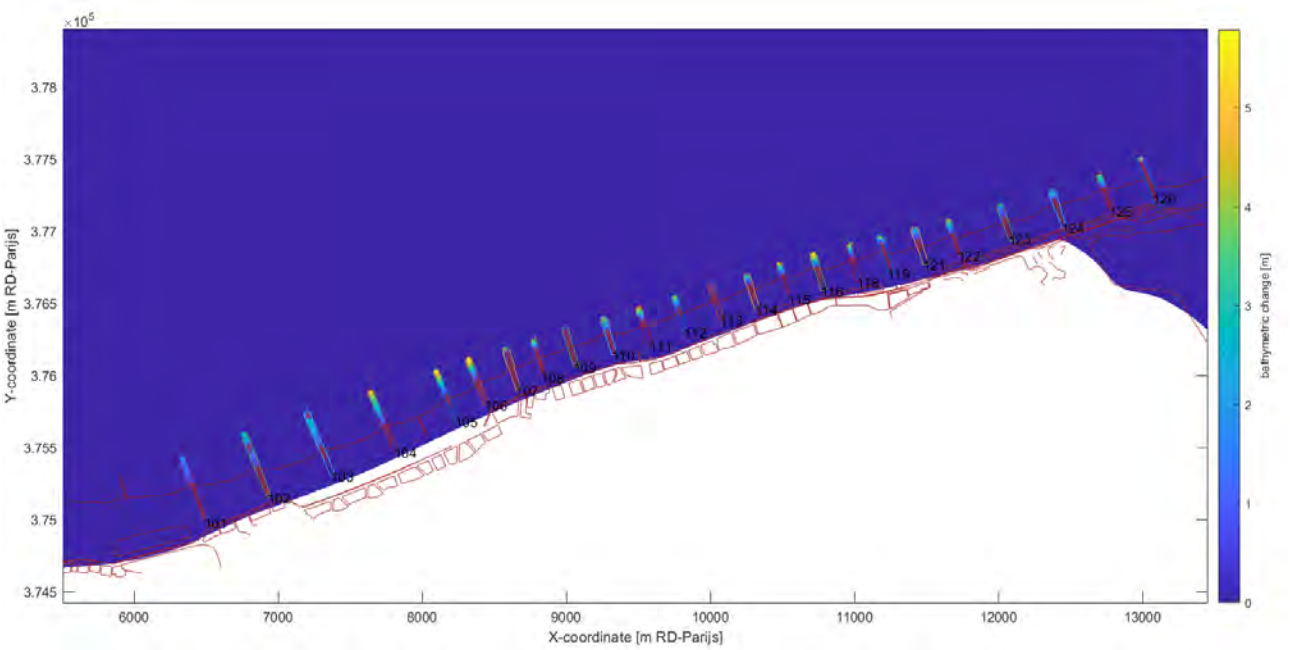

Figure 76 – Height differences between the adjusted and original bottom schematisation of the groynes in Scaldis-Coast. Blue: no change of depth; yellow: new bathymetry lies up to 5.5 m higher than in the original. Low water line, groyne contours, dike foot and some building contours are shown as brown lines.

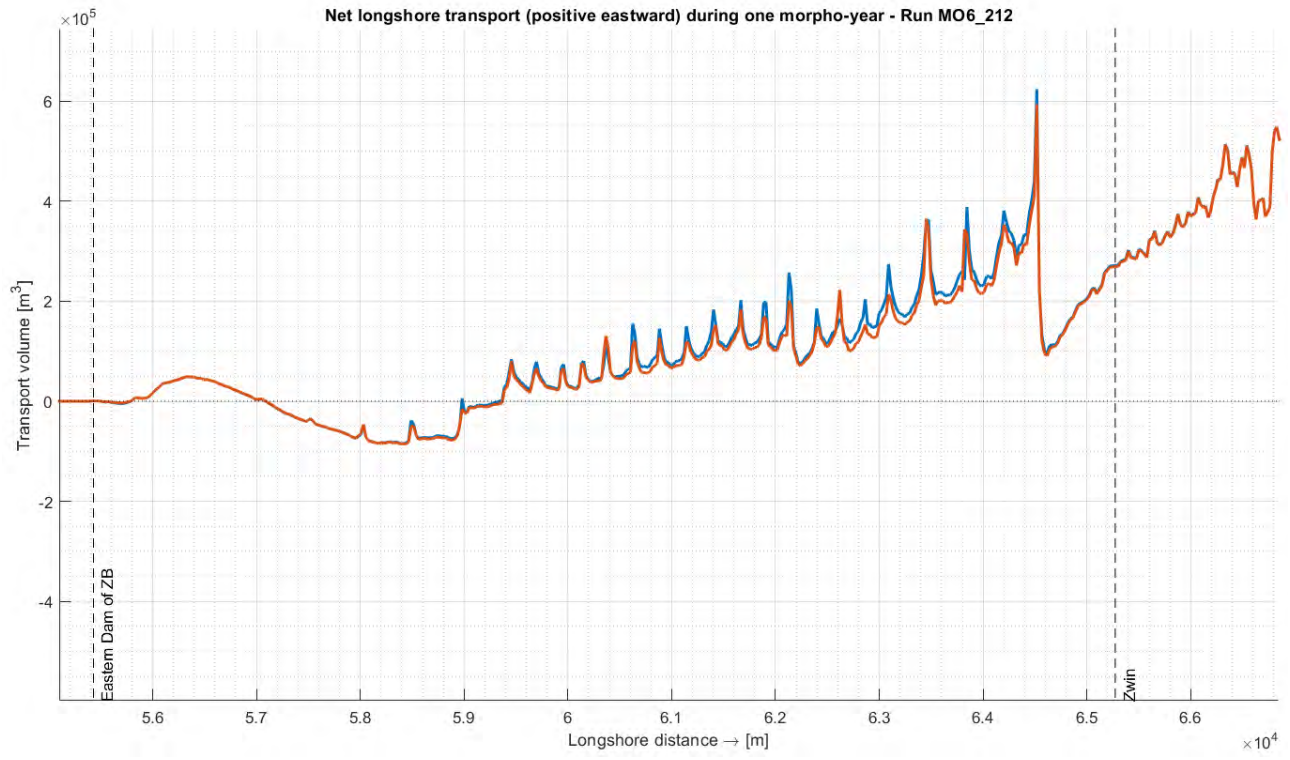

Figure 77 – Annual longshore sediment transport calculated by Scaldis-Coast. Blue: MO6_212, original bathymetry; Brown: MO6_213, higher and longer groynes as in reality.

3.3 Effect of the gradual deepening of nearshore tidal channels on the beach erosion (WP4)

3.3.1 Introduction

Task 4 of the MOZES-project (WP4) deals with the effects of the observed gradual deepening of nearshore tidal channels along the Belgian coast on beach erosion and on the intensity of beach nourishments required to maintain the coastline. The hypothesis is that a deeper and/or wider channel causes an increased erosion of the adjacent beaches, which requires larger nourishment volumes.

In the MOZES-project, Task 4 is investigated based on the example of the Appelzak channel located off the coast of Knokke-Heist between Zeebrugge harbour and the Dutch border. After the extension of Zeebrugge harbour in the year 1986, a significant deepening of the Appelzak channel has been observed, while the Paardenmarkt ridge (located seaward of the Appelzak) experienced pronounced sedimentation. The morphological development of the Appelzak channel is most probably related to the extension of Zeebrugge harbour and the observed erosion along the harbour breakwaters as well as the sedimentation on the Paardenmarkt ridge (Dujardin *et al.*, 2023; Dujardin *et al.*, 2024). Moreover, intensive beach nourishments and the presence of groynes at Knokke-Heist slow down or even prevent landward migration of the Appelzak channel.

The sedimentary processes and morphodynamics of the Appelzak area will be studied in detail in the fourth project year using the openTelemac Scaldis-Coast and the Delft3D Flexible Mesh FlemCo model. As a preparation for this model application, a first attempt of a morphological hindcast was made in current study, for the period spring 1999 to spring 2003. In this period, no nourishments have been performed and the period directly starts after a large beach and shoreface nourishment of about 413,000 m^3, which has been performed in May 1999 at Knokke-Heist between ca. Rdx = 8.5 km and Rdy = 11 km. (Houthuys *et al.*, 2022; see Figure 78 for the coordinates).

Methodology

For the morphological hindcast, two measured topo-bathymetries of the study were used – the 1999 bathymetry and the 2002/2003 bathymetry. Both topo-bathymetries are composed of different sources according to Table 16. In the case of the 2002/2003 topo-bathymetry, the beach topography derives from the December 2002 measurement *g_2002_2e*, since no corresponding measurement is available for 2003 before the following nourishment was performed at the beach of Knokke-Heist. The difference between the measured 2002/2003 and the 1999 topo-bathymetries results in the cumulative erosion/sedimentation in the study area (Figure 78), which was used for the comparison with the simulated bed level changes for the hindcast period.

Table 16 – Overview of the various sources of data used to create the measured 1999 and 2002/2003 model bathymetries. The beach and nearshore bed level data were gathered by Houthuys et al. (2022) from annual LiDar flights and depth soundings. The Vaklodingen and Jarkus data are based on RWS (1999a, 2003a) and RWS (1999b, 2003b).

Model bathymetry	Inside the study area		Outside the study area	
	Beach	Nearshore incl. shoreface	JarKus	Vaklodingen
1999	Jun 1999 (g_vo_vj1999)	Jun 1999 (g_vo_vj1999)	Summer 1999	Summer 1998 & 1999
2002/2003	Dec 2002 (g_2002_2e)	Apr 2003 (g_vo_vj2003)	Summer 2003	Summer 2003

The morphodynamic (i.e. with bed level changes) hindcast simulations with Scaldis-Coast and the FlemCo model started in 1999 and ran for the period 1999-2003. These simulations started with the measured 1999 bathymetry, which was interpolated on the computational grids of both models. In those areas, where the 1999 bathymetry does not cover the model domains, the default bathymetry of 2020 of both models was used (i.e. minimum 10 km distant to the area of interest in all directions).

Both models made use of a different hydrodynamic simulation period for the hindcast simulations. The simulation period of the Scaldis-Coast model was the morphological representative half-year period 07-11-2013 to 07-05-2014 (simulation HSW113; Kolokythas *et al.*, 2023). In the case of the FlemCo model, two different simulation periods were tested, i.e. 14-03-2014 to 13-05-2014 (earlier used by Grasmeijer *et al.,* 2020 and Dujardin *et al.,* 2023, 2024) and 28-11-2023 to 27-03-2024 (which includes the wave validation period of this study; see Chapter 3.2). Based on these simulation periods, both models were applied as described in the following two sections.

OpenTelemac Scaldis-Coast

The morphodynamic Scaldis-Coast model as developed by Kolokythas *et al*. (2023) includes tides, waves and wind. The hydrodynamic forcings consist of a representative tide (two flood-ebb cycles which are constantly repeated) and the actual measured wave and wind time series at Westhinder for the representative period. 07-11-2013 to 07-05-2014 (6 months). A morphological scale factor (MORFAC) of 7 was applied to simulate 3.5 years of morphological changes. The model uses two sand fractions in a spatially varying ratio in order to simulate one equivalent sediment transport (with spatially varying D_{50}) rather than the (default) sum of the sediment transport of each sediment fraction (details are explained in Kolokythas et al., 2023). For the Knokke-Zoute 1999–2003 hindcast run with Scaldis-Coast model presented below (runID: MO6_313), the model settings presented Wang et al. (2025) were applied. Main parameter settings are shown in Table 17.

Table 17 – Overview of selected parameter settings of the openTelemac Scaldis-Coast model run MO6_313 performed for the Knokke-Zoute 1999–2003 hindcast study.

Effect of waves	yes
Number of sediment fractions	2
Classes sediment diameters	200; 500 µm
Layers initial thickness	100; 0 m
Bed-load transport formula for all sands	4: Bijker (total transport)
Layers non cohesive bed porosity	0.4; 0.4
Slope effect	yes
Formula for slope effect	1: Koch and Flokstra
Sediment slide	yes

Delft3D Flexible Mesh FlemCo

The FlemCo model is generally based of the parameter settings according to Grasmeijer *et al. (*2020) and Dujardin *et al. (*2023, 2024) and Table 18. In contrast to Scaldis-Coast, the FlemCo model made use of the sediment transport formulation by van Rijn (2007). For the transverse bed gradient factor for bedload transport – the so-called AlfaBn parameter – we applied an increased value of 10 (default: 1.5) in order to avoid overexaggerated downslope sediment transport in the model. The wave-related suspended and bedload sediment transport factors – the so-called SusW and BedW parameters – were lowered to 0.2 (default: 1) to avoid too much landward directed wave-related sediment transport, since depth-averaged models cannot not solve the wave-related undertow current in the beach zone. For the wave velocity asymmetry in the model we applied the description according to Isobe & Horikawa *(*1982; Wform = 1).

Finally, the spatially varying sand thicknesses according to Grasmeijer *et al. (*2020) was used as initial condition in the model. These thicknesses were derived from observed sedimentary data as well as long-term observed bed level changes in the study area.

Based on the above mentions parameter settings, the FlemCo model was applied for the simulation periods 14-03-2014 to 13-05-2014 (using a morphological scale factor of 24) and 28-11-2023 to 27-03-2024 (using a morphological scale factor of 12). Generally, the second period resulted in a more accurate reproduction of the observed bed level changes in the nourishment area Knokke-Heist, which – most probably – is related to the different wave and wind climate in this period compared to the period used earlier by Grasmeijer *et al.* (2020) and Dujardin *et al.* (2023, 2024).

Table 18 – Overview of selected parameter settings of the FlemCo-model run H52 performed for the Knokke-Zoute 1999 – 2003 hindcast study.

Run ID	Transport formulation	AlfaBn	SusW/BedW	Wform	Ini. sediment thickness	Sediment fraction(s)
Run H52 (Ref.)	van Rijn 2007	10	0.2	1	Spatially varying	200 µm

3.3.2 Morphological hindcast results

Sedimentation/erosion pattern

Figure 78 shows that the observed bed level changes or the cumulative erosion and sedimentation in the period from 1999 to 2002/2003 typically range between -0.5 m to +0.5 m, locally up to -1.5 m to +1.5 m. In the area of the 1999 nourishment (red polygon), the beach is characterised by significant, uniform erosion of about 1.5 m. Also the adjacent shoreface (between the beach and ca. -8 m to -9 m NAP) and the area seawards of the red polygon (i.e. the western part of the Appelzak channel) show clear erosion, although at a smaller degree compared with the beach. Outside the nourishment area, the beaches are mainly accreting during the hindcast period by up to +0.5 m, while the bed seawards mainly shows erosion all along the coast, except for the area between Zeebrugge harbour and the red polygon, which is dominated by sedimentation.

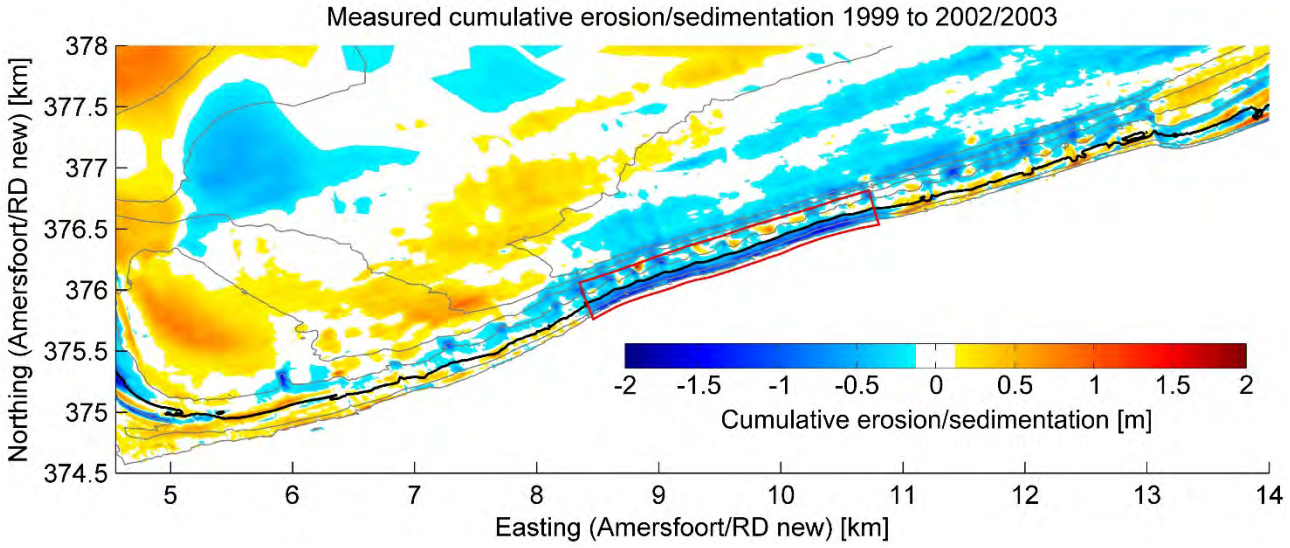

Figure 78 – Measured bed level differences between 1999 and 2002/2003 in the area between Zeebrugge harbour and the Belgian-Dutch border. The red polygon indicates the area of the nourishment performed in May 1999. The grey contour lines have an interval of 2 m. The black line indicates the coastline (0 m NAP). The black dashed lines show the groynes.

Figure 79 presents the bed level changes during the period 1999-2003 simulated by the Scaldis-Coast model. Generally, the model shows erosion inside the nourishment area which aligns with the measurements. However, it underestimates erosion along the beach in the zone above mean sea level (0 m NAP to +4 m NAP). At the seaward part of the shoreface (around - 8 m NAP), the model computes sedimentation, whereas erosion is observed in the measurement. East of the Zeebrugge harbour (north-west conner area in Figure 79), the model simulates a strong accumulation of the sediment. This feature is also evident in the observed data in Figure 78, but less pronounced.

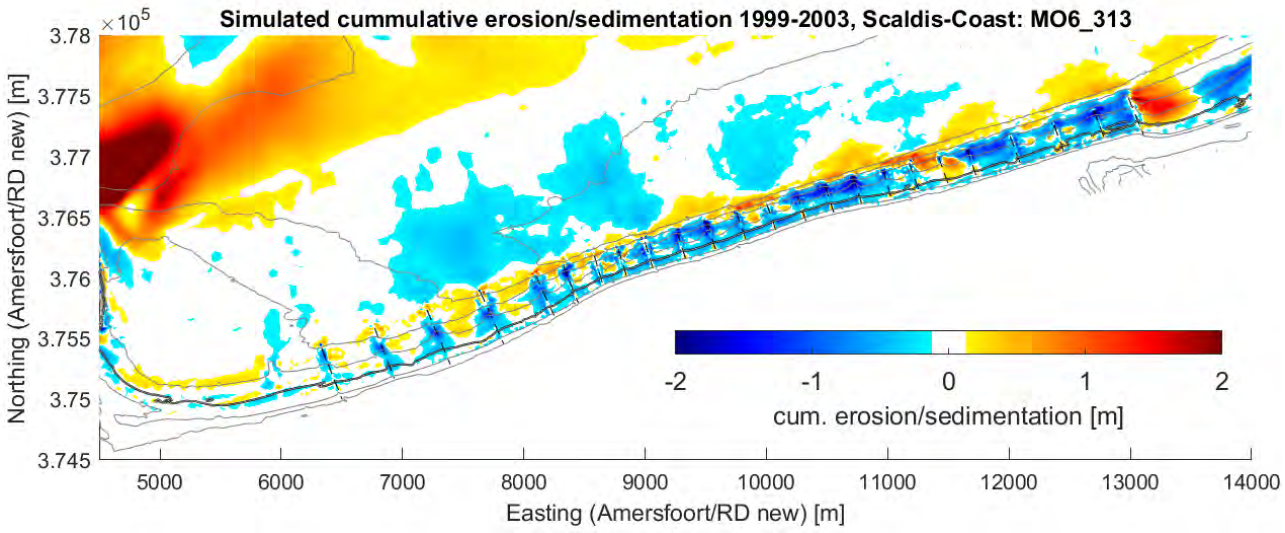

Figure 79 – Simulated bed level differences between 1999 and 2003 in the area between Zeebrugge harbour and the Belgian-Dutch border based on the openTelemac Scaldis-Coast reference run MO6_313. The grey contour lines have an interval of 2 m. The black line indicates the coastline (0 m NAP). The black dashed lines show the groynes.

The FlemCo model generally reproduces the observed morphodynamic patterns in the area of the beach and the shoreface all along the coast illustrated in Figure 80. This particularly applies to i) the observed sedimentation at beach outside the nourishment area, ii) the beach erosion inside the nourishment area and iii) the dominant erosion of the shoreface along the entire coast, which are qualitatively reproduced by the model. Nevertheless, especially the magnitude of the beach erosion inside the nourishment area is underestimated, while the shoreface erosion is overestimated. Seawards of the -6 m NAP contour line, the accuracy of the model prediction generally decreases. While the deeper shoreface (< 6 m NAP) of the area to the east of 8 km Amersfoort/RD new shows erosion according to the measurements, the FlemCo model predicts either no bed level changes or even sedimentation. Further seawards, the measurements and the model results especially disagree near Zeebrugge harbour, where significant sedimentation is predicted by the model, while the observations show a different pattern. This mismatch might be related to the role of erosion resistant layers in the bed, which are not considered in the model (cf. Grasmeijer *et al.,* 2020).

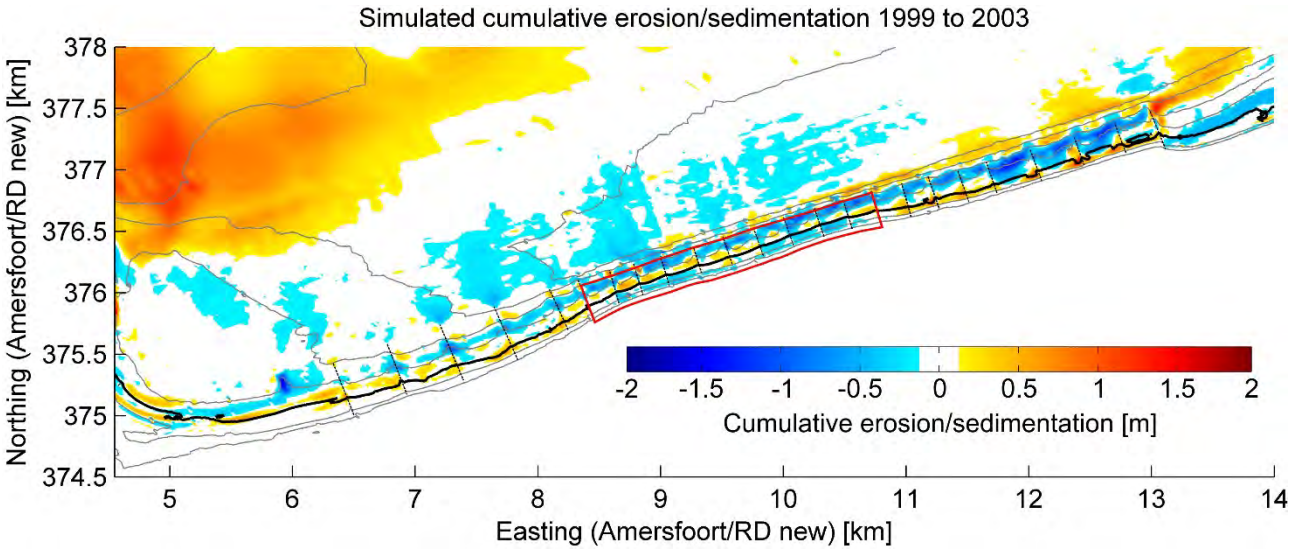

Figure 80 – Simulated bed level differences between 1999 and 2003 in the area between Zeebrugge harbour and the Belgian-Dutch border based on the Delft3D Flexible Mesh FlemCo models reference Run H52. The red polygon indicates the area of the nourishment performed in May 1999. The grey contour lines have an interval of 2 m. The black line indicates the coastline (0 m NAP). The black dashed lines show the groynes.

Residual sediment transport

Figure 81 presents the residual sediment transport and bed level changes during the period 1999-2003 resulted from the Scaldis-Coast model run MO6_313. The model simulates a sediment transport pattern characterized by eastward-directed transport in the nearshore zone - with some local changes in direction - and in the eastern part of the Zeebrugge harbour mouth (northwest corner in Figure 81), along with a divergence of the sediment movement seaward of the shoreface. A turning point in sediment transport is observed in Figure 81 where sediment moves landwards and then diverges eastward in the eastern zone and westward in the western area. This westward transport converges with the eastward-directed transport east of Zeebrugge harbour mouth, which might be one of the factors contributing to sedimentation in this zone.

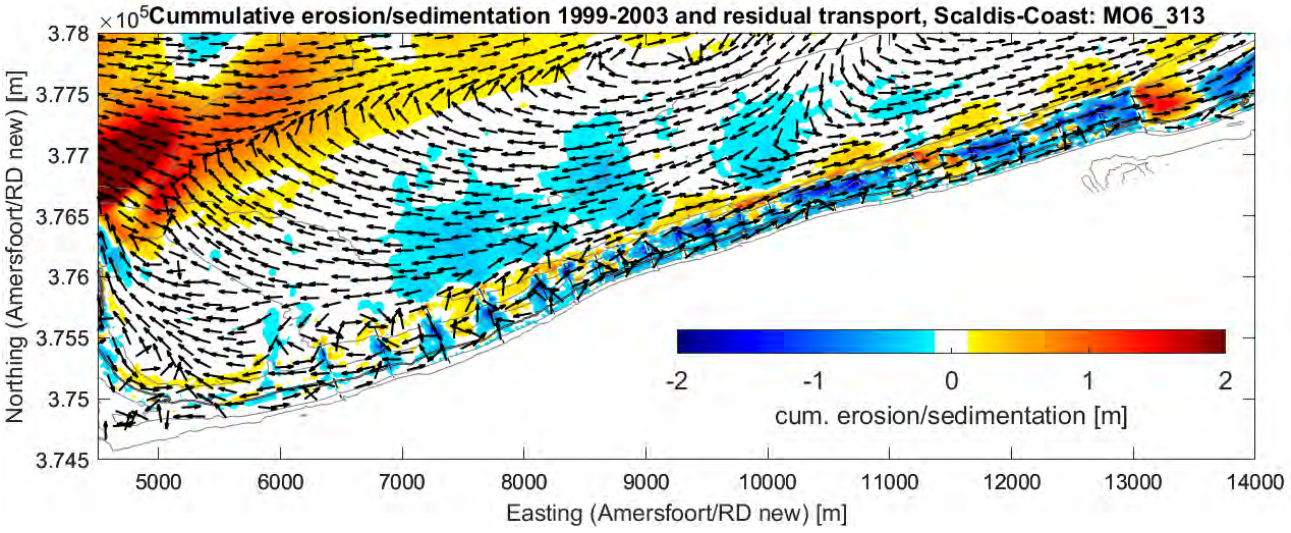

Figure 81 – Scaldis-Coast: Simulated bed level differences between 1999 and 2003 and associated total transport vectors in the area between Zeebrugge harbour and the Belgian-Dutch border based on the openTelemac Scaldis-Coast model Run MO6_313.

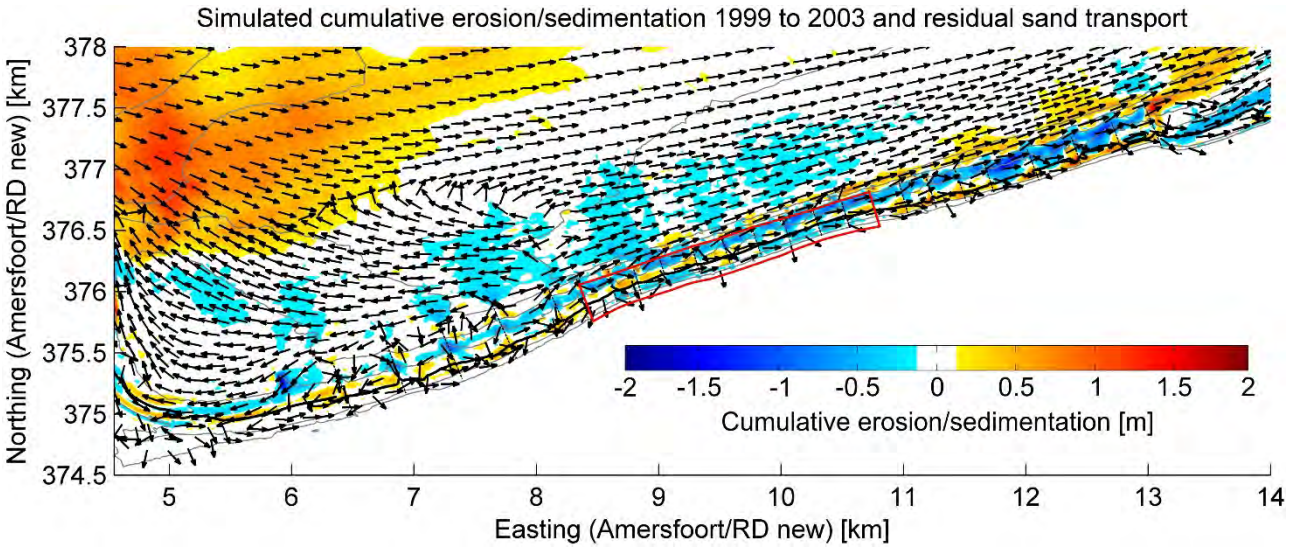

Figure 82 – Flemco: simulated bed level differences between 1999 and 2003 and associated total transport vectors in the area between Zeebrugge harbour and the Belgian-Dutch border based on the Delft3D Flexible Mesh FlemCo model reference Run H52.

The residual sediment transport of the morphodynamic FlemCo model run H52 in Figure 82 gives a better understanding of the sedimentary processes leading to the above described simulated erosion and sedimentation patterns. The dominant residual sediment transport is directed to the east, while it turns to the west near Zeebrugge harbour, which is in line with earlier findings made for the study area (e.g. Dujardin *et al.* 2023, 2024). The predicted dominant shoreface erosion is related to a clear divergence of the residual transport (see diverging vectors in these areas, which either point land- or seawards). Locally at the beaches, the residual transport is pointed towards the land, especially to the east and west of the red polygon, which is in line with the simulated and observed sedimentation in this area. Seawards of the shoreface, the residual transport is mostly parallel to the coastline except for the turning point towards Zeebrugge harbour.

Bed volume changes in the Knokke-Zoute nourishment area

The bed volume changes in the period 1999-2002/2003 based on the measurements and the two models (Scaldis-Coast and FlemCo) were calculated for the Knokke-Zoute area, where the nourishment took place in May 1999. The calculations were performed for four distinct zones (see Figure 83) which differ in this analysis from the traditionally used vertical slice definitions:

- Shoreface: ca. -8 m NAP to -2 m NAP
- Lower foreshore: ca. -2 m NAP to +1 m NAP
- Upper foreshore: ca. +1 m NAP to +4 m NAP (i.e. the high water level in the study area, up to which morphodynamics are calculated in the Scaldis-Coast and FlemCo models)
- Backshore: ca. +4 m NAP to +6 m NAP (note: this area lies higher than the high water level, which means that no morphodynamics are calculated in the Scaldis-Coast and FlemCo models for this area).

Due to the uncertainty in the topo-bathymetric measurements in the area of the groyns (see Section 3.2.3), the volume changes were calculated excluding these areas in both measurements and models. Table 19 presents the resulting bed volume changes between 1999 and 2002/2003. Figure 84 additionally shows the development of the volume changes over time for several in-between measurements.

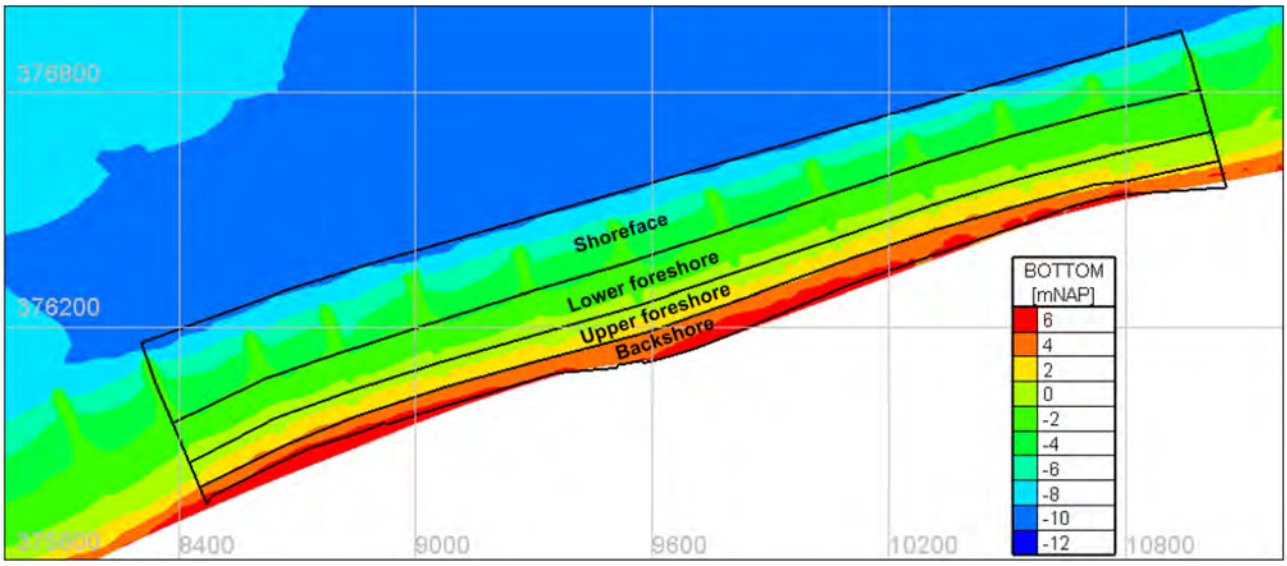

Figure 83 – Four zones in the Knokke-Zoute nourishment area used for the calculation of bed volume changes

The measurements indicate a significant sediment loss in all zones, except for the backshore, which is characterized by a slight volume increase probably due to aeolian sediment transport from the beach (Table 19). The total volume loss in all four zones after ~3.5 years amounts to 360.9 * 10^3 m^3.

For the backshore zone, the Scaldis-Coast model predicts almost no volume change since this area is located higher than the high water level and therefore dominated by aeolian sediment transport, which is not accounted for by the model. For the lower three zones (shoreface, lower and upper foreshore), the Scaldis-Coast model predicts a clear volume loss, which is consistent with the data, although the volume loss is underestimated for the shoreface and upper foreshore while overestimated for the lower foreshore. Overall, the Scaldis-Coast model predicts about 56 % of the total observed volume loss.

Similar to the Scaldis-Coast model, also the FlemCo model indicates minor volume changes for the backshore zone due to the same reason as mentioned above. The FlemCo model underestimates the observed volume loss in the shoreface zone (almost by factor 2) and in the upper foreshore (by factor 9), while it predicts almost no volume change for the lower foreshore zone, which is in contrast to the observed volume change of -77.3 * 10^3 m^3. Altogether, the FlemCo model predicts about 26 % of the total observed volume loss.

Table 19 – Bed volume changes in the nourishment area at Knokke-Heist in the period 1999-2002/2003 as derived from measured bed levels as well as from the Scaldis-Coast and FlemCo models. Negative values indicate sediment loss and positive values show sediment gain.

Polygons/Zones	Bed volume changes 1999-2002/2003 [x10^3 m^3]		
	Measurements	Scaldis-Coast	FlemCo
Backshore	29.8	-0.1	-0.5
Upper foreshore	-144.4	-19.8	-16.1
Lower foreshore	-77.3	-96.8	1.6
Shoreface	-169.0	-87.7	-79.8
All	-360.9	-204.4	-94.8

Figure 84 shows the temporal development of the observed and simulated bed volume changes in the hindcast period 1999-2002/2003 for different moments in time. It should be noted that the simulated bed volume changes over time are plotted solely to illustrate the trend of bed volume variation by the models. Only volume changes at the end of simulations (Table 19) should be considered for comparison with measurements. It is due to the fact that both models use MORFAC (7 for Scaldis-Coast and 12 for FlemCo) approach which is not intended to provide accurate intermediate results during the simulation (because representative wind/wave climate period is 6 months for Scaldis-Coast and 3,5 months for FlemCo).

Figure 84a indicates that the observed bed volume in the backshore zone slightly fluctuates throughout the hindcast period. Almost no volume loss is simulated in this zone by both the Scaldis-Coast and FlemCo models because the aeolian sediment transport is not modeled, as mentioned above. In the upper foreshore (Figure 84b), a significant volume loss can be observed during the first half year of the hindcast period, while the volume is relatively stable in the following three years. This observation is not reproduced by the two models, which predict a much smaller volume loss. In the lower foreshore zone (Figure 84c), the observed bed volume decreases during the first half year of the hindcast period, subsequently increases again, followed by a second decrease during the last year. Although the Scaldis-model nearly reproduces the observed volume loss in this zone after 3.5 years, it predicts a continuous volume decrease. In contrast, the FlemCo model shows several fluctuations of the bed volume but predicts an overall constant bed volume for the lower foreshore. Similar to the upper foreshore, the major volume loss in the shoreface zone is observed during the first half year of the hindcast period and subsequently remains stable (Figure 84d). The volume loss simulated by both models is clearly more continuous and smaller. Figure 84e shows that the major volume loss in the polygon ‘All’ (four zones) occurs during the first half year of the hindcast period, i.e. directly after the nourishment performed in May 1999. This volume loss is mainly attributed to erosion in both the upper foreshore and the shoreface zone. Both models, especially the FlemCo model predict a more constant overall volume decrease for the four zones and underestimate the total volume loss.

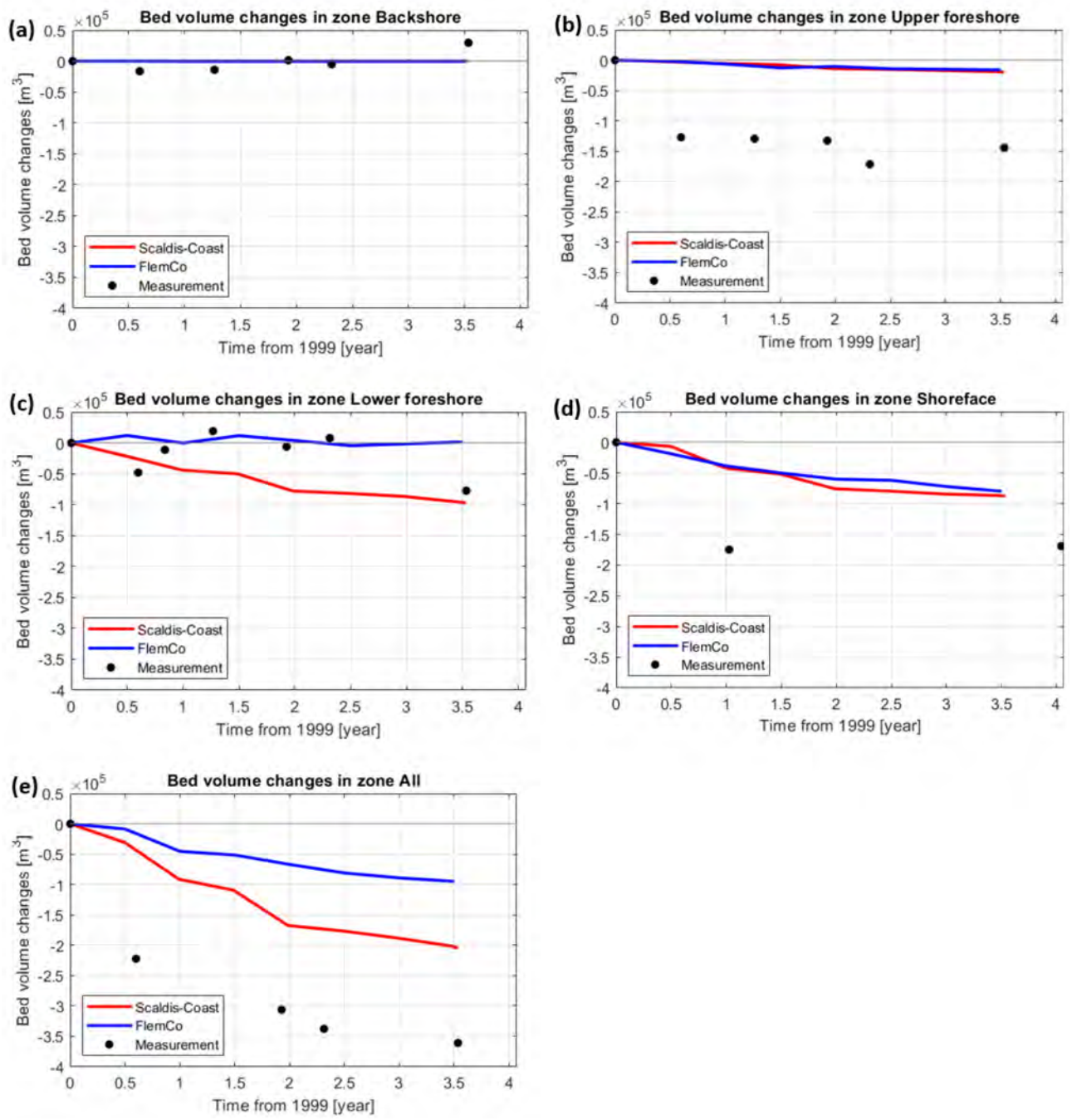

Figure 84 – Bed volume changes in the nourishment area at Knokke-Heist in the period 1999-2002/2003 for different moments in time as derived from measured bed levels as well as from the Scaldis-Coast and FlemCo models. Negative values indicate sediment loss and positive value shows sediment gain.

4 Summary and Conclusions

4.1 WP1: Data acquisition

Vectorisation of old topo-bathymetric maps continued in the 3rd working year. An additional inner shelf cover for 1974-1978 has been realised. The Spring 1992 beach maps were finalised to produce a complete cover of the Belgian coast. In addition, the Autumn 1989 and March 1990 nearshore bathymetry of the eastern part of the Belgian nearshore was vectorised, as well as the corresponding part of the Autumn 1989 beach topography.

Bathymetric rasters of the Belgian inner shelf and the surrounding parts of the French and Dutch territorial waters were also vectorised from 1804, 1866, 1908 and 1938 large scale navigation maps. The sometimes sparse data were modelled taking knowledge of the present bed morphology into account. This data set, complemented with the 1960s, 1980s and 1990s inner shelf bathymetries, allow to study the large-scale seabed evolution over the last two centuries.

In the offshore part of the inner shelf, containing the tidal sand ridges, no systematic movement of the large bedforms has been observed, while in general, this zone may have lost sediment. The loss is of the same order or just exceeds the uncertainty on the data. On the other hand, in an about 7 km wide nearshore zone, containing the shoreface-connected ridges, but excluding the beach, large and systematic movements of the large-scale bedforms to the east, smaller and systematic onshore movements, and general shallowing, albeit in the order of the data uncertainty, occur. Between the nearshore and the offshore zone, there is an about 4 km wide transition zone where the offshore trends gradually transition into the nearshore trends

The attachment points of the shoreface-connected ridges to the coast did not shift, probably so since the historic times. The shoreface tends to move landwards at rates comparable to the landward shift rate of the shoreface-connected ridges. The height of the nearshore sandbanks did not change, though often both crest and channel appear to have risen over the past two centuries. The entire Westerschelde ebb tidal delta shifted landwards, towards the Westerschelde.

It is thought that the described 1804-2022 large-scale morphological changes represent natural change, driven by natural hydrodynamic processes combined with the ongoing sea-level rise. A generalised response to sea-level rise seems to be the up-piling of sand towards the coast.

The receiving area, i.e. the nearshore zone, is not allowed to migrated inland. As a result, accommodation is lost in the nearshore area. Combined with the shoreward long-term movement of sandbanks, this may lead to channel deepening. If sediment up-piling near the coast would continue, a flipping point might be attained where general sanding up of the nearshore may set in. The volume and time scale of this flipping point is unknown.

Human interference also triggered important morphological changes. The creation of navigation channels cross-cutting the nearshore sandbanks depleted the downdrift (eastward) part of the affected sandbanks, thus probably also depriving the downdrift beach of sand supply. In the neighbourhood of Wielingen-Scheur and Pas van 't Zand, a wide surrounding area deepened after the 1960s survey by 1 to 2 m, demonstrating the fact that large-scale dredging below the generalised seabed depth also affects the environment. Due to flow constriction, scour channels developed at the seaward side of the new harbour dams that protrude in the nearshore area. At the same time, sedimentation occurs updrift and downdrift of the new harbour dams. Combined nearshore and beach accretion is observed at the updrift (west) side of the outer harbours, while accretion at the downdrift (east) side is also important but only affects the nearshore.

The abandonment of the old navigation channel to Oostende crosscutting Stroombank in 2009 allowed to obtain another measure for the average longshore sediment transport at the intersection of the channel with Stroombank crest. An estimate of 280 $\pm$ 80 m³/m/yr was obtained. It is thought to be a better estimate than 75 to 100 m³/m/yr found earlier based on morphological change in 2014-2015 in the new navigation channel Pas van Stroombank, as it appeared that repair of Stroombank crest continued at least till 2022, and thus intercepted part of the longshore transport over Stroombank crest. The result also compares well to the earlier estimate of 300 to 500 m³/m/yr at the crossing of Kleine Rede.

4.2 Numerical modelling

4.2.1 WP2: Coupled Shelf-shoreline model morphodynamics

In WP2 of the MOZES project, the third year focused on two main activities (Activity 1 and 2) aimed at further developing the coupled shelf-shoreline model (Activity 1) and the morphodynamic shelf model (Activity 2), both established during the first two years. The morphodynamic model allows a changing shelf bottom in time, whereas the coupled shelf-shoreline model assumes a “frozen” (morphostatic) shelf bottom, while the shoreline evolves in time.

Activity 1: The coupled shelf-shoreline model, which couples a morphostatic shelf model to a morphodynamic nearshore model, is further refined by implementing a ridge configuration resembling that of the Belgian shelf, whereby multiple sfcr and tsr are present on the shelf.

Activity 2: The morphodynamic shelf model is further improved by incorporating a wind climate more representative for the Belgian shelf and 2) including tides in the model.

Key achievements in the third year include:

1. **Realistic ridge configuration**: A ridge system of sfcr and tsr resembling the Belgian shelf was successfully implemented in the coupled shelf-shoreline model. Additionally, a realistic wind climate was derived using data from an offshore wind buoy.
2. **Improved coupled shelf-shoreline model**: The model reproduces observed shoreline progradation near ridge crests and retreat near channels. Simulations indicate that the observed onshore movement of sfcr on the Belgian shelf is likely to intensify shoreline retreat near the channels and progradation near the ridge crests. While tsr have less impact on shoreline evolution than sfcr, their influence is still significant. Results from this model are currently in the process of being published in the *Journal of Geophysical Research – Earth Surface.*
3. **Improved morphodynamic shelf model**: The model now simulates the simultaneous development of sfcr and tsr on the shelf under waves, wind, and tides. The simulated ridge configuration does not resemble that of the Belgian shelf, although the typical orientations of sfcr and tsr are well captured by the model. One difference is that observed sfcr are more oblique, and their migration rates are slower than the simulated ones. A time-varying wind climate alternating between stormy and fair weather reduces migration rates and ridge growth. A time-varying wave climate, a focus of year 4 of the MOZES project, is expected to further reduce these discrepancies. Another difference is the tsr location: observed tsr occur offshore, whereas model generated tsr are situated more shoreward. This mismatch likely stems from the assumption of constant stormy waves and the absence of sea level rise in the model, aspects that will also be investigated in year 4 of the MOZES project.
4. **Innovative sediment formulations**: For the first time, the morphodynamic shelf model simulates sfcr using sediment formulations other than those traditionally used. This is attributed to the presence of directional wave spreading in the SWAN wave model, unlike in earlier modelling studies where directional spreading was absent

Outlook WP2:

The following activities are planned for the fourth year of the project:

1. **Activity 1**: Quantify the effects of sea level rise and changes in tidal forcing on shoreline evolution. Different scenarios of sea level rise will be explored, which will be based on IPCC scenarios. The coupled shelf-shoreline model will be used for this activity.
2. **Activity 2**: Further development of the morphodynamic shelf model. If this model would successfully reproduce the ridge configuration of the Belgian shelf (i.e., tsr offshore, sfcr onshore), it will be coupled with the shoreline evolution model. This coupling will allow for the study of the effects of sea level rise and changes in tidal forcing on both shelf ridge morphodynamics and shoreline evolution, but also how this evolution will influence the shelf ridges.

4.2.2 2DH models development for Knokke-Heist area

The modelling study performed in the second project year revealed that it is mainly the wave related longshore sediment transport that differs between the Scaldis-Coast and FlemCo models, while the tide related transports show a closer match. In the current study, both the Scaldis-Coast and FlemCo models were therefore applied for a simulation period that allowed for a more detailed calibration and validation of the wave models in the nearshore zone between Zeebrugge harbour and the Belgian-Dutch border, especially with regard to the predicted wave directions and wave heights.

The validation showed that the dominant southwestern and northern waves in the offshore area of the model domains (MP7 – Westhinder and Thorntonbank Zuid) are generally simulated fairly well by both models, although the Scaldis-Coast model overestimates the western directions and the FlemCo model underestimates both the western and the northern waves and shows more directional spreading than the measurements and the Scaldis-Coast model. Towards the coast FlemCo tends to represent more the directional spreading, where Scaldis-Coast has a more pronounced wave direction with limited directional spreading. The measurements show a strong undulation in the wave direction caused by the tide, up to 45 degrees. In Scaldis-Coast a similar behaviour can be noticed only it is limited to some 30 degrees. This is a relevant finding with regard to the simulated longshore sediment transport, which – most probably – will be higher in the case of a clearly peaked wave direction near the coast (and resulting stronger wave-induced longshore current) as predicted by the Scaldis-Coast model. Since the current study only dealt with the wave validation, future research could focus on the impact of a more peaked wave direction near the coast on the longshore sediment transport. For this, a suggestion is to apply both models based on the wave validation period for longshore sediment transport simulations and to re-compare the longshore transport predictions between models.

4.2.3 WP4: Effect of the gradual deepening of nearshore tidal channels on beach erosion

In order to simulate and analyse the sedimentary processes and morphodynamics of the Appelzak area in detail in the coming fourth project year using the Scaldis-Coast and FlemCo models, a first attempt of a morphological hindcast of the period 1999 to 2002/2003 was made with both models.

The Scaldis-Coast model generally captures the main morphological changes during the period 1999-2002/2003 with erosion in the nourishment area. However, discrepancies remain in the magnitude and spatial distribution of bed level changes. It underestimates erosion along the beach and predicts sedimentation on the seaward shoreface where erosion is observed. The model overestimates sediment accumulation east of the Zeebrugge harbour.

The FlemCo model generally reproduces the observed morphodynamic patterns in the area of the beach and the shoreface all along the coast although the magnitude of the beach erosion inside the nourishment area is underestimated, while the shoreface erosion is overestimated. Seawards of the -6 m NAP contour line, the accuracy of the model prediction generally decreases. This is especially the case near Zeebrugge harbour, where significant sedimentation is predicted by the model, while the observations show a different pattern. This mismatch is possibly related to the role of erosion resistant layers in the bed/limited sediment availability around Zeebrugge harbour, which are not accounted for in the model.

A comparison between the measured and simulated bed volume changes in the hindcast period indicates that both models but especially the FlemCo model underestimate the total observed volume loss, which mainly occurs in the upper foreshore and the shoreface zones. Moreover, the measured bed levels indicate that the major volume loss occurred during the first half year of the hindcast period (i.e. directly after the nourishment performed in May 1999), while both models predict a more constant volume loss.

The results of this hindcast study must be regarded as a first benchmark of both models. Both models need further calibration and validation before they can be applied to study the nourishments lifetime of the Knokke-Heist coast in more detail. In particular, we suggest to further study the models' sensitivity with regard to i) the predicted (unimodal) wave directions in the nearshore zone, ii) the applied sediment transport formulation (e.g. the more complex transport formulation instead of Bijker, 1971 in Scaldis-Coast), iii) the wave related (SusW, BedW) and transverse slope sediment transport (AlfaBn) parameters, iv) the applied description of the wave velocity asymmetry (WForm), v) considered sediment fractions (e.g. more combinations of different fractions), vi) account for erosion resistant (mud) layers in the model domain (see e.g. Grasmeijer et al., 2020) in order to achieve more realistic morphodynamics near Zeebrugge harbour, vii) alternative hydrodynamic simulation periods and viii) a three-dimensional simulation approach to better reproduce the complex three-dimensional wave processes near the coast.

4.3 Outlook ShorelineS modelling study

The aim of this activity is to gain a better understanding of the coastline development of the coastal zone between Heist and Knokke during the past decades. It also aims to get an indication of expected future shoreline developments. The chosen approach is to perform a hindcast for the shoreline (volume) development in the period from 1983 to 2023, using the recently developed shoreline model ShorelineS (Trouw *et al.*, 2024).

ShorelineS is an open-source numerical model used to calculate shoreline evolution. The model concept is based on one-dimensional equations for sediment transport along the coast, with mass conservation. Evolution takes place on a free-form grid that can consist of several shoreline sections, which are represented as series of shoreline points. The shoreline sections can evolve freely and can include coastal undulations, islands, spits and tombolos; the sections can influence each other by shading and can merge or split. Simulated processes include sediment bypassing and diffraction. Several formulations for coastal sediment transport (bulk) are available and "soft" engineering measures such as beach and coastal nourishment can be simulated. In addition, several hard coastal protection measures can also be included, such as groynes, T-shaped groynes, offshore breakwaters and revetments.

In the fourth project year, the following steps will be performed:

- Merging the current ShorelineS model for Knokke-Heist, developed by Trouw *et al.* (2024), with the latest code from the ShorelineS TKI project.
- Analysing and post-processing measured volume changes based on Houthuys *et al.* (2022).
- Model calibration (1999-2004) and validation (1983-2023) based on measured coastal zone volume changes.

- In-depth analysis into role of groynes, nourishments, wave climate and tide.
- Possible sensitivity analyses for improved model functionality:
    - Contour lines: To minimise spin-up differences, use contour lines where the effect of the groynes is visible. E.g. +2 – 3 m as coastline, then shift back to MSL.
    - Variable coastal cross-shore profiles: Now only one representative cross-shore profile is used for the whole coast section, which means the connection to groynes is not correct everywhere.
    - Grain size: make profile variable.
    - Diffraction: With oblique-incoming waves a too large shadow zone seems to be created.

5 References

Anthony, Edward J., and Troels Aagaard. (2020). "The Lower Shoreface: Morphodynamics and Sediment Connectivity with the Upper Shoreface and Beach." *Earth-Science Reviews* 210: 103334. https://doi.org/10.1016/j.earscirev.2020.103334.

Anthony, E. J., & Orford, J. D. (2002)**.** Between wave- and tide-dominated coasts: the middle ground revisited. *Journal of Coastal Research*, 36 (sp1), 8 – 15. https://doi.org/10.2112/1551-5036-36.sp1.8

Antia, E. E. (1996). "Shoreface-connected ridges in German and US Mid-Atlantic Bights: similarities and contrasts." *Journal of Coastal Research* 12 (1): 141–46.

Arriaga, J.; Rutten, J.; Ribas, F.; Falqués, A.; Ruessink, G. (2017). "Modeling the Long-Term Diffusion and Feeding Capability of a Mega-Nourishment." *Coastal Engineering* 121: 1–13. https://doi.org/10.1016/j.coastaleng.2016.11.011.

Ashton, A.; A Brad Murray; Arnoult, E. (2001). "Formation of coastline features by large-scale instabilities induced by high-angle waves." *Nature* 414 (6861): 296–300. https://doi.org/10.1038/35104541.

Bagnold, R. (1966). An approach to the sediment transport problem from general physics. *Geological Survey*, USA, 422-I.

Bailard, J. A. (1981). An energetics total load sediment transport model for a plane sloping beach. *Journal of Geophysical Research*, 86 (C11), 10938–10954.

Battiau-Queney, Y.; Billet, J. F.; Chaverot, S.; Lanoy-Ratel, P. (2003). "Recent shoreline mobility and geomorphologic evolution of macrotidal sandy beaches in the north of France." *Marine Geology* 194 (1): 31–45. https://doi.org/10.1016/S0025-3227(02)00697-7.

Battjes, J. A., & Janssen, J. P. F. M. (1978). Energy loss and set-up due to breaking of random waves. *In Coastal Engineering Proceedings 1978* (p. 569-587). https://doi.org/10.1061/9780872621909.034

Baudez, L. (1989). De Scheldekaarten van Beautemps-Beaupré. Tijdschrift der stad Antwerpen, 35(1), 13 p.

Belderson, R. H.; Pingree R. D.; Griffiths D.K. (1986). "Low Sea-Level Tidal Origin of Celtic Sea Sand Banks—Evidence from Numerical Modelling of M2 Tidal Streams." *Marine Geology* 73 (1-2): 99–108.

Berg, N. van den; Falqués, A.; Ribas F. (2012). "Modeling Large Scale Shoreline Sand Waves Under Oblique Wave Incidence." *Journal of Geophysical Research: Earth Surface* 117 (F3). https://doi.org/10.1029/2011JF002177.

Bijker, E.W. (1971). Longshore transport computations. ASCE, J. Waterw., *Harbours Coastal Eng*. Div., 97 (WW4).

Booij, N.; Ris, R. C.; Holthuijsen L. H. (1999). "A third-generation wave model for coastal regions: 1. Model description and validation." *Journal of Geophysical Research: Oceans* 104 (C4): 7649–66. https://doi.org/10.1029/98JC02622.

Calvete, D., A. Falqués, H. E. de Swart, and M. Walgreen. (2001). "Modelling the formation of shoreface-connected sand ridges on storm-dominated inner shelves." *Journal of Fluid Mechanics* 441: 169–93. https://doi.org/10.1017/S0022112001004815.

Cartier, A.; Tresca, A.; Forain, N.; Cotonnec, G.; Héquette, A. (2020) Valorisation du sable issu des dragages d'entretien pour la lutte contre l'érosion côtière: le cas du Port de Dunkerque. XVI^{ièmes} Journées Nationales Génie Côtier – Génie Civil, Le Havre, 2020. DOI: 10.5150/jngcgc.2020.066

Castelle, B., G. Ruessink, P. Bonneton, V. Marieu, N. Bruneau, and T. Price. (2010). "Coupling Mechanisms in Double Sandbar Systems. Part 1: Patterns and Physical Explanation." *Earth Surface Processes and Landforms* 35: 476–86. https://doi.org/10.1002/esp.1929.

Catuneanu, O. (2006). Principles of Sequence Stratigraphy. Elsevier, Amsterdam, 375 p.

Cooper, JAG, and F Navas. (2004). "Natural Bathymetric Change as a Control on Century-Scale Shoreline Behavior." *Geology* 32 (6): 513–16. https://doi.org/10.1130/G20377.1.

Damgaard, J., Dodd, N., Hall, L., & Chesher, T. (2002). Morphodynamic modelling of rip channel growth. *Coastal Engineering, 45* (3), 199-221. https://doi.org/0.1016/S0378-3839(02)00034-0

Davis, Richard A, Jonathan Klay, and Pliny Jewell. (1993). "Sedimentology and stratigraphy of tidal sand ridges southwest Florida inner shelf." *Journal of Sedimentary Research* 63 (1): 91–104.

Delft, T U. (2024). "SWAN: A third-generation wave model (Linux version 4145) [Software]. Delft University of Technology, Delft, The Netherlands." https://swanmodel.sourceforge.io/download/download.htm.

Deltares. (2022). "User Manual Delft3D-Flow: Simulation of Multi-Dimensional Hydrodynamic Flows and Transport Phenomena, Including Sediments." Version 4.05, SNV revision: 75129, Delft, The Netherlands. https://oss.deltares.nl/web/delft3d/manuals.

De Moor, G. (1991). De februari-stormen van 1990 en hun weerslag op de stranddynamiek langs de Belgische kust. *De Aardrijkskunde 15(3)*: 251-316

Devos, M., Desnerck, R., Fockedey, N., Haspeslagh, J., Termote, J., Termote, T., Tys, D., Van Cauwenberghe, C., Zwaenepoel, A., Seys, J. (2014). Zeewoorden: een speurtocht naar de naamsverklaring van zandbanken, geulen en andere 'zee-begrippen'. Stroombank; Haven. De Grote Rede: Nieuws over onze Kust en Zee, 39, 29-33

Dissanayake, D. M. P. K., Roelvink, J. A., & van der Wegen, M. (2009). Modelled channel patterns in a schematized tidal inlet. *Coastal Engineering*, 56 (11), 1069 - 1083. https://doi.org/10.1016/j.coastaleng.2009.08.008

Duane, David B, Michael E Field, Edward P Meisburger, Donald JP Swift, and S Jeffress Williams. (1972). "Linear Shoals on the Atlantic Inner Continental Shelf, Florida to Long Island." Edited by D. J. P. Swift D. B. Duane, Hutchinson O. H. Pilkey; Dowden, and Stroudsburg Ross. *In: Shelf Sediment Transport: Process and Pattern*, 447–98.

Dujardin, A.; Houthuys, R.; Nnafie, A.; Röbke, B.; van der Werf, J.; de Swart, H.E.; Biernaux, V.; De Maerschalck, B.; Dan, S.; Verwaest, T. (2023). MOZES – Research on the Morphological Interaction between the Sea bottom and the Belgian Coastline: Working year 1. Version 4.0. FH Reports, 20_079_1. Flanders Hydraulics: Antwerp.

Dujardin, A.; Houthuys, R.; Nnafie, A.; Röbke, B.; van der Werf, J.; de Swart, H.E.; Biernaux, V.; De Maerschalck, B.; Dan, S.; Verwaest, T. (2024). MOZES – Research on the Morphological Interaction between the Sea bottom and the Belgian Coastline: Working year 2. Version 4.0. FH Reports, 20_079_2. Flanders Hydraulics: Antwerp.

Dyer, Keith R., and David A. Huntley. (1999). "The Origin, Classification and Modelling of Sand Banks and Ridges." *Continental Shelf Research* 19 (10): 1285–1330.

Elias E.P.L., van der Spek, A.J.F., Lazar, M. (2016). The 'Voordelta', the contiguous ebb-tidal deltas in the SW Netherlands: large-scale morphological changes and sediment budget 1965–2013; impacts of large-scale engineering. Netherlands Journal of Geosciences, 27 p. doi:10.1017/njg.2016.37

Falqués, A., and D. Calvete. (2005). "Large-scale dynamics of sandy coastlines: Diffusivity and instability." *Journal of Geophysical Research: Oceans* 110 (C3). https://doi.org/10.1029/2004JC002587.

Falqués, Albert, Francesca Ribas, Déborah Idier, and Jaime Arriaga. (2017). "Formation mechanisms for self-organized kilometer-scale shoreline sand waves." *Journal of Geophysical Research: Earth Surface* 122 (5): 1121–38. https://doi.org/10.1002/2016JF003964.

Galappatti, R. (1983). A depth integrated model for suspended transport. *Communications on Hydraulics*, 1983-07, Delft University of Technology.

Garnier, R., Calvete, D., Falqués, A., & Caballeria, M. (2006). Generation and nonlinear evolution of shore-oblique/transverse sand bars. Journal of Fluid Mechanics, 567, 327–360. https://doi.org/110.1017/S0022112006002126

Grasmeijer, B.; Röbke, B.R.; van der Werf, J. (2020). The Delft3D-FM Flemish Coast Model. Set-up of sediment transport and morphology and first steps towards calibration and validation. Deltares report, vol. 1210301-001-ZKS-0014. Delft, The Netherlands.

Hasselmann, K., Barnett, T., Bouws, E., Carlson, H., Cartwright, D., Enke, K., . . . Kruseman, P. (1973). Measurements of wind-wave growth and swell decay during the Joint North Sea Wave Project (JONSWAP). *Deutsche Hydrographische Zeitschrift*, Reihe A, 12 (A8), 1–95.

Héquette, Arnaud, and David Aernouts. (2010). "The influence of nearshore sand bank dynamics on shoreline evolution in a macrotidal coastal environment, Calais, northern France." *Continental Shelf Research* 30 (12): 1349–61. https://doi.org/10.1016/j.csr.2010.04.017.

Holthuijsen, Leo H. (2007). *Waves in Oceanic and Coastal Waters*. Cambridge University Press.

Houthuys; R., Vos, G.; Dan, S.; Verwaest, T. (2021). Long-term morphological evolution of the Flemish coast: Holocene, Late Middle Ages to present. Version 1.0. FHR Reports, 14_023_1. Flanders Hydraulics Research: Antwerp

Houthuys, R.; Verwaest, T.; Dan, S. (2022). Morfologische trends aan de Belgische Kust: Evolutie van de Vlaamse kust tot 2019. Versie 3.0. WL Rapporten, 18_142_1. Waterbouwkundig Laboratorium: Antwerpen.

Huthnance, J. M. (1982). "On One Mechanism Forming Linear Sand Banks." *Estuarine, Coastal and Shelf Science* 14 (1): 79–99.

Huybrechts, P.; Van den Eynde, D.; Slangen, A.; Pattyn, F.; Hamdi, R. (2023). Zeespiegelstijging voor Vlaanderen. Studie voor het Dep Mobiliteit en Openbare Werken, Waterbouwkundig Laboratorium, door VUB, NOIZ, KMI, KBIN, ULB (text in English, 21 p.).

Ikeda, S. (1982). Lateral bed load transport on side slopes. *Journal of the Hydraulics Division*, 108 (11), 1369–1373.

Isobe, M.; K. Horikawa (1982). Study on water particle velocities of shoaling and breaking waves. Coastal Engineering in Japan 25: 109–123.

Janssens, J.; Reyns, J.; Verwaest, T.; Mostaert, F. (2012). Morfologische evolutie van het Belgisch continentaal plat gedurende de laatste 150 jaar: Deelrapport in het kader van het Quest4D-project. Versie 2_0. WL Rapporten, 814_02. Waterbouwkundig Laboratorium: Antwerpen, België

Kolokythas, G.; Fonias, S.; Wang, L.; De Maerschalck, B.; Vanlede, J. (2023). Modelling Belgian Coastal zone and Scheldt mouth area: Sub report 14: Scaldis-Coast model – Model setup and validation of the morphodynamic model. Version 4.0. FH Reports, 15_068_14. Flanders Hydraulics: Antwerp.

Kolokythas, G.; Breugem, A.; De Maerschalck, B. (2024a). Morphodynamic modelling of the Belgian Coastal zone: Sub report 3 – Implementation and testing cross-shore transport processes in GAIA. Version 4.0. FH Reports, 21_104_3. Flanders Hydraulics: Antwerp

Kolokythas, G.; Breugem, A.; De Maerschalck, B. (2024b). Morphodynamic modelling of the Belgian Coastal zone: Sub report 4 – Cross-shore transport modelling with GAIA: Ostend model. Version 4.0. FH Reports, 21_104_4. Flanders Hydraulics: Antwerp

Komar, P. D. (1998). Beach processes and sedimentation, 2nd edition. Prentice Hall, Englewood Cliffs, N.J.

Komen, G. J., & Hasselmann, K. (1984). On the existence of a fully developed wind-sea spectrum. *Journal of Physical Oceanography*, 14 (8), 1271–1285.

Lesser, G R, J A Roelvink, J A T M Van Kester, and G S Stelling. (2004). "Development and Validation of a Three-Dimensional Morphological Model." *Coastal Engineering* 51 (8): 883–915. https://doi.org/10.1016/j.coastaleng.2004.07.014.

Li, Cong Xian, Jia Qiang Zhang, Dai Du Fan, and Bing Deng. (2001). "Holocene regression and the tidal radial sand ridge system formation in the Jiangsu coastal zone, east China." *Marine Geology* 173 (1): 97–120. https://doi.org/10.1016/S0025-3227(00)00169-9.

Liu, Zhenxia, Serge Berné, Yoshiki Saito, Hua Yu, Alain Trentesaux, Katsuto Uehara, Ping Yin, et al. (2007). "Internal architecture and mobility of tidal sand ridges in the East China Sea." *Continental Shelf Research* 27 (13): 1820–34.

Longuet-Higgins, M. S., and R. W. Stewart. (1964). "Radiation Stresses in Water Waves; a Physical Discussion, with Applications." *Deep Sea Research* 11 (4): 529–62.

Meetnet Vlaamse Banken (2024): Data download https://meetnetvlaamsebanken.be/Download/Welcome dd. 20240615.

Nnafie, A., de Swart, H. E., Boersma, J. M., Verwaest, T., Falqués, A., & Calvete, D. (2024). Presence and position of sand ridges on the shelf strongly impact decadal evolution of adjacent shorelines: A model study. *Journal of Geophysical Research: Earth Surface.*

Nnafie, A., H. E. de Swart, A. Falqués, and D. Calvete. (2021). "Long-Term Morphodynamics of a Coupled Shelf-Shoreline System Forced by Waves and Tides, a Model Approach." *Journal of Geophysical Research: Earth Surface* 126 (12).

Nnafie, A., H. E. de Swart, R. Garnier, and D. Calvete. (2014). "Formation and Long-Term Evolution of Shoreface-Connected Sand Ridges: Modeling the Effects of Sand Extraction and Sea Level Rise." PhD thesis, Utrecht University.

Nnafie, A., T. B. J. Wolf, and H. E. de Swart. (2020). "Tidal Sand Ridges on the Shelf: A Numerical Study of Their Natural Morphodynamic Evolution and Response to Interventions." *Continental Shelf Research* 205: 104195. https://doi.org/10.1016/j.csr.2020.104195.

Nnafie, A., H. E. de Swart, R. Garnier, and D. Calvete. (2014-2). "Effects of sea level rise on the formation and drowning of shoreface-connected sand ridges, a model study". *Continental Shelf Research*, *80*, 32-48. https://doi.org/10.1016/j.csr.2014.02.017

Ozer, J.; Ponsar S.; Van den Eynde, D. (2019). Revisiting the trend analysis of relative mean sea level rise at Oostende (southern North Sea – Belgian coast). Report CREST/X/JO/201906/EN/TR02. Prepared for the CREST Project, Royal Belgian Institute of Natural Sciences, Operational Directorate Natural Environment, Brussels, 28 pp.

Parker, G., N. W. Lanfredi, and D. J. P. Swift. (1982). "Seafloor response to flow in a southern hemisphere sand-ridge field: Argentine inner shelf." *Sedimentary Geology* 33 (3): 195–216.

Pawlowicz, Rich, Bob Beardsley, and Steve Lentz. (2002). "Classical Tidal Harmonic Analysis Including Error Estimates in MATLAB Using t_TIDE." *Computers & Geosciences* 28 (8): 929–37.

Quant, P. (1828). Algemeene kaart in 35 bladen van de duinen en duingronden langs de Noord-Zee in het Koningrijk der Nederlanden behoorende bij het Verslag van de HH. Gecommitteerden tot het Onderzoek naar de mogelijkheid om de Wijze van bevestiging der Fransche duinen toe te passen op die in Nederland. Gedeelte B. van Ostende tot aan het Zwin.

Ribas, F., A. Falqués, H. E. de Swart, N. Dodd, R. Garnier, and D. Calvete. (2015). "Understanding Coastal Morphodynamic Patterns from Depth-Averaged Sediment Concentration." *Reviews of Geophysics* 53. https://doi.org/10.1002/2014RG000457.

Ridderinkhof, W., H. E. de Swart, M. van der Vegt, and P. Hoekstra. (2016). "Modeling the Growth and Migration of Sandy Shoals on Ebb-Tidal Deltas." *Journal of Geophysical Research: Earth Surface* 121 (7): 1351–72. https://doi.org/10.1002/2016JF003823.

Röbke, B.R.; Grasmeijer, B.; van der Werf, J. (2020). The Delft3D-FM Flemish Coast Model. Model set-up and hydrodynamic validation. Deltares report, vol. 1210301-001-ZKS-0008. Delft, The Netherlands.

RWS — Rijkwaterstaat Ministerie van Infrastructuur en Milieu (1999a). Bathymetrie Nederland - kust en vaklodingen 20 mtr. https://maps.rijkswaterstaat.nl/dataregister/srv/api/records/21387166-c765-46a6-9155-32df333388fa, 2024-09-30.

RWS — Rijkwaterstaat Ministerie van Infrastructuur en Milieu (1999b). Jarkus serie. https://maps.rijkswaterstaat.nl/dataregister/srv/api/records/e495f045-412b-4d3a-bdb6-4c64ddf2bef4, 2024-09-30.

RWS — Rijkwaterstaat Ministerie van Infrastructuur en Milieu (2003a). Bathymetrie Nederland - kust en vaklodingen 20 mtr. https://maps.rijkswaterstaat.nl/dataregister/srv/api/records/21387166-c765-46a6-9155-32df333388fa, 2024-09-30.

RWS — Rijkwaterstaat Ministerie van Infrastructuur en Milieu (2003b). Jarkus serie. https://maps.rijkswaterstaat.nl/dataregister/srv/api/records/e495f045-412b-4d3a-bdb6-4c64ddf2bef4, 2024-09-30.

RWS — Rijkwaterstaat Ministerie van Infrastructuur en Milieu (2017). Rijkswaterstaat Matroos NOOS_E. http://noos.matroos.rws.nl/index.php, 2024-03-30.

Safak, Ilgar, Jeffrey H. List, John C. Warner, and William C. Schwab. (2017). "Persistent shoreline shape induced from offshore geologic framework: Effects of shoreface connected ridges." *Journal of Geophysical Research: Oceans* 122 (11): 8721–38. https://doi.org/10.1002/2017JC012808.

Schwab, William C, Wayne E Baldwin, Cheryl J Hapke, Erika E Lentz, Paul T Gayes, Jane F Denny, Jeffrey H List, and John C Warner. (2013). "Geologic Evidence for Onshore Sediment Transport from the Inner Continental Shelf: Fire Island, New York." *Journal of Coastal Research* 29 (3): 526–44. https://doi.org/10.2112/JCOASTRES-D-12-00160.1.

Soulsby, Richard. (1997). *Dynamics of Marine Sands: A Manual for Practical Applications*. Thomas Telford.

Southgate, H. N. (1989). A nearshore profile model of wave and tidal current interaction. *Coastal Engineering*, 13 (3), 219-245. https://doi.org/10.1016/0378-3839(89)90050-1

Steffelbauer, David B, Riccardo E M Riva, Jos S Timmermans, Jan H Kwakkel, and Mark Bakker. (2022). "Evidence of regional sea-level rise acceleration for the North Sea." *Environmental Research Letters* 17 (7): 074002. https://doi.org/10.1088/1748-9326/ac753a.

Stessels, A. (1866). Carte g´en´erale des Bancs de Flandres compris entre Gravelines etl'embouchure de l'Escaut. 1/88,888 scale bathymetric map of the Belgian nearshore shelf published in Antwerp.

Strypsteen, Glenn, Rik Houthuys, and Pieter Rauwoens. (2019). "Dune Volume Changes at Decadal Timescales and Its Relation with Potential Aeolian Transport." *Journal of Marine Science and Engineering* 7 (October): 357. https://doi.org/10.3390/jmse7100357.

Swart, Huib E de, and Bing Yuan. (2019). "Dynamics of Offshore Tidal Sand Ridges, a Review." *Environmental Fluid Mechanics*, 1047–71. https://doi.org/10.1007/s10652-018-9630-8.

Swift, D. J. P., G. Parker, N. W. Lanfredi, G. Perillo, and K. Figge. (1978). "Shoreface-connected sand ridges on American and European shelves: a comparison." *Estuarine and Coastal Marine Science* 7 (3): 257–73.

Swift, Donald J P, and George L Freeland. (1978). "Current Lineations and Sand Waves on the Inner Shelf, Middle Atlantic Bight of North America." *Journal of Sedimentary Research* 48 (4): 1257–66.

Termote, J. (1992). Wonen op het duin. De bewoningsgeschiedenis van het duingebied tot aan de Franse revolutie. Chapter 2 in: Termote, J. (ed.), Tussen land en zee. Het duingebied van Nieuwpoort tot De Panne. Lannoo nv, Tielt, Belgium, p. 46-87.

Trouw, K., Verwaest, T., Dujardin, A., Dan, S. (2024). ShorelineS Knokke-Heist model: Set up of the numerical model. Version 1.0. FHR Reports, 21_091_1. Flanders Hydraulics Research: Antwerp

Trowbridge, J. H. (1995). A mechanism for the formation and maintenance of shore-oblique sand ridges on storm-dominated shelves. *Journal of Geophysical Research*, 100 (C16), 16071-16086.

Van Cauwenberghe, C. (1971). Hydrografische analyse van de Vlaamse banken langs de Belgisch-Franse kust. *Het Ingenieursblad* 40 (19): 563-571

Van de Meene, J. W. H., J. R. Boersma, and J. H. J. Terwindt. (1996). "Sedimentary structures of combined flow deposits from the shoreface-connected ridges along the central Dutch coast." *Marine Geology* 131 (3-4): 151–75.

Van der Spek, A. (1997). Tidal asymmetry and long-term evolution of Holocene tidal basins in The Netherlands: simulation of palaeo-tides in the Schelde estuary. *Marine Geology*, 141 (1), 71–90. https://doi.org/10.1016/S0025-3227(97)00064-9

Van Lancker, Vera R M, Wendy M I Bonne, Erwan Garel, Koen Degrendele, Marc Roche, Dries Van den Eynde, Valérie K Bellec, Christophe Brière, Michael B Collins, and Adonis F Velegrakis. (2010). "Recommendations for the Sustainable Exploitation of Tidal Sandbanks." *Journal of Coastal Research, SI 51*, 151–64.

van Rijn, L. C. (1993). Principles of Sediment Transport in Rivers, Estuaries and Coastal Seas. Aqua Publications, The Netherlands.

van Rijn, L. (2007). Unified view of sediment transport by currents and waves. I: Initiation of motion, bed roughness, and bed-load transport. Journal of Hydraulic Engineering, 133, pp. 649–667. doi: 10.1061/(ASCE)0733-9429(2007)133:6(649).

Verwaest, T; Dujardin, A.; Montreuil, A.-L.; Trouw, K. (2022). "Understanding Coastal Resilience of the Belgian West Coast." *Water* 14 (13). https://doi.org/10.3390/w14132104.

Vis-Star, N. C., de Swart, H. E., & Calvete, D. (2008). Patch behaviour and predictability properties of modelled finite-amplitude sand ridges on the inner shelf. *Nonlinear Processes in Geophysics*, 15, 943-955.

Wahl, T.; Haigh, I.D.; Woodworth, P.L., Albrecht, F.; Dillingh, D.; Jensen, J.; Nicholls, R.J.. Weisse, R.; Wöppelmann, G. (2013). Observed mean sea level changes around the North Sea coastline from 1800 to present. Earth-Science Reviews **124**: 51-97. http://dx.doi.org/10.1016/j.earscirev.2013.05.003

Walgreen, M., Calvete, D., & de Swart, H. E. (2002). Growth of large-scale bed forms due to storm-driven and tidal currents: a model approach. Continental Shelf Research (18-19), 2777–2793. https://doi.org/10.1016/S0278-4343(02)00126-7

Wang, L.; Kolokythas, G.; Fonias, S.; De Maerschalck, B.; Vanlede, J.; Mostaert, F. (2021). Modelling Belgian Coastal zone and Scheldt mouth area: Sub report 13: Scaldis-Coast model – Model setup and validation of the wave propagation model. Version 4.0. FHR Reports, 15_068_13. Flanders Hydraulics Research: Antwerp.

Wang, L.; Kolokythas, G.; Breughem, A.; De Maerschalck, B.Wang, L.; Kolokythas, G.; Breugem, W.A.; De Maerschalck, B. (2025). Modelling Belgian Coast: ScaldisCoast: Sub report 2 – Release notes ScaldisCoast 2024. Version 0.1. FHR Reports, 21_104_2. Flanders Hydraulics Research: Antwerp.

Wyns, Liam, Marc Roche, Florian Barette, Vera Van Lancker, Koen Degrendele, Kris Hostens, and Annelies De Backer. (2021). "Near-Field Changes in the Seabed and Associated Macrobenthic Communities Due to

Marine Aggregate Extraction on Tidal Sandbanks: A Spatially Explicit Bio-Physical Approach Considering Geological Context and Extraction Regimes." *Continental Shelf Research* 229: 104546. https://doi.org/10.1016/j.csr.2021.104546.

Xu, Tongtong. (2015). "Wave Transformation and Alongshore Sediment Transport Due to Obliquely Oriented Shoreface-Connected Ridges." PhD thesis, Georgia Institute of Technology. http://hdl.handle.net/1853/54466.

Zimmerman, JTF. (1980). "Vorticity Transfer by Tidal Currents over an Irregular Topography." *J. Mar. Res.* 38: 601–30.

Appendix A

Morphodynamic shelf model: Sediment transport and morphology

In the morphodynamic shelf model, sediment transport, assumed to be non-cohesive and characterized by a spatially uniform d_{50}, is calculated according to the formulations of Van Rijn (1993). These formulations included both bedload and suspended load transport under the joint action of waves and currents, i.e.,

$$\vec{q} = \vec{q}_b + \vec{q}_s. \qquad \text{(A1)}$$

The magnitude of bedload transport, $|\vec{q}_b|$, is expressed as

$$|\vec{q}_b| = 0.006 w_s d_{50} M^{0.5} M_e^{0.7}. \qquad \text{(A2)}$$

Here, w_s represents the sediment setting velocity, which is computed using the following expression

$$w_s = \frac{10\nu_k}{d_{50}}\left[\sqrt{1 + \frac{0.01(s-1)g d_{50}}{\nu_k^2}} - 1\right], \qquad \text{(A3)}$$

in which ν_k is the kinematic viscosity of water ($1 \cdot 10^{-6}$ m^{2}s^{-1}). Furthermore, M and M_e denote the sediment mobility numbers:

$$\begin{aligned} M &= \frac{|\vec{v}|^2 + U_w^2}{(s-1)g d_{50}}, \\ M_e &= \begin{cases} \dfrac{[\sqrt{|\vec{v}|^2 + U_w^2} - v_{cr}]^2}{(s-1)g d_{50}} & \text{if} \quad \sqrt{|\vec{v}|^2 + U_w^2} \geq v_{cr}, \\ 0 & \text{if} \quad \sqrt{|\vec{v}|^2 + U_w^2} < v_{cr}. \end{cases} \end{aligned} \qquad \text{(A4)}$$

In these expressions, U_w represents the magnitude of the near-bed peak wave orbital velocity (computed by SWAN), $s = \rho_s/\rho$ (with ρ_s the sediment density) is the relative density, and v_{cr} is the critical depth-averaged velocity for the initiation of motion. Critical velocity v_{cr} comprises a component due to currents ($v_{cr,c}$) and another due to waves ($v_{cr,w}$):

$$v_{cr} = \Gamma v_{cr,c} + (1-\Gamma) v_{cr,w}, \quad \Gamma = \frac{|\vec{v}|}{|\vec{v}| + U_w}. \qquad \text{(A5)}$$

These critical velocities are computed using the following formulations:

$$v_{cr,c} = \begin{cases} 0.19(d_{50})^{0.1} \log\left(\dfrac{12D}{3d_{90}}\right) & \text{for} \quad 0.1 < d_{50} < 0.5 \text{ mm}, \\ 8.5(d_{50})^{0.6} \log\left(\dfrac{12D}{3d_{90}}\right) & \text{for} \quad 0.5 < d_{50} < 2 \text{ mm}, \end{cases} \qquad \text{(A6)}$$

and

$$v_{cr,w} = \begin{cases} 0.24[(s-1)g]^{0.66} (d_{50})^{0.33} T_p^{0.33} & \text{for} \quad 0.1 < d_{50} < 0.5 \text{ mm}, \\ 0.95[(s-1)g]^{0.57} (d_{50})^{0.43} T_p^{0.14} & \text{for} \quad 0.1 < d_{50} < 0.5 \text{ mm}, \end{cases} \qquad \text{(A7)}$$

where d_{90} is the sediment diameter corresponding to the 90% cumulative percentile value, while T_p is the peak wave period.

The suspended load transport ($\vec{q}_s$) is calculated by solving the depth-averaged advection-diffusion equation, expressed as

$$\frac{\partial(Dc)}{\partial t}+\frac{\partial(Duc)}{\partial x}+\frac{\partial(Dvc)}{\partial y}-\epsilon_H\left[\frac{\partial}{\partial x}\left(D\frac{\partial c}{\partial x}\right)+\frac{\partial}{\partial y}\left(D\frac{\partial c}{\partial y}\right)\right]=\frac{w_s\left(c_{eq}-c\right)}{T_{sd}}, \quad \text{(A8)}$$

where c is the depth-averaged sediment volume concentration, and ϵ_H is the horizontal eddy diffusion coefficient, which is calculated using the following expression

$$w_s=\frac{10\nu_k}{d_{50}}\left[\sqrt{1+\frac{0.01(s-1)gd_{50}}{\nu_k^2}}-1\right], \quad \text{(A9)}$$

in which ν_k is the kinematic viscosity of water ($1\cdot10^{-6}$ m^{2}s^{-1}), T_{sd} represents a dimensionless adaptation time scale, determined using the following empirical function (Galappatti 1983):

$$\begin{aligned}T_{sd} &= \widetilde{w_s}\exp[(1.547-20.12\widetilde{u^*})\widetilde{w_s}^3+\left(326.832\widetilde{u^*}^{2.2047}-0.2\right)\widetilde{w_s}^2\\ &+(0.1385\ln(\widetilde{u^*})-6.4061)\widetilde{w_s}+(0.5467\widetilde{u^*}+2.1963)]. \quad \text{(A10)}\end{aligned}$$

Here, $\widetilde{w_s}\equiv w_s/u^*$ is the dimensionless fall velocity, where u^* is friction velocity, and $\widetilde{u^*}\equiv u^*/\sqrt{u^2+v^2}$ represents the dimensionless friction velocity. Finally, c_{eq} is the depth-averaged equilibrium sediment concentration as defined by Van Rijn (1993).

Bed slope effects on sediment transport, considered only on for bedload transport, are calculated with the formulations of Bagnold (1966) and Ikeda (1982). These effects are incorporated both in the direction of the local flow and perpendicular to it, with coefficients α_{BS} and α_{BN}, respectively (Dissanayake et a., 2009).

The time evolution of the shelf bed level ($\partial z_b/\partial t$) is determined by dynamically updating z_b based on the net exchange of sediment between the water column and the bed, as well as the spatial gradients in the bedload sediment transport vector $\vec{q}_b$, i.e.,

$$\frac{\partial z_b}{\partial t}=-\frac{1}{1-p}\left[\vec{\nabla}\cdot\vec{q}_b+\frac{w_s\left(c_{eq}-c\right)}{T_{sd}}\right], \quad \text{(A11)}$$

with $p(=0.4)$ the porosity of the bed.

Appendix B

FlemCo and Scaldis-Coast wave calibration/validation

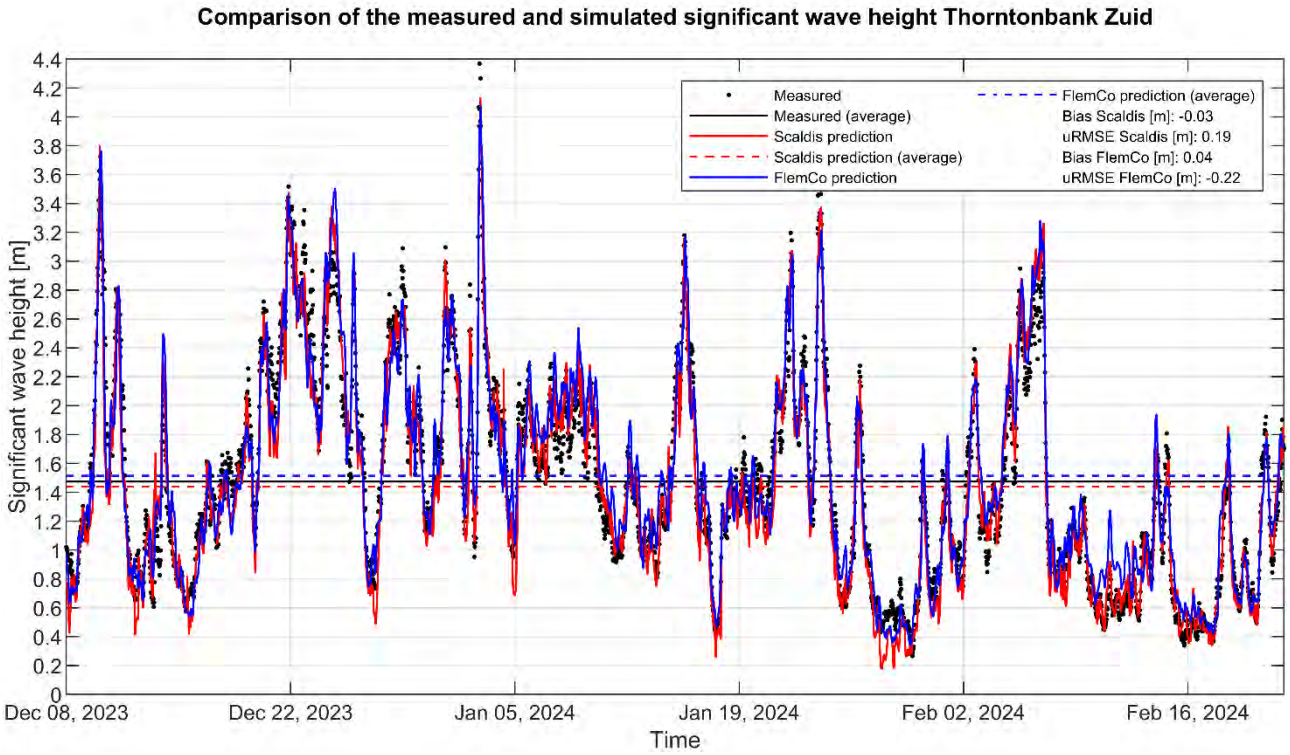

Figure A 1: Comparison of the measured and simulated significant wave height at wave buoy Thorntonbank Zuid based on Scaldis-Coast model reference Run MO6_207 and on FlemCo model reference Run 35. The measured significant wave height is derived from Meetnet Vlaamse Banken (2024).

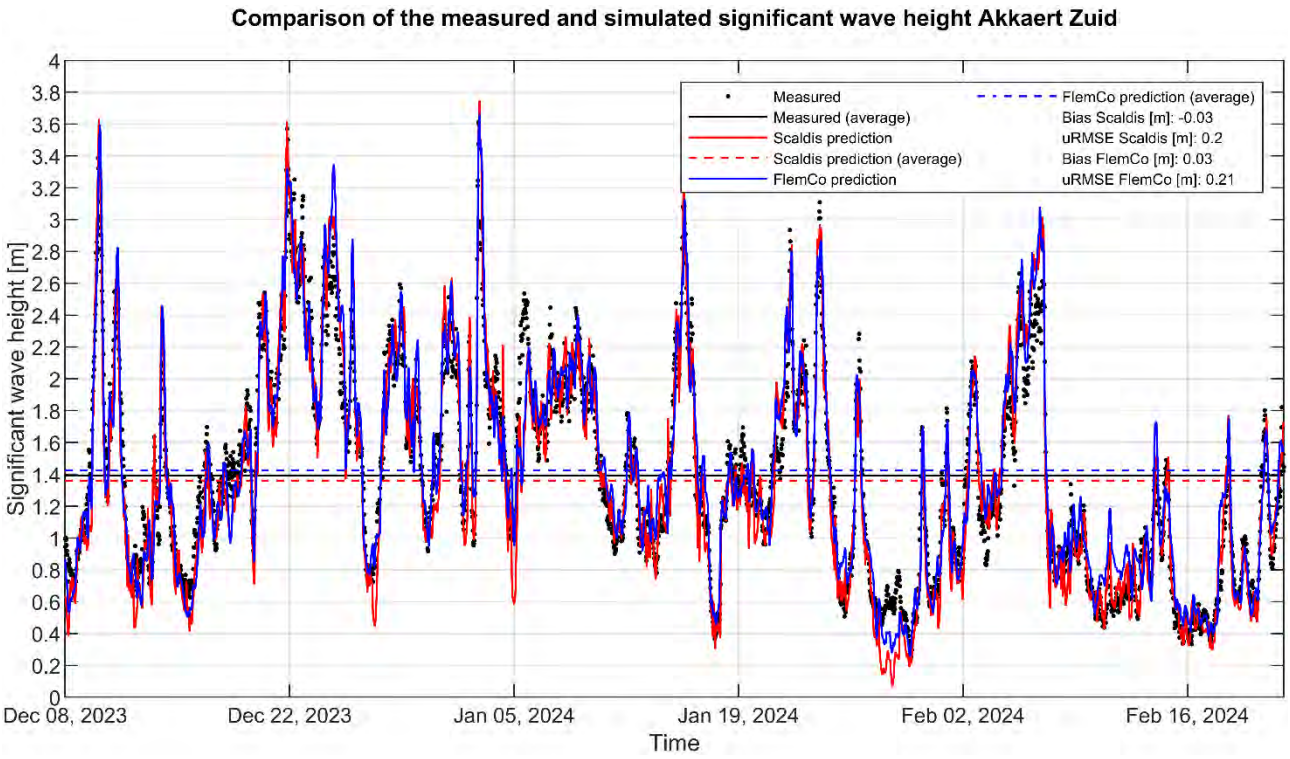

Figure A 2: Comparison of the measured and simulated significant wave height at wave buoy Akkaert Zuid based on Scaldis-Coast model reference Run MO6_207 and on FlemCo model reference Run 35. The measured significant wave height is derived from Meetnet Vlaamse Banken (2024).

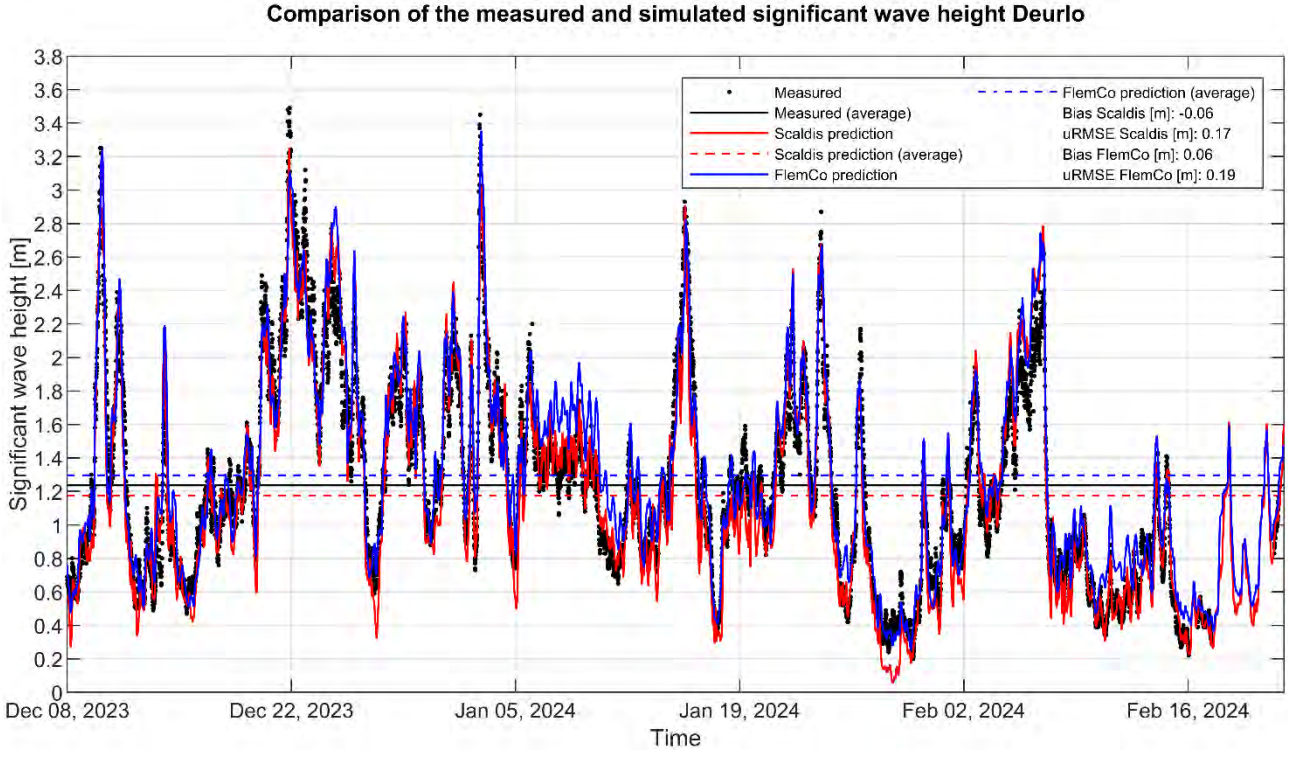

Figure A 3: Comparison of the measured and simulated significant wave height at wave buoy Deurlo based on Scaldis-Coast model reference Run MO6_207 and on FlemCo model reference Run 35. The measured significant wave height is derived from RWS (2024).

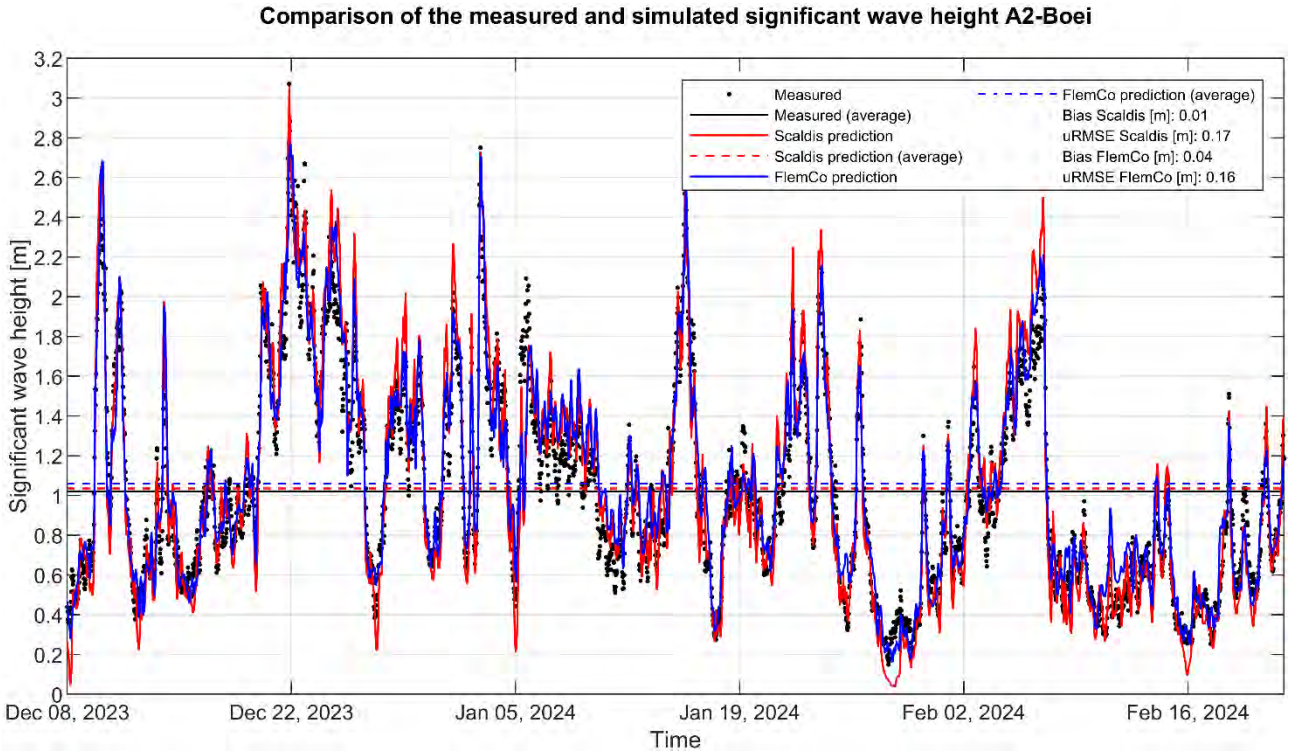

Figure A 4: Comparison of the measured and simulated significant wave height at wave buoy A2-Boei based on Scaldis-Coast model reference Run MO6_207 and on FlemCo model reference Run 35. The measured significant wave height is derived from Meetnet Vlaamse Banken (2024).

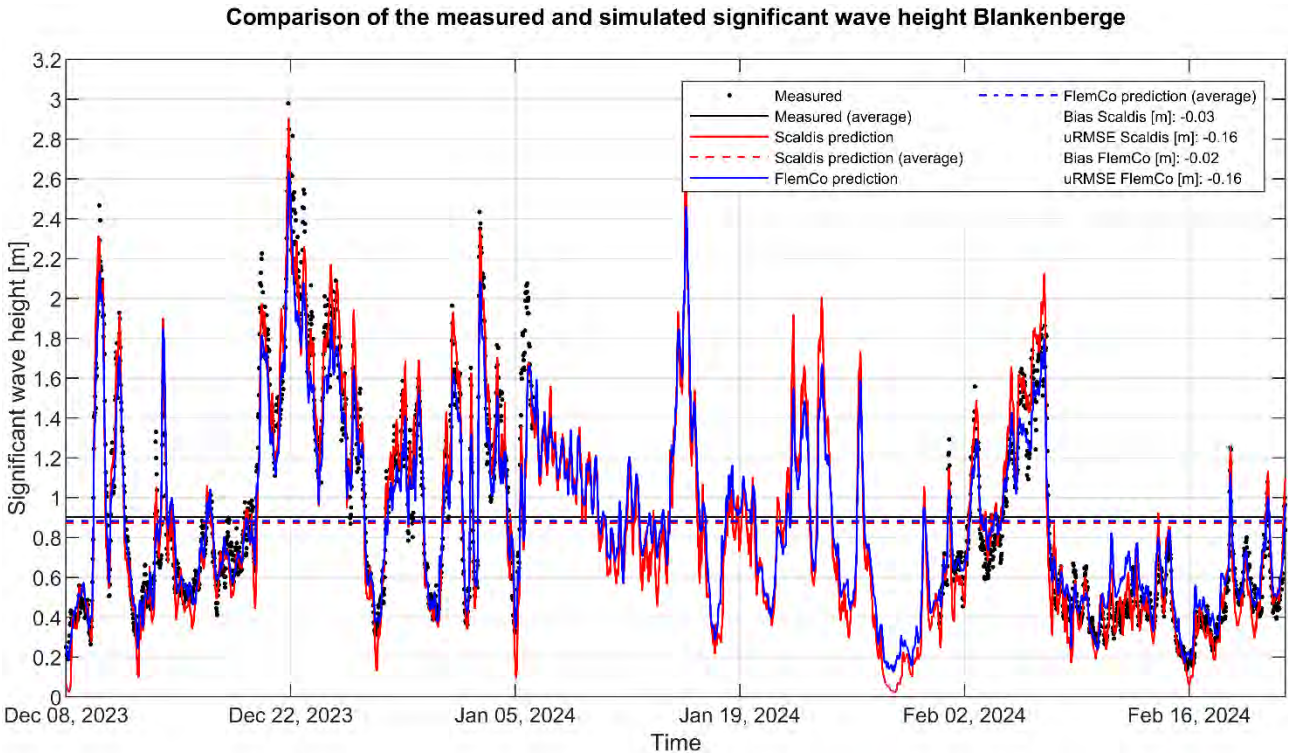

Figure A 5: Comparison of the measured and simulated significant wave height at wave buoy Blankenberge based on Scaldis-Coast model reference Run MO6_207 and on FlemCo model reference Run 35. The measured significant wave height is derived from Meetnet Vlaamse Banken (2024).

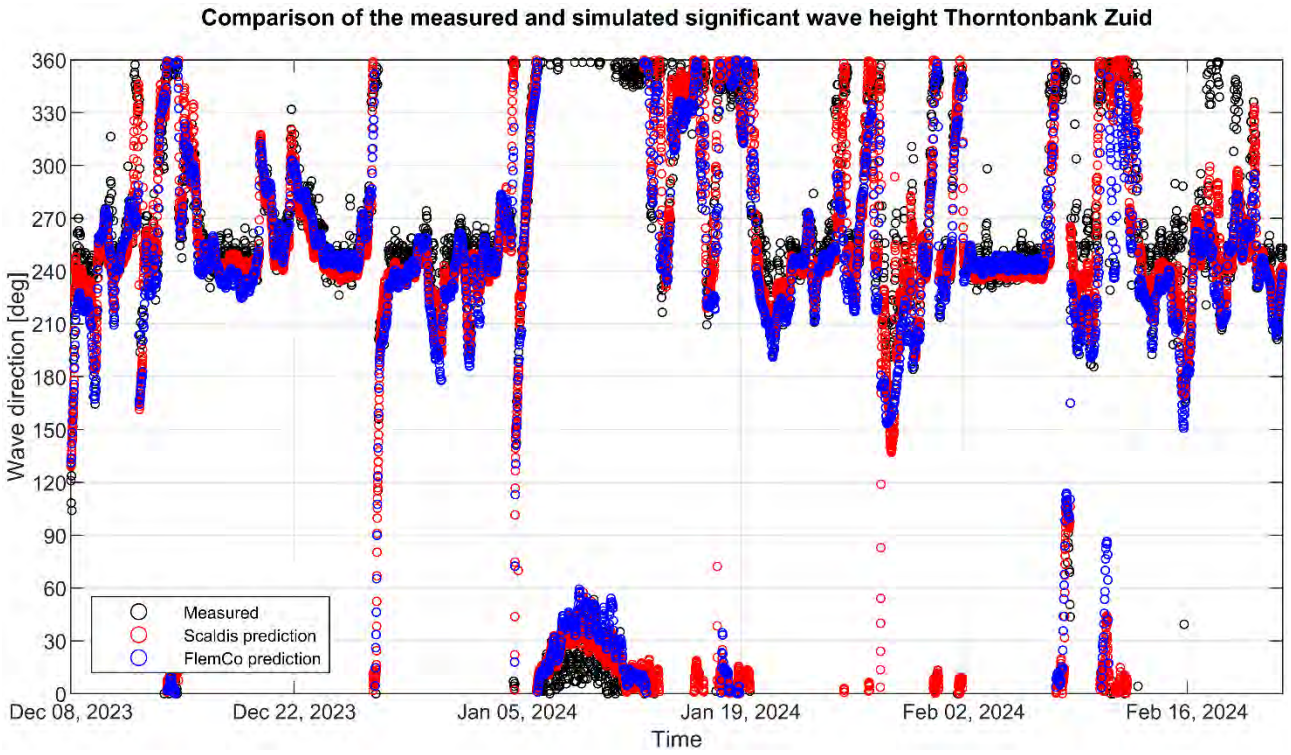

Figure A 6: Comparison of the measured and simulated wave direction (= direction associated with the maximum wave energy) at wave buoy Thorntonbank Zuid based on Scaldis-Coast model reference Run MO6_207 and on FlemCo model reference Run 35. The measured wave direction is derived from Meetnet Vlaamse Banken (2024).

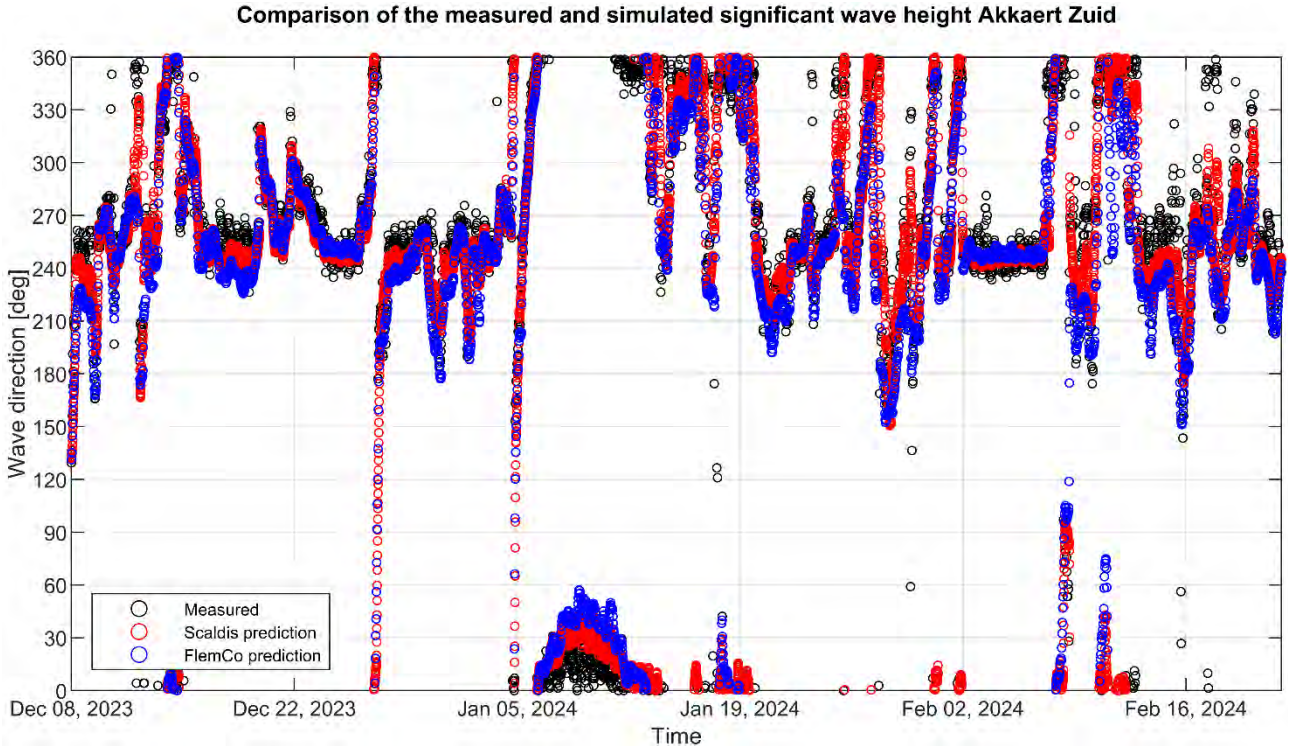

Figure A 7: Comparison of the measured and simulated wave direction (= direction associated with the maximum wave energy) at wave buoy Akkaert Zuid based on Scaldis-Coast model reference Run MO6_207 and on FlemCo model reference Run 35. The measured wave direction is derived from Meetnet Vlaamse Banken (2024).

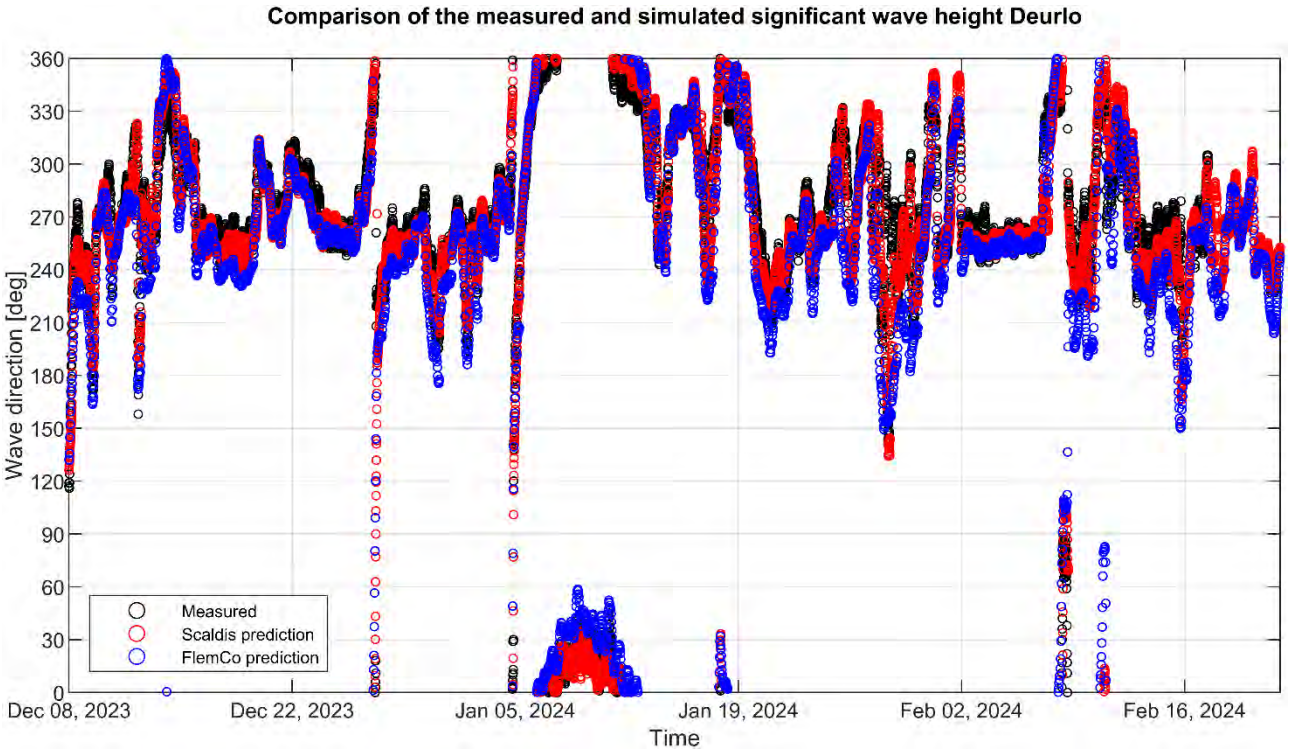

Figure A 8: Comparison of the measured and simulated wave direction (= direction associated with the maximum wave energy) at wave buoy Deurlo based on Scaldis-Coast model reference Run MO6_207 and on FlemCo model reference Run 35. The measured wave direction is derived from RWS (2024).

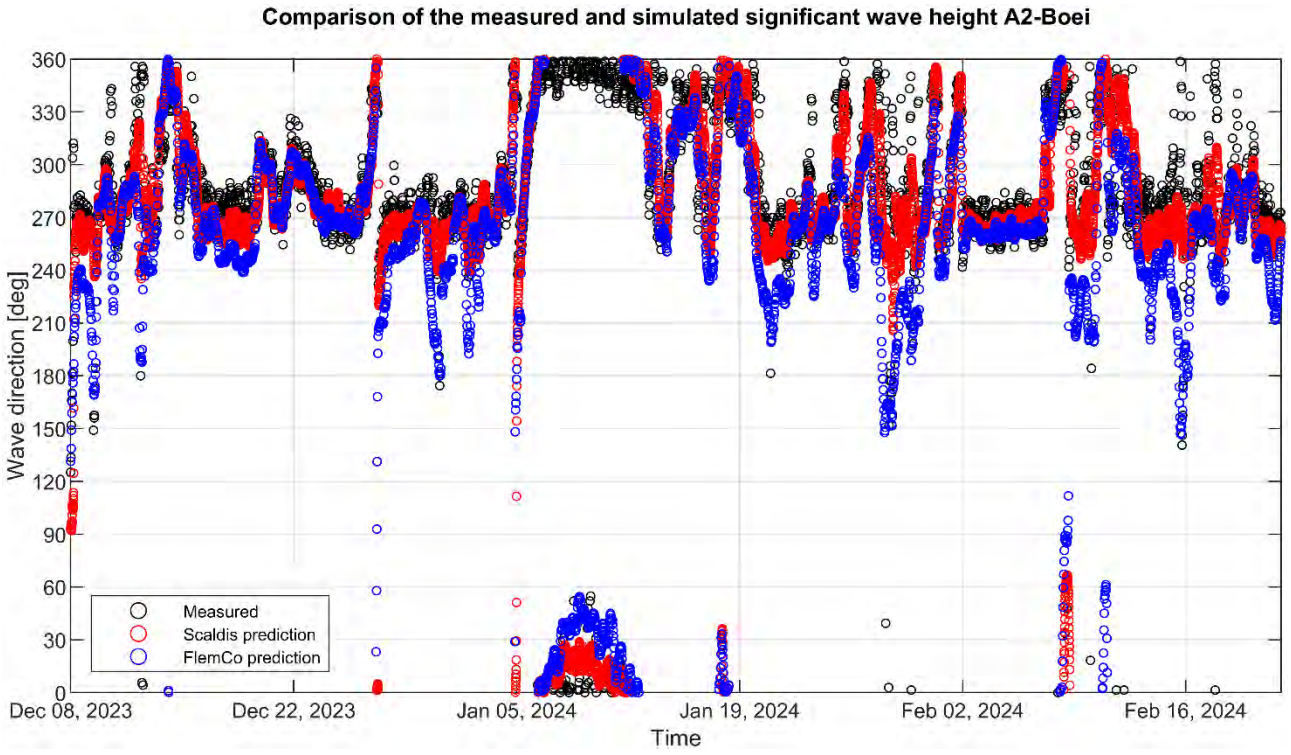

Figure A 9: Comparison of the measured and simulated wave direction (= direction associated with the maximum wave energy) at wave buoy A2-Boei based on Scaldis-Coast model reference Run MO6_207 and on FlemCo model reference Run 35. The measured wave direction is derived from Meetnet Vlaamse Banken (2024).

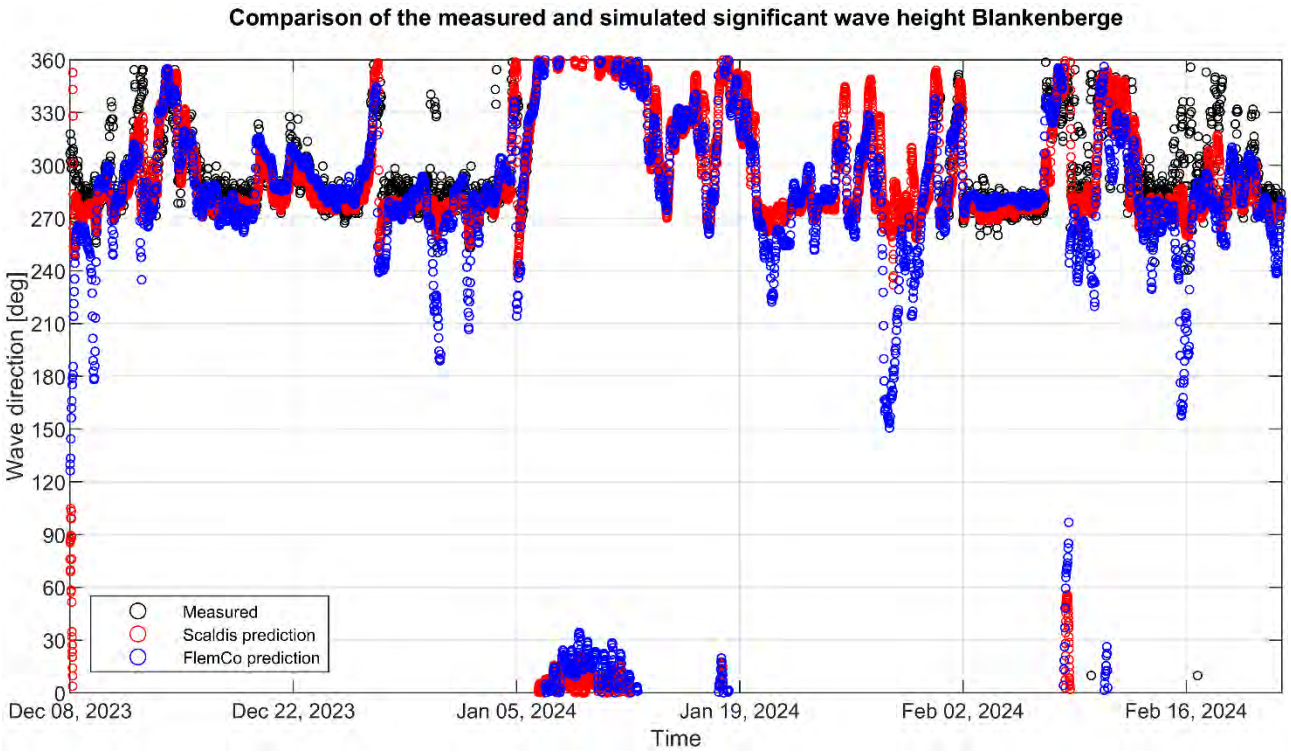

Figure A 10: Comparison of the measured and simulated wave direction (= direction associated with the maximum wave energy) at wave buoy Blankenberge based on Scaldis-Coast model reference Run MO6_207 and on FlemCo model reference Run 35. The measured wave direction is derived from Meetnet Vlaamse Banken (2024).

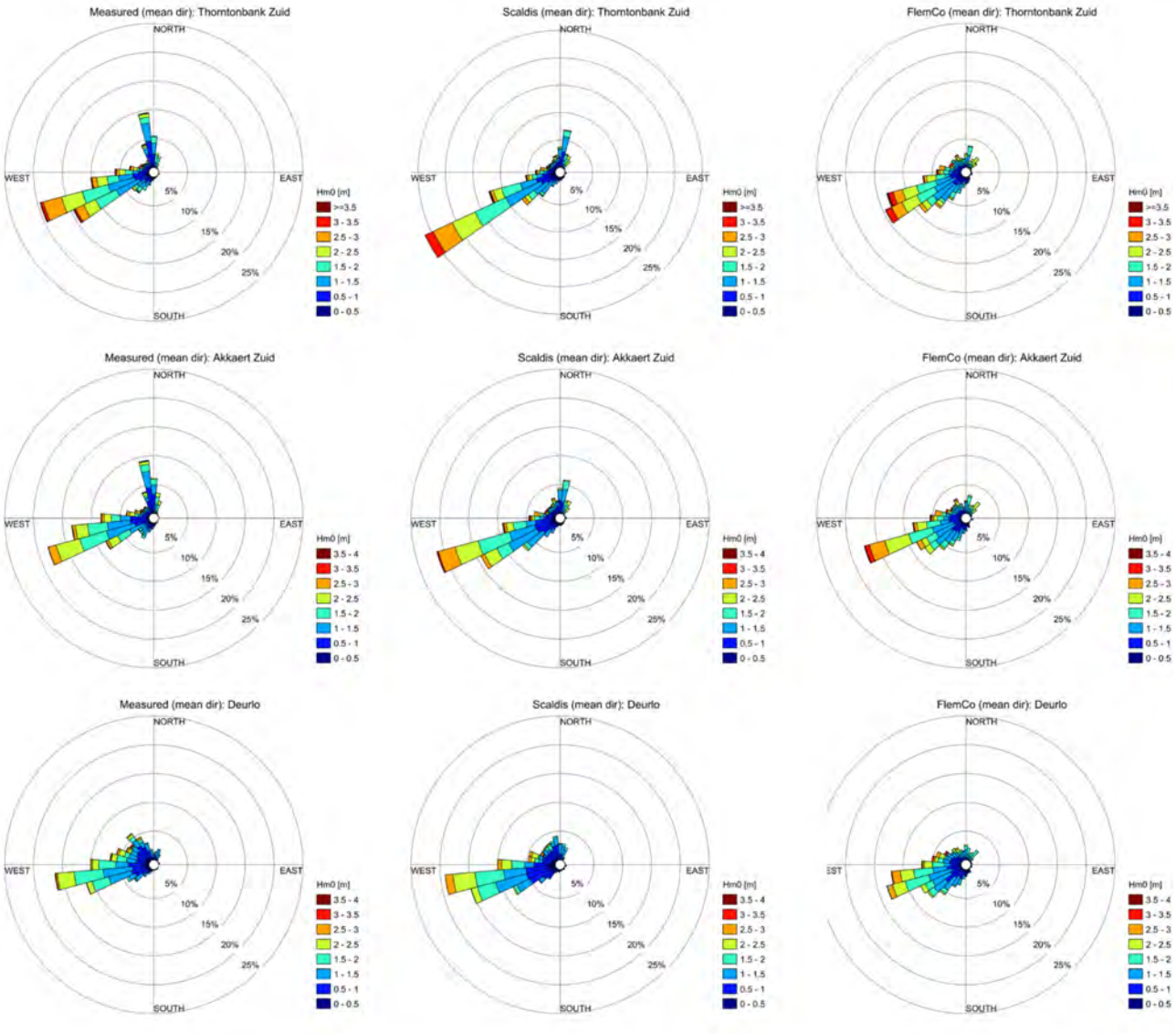

Figure A 11: Wave roses of the measured (left) and simulated (right) significant wave height and wave direction (= direction associated with the maximum wave energy) at wave buoys Thorntonbank Zuid, Akkaert Zuid and Deurlo based on Scaldis-Coast model reference Run MO6_207 and on FlemCo model reference Run 35. The measured significant wave height and wave direction is derived from Meetnet Vlaamse Banken (2024).

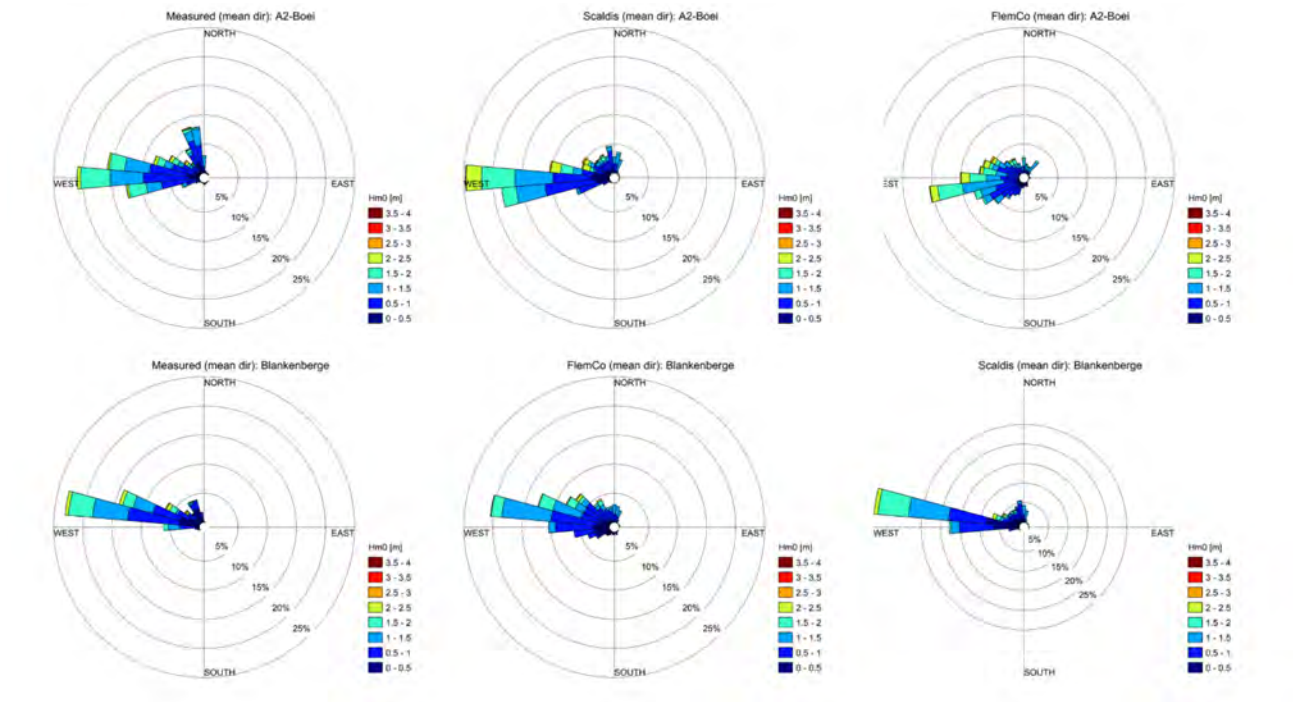

Figure A 12: Wave roses of the measured (left) and simulated (right) significant wave height and wave direction (= direction associated with the maximum wave energy) at wave buoys A2-Boei and and Blankenberge based on FlemCo model reference Run 35. The measured significant wave height and wave direction is derived from Meetnet Vlaamse Banken (2024).

Appendix C

Groyne crest height

The following figures show bathy-topographic profiles over the centre line of the groynes east of Zeebrugge. The curves derived from LiDar data are shown as thin coloured lines; the colour indicates the year. Data derived from the scanned design plans is shown as a grey shaded area. Scaldis-Coast bathymetry is shown as thick black lines: full line – telemac2d mesh, dashed line – tomawac mesh.

The profiles over the groynes Duinbergen 9 to Knokke 11 additionally show the combined multibeam echo sounding and topographic drone measurements conducted by DEME pre- and post-nourishment (respectively October 2023 and March 2024) as thick brown lines.

Generally there's good agreement between all measured datasets and the design plans. For some older LiDar flights however, the water surface was not filtered out.

The Scaldis-Coast model bathymetry matches the data for some groynes (e.g. Knokke 7), but for other groynes the adjacent beach topography is clearly interpolated over the groyne (e.g. Duinbergen 7).

Groyne Heist 51 was demolished late 2009.

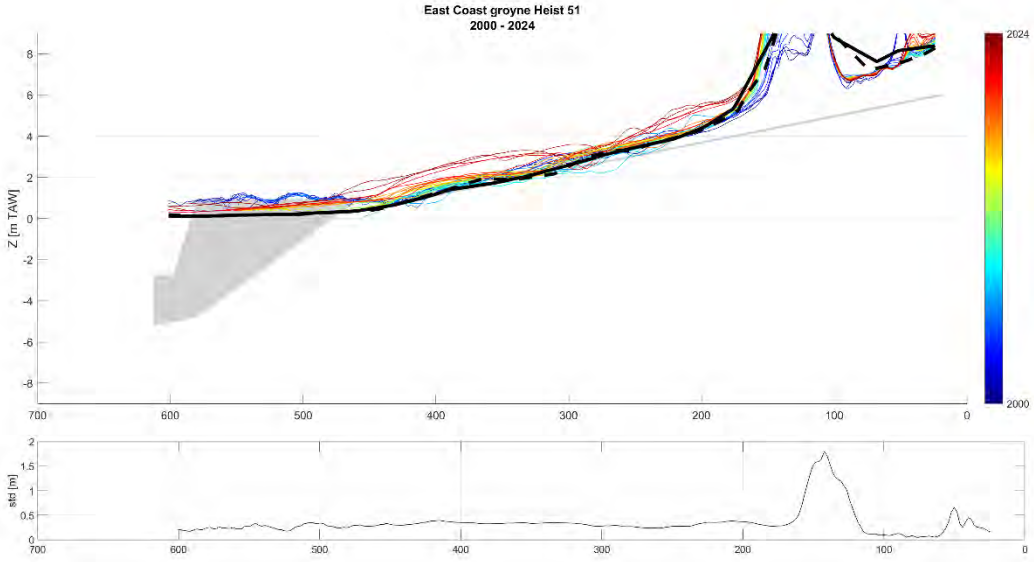
East Coast groyne Heist 51
2000 - 2024
Z [m TAW]
std [m]
2024
2000

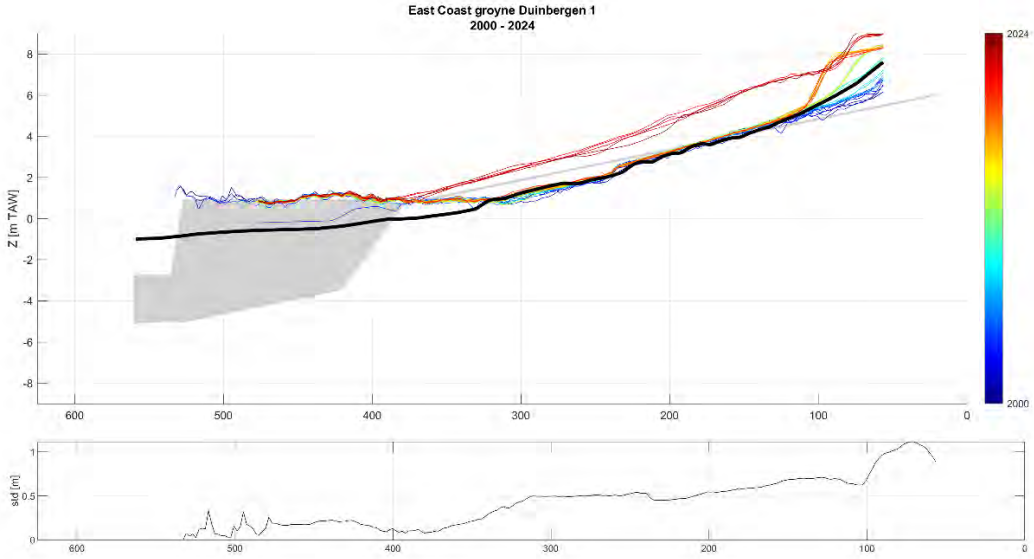
East Coast groyne Duinbergen 1
2000 - 2024
Z [m TAW]
std [m]
2024
2000

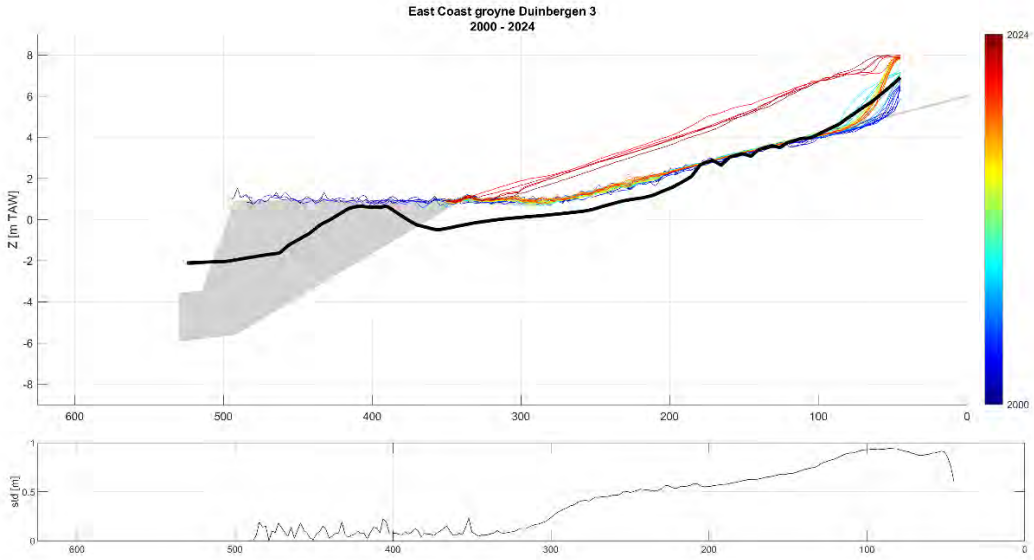
East Coast groyne Duinbergen 3
2000 - 2024
Z [m TAW]
std [m]
2024
2000

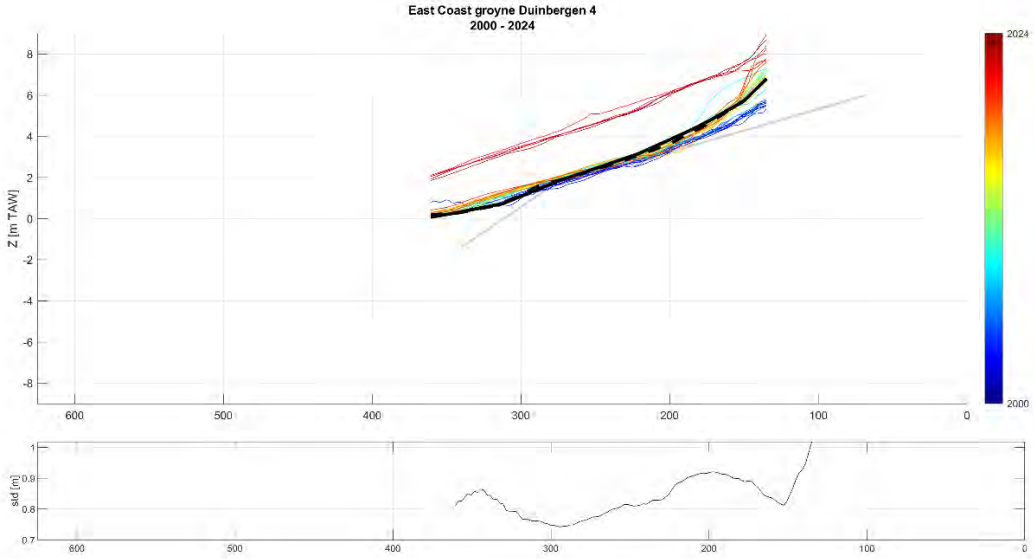
East Coast groyne Duinbergen 4
2000 - 2024
Z [m TAW]
std [m]
2024
2000

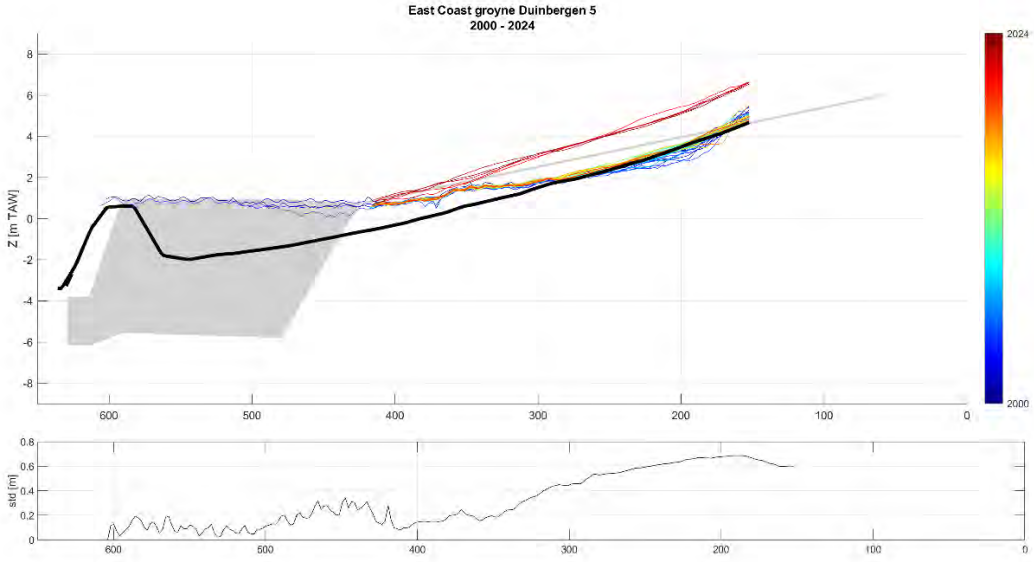
East Coast groyne Duinbergen 5
2000 - 2024
Z [m TAW]
std [m]
2024
2000

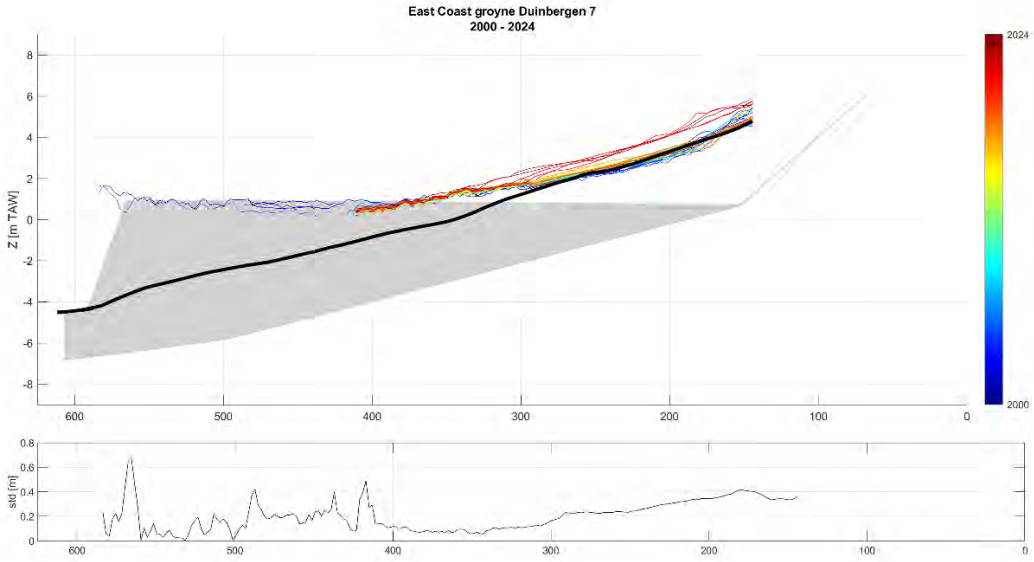
East Coast groyne Duinbergen 7
2000 - 2024
Z [m TAW]
std [m]
2024
2000

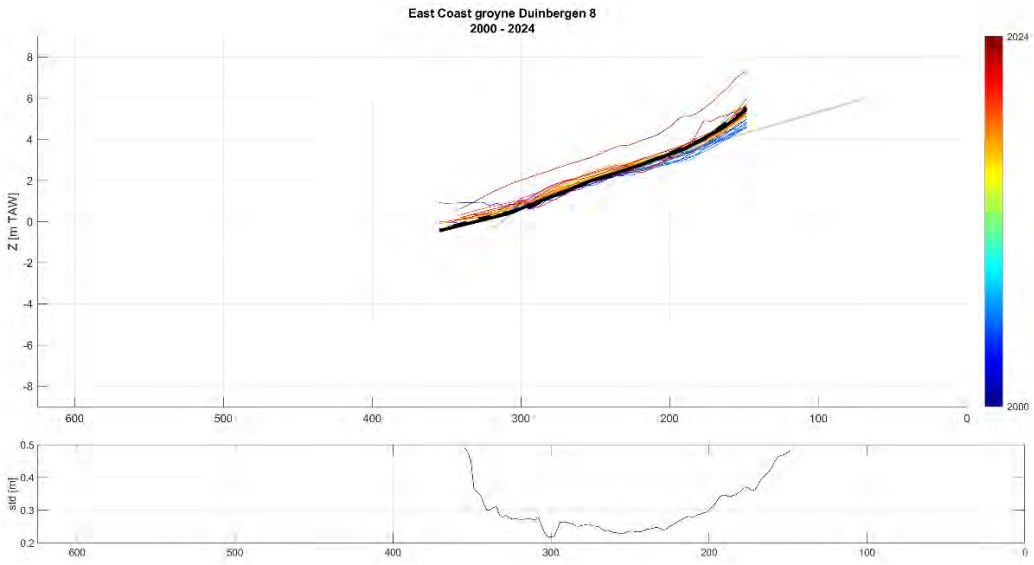
East Coast groyne Duinbergen 8
2000 - 2024
Z [m TAW]
std [m]
2024
2000

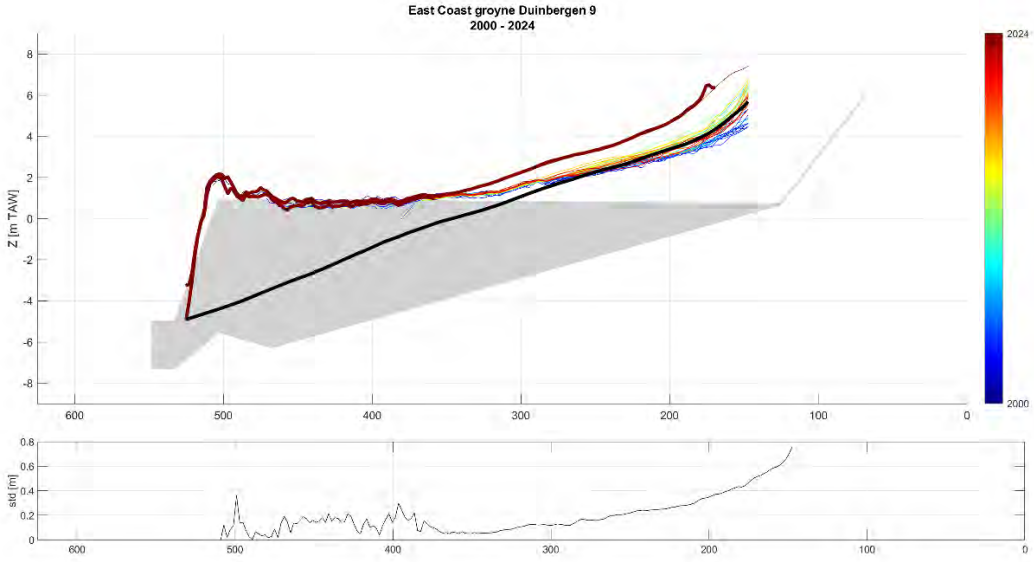
East Coast groyne Duinbergen 9
2000 - 2024
Z [m TAW]
std [m]
2024
2000

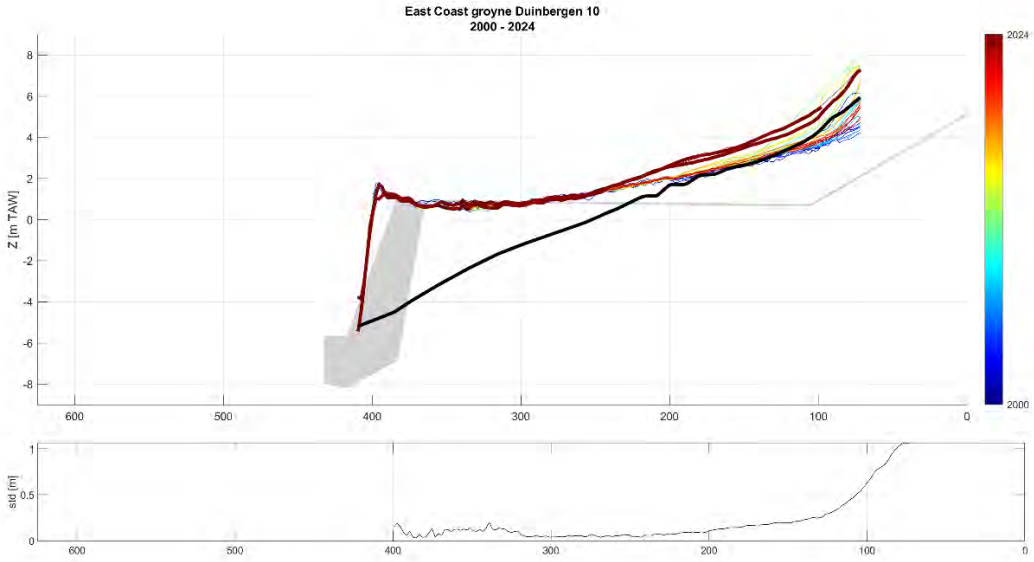
East Coast groyne Duinbergen 10
2000 - 2024
Z [m TAW]
std [m]
2024
2000

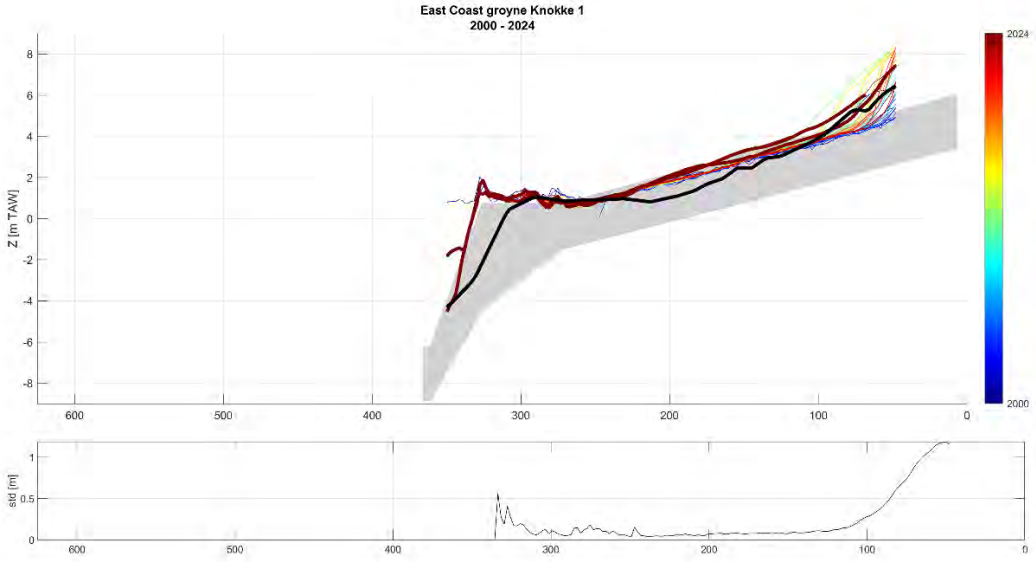
East Coast groyne Knokke 1
2000 - 2024
Z [m TAW]
std [m]
2024
2000

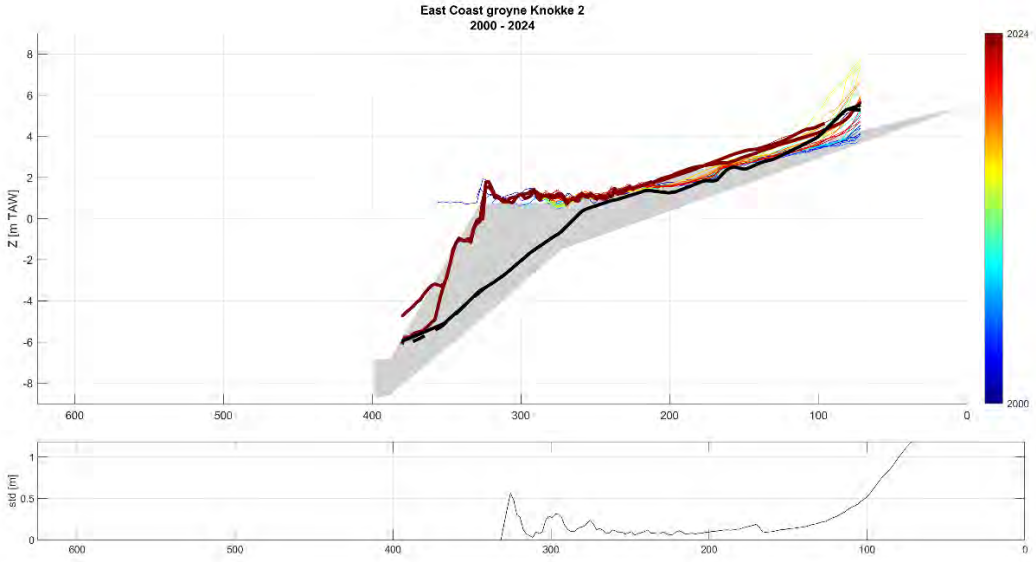
East Coast groyne Knokke 2
2000 - 2024
Z [m TAW]
std [m]
2024
2000

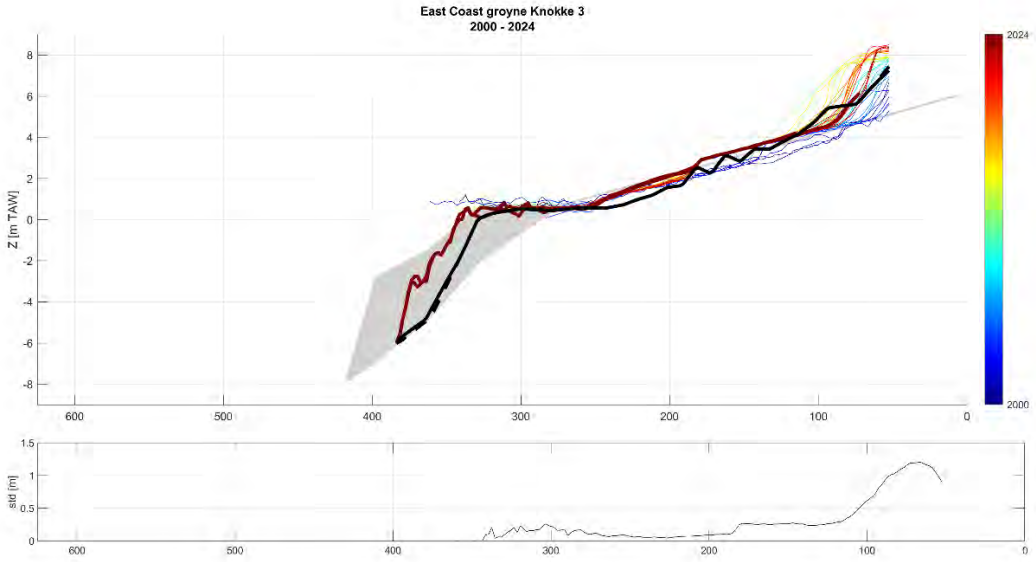
East Coast groyne Knokke 3
2000 - 2024
Z [m TAW]
std [m]
2024
2000

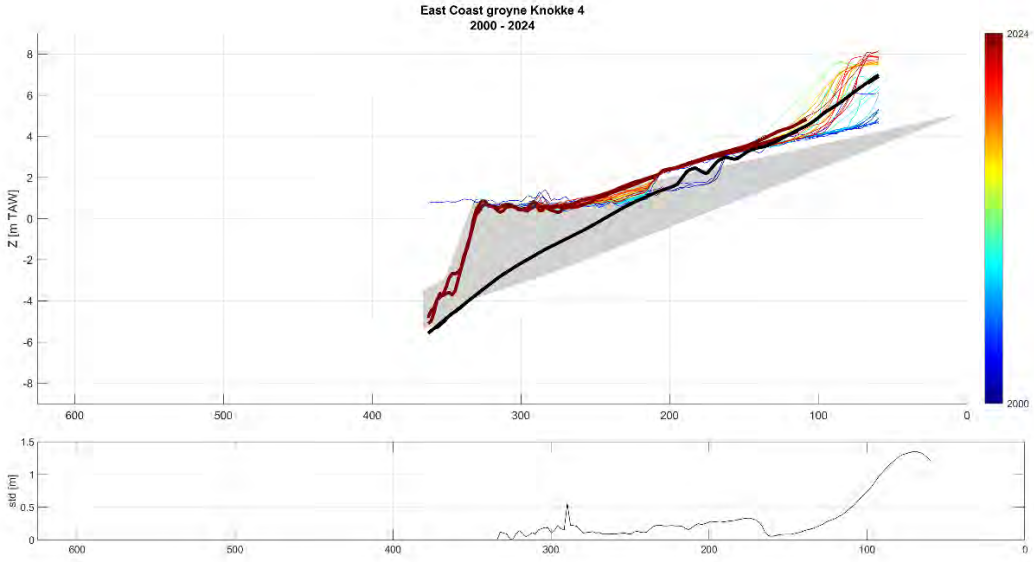
East Coast groyne Knokke 4
2000 - 2024
Z [m TAW]
std [m]
2024
2000

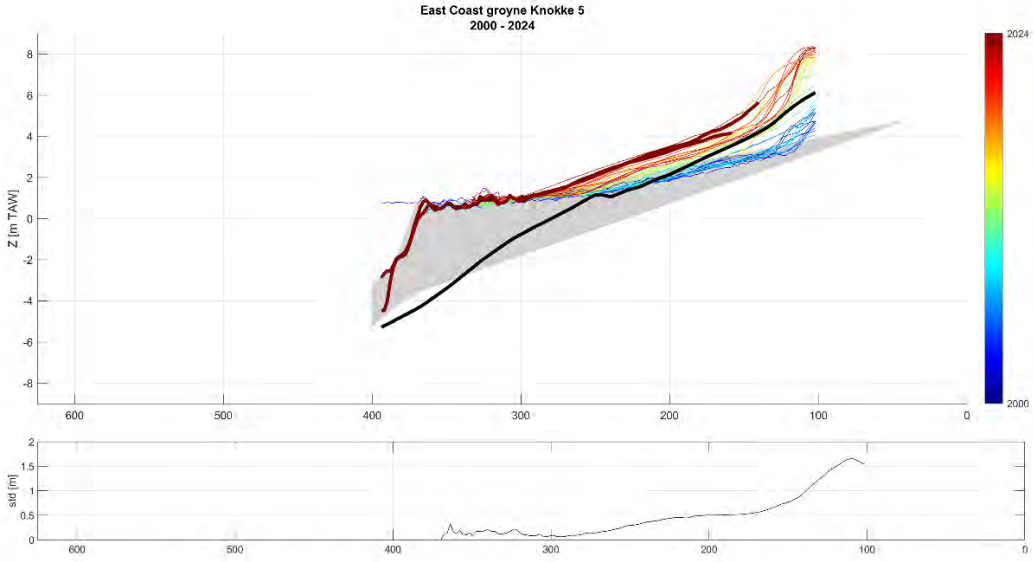
East Coast groyne Knokke 5
2000 - 2024
Z [m TAW]
std [m]
2024
2000

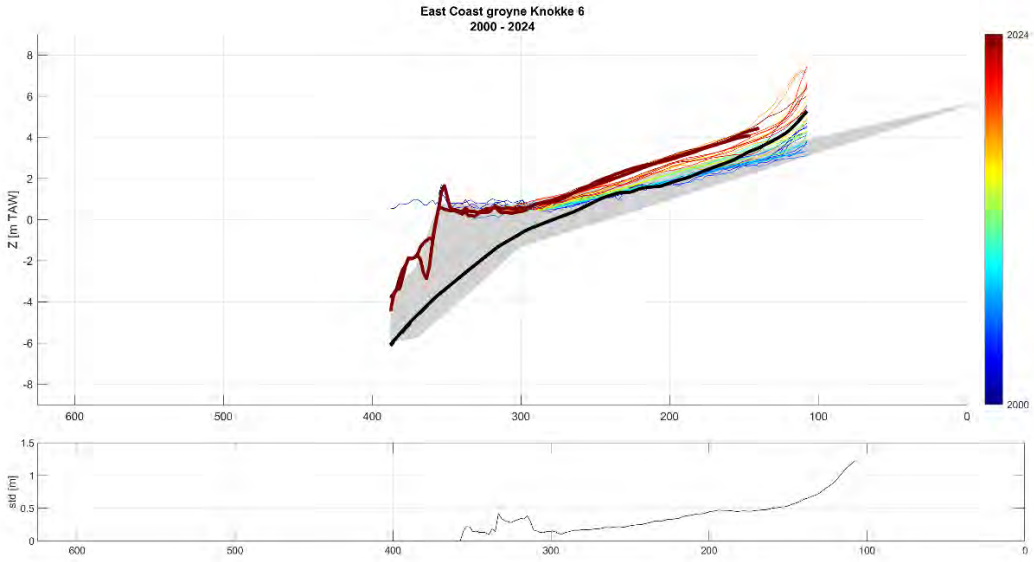
East Coast groyne Knokke 6
2000 - 2024
Z [m TAW]
std [m]
2024
2000

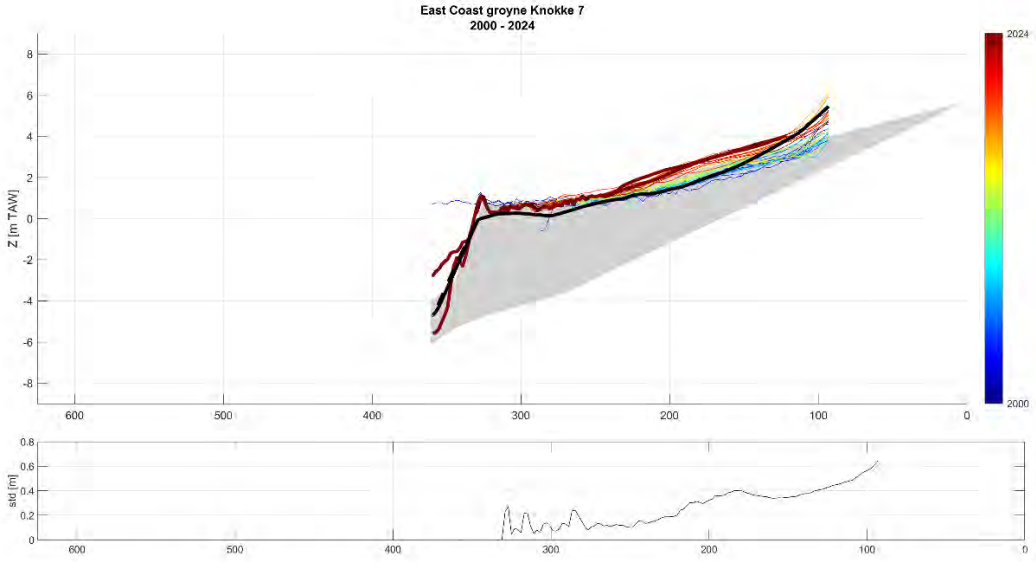
East Coast groyne Knokke 7
2000 - 2024
Z [m TAW]
std [m]
2024
2000

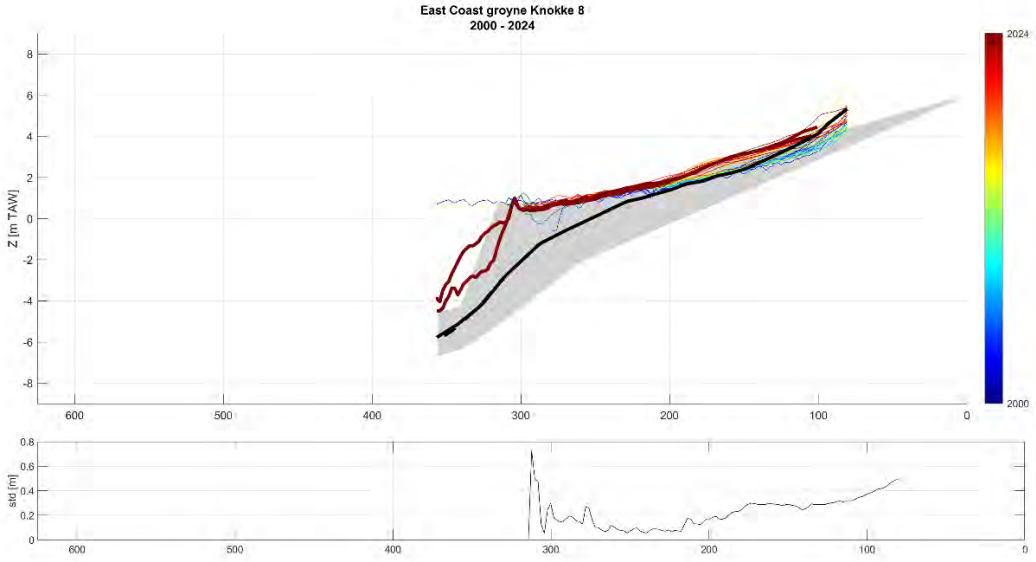
East Coast groyne Knokke 8
2000 - 2024
Z [m TAW]
std [m]
2024
2000

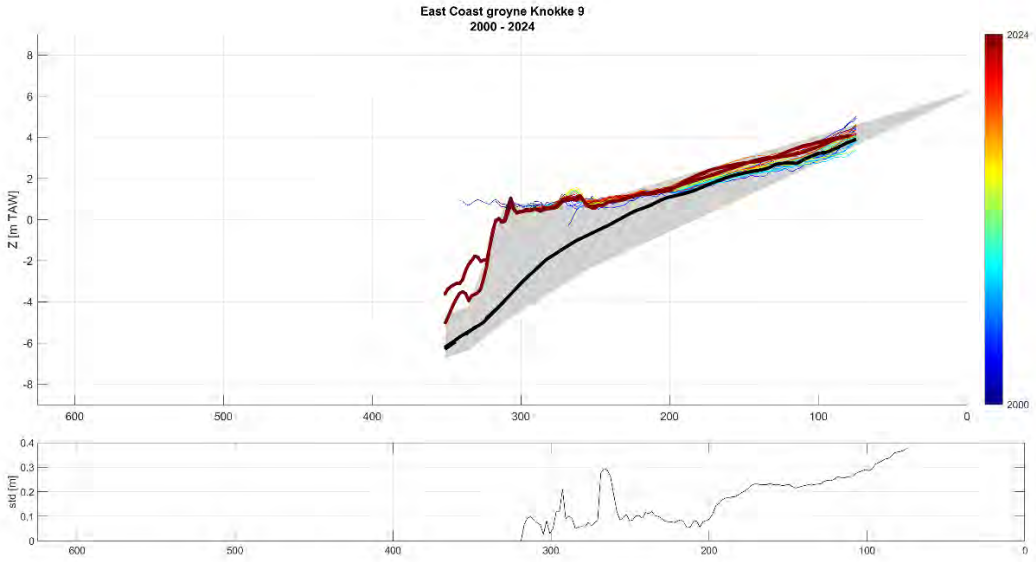
East Coast groyne Knokke 9
2000 - 2024
Z [m TAW]
std [m]
2024
2000

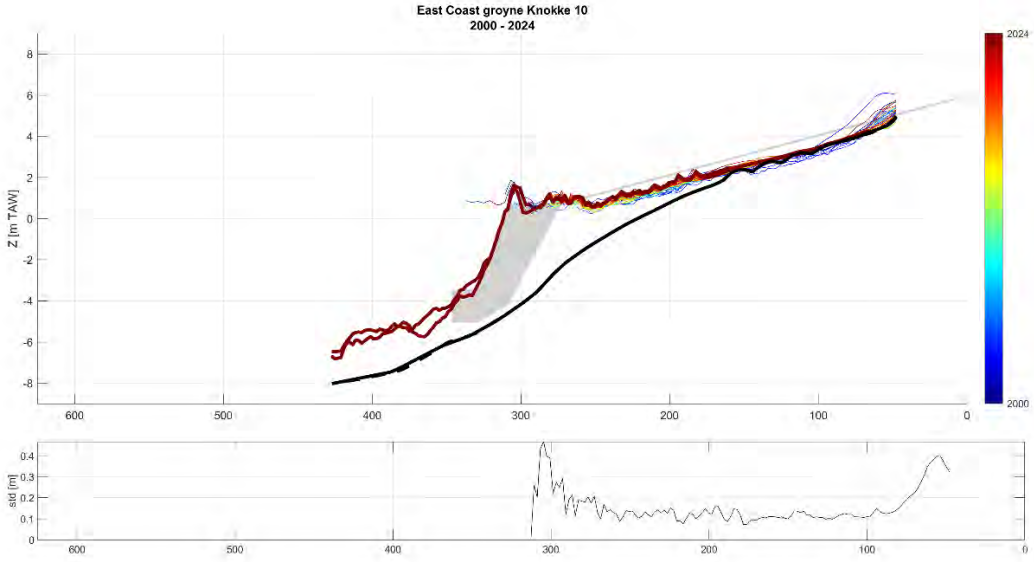
East Coast groyne Knokke 10
2000 - 2024
Z [m TAW]
std [m]
2024
2000

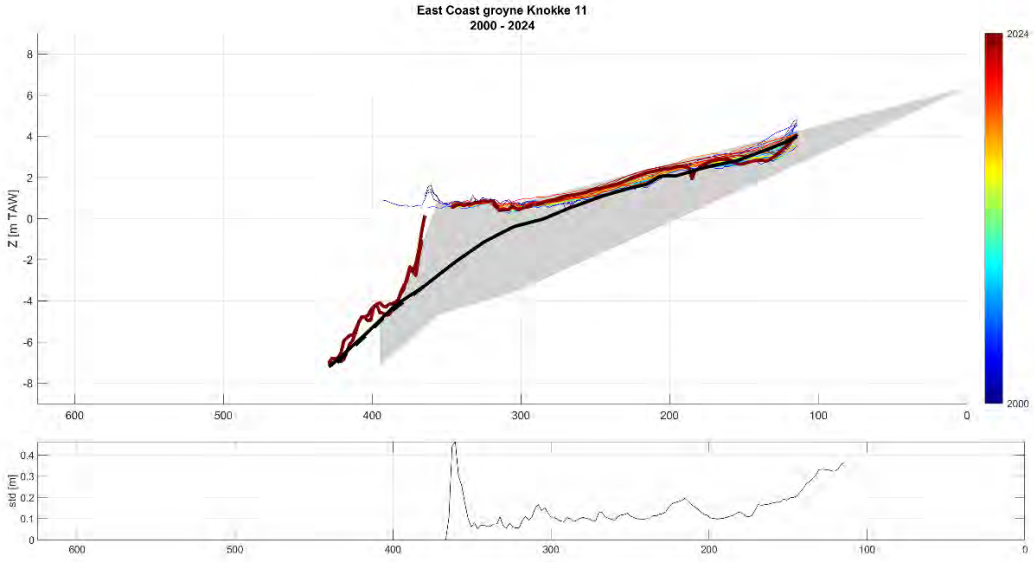
East Coast groyne Knokke 11
2000 - 2024
Z [m TAW]
std [m]
2024
2000

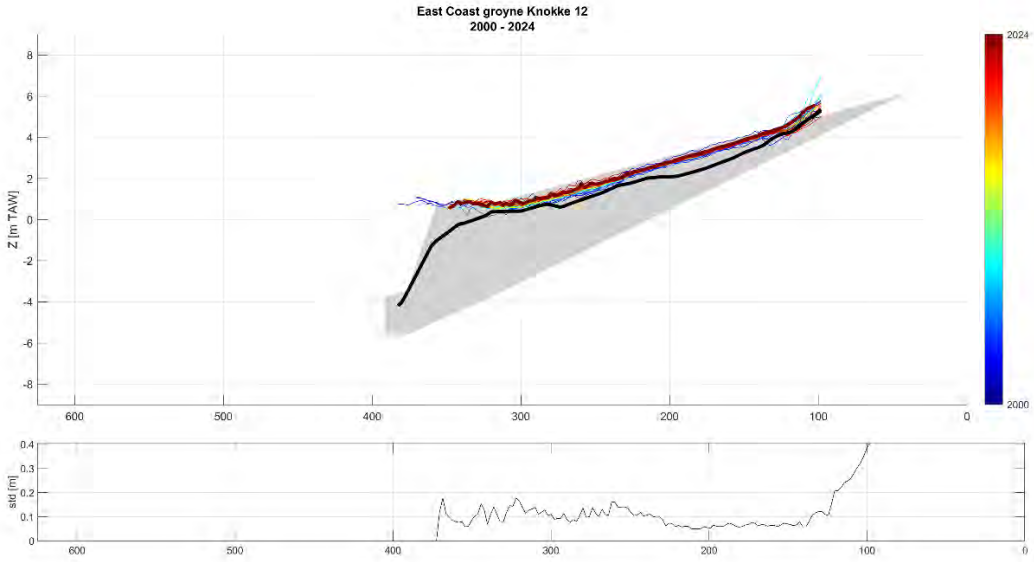
East Coast groyne Knokke 12
2000 - 2024
Z [m TAW]
std [m]
2024
2000

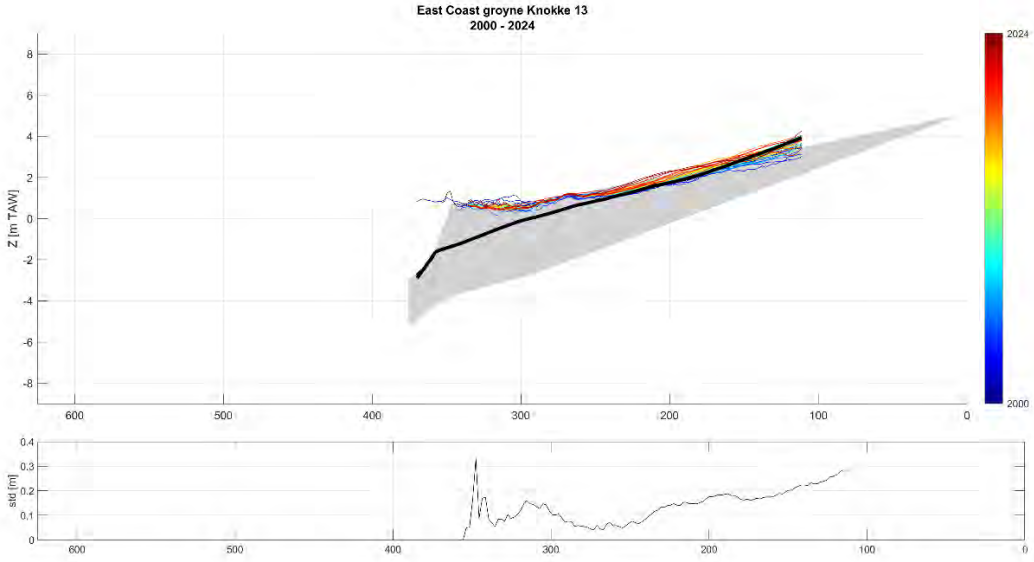
East Coast groyne Knokke 13
2000 - 2024
Z [m TAW]
std [m]
2024
2000

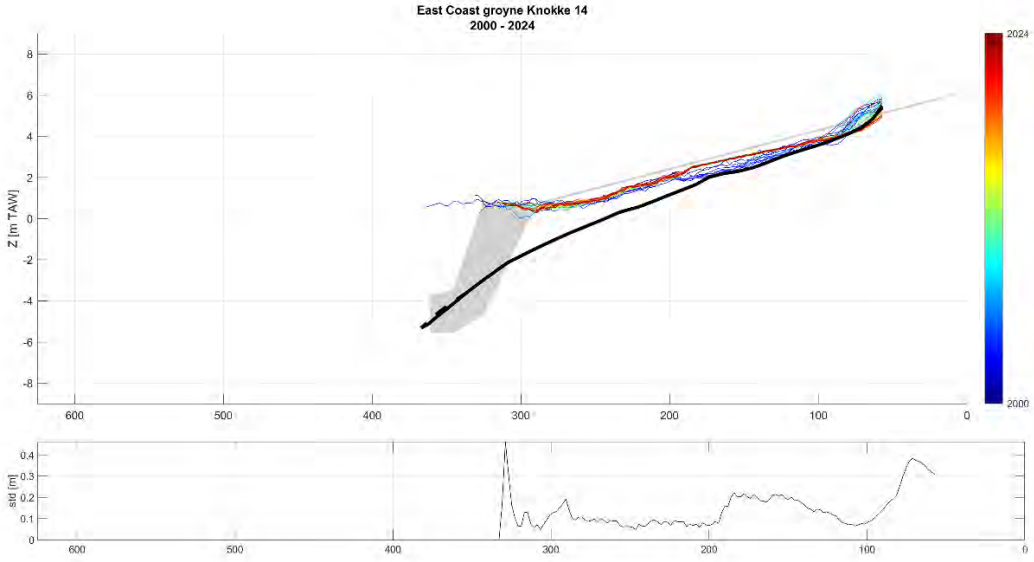
East Coast groyne Knokke 14
2000 - 2024
Z [m TAW]
std [m]
2024
2000

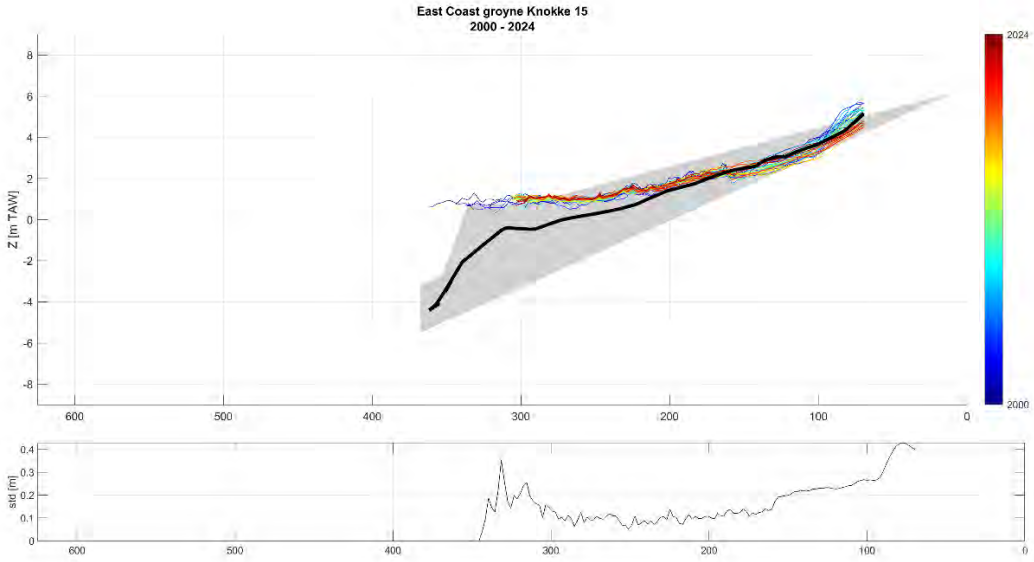
East Coast groyne Knokke 15
2000 - 2024
Z [m TAW]
std [m]
2024
2000

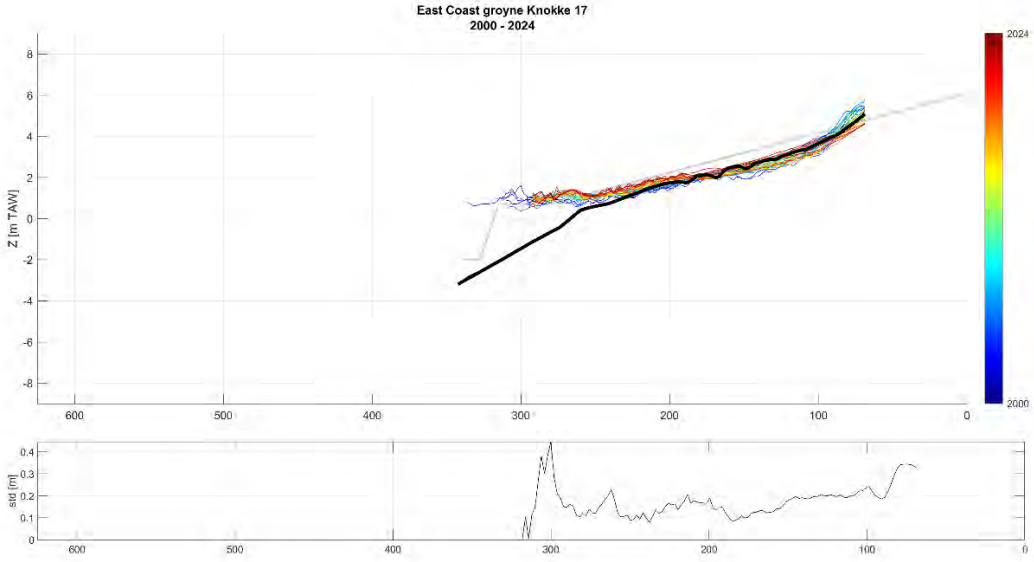
East Coast groyne Knokke 17
2000 - 2024
Z [m TAW]
std [m]
2024
2000

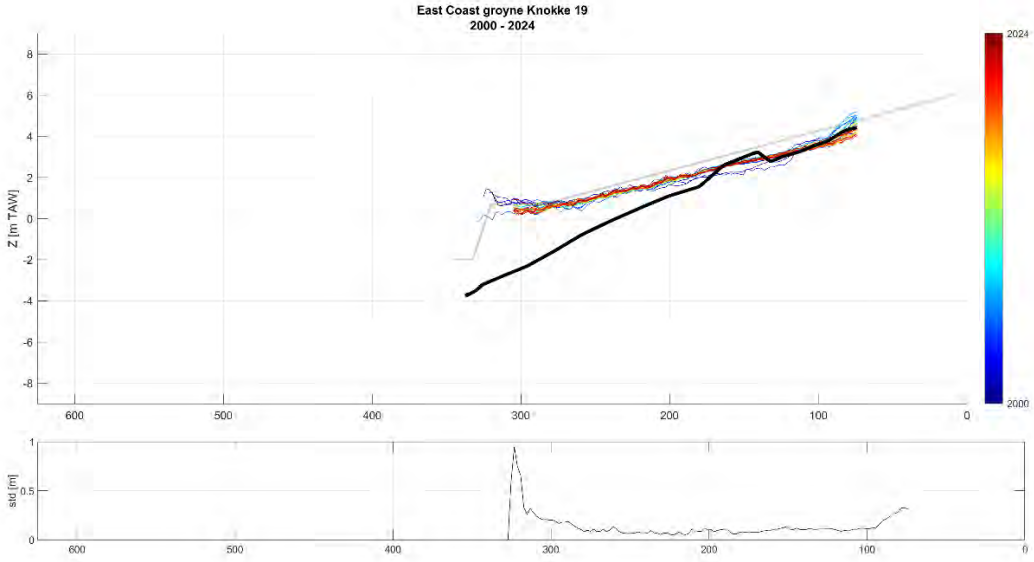
East Coast groyne Knokke 19
2000 - 2024
Z [m TAW]
std [m]
2024
2000

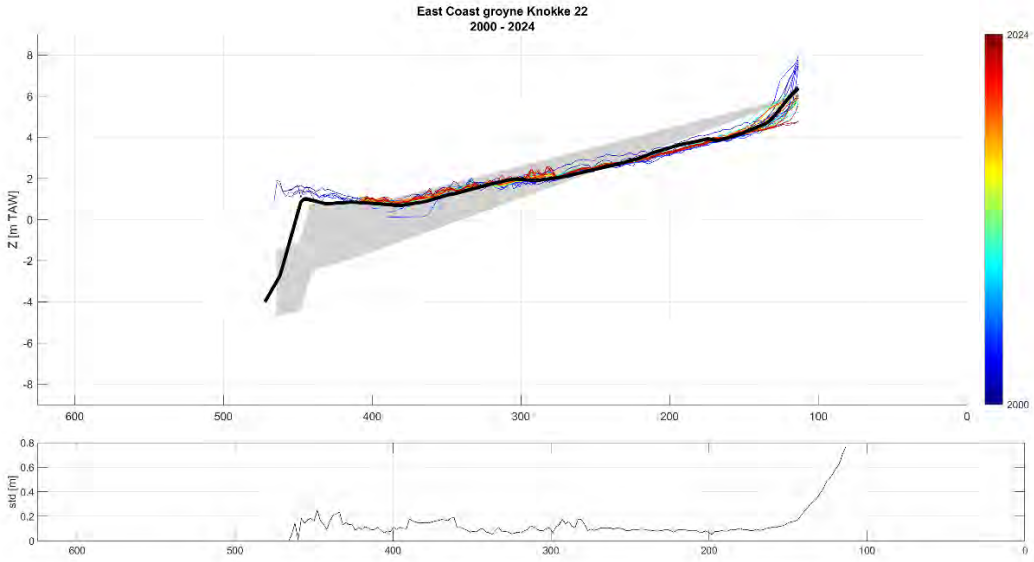
East Coast groyne Knokke 22
2000 - 2024
Z [m TAW]
std [m]
2024
2000

Alongshore profiles

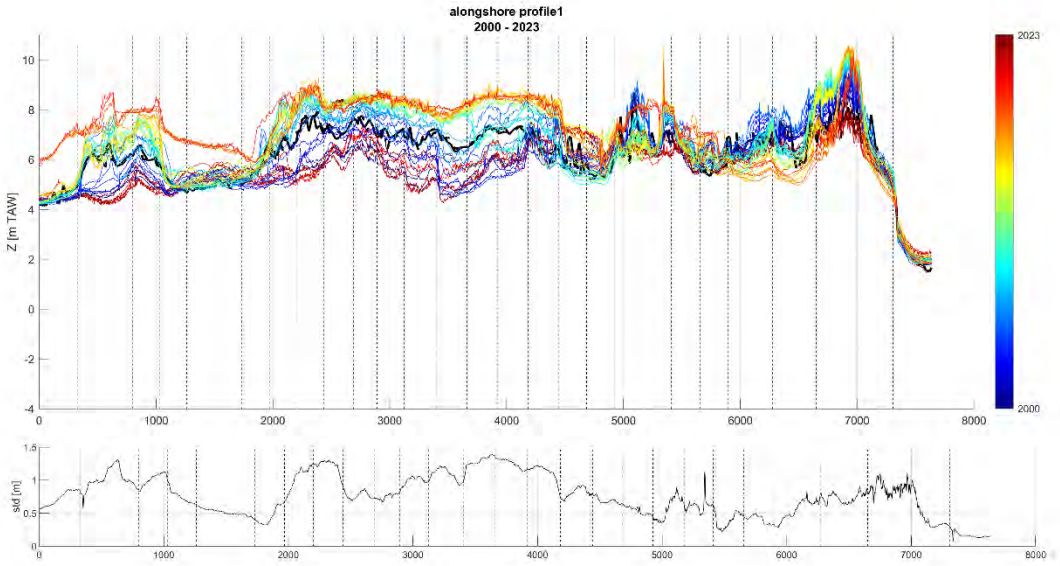

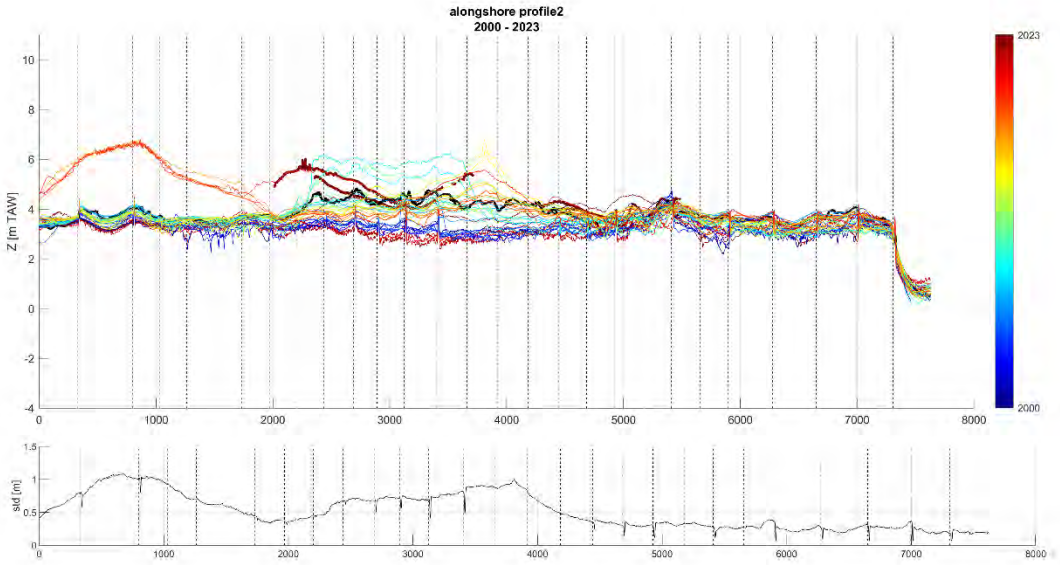

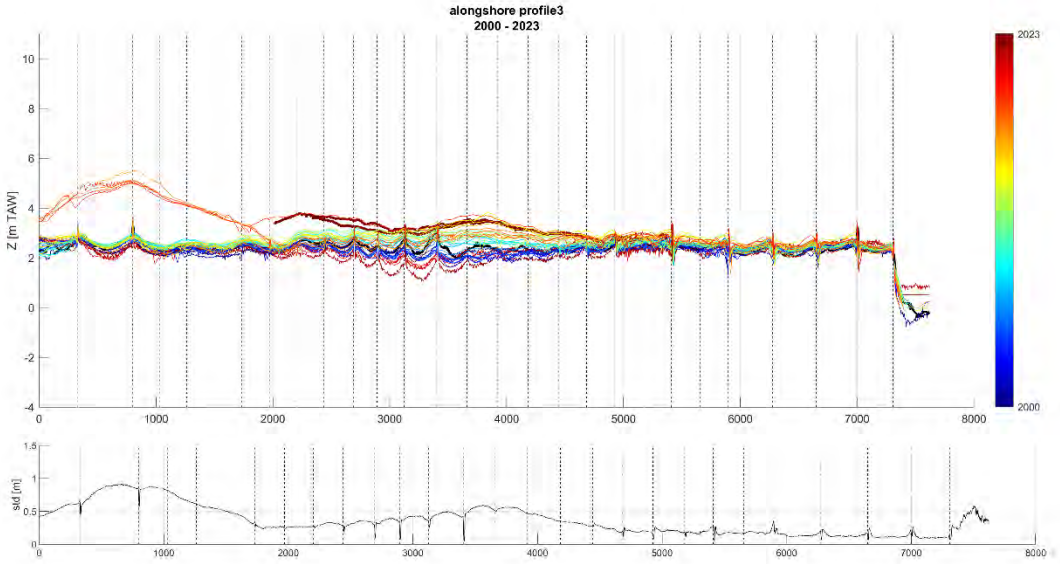
alongshore profile3
2000 - 2023
Z [m TAW]
std [m]
2023
2000

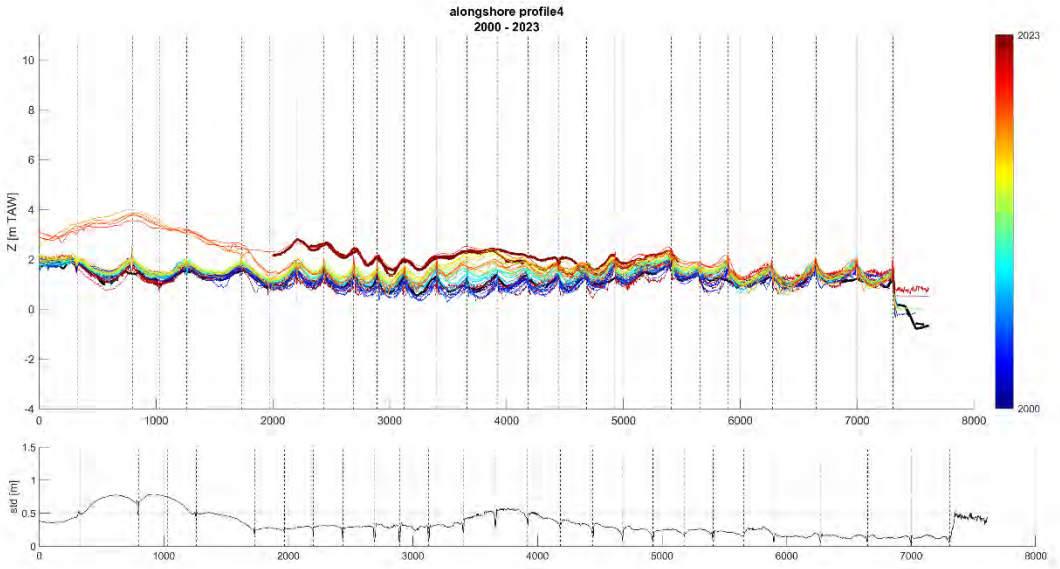
alongshore profile4
2000 - 2023
Z [m TAW]
std [m]
2023
2000

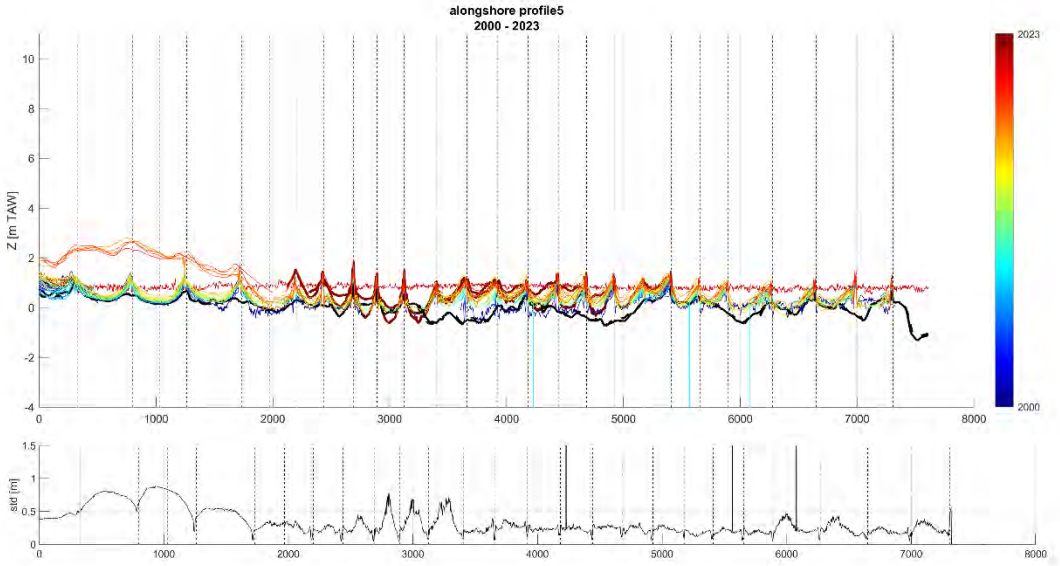
alongshore profile5
2000 - 2023
Z [m TAW]
std [m]
2023
2000

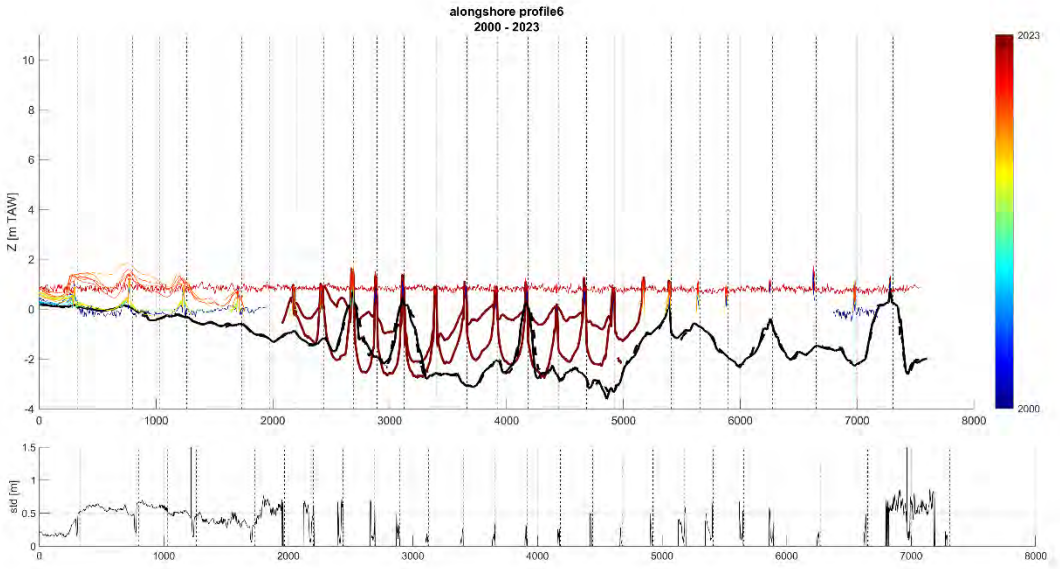
alongshore profile6
2000 - 2023
Z [m TAW]
std [m]
2023
2000

DEPARTMENT **MOBILITY & PUBLIC WORKS**
Flanders hydraulics

Berchemlei 115, 2140 Antwerp
T +32 (0)3 224 60 35
F +32 (0)3 224 60 36
flanders.hydraulics@vlaanderen.be
www.flandershydraulics.be